SUPERABSORBENT POLYMER NANOCOMPOSITES AS WATER RESERVOIR FOR THE SUSTAINED RELEASE OF ACTIVE AGENTS

by
OGEDAY RODOP

Submitted to the Graduate School of Engineering and Natural Sciences
in partial fulfillment of the requirements for the degree of Doctor of Philosophy

Sabancı University
December 2024

ABSTRACT

SUPERABSORBENT POLYMER NANOCOMPOSITES AS WATER RESERVOIR FOR THE SUSTAINED RELEASE OF ACTIVE AGENTS

OGEDAY RODOP

Materials Science and Nano Engineering, Ph.D. Thesis, July 2024

Prof. Dr. Yusuf Ziya Menceloğlu

Keywords: superabsorbent polymers, water reservoir, sustainable agriculture, micronutrient release, biodegradable SAP

Globally, 80% of all farmlands is rainfed, making irregular rainfall regimes a significant threat to food security. Farmers urgently need technologies that minimize water loss to alleviate yield loss in times of drought. Fertilizers and plant protection products (PPPs) are crucial for improved yields. However, the bulk application of these agrochemicals can lead to environmental leaching due to runoff and evaporation. Sustained delivery can improve the efficiency of agrochemicals.

To address the above-mentioned challenges, we propose superabsorbent polymer (SAP) nanocomposites as underground water reservoirs with the ability to integrate water and active agent delivery. SAPs absorb water during rainfall and release it during dry spells. Composite SAPs can allow sustained delivery of agrochemicals, prevent their runoff due to heavy rainfalls, and keep them closer to the root area for optimum plant uptake.

In this study, fertilizer-SAP composites containing 17 wt% micronutrients have achieved superior water absorption capacities of 1460-1630 g/g, compared to 500 g/g for traditional SAPs.

Commercial SAPs have very limited biodegradability. Developing biodegradable SAP formulations is important to combat plastic accumulation in agricultural lands. There is a lack of studies on bio-SAPs with 25-70 wt% biomaterial contents.

We have incorporated 5-60 wt% carboxymethyl cellulose (CMC) into an otherwise polyacrylate-based SAP formulation. A maximum water absorption of 600 g/g was achieved with SAP containing 10 wt% CMC. Up to 40 wt% CMC, SAPs exhibited water absorption comparable to commercial SAPs. SAPs with 40 wt% or more CMC biodegraded completely by cellulase enzyme within 3 days.

ÖZET

AKTİF MADDELERİN YAVAŞ SALINIMI İÇİN SU REZERVUARI OLARAK SÜPER EMİCİ POLİMER NANOKOMPOZİTLER

OGEDAY RODOP

Malzeme Bilimi ve Nano Mühendislik, Doktora Tezi, Temmuz 2024

Prof. Dr. Yusuf Ziya Menceloğlu

Anahtar Kelimeler: süper emici polimerler, su rezervuarı, sürdürülebilir tarım, mikro besin salınımı, biyolojik olarak parçalanabilir SAP

Küresel olarak tarım alanlarının %80'i yağmurla beslenmektedir ve bu da düzensiz yağış rejimlerini gıda güvenliği için önemli bir tehdit haline getirmektedir. Çiftçiler, kuraklık dönemlerinde verim kaybını azaltmak için su kaybını en aza indiren teknolojilere acilen ihtiyaç duymaktadır. Gübreler ve bitki koruma ürünleri (BKÜ'ler) hasat verimini artırmak için çok önemlidir. Ancak, bu tarımsal girdilerin dökme yöntemiyle uygulanması, yüzeysel akış ve buharlaşma nedeniyle çevresel sızıntılara yol açabilir. Öte yandan, yavaş salım, tarımsal girdilerin verimliliğini artırabilir.

Yukarıda bahsedilen zorlukların üstesinden gelmek için, su ve aktif madde salımını entegre etme kapasitesine sahip yeraltı su rezervuarları olarak süper emici polimer (SAP) nanokompozitleri öneriyoruz. SAP'lar yağış sırasında suyu emer ve kurak dönemlerde serbest bırakır. Kompozit SAP'lar tarımsal girdiler ihtiva eder, bunların yavaş salımını sağlar, şiddetli yağışlar nedeniyle akmalarını önleyebilir ve verimli bitki alımı için onları kök bölgesine daha yakın tutar.

Bu çalışmada, ağırlıkça %17 mikro besin içeren gübre-SAP kompozitleri, geleneksel SAP'lara (500 g/g) kıyasla 1460-1630 g/g'lık üstün su emme kapasitelerine ulaşmıştır.

Ticari SAP'ların biyolojik olarak parçalanabilirliği çok sınırlıdır. Biyolojik olarak parçalanabilen SAP formülasyonlarının geliştirilmesi, tarım arazilerindeki plastik

birikimiyle mücadele etmek için önemlidir. Literatürde, ağırlıkça %25-70 biyomateryal içeriğine sahip biyo-SAP'lar hakkında yayımlanan çalışmalar kısıtlıdır.

Poliakrilat bazlı bir SAP formülasyonuna ağırlıkça %5-60 oranında karboksimetil selüloz (CMC) ekledik. Ağırlıkça %10 CMC içeren SAP ile maksimum 600 g/g su emilimi elde edilmiştir. Ağırlıkça %40'a kadar CMC ihtiva eden SAP'lar, ticari SAP'lara yakın bir su emilimi performansı sergilemiştir. Ağırlıkça %40 veya daha fazla CMC içeren SAP'lar 3 gün içinde selülaz enzimi tarafından tamamen biyolojik olarak parçalanmıştır.

Aileme

TABLE OF CONTENTS

LIST OF TABLES

TABLE OF FIGURES

LIST OF SYMBOLS

G'	:	Storage modulus
G"	:	Loss modulus
μ	:	Mu, micro, a unit prefix denoting a factor of 10^{-6} (one millionth)
S	:	Siemens, the unit of electric conductance in SI unit system

LIST OF ABBREVIATIONS

AMPS	:	2-acrylamido-2-methylpropane sulfonic acid
APTES	:	(3-Aminopropyl)triethoxysilane
IPTS	:	3-(Triethoxysilyl)propyl isocyanate
AAm	:	Acrylamide
AA	:	Acrylic acid
BET	:	Brunauer, Emmett and Teller
Ca:SAP	:	Calcium nitrate – superabsorbent polymer composites
CMC	:	Carboxymethyl cellulose
HNT	:	Halloysite nanotube
Mg: SAP	:	Magnesium sulfate – superabsorbent polymer composites
PPP	:	Plant protection products
PEG	:	Poly(ethylene glycol)
KOH	:	Potassium hydroxide
SEM	:	Scanning electron microscopy
NaOH	:	Sodium hydroxide
SAP	:	Superabsorbent polymer
SAP-HNT	:	Superabsorbent polymer nanocomposites with halloysite nanotubes as nano-filler
CMC-SAP	:	Superabsorbent polymer synthesized with carboxymethyl cellulose
TGA	:	Thermogravimetric analysis
VTMS	:	Vinyltrimethoxysilane
Zn:SAP	:	Zinc sulfate – superabsorbent polymer composites

Chapter 1

INTRODUCTION

1.1. Our Greatest Endeavour

Agriculture is humanity's foremost pursuit, necessary for our survival and progress in the world. During most of our 12,000-year history as farmers, our cultivation methods and population remained largely unchanged. However, two revolutions arose during this agricultural era, which lead to significant changes in our lives.

The first revolution, known as the British Agricultural Revolution, implemented innovative techniques to greatly improve agricultural productivity. These techniques included the use of machinery for plowing instead of relying on manual labor or animals, selective breeding to cultivate higher-yielding crops, and advancements in infrastructure such as canals to ensure proper irrigation, resulting in increased production. The higher yields achieved allowed a reduced number of farmers to produce an ample food supply. As a result, a larger proportion of the workforce started to take part in urban occupations, which promoted industrial production. Subsequently, the British Agricultural Revolution played a pivotal role in triggering the onset of the Industrial Revolution.

Subsequently, the Green Revolution emerged, enabling a significant increase in food production from the same land area. Various factors contributed to this boost in yields. In

addition to selective breeding and genetic modification to develop high-yielding crop varieties, pesticides and fertilizers played a vital role. Pesticides were employed to safeguard crops against pests, preventing substantial losses in yield. Furthermore, fertilizers were utilized to supplement essential nutrients in the soil, ensuring robust plant growth. Without nutrient replenishment, high yielding crop varieties would make soil unproductive during upcoming growing seasons. This situation renders the use of fertilizers imperative to sustain the intensive growth of plants.

Between 1950 and 1985, the global population doubled while global grain output increased by a factor of 2.6, resulting in increased food accessibility and economic growth in many countries. (European Environment Agency, 2021) From the perspective of effectively feeding people and driving the economy, the Green Revolution proved highly successful. However, it also led to adverse effects on our agricultural practices, posing environmental challenges that necessitate another revolution to address them. The ongoing growth of the global population further complicates this task. Balancing the need for increased yields with the urgent requirement to mitigate unsustainable practices introduced during the initial push for higher yields seems contradictory and exceedingly challenging.

Meeting the global food demand is a complex and challenging task that involves numerous factors, stakeholders, and variables, potentially requiring a third agricultural revolution. Water, plant protection products, and fertilizers are essential inputs in agriculture, and the next revolution should focus on finding optimal methods of their application in fields. Our primary challenge goes beyond simply producing more food; it lies in meeting the nutrition needs of an estimated 11 billion people by 2050 while respecting the sustainable boundaries of our planet.

Historically, the expansion of food production was enabled by converting natural ecosystems into agricultural land, leading to deforestation. However, owed to previous agricultural revolutions, food production per capita was significantly increased while utilizing less land per capita. For instance, in 1961, the arable land per person was 0.36 hectares, which decreased to 0.18 hectares in 2020, and is projected to decrease to 0.16 hectares by 2080. (Alexandratos & Bruinsma, 2012; The World Bank, n.d.-b) These statistics suggest the need for an even more efficient food production.

We must continue to advance our farming methods to ensure sufficient food production, despite limited availability of arable land. Finding sustainable ways to meet the nutritional needs of a growing population is crucial, and a third agricultural revolution may be necessary to address these challenges effectively.

1.2. Climate Change and its Effects on Agriculture

The anticipated impact of climate change on food production is intricate. Temperature increases, rising sea levels, and atmospheric CO_2 concentration may be the most trending effects of climate change. However, in terms of food security, rainfall irregularities possibly pose a bigger threat. Water management plays a crucial role in plant health. Although total rainfall received globally is roughly stable, there are more and more instances of heavy rainfall and longer periods of drought, throughout the world. Such an increase in the intensity of rain is neither suitable for plant uptake nor for soil water absorption; and longer dry periods are harmful for plant growth. The harvest of the farmers who rely solely on rainwater fluctuates with rain. People with access to irrigation can compensate for the lack of precipitation. However, if exploited, this will result in the depletion of underground water reserves, which will affect successive growing seasons.

It is forecasted that global warming will result in a temperature increase of 1.5-2 °C, along with more frequent rainfall irregularities. While certain regions may experience increased overall rainfall (e.g., Eastern Europe), others may face more instances of drought (e.g., South Europe). The distribution of rainfall is expected to become more irregular, with heavy rainfalls followed by prolonged dry spells. These precipitation swings can have detrimental effects on water uptake by plants. Recent examples of irregular precipitation patterns include severe droughts in Spain and Portugal in 2022 and the destructive floods in South Africa.

On the other hand, rising temperatures will contribute to crop losses by promoting the growth and metabolism of insects, leading to increased pest populations. This will be

particularly impactful in temperate regions where grains are predominantly grown. Furthermore, new pest species may emerge, posing additional threats to crops and necessitating the development of new plant protection methods.

The Mediterranean fruit fly, a highly invasive and damaging pest in horticulture, is expected to expand its range northward into temperate regions due to climate change. This expansion may occur in areas such as inland France, southern Germany, Switzerland, Austria, and Hungary. Conversely, regions that become less suitable for fruit flies, like North Africa, may experience a decrease in populations.

Overall, the following are the most anticipated effects of climate change on food production: (i) increased droughts, floods, and related soil erosion, (ii) reduced average crop yields, (iii) intensified pest populations, (iv) shift in planting schedules, and (v) the risk of extinction for certain crop types.

1.3. Water in Agriculture

Water is the most important resource in agriculture. Although they represent only 20% of cultivated land, irrigated farmlands contribute 40% of the global food supply. (Dowgert, 2010; The World Bank, n.d.-c) However, the limited availability of freshwater resources makes them highly precious. Agriculture is responsible for 70% of global water consumption. This percentage can even exceed 95% in some developing countries, making farming the largest consumer of water. (The World Bank, n.d.-a) Unfortunately, the use of chemical pesticides to combat pests and mineral fertilizers to promote plant growth, also makes agriculture the biggest polluter of water.

One of the greatest problems faced by conventional agriculture is water scarcity. The challenges associated with water usage in agriculture begin even before water reaches the fields. Inefficient water pipe infrastructure, particularly in open canals, leads to significant water loss through evaporation. For example, in Türkiye, 50% of irrigation water is lost through open canals.

Although manual or surface irrigation is an inefficient method, it remains widely used, covering over 83% of irrigated farmland globally, albeit with only 60% efficiency. (Brouwer et al., 1989; Gonçalves et al., 2021; Lehrsch et al., 2014) Farmers require technologies that can optimize the utilization of available water by plants. So far, to combat water scarcity, engineers have developed techniques that are designed to apply water in a sustained fashion, such as drip or spray irrigation.

Drip irrigation is a highly efficient system that delivers water directly to the soil through a network of plastic pipes at low rates. It achieves more than 90% water use efficiency and can also provide nutrients directly to plant roots. (Brouwer et al., 1989) Drip irrigation is suitable for high-value crops such as vegetables, fruit trees, and vine crops. On the other hand, sprinkler irrigation mimics rainfall by applying water over the crop canopy. These systems are typically 75% efficient and require lower investment and maintenance costs compared to drip irrigation. (Brouwer et al., 1989) Sprinklers are preferable for lower revenue-generating crops and both annual and perennial crops.

1.4. Superabsorbent Polymers

Superabsorbent polymers (SAP) are hydrophilic polymers, with three-dimensional crosslinked structures. With an optimized crosslinked structure, SAPs can absorb and retain extensive amount of water while maintaining their structural integrities. When in contact with water, SAPs absorb water due to osmotic pressure difference and the presence of hydrophilic functional groups (-OH, -COOH, -CONH-, -CHO, -COONa, -SO3H, -NH2) in their polymer backbone. The absorption of water is allowed by the expansion of the polymer network, which is possible owed to chemical and physical crosslinking introduced during or after polymerization. The crosslinked structure of SAP prevents its dissolution in water. This characteristic allows SAPs to absorb and retain significant quantities of water within their 3D structure. (Ahmed, 2015; Kabiri et al., 2011; Venkatachalam & Kaliappa, 2023; Zohuriaan-Mehr et al., 2010) Parameters such as crosslinking characteristics, density, and length of crosslinks determine water absorption properties of SAPs. Water absorbency of SAPs is also greatly affected by the ionic concentration of the solution, deteriorating significantly in saline conditions.

Often, the terms hydrogel and superabsorbent polymers (SAPs) are used interchangeably. However, for the polymer discussed in this study, using the word superabsorbent polymer is more appropriate. Hydrogels are defined as polymer networks that have hydrophilic properties, are water-insoluble, and can hold large amounts of water. Usually, the polymers that can hold up to 10 times their own weight are referred to as hydrogels. Whereas, superabsorbent polymers represent a subcategory of hydrogels, with high water absorption capacities, up to 1500 times their own weight. (Farzanian & Ghahremaninezhad, 2018)

SAPs can be synthesized from either natural or synthetic sources, or from a combination of both. Commercially, almost all SAP is manufactured from synthetic monomers, of which the most common are acrylamide and acrylic acid. (Anil et al., 2019; Ghazali et al., 2016; Kiatkamjornwong, 2007) Methacrylic acid (Bajpai et al., 2007), 2-acrylamido-2-methylpropanesulfonic acid (AMPS) (Tang et al., 2019), hydroxyethyl-methacrylate (Chauhan et al., 2009), polyvinyl alcohol (Czarnecka & Nowaczyk, 2021; Patachia & Croitoru, 2015), and various other acrylates (Macdougall & Anseth, 2020; Sánchez-Correa et al., 2018) are also used for the synthesis of superabsorbent polymers.

Sources for natural sources include cellulose, starch, collagen, alginate, and chitosan. (Aljohani et al., 2017; Dinescu et al., 2018; Kabir et al., 2018; Sadeghi & Soleimani, 2012; S. Song et al., 2019) Synthetic SAPs are preferred over their natural counterparts due to their higher water absorption capacities, longer service life, and improved mechanical strength. (Ahmed, 2015) Furthermore, hybridized SAPs can be synthesized by graft polymerization, using both natural and synthetic polymers. (Bao et al., 2011; Czarnecka & Nowaczyk, 2020, 2021; Mignon et al., 2019)

SAPs suffer from low elastic modulus, low fracture energies, and negligible fatigue resistance, leading to weak and brittle mechanical properties. The uneven distribution of crosslinking points in the polymer network prevents effective dissipation of stress and results in the formation of microcracks. (Huang et al., 2007; Islam et al., 2023; Y. Wu et al., 2022) Even though synthetic SAPs have a gel strength that is comparatively higher than that of natural SAPs, the gel typically disintegrates under load and loses its strength after reaching equilibrium swelling. (Ramazani-Harandi et al., 2006a) Various

approaches have been evaluated to improve the mechanical strength and fatigue resistance of SAPs, such as grafting with clays (R. Singh & Mahto, 2017), synthesizing double network hydrogels (Gong et al., 2003; Nakayama et al., 2004), nanocomposite hydrogels (Rodrigues et al., 2013), macromolecular microsphere hydrogels (Huang et al., 2007), or by introducing ionic coordination interactions (Q. Chen et al., 2016) or polyzwitterions (Yin et al., 2013) in double network hydrogels.

SAPs exhibit unique responses to external stimuli, such as pH, ionic strength, solvent composition, temperature, and light, making them versatile materials in various fields. Although most SAPs are produced for personal care products like diapers and sanitary pads, they have found applications in tissue engineering (Sargeant et al., 2012), cement (Sun et al., 2019), food packaging (Batista et al., 2019; Sudheer et al., 2023), drug delivery (Noppakundilograt et al., 2018; Rossi et al., 2015), adhesives (Xue et al., 2021), agriculture (Behera & Mahanwar, 2020), and wastewater treatment (Sinha & Chakma, 2019). SAPs are preferred for a variety of applications due to their high-water absorption capacity, biocompatibility, softness, and sensitivity to environmental stimuli.

1.4.1. Superabsorbent Polymers in Agriculture

Traditionally, SAPs have been and still are being widely used in diapers and in feminine hygiene products. They have recently found applications in agriculture, owed to their ability to improve the water retention capacity of the soil. (Takahashi et al., 2023)

One of the greatest problems faced by conventional agriculture is water scarcity and rain irregularity. Farmers require technologies that can optimize the utilization of available water by plants. So far, to combat water scarcity, engineers have developed techniques that are designed to apply water in a sustained fashion, such as drip or spray irrigation systems. However, due to their high upfront materials and labor cost, maintenance, economic lifetime, and the unsuitability of hilly lands, these methods are far from being prevalent in most developing countries, where mostly flood irrigation is used.

Another approach to reduce the agricultural water footprint, is enhancing soil water retention capacity. One such method is the use of superabsorbent polymers (SAPs) as water reservoirs that can regulate water delivery to plants by swelling during rainfall and

releasing water during dry periods. Thus, plant growth continues even in drought conditions. This prolongs water availability near plant roots, leading to increased water uptake, biomass, and yield. SAPs are particularly effective in fields with surface irrigation or non-irrigated agriculture. SAPs can reduce the irrigation need of plants in fields watered by flood irrigation, and hence prevent excessive water use. Depending on crop type and field conditions, they can potentially reduce water demand by 25-50% and result in a 20-40% yield increase. (Cerasola et al., 2022; Mao et al., 2011) SAPs are mainly suitable for annual crops but can also be applied to saplings or trees.

In conventional agriculture on open fields, SAPs are applied during the seeding stage, near the root area of the plants. SAPs are produced granular form, like mineral fertilizers. This allows them to be applied with conventional equipment, already developed for fertilizers or seeds. They can be readily integrated into zero-till or seed-cum-fertilizer drills, be applied together with the seeds or fertilizers, and cause no extra burden for the farmer.

Numerous studies have shown that the presence of SAPs near plant roots increases soil water absorption and retention, leading to improved plant growth. Mixing SAPs with soil increases plant yield and seed germination. (Oladosu et al., 2022) The increasing importance of SAPs in agriculture holds promise for achieving more productive lands.

1.5. Efficient Use of Plant Protection Products (PPP) and Nutrients

Arable land is limited, and to feed the ever-growing population, we need to maximize crop yields. Harmful pests have a drastically negative effect on crop yields, and not taking any preventative measures, e.g., using plant protection products (PPPs), could result in up to a 70% yield loss. (Gordon, 2022) So, unless we double the amount of land used for agriculture, eliminating pesticides is not a viable option. However, significantly increasing the amount of arable land would also be detrimental to biodiversity, because making up land for agriculture is usually through deforestation. In fact, almost 90% of global deforestation is due to food production and animal husbandry. (FAO, 2021) So, a

strategy that aims to increase the amount of arable land at the expense of lower crop yields with the use of minimal pesticides (PPPs) is not a sustainable option.

Water, fertilizers and pesticides are the key inputs of modern agriculture. To maximize crop yields they should be applied in appropriate amounts. Their excessive application can be as destructive as their shortage. In this regard, these inputs' method of application is as important as their application doses.

1.5.1. Plant Protection Products - Current Situation

Pesticides play a crucial role in enhancing crop productivity. Before delving into the importance and shortcomings of and challenges faced by pesticides let us concisely describe what we mean by pests. A pest is any destructive insect, animal, or more generally any organism that attacks crops, food or livestock, for example, through feeding on plants or parasitizing livestock. As its name suggests, pesticides are then any substance or a combination or substances that destroys, repels, or weakens any pest. Pesticides can be classified according to different criteria. According to their target organisms, pesticides are classified into insecticides (insects), herbicides (plants), fungicides (fungi), nematicides (worms), rodenticides (rats and mice), and miticides (mites and ticks). Further, according to their intended use, they are classified as defoliants, desiccants, fumigants, and plant growth regulators. Further still, we can distinguish between pesticides according to their modes of actions: non-systemic (exterior of the plant), systemic (absorbed by the plant), broad-spectrum (non-selective, for various pests), curative (applied after damage), and preventative (applied to stop the loss before it starts). (A. Singh et al., 2020)

Numerous advances accomplished in agriculture to date are ascribed to the development of pesticides and fertilizers, both of which increased productivity tremendously. In fact, we tend to associate these developments with the extensive and mostly indiscriminate use of pesticides. However, on the other side of the medallion, these chemicals have become the main contaminants of both our surface and groundwater reservoirs. Pesticides are unfortunately used excessively due to their desperately ineffective application. To better explain just how serious the situation is, let us give two simple statistics: 60-90% of all

pesticides used are lost to the environment due to degradation, photolysis, evaporation, and surface runoff; and even more shockingly, only a mere 0.1% of pesticides coat the harmful pests. (B. Liu et al., 2016; Rosenbom et al., 2015) Pesticide usage is expected to reach 3.5 million tonnes in 2020. (Sharma et al., 2019)

The reason behind the ineffectiveness of pesticides lies in their method of application. Pesticides are applied to fields in bulk and mostly in pure form without any adjuvants. Spraying, dusting, mixing with soil, seed pelleting, and sett treatment are some of the most common application techniques of pesticides. With these traditional methods, active molecules are applied at high initial doses (often at toxic levels), but their concentration usually rapidly drops below the effective level after a primary burst release. Weather conditions also greatly impact their efficiency. For instance, a rainfall soon after pesticide application causes substances to move freely through soil, without contacting pests; and eventually to be transported in water and contaminate rivers and other water bodies. As a result of limiting factors, such as leaching, degradation, mineralization, and bioconversion, a significant portion of agro-chemicals remains unused and is lost to the environment. This not only renders pesticides environmentally threatening due to bioaccumulation, but also demands their repeated applications, to achieve effective pest control. (Campos et al., 2014)

Moreover, due to indiscriminate use of especially broad-spectrum pesticides, many benign non-target organisms are negatively affected, and soil biodiversity is damaged. Thus, pesticides have a serious detrimental impact on terrestrial and aquatic systems, flora, and fauna. On another note, the repeated use of the same active ingredients makes target pests and diseases resistant to certain chemicals, rendering further pesticide use less and less effective.

Pesticides are toxic not only to the ecosystem but also to human health as they can remain as residues on agricultural harvest or get bio-magnified along to food chain and pose occupational exposure risk to farm workers. Many pesticides are carcinogenic, mutagenic, and teratogenic; meaning they can cause cancer, miscarriages, and disrupt human hormones. (Campos et al., 2014) Other health risks associated with pesticides include skin, eye and lung irritation, blood disorders, brain and nervous system toxicity, reproduction effects, birth defects, nerve disorders, and blood disorders. (Neem.World,

2016) Toxicity of pesticides is particularly a threat for children; due to their underdeveloped immune system and large skin surface to body mass ratio. Since most chemical absorption occurs through our skins, children are more susceptible to being exposed to toxic doses of pesticides. However, the problem is more widespread than it seems. Pesticides do not only affect the organisms that they encounter. Some pesticides are highly persistent in the environment as they are resistant to degradation due to their lipophilic nature. Hence, they accumulate in the adipose tissue of organisms and get biomagnified along the food chain. For instance, we can be exposed to pesticides by eating a steak chopped from a cow, which had been eating grass from a land very close to an agricultural land that is continually being sprayed with insecticides that are leached to neighboring lands. (A. Singh et al., 2020)

1.5.2. Fertilizers – Current Situation

Efficient fertilizer application in agriculture is vital for maximizing crop yields. Intensive farming practices lead to soil nutrient depletion, necessitating the replenishment of soil nutrients to sustain plant growth in successive seasons. While organic approaches like animal manure, compost, and rock salt are commonly employed, they often fall short in providing optimal yields. Chemical fertilizers, with the first nitrogen fertilizer developed in 1913, through the Haber-Bosch process, have become indispensable in sustaining agricultural productivity and feeding the world's population.

Fertilizers are broadly categorized into mineral and organic. Mineral fertilizers are produced through chemical reactions involving air, natural gas, and mined ores, and are in the form of inorganic salts. Mineral fertilizers usually provide a single, or a few plant nutrients, at high concentrations. Whereas organic fertilizers mainly include crop residues, food waste, animal manures, and slurries. Organic fertilizers provide a wide variety of essential nutrients, albeit in low concentrations. Other types of fertilizers are also being developed, including organo-mineral fertilizers, mineral fertilizers including inhibitors, liming material, and plant biostimulants. Organo-minerals are a mixture of animal manure and mineral fertilizers. (International Fertilizer Association, n.d.)

Inhibitors that are used as fertilizer additives are mostly nitrification inhibitors and urease inhibitors, which combat nitrogen loss and consequent N_2O release into the atmosphere. Nitrogen loss, one of the greatest challenges in the conventional agricultural sector, can be in the form of leaching of nitrate, and gaseous losses of ammonia, nitrogen, and nitrous oxide. Nitrogen loss results in the reduction of nitrogen use efficiency. This represents both a major economic loss, crop yield loss, and a significant threat to groundwater quality. Nitrogen inhibitors hinder the microbial conversion of ammonium to nitrate, which further converts to gases of nitrogen gas and nitrous oxide in the soil. Similarly, urease inhibitors hinder the conversion of urea and urine to ammonium, which consequently converts to nitrate, in soils. Ammonium is positively charged and hence persists to a certain extent in soil, according to the cation exchange capacity (CEC) of soil. Nitrate, on the other hand, is negatively charged and soluble in soil (i.e., not retained by soil), and therefore, susceptible to leaching. (Abalos et al., 2014; Edmeades, 2004) Main nitrification inhibitors are Dicyandiamide (DCD) (Guardia et al., 2018) and 3,4-dimethylpyrazole phosphate (DMPP) (Kong et al., 2016). They reduce N loss through denitrification of nitrate. Main urease inhibitor is NBPT, N-(n-butyl) thiophosphoric triamide – trade name: Agrotain™, which reduces ammonium volatilization. (G. Liu et al., 2020)

Nutrients are broadly categorized as macro- and micronutrients. Macronutrients are used in substantial quantities by the plants. They are composed of (i) structural nutrients, (ii) primary nutrients, and (iii) secondary nutrients. Structural nutrients are carbon, hydrogen, and oxygen. Primary nutrients are nitrogen, phosphorous, and potassium. Lastly, secondary nutrients are calcium, magnesium, and sulfur. The main nutrients provided by mineral fertilizers are nitrogen, phosphorous, and potassium. They are commonly abbreviated according to their chemical symbols, NPK. Micronutrients, on the other hand, are used in much smaller quantities by the plants. These are iron, boron, copper, chloride, manganese, molybdenum, zinc, cobalt, and nickel. Together with macronutrients, the above-mentioned elements make up the 18 essential elements required for plant nutrition. (Cornell University Northeast Region Certified Crop Adviser (NRCCA) Study Resources, n.d.)

Fertilizers are essential for human nourishment. Nonetheless, their improper application can result in environmental issues such as water pollution. Due to inefficient application

methods and consequent environmental leaching, fertilizers are applied in excessive amounts. If applied inappropriately, excessive fertilizer use can disrupt the nutrient balance in the soil, mostly overloading it with nitrogen and phosphorus. Excessive nutrient concentrations damage soil microbial activity and beneficial organisms, thereby harming biodiversity. Fertilizer runoffs carry nutrients to water bodies, such as lakes and rivers, causing eutrophication, which depletes the oxygen levels in the water and causes damage to aquatic systems. (Rahman & Zhang, 2018) Fertilizer leaching also increases the pH of natural freshwater lakes. (Li et al., 2023) Moreover, excessive fertilizers also affect the water uptake capacity of plant roots. Elevated nutrient concentrations in the soil create an osmotic pressure difference between the soil and the plant root. This results in reduced water uptake.

1.5.3. Towards Sustainable Crop Protection

The challenges associated with crop protection by pesticide use includes limiting their loss to the environment, minimizing harm to non-target species, accurate delivery on pests, eliminating residues on harvest and thus reducing impact on human health, minimizing repeated applications, and ultimately using less pesticides. Other than developing less malign pesticide formulations, all these goals ultimately require the slow release and protection of active molecules from environmental factors, such as rainfall, UV, or high temperatures. Controlled pesticide release systems are promising solutions to involved challenges faced by crop protection.

In developed countries, the use of highly toxic pesticides (classified by WHO) is banned, whereas the lack of stringent regulations and awareness in developing and underdeveloped countries leads to the continued use of such pesticides. Moreover, EU continues to tighten its restrictions on maximum acceptable levels of pesticides residues on agricultural produce. Accordingly, producers seek for alternate ways to minimize their pesticide use. Government regulations are hence vital for a successful quest for sustainable agriculture.

Crop protection involves not only PPPs but also other strategies, such as crop rotation, biological control, resistant cultivars, and soil management. However, the use of PPPs is much more effective in decreasing crop yield losses and is also the subject of many

controversies, especially regarding biodiversity and possible environmental and health hazards.

The following table provides data for actual and potential yield losses for major crops. Potential losses represent the total percentage of crop loss in the case of no crop protection while the percentage loss without PPPs denotes an estimated loss in practices that exclude PPPs but include crop rotation, biological control, soil management, and resistant varieties. (OERKE, 2006; Savary et al., 2019)

Table 1: Effect of plant protection products on yield losses.

Crop	% losses with PPPs	% losses without PPPs (estimation)	% potential losses	Yield gain by PPPs
Wheat	21% (10.1-28.1)	40%	50%	19%
Rice	30% (24.6-40.9)	62%	77%	32%
Maize	22% (19.5-41.1)	55%	69%	33%
Potato	18% (8.1-21)	60%	75%	42%
Soybean	21% (11-32.4)	48%	60%	27%

PPP usage provides significant yield gains for all the major crops listed in the table above. Although the usage of PPPs has doubled since 1980, the development of synthetic PPPs has declined, and the number of biopesticides has increased. The increase in PPPs was largely due to the shift from broad spectrum PPPs to more specific PPPs, which only target specific pests and avoid non-target organisms. Strict regulation is a significant hurdle in developing new formulations. New PPPs are subject to extensive, science-based risk assessments. In fact, the average cost of such assessments per active substance is US$71 million, almost double their cost from 15 years ago. The evaluation of PPPs' toxic effects on humans and other organisms, strict control of their residues, and a safety factor of a 100 when determining their maximum allowed doses, allow for lower environmental impacts and fewer negative health effects. It can be concluded that PPPs are much safer than in the past if applied properly. (Bylemans et al., 2019)

The “Panel for the Future of Science and Technology”, which was sponsored by the European Parliament, determined that: “based on the required extensive risk assessments, plant protection products and their active ingredients are one of the best-studied and safest products worldwide.” (Bylemans et al., 2019) It is noteworthy that this conclusion was not reached in a report financed by a pesticide producer but by an in-depth intergovernmental research study. Due in large part to the oversimplified and one-sided messages circulating in the media, the public believes that chemical PPPs are, by definition, harmful to human health and the environment. Public opinion is similarly misinformed on organic farming and the overstated advantages of using natural PPPs. Poorly informed public opinion, in turn, has a strong influence on policymakers and can lead to poorly conceived strategies for addressing food demand.

The problem with most pesticides and fertilizers lies not so much in their chemical compositions but in how they are applied. Pesticides are lost to the environment due to runoffs and evaporation. Only a very small percentage of pesticides reach target insects. This value can be 0.03% or even lower for certain insecticides. (Pimentel & Burgess, 2012) Overall, 99.9% of pesticides do not kill pests. (Pimentel & Levitan, 1986) Moreover, up to 60% leach to a depth of 1 meter in the soil and groundwater, according to a more recent long-term study by the Danish Pesticide Leaching Assessment Programme. (Rosenbom et al., 2015) Pesticide leaching depends on soil type and irrigation, such that loamy or other permeable soils and flood irrigation accelerate leaching; this is one of the main causes of underground water pollution. The most effective solution for mitigating the harmful effects of pesticides is to apply PPPs when and where needed, which is suitable for both chemical pesticides and their bio-alternatives. This is where integrated smart pest detection and application systems can play a vital role, thanks especially to advancements in sensing and communication technologies.

Without preventive measures against pests, crop yields could diminish significantly, by up to 70%, depending on the type of plant. So even a mere 10% more effective protection against pests would result in 10% more produce from the same lands. However, the widespread and indiscriminate use of pesticides results in environmental pollution.

Yet the use of pesticides comes with a hefty price tag. Due to their excessive and indiscriminate use, pesticides are a major source of environmental pollution. Therefore, the real challenge in this quest to feed more people is to fight with pests effectively and in a sustainable manner. In other words, to make sure pesticides remain where there is a potential pest threat for the maximum amount of time, by minimizing their loss to environment, and consequently using less of them.

Achieving sustainable pesticide use involves several measures, such as reducing environmental contamination, minimizing harm to non-target species, precise targeting of pests, preventing residue accumulation on harvested crops to safeguard human health, minimizing the need for repeated applications, and ultimately reducing overall pesticide usage. To address these challenges, the development of less harmful pesticide formulations is important. Additionally, controlled release systems for pesticides offer promising solutions by ensuring slow and targeted release of active molecules, protecting them from environmental factors like rainfall, UV radiation, and high temperatures. These systems aim to minimize pollution, health risks, labor requirements, and costs associated with crop protection.

1.5.4. How to Reduce Chemical PPP Usage

One fruitful strategy for the reduction of PPP use is precision farming. In precision farming, remote sensing equipment is used to detect pests, artificial intelligence algorithms are developed to foresee potential threats to crops, and the farmer is advised to where to apply the necessary PPP and in what dose. This integrated strategy can allow farmers to combat pests in a much more effective way and significantly reduce the use of PPPs. Furthermore, moisture sensors, weather forecasts, and nutrient sensors can recommend an optimum irrigation and fertigation schedule for farmers. An ideal application of water and nutrients helps reduce the vulnerability of plants to pests and thus reduces the need for PPPs.

The use of resistant cultivars can also reduce PPP usage significantly. For most crops, there are many cultivars and varieties that are resistant to certain pests and diseases. A major reason why current crops are vulnerable to most pests lies in traditional

domestication strategies. In these breeding programs, easy harvest, high yield, and low toxicity traits were selectively improved. Since PPPs became available to combat pests, traits that protect plants from biotic stress have not been prioritized. Current breeding programs prioritize the identification and selection of resistance genes, which are mostly preserved in wild cultivars. For this strategy to be successful, traits important for food quality and yield need to be preserved, while original plant survival traits are re-introduced. Insect resistant crops (GMIR) have shown to be very successful in reducing PPP usage. For example, in 2016, GMIR cotton and maize respectively allowed for a 56% and 82% reduction in PPPs compared to their non-GMO versions. (Brookes & Barfoot, 2018)

Although crop production without PPPs is unrealistic, reductions in usage are possible, some with acceptable yield losses. PPP reduction is currently possible for cases of high use, but not so much for those that are already low use. However, the major obstacle here is the financial risk for the grower, which can be subsidized by incentive programs.

By their nature, PPPs have negative impacts on biodiversity since their aim is to kill unwanted plants and pests. From this perspective, one might think that organic farming with no synthetic PPPs would be better for biodiversity. Unfortunately, the solution is not that simple. Organic farming, on average, is 25% less productive than conventional farming. (Seufert et al., 2012) Thus, to produce the same amount of food, more farmland is needed. Having more farmlands requires deforestation, which is detrimental to biodiversity, greatly outweighing the negative effects of PPPs.

Using natural products for pest protection would only be meaningful with regards to sustainability if they can provide a similar reduction in yield losses compared to their chemical alternatives. This way, since the yield per area of land will be conserved, biodiversity will improve as there will be no increase in land use. Natural PPPs, or biopesticides, can be of plant, microbial, or mineral origin, or comprise living micro-organisms, such as nematodes that feed on pest insects. Unlike their chemical alternatives, biopesticides are harmless to non-target organisms. However, since these natural PPPs are more expensive than traditional PPPs, farmers would be hesitant to make the switch if they are not incentivized to use higher cost natural PPPs, and if they do not achieve crop yields similar to the levels obtained through traditional crop protection.

1.5.5. Controlled Release Systems

Controlled release systems (CRS) have been extensively studied and developed in the biomedical field over the past 70 years. However, due to stringent regulations, their clinical applications have been limited. In contrast, the agricultural sector, with less stringent regulations, has recognized the potential of CRS for sustainable agriculture. CRS involves the permeation-driven relocation of an active ingredient from its entrapped compartments to a targeted surface, with the aim of maintaining a predetermined concentration level for a specific period.

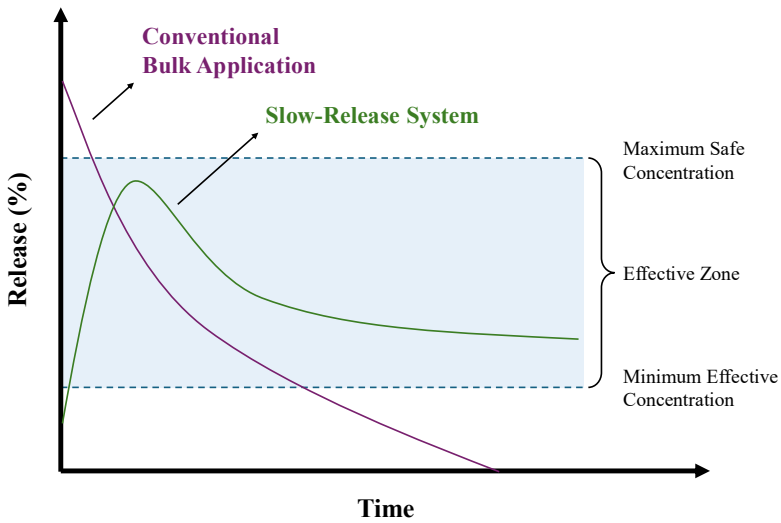

Figure 1: Release Mechanisms of Conventional (Bulk) vs Controlled Release Systems.

The main issue with conventional pesticides and fertilizers lies in their application methods, which often result in significant loss to the environment. Factors such as leaching and volatilization contribute to the low efficiency of these products, with only a small percentage reaching the target pests. This inefficiency not only wastes resources but also contributes to environmental pollution, particularly through leaching into groundwater. The ideal solution lies in applying pesticides and fertilizers when and where they are needed, regardless of whether they are chemical or bio-based.

To address the challenges associated with pesticide use in crop protection, controlled release systems offer promising solutions. These systems aim to limit the loss of active molecules to the environment, minimize harm to non-target species, accurately deliver the pesticides to pests, eliminate residues on harvested crops to reduce human health risks,

minimize repeated applications, and ultimately reduce overall pesticide usage. By using controlled release systems, the slow release and protection of active molecules from environmental factors such as rainfall, UV radiation, and high temperatures can be achieved. This approach not only prolongs the effectiveness of pesticides but also significantly reduces environmental contamination. Additionally, insoluble active ingredients can be transformed into more readily dispersed formulations.

The thermodynamics of biocide delivery from CRS depend on the complex interactions between carrier materials, biocides, and the environment. The architecture and morphology of carrier materials play a crucial role in determining the release kinetics. Furthermore, environmental factors such as temperature, soil humidity, and salinity can influence the performance of CRS.

1.6. Integration of Water Management and Efficient PPP and Nutrient Use

Climate change causes extended drought periods, which results in significant crop losses. Most farms rely solely on rainwater and irrigated lands are mostly watered by manual irrigation. Fertilizer and pesticide run-offs are triggered by heavy rainfalls and manual irrigation. To address these problems, superabsorbent polymers (SAP) can be used as underground soil water reservoirs. Upon rain or irrigation, SAPs swell with water and release this water when their surroundings start to dry, to regulate water delivery to plants. Currently, SAPs are primarily used as water reservoirs in agriculture without the addition of pesticides or nutrients. However, SAPs can further be incorporated with fertilizers or pesticides. This allows them to act both as a water and fertilizer or pesticide reservoir. Moreover, fertilizer and pesticide run-offs can be alleviated by this approach.

While efficient water delivery methods are available, their widespread adoption is hindered by various factors in developing nations. Consequently, flood irrigation remains the dominant technique globally, despite its inefficiencies. To address the water needs of crops in regions with irregular rainfall and limited water supply, superabsorbent polymers (SAPs) offer a realistic and practical solution. By absorbing and releasing moisture, SAPs

enhance the water retention capacity of the soil, providing plants with access to water for extended periods. The granular form of SAPs enables their application using existing equipment developed for fertilizers or seeds, making them compatible with current farming practices.

One of the major drawbacks of conventional fertilizers is their tendency to readily leach into the environment. Since fertilizers readily dissolve in water, they do not stay near the root area of plants for a long time and reach lower levels of the soil. Also, due to climatic conditions, such as strong winds, they can easily be carried away to other parts of the field. So, with their current application method, fertilizer leaching into the unwanted parts of the field is inevitable. In fact, the utilization efficiencies of urea and phosphorus fertilizers are between 30-40% and 15-25%, respectively. (Sarkar & Datta, 2014) This problem is also highly common among pesticides. In fact, up to 60% of plant protection products leach into the environment (Rosenbom et al., 2015), and often, more than 99% do not affect pests. (Pimentel & Burgess, 2012; Pimentel & Levitan, 1986)

In addition to improving water management in soil, SAPs can enhance the use efficiency of fertilizers. SAPs absorb water from the soil that already contains dissolved nutrients from conventional fertilizer applications. Hence, they retain dissolved nutrients near the root area of the plants for a longer time and impede nutrient leaching to the environment. In fact, studies have demonstrated that SAPs increase fertilizer retention in soil and reduce nutrient leaching.

In this context, a superabsorbent polymer composite incorporated with mineral nutrients can enhance both fertilizer and water use efficiency in agriculture. SAPs can be loaded with fertilizers to serve as slow-release nutrient carriers and enhance nutrient availability to plant roots. (Cheng et al., 2018) Integrating nutrients into SAPs provides controlled release and improved use efficiency. The controlled release of fertilizers from SAPs can promote plant germination, root biomass, and above-ground biomass.

Encapsulation techniques have been developed to improve fertilizer utilization, ensuring controlled release, and minimizing nutrient loss. (Guo et al., 2005) Carrier materials, such as halloysite nanotubes, can be also used to load nutrients. The loaded carrier materials can be integrated in the SAP structure during synthesis, to achieve a nanocomposite

structure. However, the fraction of these filler materials in the SAP structure is limited, usually around 5-10 wt%. Also, the nutrient loading efficiency on these carrier materials is minimal. However, nanocomposite superabsorbent polymers have improved mechanical properties. The improved mechanical properties improve their water absorption capacity under load and prolong their water retention.

In a facile approach, nutrients can also be integrated in the SAP structure by directly mixing the SAP solutions after polymerization, with fertilizer solutions. Upon thorough stirring, the mixture is dried, and a homogeneous product is achieved. In this method, it is possible to obtain SAP composites with approximately 30 wt% fertilizer content without compromising their water absorption capacities when compared to commercial SAPs. In another simple approach, SAPs can be allowed to swell in a nutrient solution, thereby incorporating nutrients in its structure. These swollen SAP gels can be applied as-is, as well as upon drying.

In the literature, there are studies that report composite SAPs incorporating fertilizers. One interesting study reports the use of a combination of various micro- and macronutrients. (Tubert et al., 2018) However, in almost all these studies, macronutrients are utilized, such as urea, NPK, and DAP. (Ahmed Khan et al., 2020; Qiao et al., 2016; Sarkar et al., 2015; Xiao et al., 2017) There are hardly any studies on SAPs incorporated with nutrients that are applied at smaller doses, such as micronutrients. Fertilizers are incorporated in SAPs at varying doses throughout these studies, although most papers only report one or a few similar fertilizer:SAP ratios. (Joshi et al., 2020; Sarmah & Karak, 2020; W. Wang et al., 2020; Zhan et al., 2004; Zhang et al., 2017) Also, the water absorption performances of these composite SAPs are generally inferior compared to commercial SAPs.

Moreover, most studies integrate fertilizers in SAPs by allowing them to swell in fertilizer-rich solutions. This approach requires additional processing steps of swelling and drying. Our work contributes to the literature on fertilizer-SAPs, to create new knowledge on zinc sulfate and calcium nitrate-incorporated SAPs. Furthermore, in our study, the fertilizers are integrated into the SAP structure after polymer synthesis, before drying. This eliminates the need for additional swelling and drying steps.

Globally, the average fertilizer application dose per hectare is 140 kg (Food and Agriculture Organization, 2021), of which urea and NPK are the major constituents. In comparison, the suggested SAP application is 15-45 kg/ha. (Mao et al., 2011; Y. Yang et al., 2022) The highest fertilizer incorporation in SAP reported in the literature is approximately 60 wt%, which significantly deteriorates water absorption and renders them impractical for agricultural applications. (Mulyani et al., 2021) Therefore, even with a very high loading ratio, fertilizer loaded SAP composites would not be enough to supply the macronutrient needs (urea, NPK, or DAP) of agricultural soils.

On the other hand, calcium and zinc fertilizers are applied at much lower doses compared to urea and NPK. Considering SAPs are applied at a dose of 15-45 kg/ha, applying zinc- and calcium-SAPs can satisfy the nutrient needs of the soil. A single application of fertilizer incorporating composite SAPs can supply the majority of the calcium and zinc requirement, thereby eliminating the need for respective nutrient applications. Therefore, our aim in this study has been to develop Ca and Zn-SAP composites.

To maximize their uptake by the plants, and to limit their loss to the environment, we integrated zinc and calcium fertilizers in nanocomposite superabsorbent polymers. By applying fertilizer-containing SAP composites near the root area of the plants, nutrients can be made readily available for plant uptake. Also, the dissolution and leaching of fertilizers into the soil will be delayed owed to SAPs, which will act as a host matrix for these nutrients.

Similar to the above-mentioned mechanism involving fertilizers, SAPs can enhance the effectiveness of pesticides. SAPs can soak up water that contains plant protection products, which are already present in the soil due to the application of conventional pesticides. Consequently, the SAPs can retain these dissolved pesticides in the vicinity of the plant roots for an extended duration, limiting their runoff into the environment.

Furthermore, SAPs can be utilized as delivery matrices for the controlled or sustained release of plant protection products, addressing the issue of excessive pesticide use in agriculture. Compared to virgin pesticides, those integrated into SAPs exhibit slower release, leading to enhanced plant uptake. Hence, SAPs can help improve pesticide

efficiency and minimize environmental and health risks associated with pesticide residue in the soil and crops. (B. Singh et al., 2009, 2015)

Different carrier materials can be loaded with active agents, such as pesticides. For example, halloysite nanotubes can be loaded with a variety of pesticides, including fungicides and herbicides. (X. Jin et al., 2019; Zeng et al., 2019) However, these loaded HNTs are not suitable for the field as-is since they are in a powder form and can quickly become airborne. Thus, to be applied to the field, HNTs need a delivery matrix to host them for a certain time. SAPs are the perfect delivery matrices to host carrier materials such as HNTs.

SAPs can also be incorporated directly with pesticides, without the need for carrier materials. In the first method, SAP solutions after polymerization can be directly mixed with pesticide solutions. When this mixture is dried, a homogeneous product is achieved. In the second simple approach, SAPs can be allowed to swell in a pesticide. Loaded or pristine carrier materials, such as HNTs, can also be utilized in the SAP syntheses, to act as nanofillers, to impart mechanical strengthening to the polymer network. With these approaches, a higher pesticide incorporation in SAPs can be achieved.

Superabsorbent polymers offer promising approaches for increasing fertilizer, pesticide, and water use efficiency in agriculture. By serving as water reservoirs, SAPs enhance soil water retention capacity, prolonging plant access to moisture and improving overall crop health. Incorporating mineral nutrients or pesticides into SAPs enables their controlled release and prevents nutrient and pesticide leaching, reducing environmental impacts and enhancing their use efficiencies.

By implementing SAP-based solutions, we can foster sustainable agricultural practices, optimize resource utilization, and mitigate environmental challenges associated with conventional fertilizer and pesticide applications.

This work can be advanced further by studying the incorporation of other micronutrients and plant protection products in SAPs. Nutrients or active agents that need to be applied at small doses can be incorporated into SAPs, which would also reduce labor for their isolated applications.

1.7. Bio-Based Superabsorbent Polymers

Currently, most commercially available superabsorbent polymers (SAPs) are fully synthetic and primarily composed of acrylic acid and/or acrylamide, which exhibit limited biodegradability. In fact, poly-acrylic acid sodium salt is the most widely used SAP worldwide. Acrylate-based SAPs possess excellent water-absorption properties due to their high molecular weight and cross-linked structure. However, these characteristics also make them challenging to biodegrade. Polyacrylate-based SAPs have very limited biodegradabilities. (Braun et al., 2021)

To improve the sustainability of SAPs and to render them biodegradable for optimum soil health, numerous studies in the literature have focused on synthesizing bio-based SAPs from bio-based and/or biodegradable starting materials. (Arredondo Ramirez, 2022; Djafari Petroudy et al., 2018; Fujita et al., 2022; Zhu et al., 2020)

Cellulose is a perfect choice to be used as a natural polymer to produce bio-based superabsorbent polymers. It is a hydrophilic polymer; and being the most abundant natural compound derived from biomass, cellulose is highly sustainable and has excellent biodegradability. (Bao et al., 2011) In the literature, there are various studies on bio-based SAPs that incorporate cellulose in their structure. Although mostly carboxymethyl cellulose is used in such work (Klinpituksa & Kosaiyakanon, 2017; Shen et al., 2018), there are reports on SAPs based on nanocellulose (Barajas-Ledesma et al., 2022), carboxylated nanocellulose (Barajas-Ledesma et al., 2022), alpha-cellulose (Fu et al., 2022), corn straw cellulose (W. Wang et al., 2020), and bacterial cellulose (Chaiyasat et al., 2019). In these works, the studied formulations either contain very small amounts of cellulose and have good water absorption, or they are almost entirely bio-based, but with inferior water absorption, which is not suitable for agriculture.

Our aim in this study was to develop SAP formulations using sustainable raw materials and to minimize polymer contamination in agricultural lands due to their use. To impart sustainability and biodegradability to commercial SAPs that are polyacrylate-based and fully synthetic, we developed bio-based SAPs. To do so, we have used carboxymethyl cellulose (CMC), which is hydrophilic, highly sustainable, and has excellent

biodegradability. In the literature, there exist studies on cellulose-based SAPs. However, the studied SAPs either contain minimal cellulose and have good water absorption, or they are almost entirely bio-based but have inferior water absorption that is not suitable for agriculture. In the literature, there is a large gap in the range of bio-based material concentrations within the SAP structure.

Specifically, there is a lack of papers studying bio-based SAPs with 25 to 70 wt% cellulose contents. In terms of sustainability, a bio-based SAP with a cellulose content in this range, and a water absorption capacity comparable to synthetic, commercial SAPs, would be the optimum solution for agricultural applications.

In this study, a bio-based material, 5 wt% to 60 wt% carboxymethyl cellulose, was incorporated in an otherwise polyacrylate-based synthetic SAP formulation described in the patent TR202002652A, “A polymer matrix based superabsorbent material” (M. S. Seven et al., 2020), to improve its biodegradability, while maintaining, and even improving its water absorption characteristics. 7 different bio-based SAPs were synthesized, containing 5 to 60 wt% CMC. Their water and saline absorption capacities, water retention performances, and biodegradability are discussed in this study, along with their surface morphologies. We aim to provide new knowledge on the properties and performance of CMC-based SAPs belonging to such a wide range of bio-material incorporations. This work will impact the field of agricultural science and technology because it provides insight into the suitability of bio-based SAPs to be used in agriculture.

Chapter 2

LITERATURE REVIEW

2.1. Superabsorbent Polymers

The first commercially available superabsorbent polymer (SAP) was produced in 1970 through the alkaline hydrolysis of starch-g-polyacrylonitrile. It had the ability to absorb up to 500 g/g of water but exhibited mechanical weakness when swollen. Presently, synthetic SAPs have advanced and can absorb up to 2000 g/g of water. The SAP market is primarily dominated by two monomers: acrylic acid and acrylamide. (Kabiri et al., 2011)

Superabsorbent polymers (SAPs) are hydrogels lightly crosslinked to form a network. They have found applications as underground water reservoirs in agriculture. SAPs are strategically placed near plant roots, such as during seeding or encircling mature trees. By swelling with water to more than 100 times their own weight, SAPs slowly release water, effectively regulating water delivery to plants. (Al-Jabari et al., 2019; Elshafie & Camele, 2021) This prolonged proximity of water to plant roots enables enhanced water uptake, resulting in increased biomass and yield. To date, SAPs have primarily been used solely as water reservoirs without the addition of nutrients, particularly micro-nutrients or pesticides. (Bao et al., 2011; Tang et al., 2019)

In addition to absorption capacity, gel strength is a critical parameter in agriculture as it determines absorption under load, specifically in soil. Gel strength of SAPs can be enhanced by increasing crosslinking density and incorporating inorganic micro- or nanoparticles. Consequently, substantial research has been conducted over the past two decades on particulate composites of hydrogels. Natural aluminosilicate inorganic compounds, especially clays, have emerged as popular choices for the preparation of SAP nanocomposites. For instance, extensive studies have focused on kaolin, montmorillonite, and halloysite nanotube nanofillers in superabsorbent polymers. (Kabiri et al., 2011)

Solution polymerization stands as the most convenient method for nanocomposite SAP preparation. In this approach, clay is dispersed in the monomer solution prior to polymerization. Bulk polymerization, on the other hand, is a straightforward technique that involves only monomer, monomer-soluble initiators, and crosslinkers. (Kiatkamjornwong, 2007)

Satriani et al. investigated the impact of a biodegradable cellulose-based superabsorbent polymer in the cultivation of bean crops (Phaseolus vulgaris L.) in water-scarce fields. Field tests were carried out in the Mediterranean region during summer seasons. The surrounding soil was mixed with SAP at a depth of 10 cm. In the first treatment (A), the soil was irrigated to meet 100% of the crop's evapotranspiration (ETc) demand without the addition of SAP. In treatment B, the soil was irrigated to 70% of ETc demand and treated with 5 grams of SAP. In the final treatment, irrigation was reduced to 50% of ETc demand, and 10 grams of SAP was mixed with the soil. Although the maximum dry grain yield was observed when the soil was irrigated to meet 100% of ETc demand, as expected, the inclusion of SAP successfully conserved irrigation water. Notably, even with reduced irrigation, SAP-treated soils maintained at least 90% of crop production. In fact, irrigation water use efficiency and agricultural water productivity index were significantly higher for SAP-treated soils compared to soils irrigated to 100% of ETc demand. (Satriani et al., 2018)

2.1.1. Improving Mechanical Properties of SAPs with HNTs

Halloysite nanotubes can be utilized as strengthening fillers in nanocomposite superabsorbent polymer systems. HNT can improve the strength of the SAP structure by imparting additional physical crosslinking. There is limited and conflicting information available in the literature regarding the Young's modulus of HNTs. Additionally, thorough analyses of the impact of HNTs on the mechanical properties of polymer nanocomposite systems are scarce.

In an article published in Nature, Zare and Rhee developed a model to determine the Young's modulus of HNTs in polymer-HNT nanocomposites. They extended the advanced Takayanagi equation by incorporating interphase zones surrounding the dispersed and networked HNTs above the percolation onset threshold. Through their calculations, they derived the Young's modulus of HNTs as 140 GPa. Furthermore, their model provided insights into how the geometry, volume fraction, and interphase depth of HNTs influence their strengthening properties. For example, the study revealed that HNTs do not contribute to strengthening polymer matrices until their volume fraction reaches 1% or when the interphase depth is less than 5 nm. Another valuable finding of this study was that composite systems were reinforced by slender and elongated HNTs rather than thick and short ones. (Zare & Rhee, 2022a)

2.2. Efficient Use of Plant Protection Products (PPP) and Nutrients

In the literature, several studies have investigated the use of sustained delivery systems for various biocides, such as herbicides (Tan et al., 2015; Zeng et al., 2019), fungicides, acaricides, salicylates, nutrients, and growth hormones, in applications related to crop and wood protection, as well as active food packaging (Ghezzi et al., 2018; Santos et al., 2018). Surface modification of carrier materials plays a critical role in tailoring their properties, including the introduction of functional groups to enhance loading capabilities, improve stability of nanoparticles, and impart desired electrical, thermal, and antibacterial characteristics. (Massaro, Campofelice, et al., 2018; Tharmavaram et al., 2018; Yamina et al., 2018; Y. Yang et al., 2017; Yuan et al., 2008)

Various techniques have been employed in the literature to load pesticides onto carrier materials. One straightforward method involves mixing pesticides with carrier materials dispersed in water and stirring the mixture for 2 to 24 hours. Subsequently, the mixture is centrifuged or filtered to remove any unentrapped pesticides, followed by washing with deionized water or other solvents to eliminate residual chemicals. (Zhao et al., 2020; Zou et al., 2018)

Another technique used for pesticide loading is emulsification-solvent evaporation. For instance, in a study by Y. Wang et al. (2020), a mixture of PLA-GOs (graphene oxides) and the fungicide pyraclostrobin was dissolved in an organic solvent to form the organic phase. Aqueous phase composed of PVA-1788 (1% w/v) was used, and the organic phase was added to the aqueous phase under high-speed shearing to generate an oil-in-water emulsion. The emulsion was stirred until the solvent completely evaporated, after which the resulting product was centrifuged, washed with methanol, and dried in a desiccator. (Y. Wang et al., 2020)

Emulsion crosslinking is another technique employed to load pesticides onto nanocarriers. Patel et al. (2018) utilized this method to load the broad-spectrum insecticide cypermethrin onto calcium alginate nanocarriers. In this approach, a stable emulsion was formed by mixing paraffin oil with sodium alginate dissolved in water. The emulsion was continuously stirred while calcium chloride solution and cypermethrin were added, leading to the formation of cypermethrin-loaded calcium alginate nanocarriers through crosslinking of the alginate with Ca2+ ions. The loaded carriers were subsequently precipitated, filtered, and washed with water and acetone to remove any unloaded chemicals and paraffin oil. (Patel et al., 2018)

Additionally, pesticides have been directly loaded onto nanocomposite superabsorbent polymers (SAPs) by allowing the SAPs to swell in a solution containing the desired pesticides, followed by freeze drying. The concentration of the pesticide in the solution before and after swelling is compared to determine the pesticide loading. (He et al., 2019)

The fundamental objectives of controlled release systems (CRS) are to provide sustained release of active molecules for a specific duration, maintain effective dosages, and target pests accordingly. These carrier systems serve a dual purpose by gradually releasing

active molecules through desorption from the carrier's surface and/or diffusion through its matrix, while also acting as protective barriers against drifting, leaching, and pesticide degradation. By minimizing pesticide loss and keeping them localized at the intended site of action, CRS prolong the efficacy of pesticides, reduce environmental contamination, and significantly decrease the amount of pesticide application per unit area.

The release kinetics of CRS are determined by the competitive interactions among the carrier, pesticide molecules, and the surrounding environment. Achieving the desired sustained release of pesticides relies on maintaining an appropriate balance in these interactions. The architecture and morphology of carrier materials play a crucial role in release kinetics. Furthermore, environmental factors such as temperature, soil humidity, and salinity can influence the performance of CRS. While we can manipulate carrier-pesticide and carrier-water interactions, it is essential to carefully select carrier materials that strike the optimal balance between water and pesticide interactions. This can be achieved by designing carriers with high chemical affinity for the pesticide molecules, such as those bonded through strong covalent bonds that require more energy for dissolution compared to weak hydrogen bonds. Alternatively, tuning carrier-water interactions through surface chemical group modifications can enhance the dissolution and diffusion of pesticide molecules, resulting in increased release rates. The selection of materials is crucial to achieve the desired balance between water and pesticide interactions with the carrier. (Mattos, Tardy, et al., 2017)

Mass transport mechanisms during pesticide release are primarily attributed to the architecture of carrier material. Nanostructures are among the most promising for controlled release. Materials in the nanometer scale exhibit high surface area to mass ratio, which means more active sites for active molecule adsorption. Some controlled release systems with such structures are aerogels, mesoporous structures, tubules, fractal-like structures, platelets, and spheroids.

CRS can be classified most broadly in terms of constant or variable pesticide release activity; namely as core-shell and matrix systems. In a core-shell arrangement, active molecule and carrier are separated, which results in a temporal lag in release. The shell, carrier material, surrounds the active molecule, thus the release to the environment will not commence until the time has passed necessary for the active molecule to diffuse

through the shell, and the pesticide activity here can be described as variable. In contrast, matrix systems are characterized by the homogeneous distribution of active molecules and carrier material. There are as many active molecules on the surfaces of the system as there are in the bulk. Thus, matrix systems enable an initial burst dispatch of pesticides from its surfaces and an extended delivery governed by diffusive mass transfer (according to the strength of carrier-pesticide interactions), hence achieving a constant pesticide activity. Moreover, carrier systems can be designed to be prone to microbiological decomposition or chemical degradation, which enable a prolonged release.

A narrower classification of carrier architectures can be made according to their shapes: slabs (films, lamellae structures), cylinders (nanofibers, nanotubes) or spheres (micro/mesoporous inorganic particles, polymeric capsules, carbohydrate beads).

Carriers can also be categorized according to their material origins, natural or synthetic, and whether they are biodegradable or not. Cellulose, lignin, alginates, chitin, and starch are bio-based, biodegradable represent sustainable carrier material alternatives. Biogenic silica, halloysite, kaolin, are other alternative carrier materials obtained from natural resources; however, they are not biodegradable. Carbon nanotubes, polymers, mesoporous silica are examples of synthetic alternatives.

Various simultaneous mechanisms determine the release kinetics of CRS, which depend on physical and chemical properties of carrier material. Such mechanisms comprise surface wetting, water penetration, diffusion through carrier, phase transitions, pore closing or opening upon swelling, chemical interactions, crack generations, and changes in the geometry. The interplay between these phenomena regulates the release behaviour of CRS.

In the biomedical field, controlled release systems are designed with similar carrier materials and loading techniques. (Pierchala et al., 2018; Yamina et al., 2018; Zargarian et al., 2015) For example, in a 2018 study by Massaro et al., halloysite nanotubes were used to load insulin. Loaded nanotubes were incorporated into a chitosan matrix to prepare a bio-nanocomposite film to be used for transdermal delivery. (Massaro, Cavallaro, et al., 2018) In another study from the same research group, halloysite

nanotubes were functionalized with cyclodextrin moieties, which were later loaded with clotrimazole, an anti-fungal drug. (Massaro, Campofelice, et al., 2018)

In conclusion, controlled release systems for pesticides and biomedical applications rely on the proper selection of carrier materials, surface modification, and loading techniques. The interactions between carrier materials, pesticide molecules, and the surrounding environment determine the release kinetics, with the architecture and morphology of the carriers playing a crucial role. By understanding these mechanisms, it is possible to design effective CRS that prolong pesticide efficacy, reduce environmental contamination, and achieve sustained release of active molecules.

2.2.1. Natural Carriers

Chemical and physical heterogeneity of natural resources is the major shortcoming of their utilization as pesticide carrier materials.

2.2.1.2. Lignin

Lignin-based pesticide carriers have been reported more than two decades ago. Owed to its aromatic nature, it acts as an excellent protective matrix for pesticides, which are sensitive to degradation by sunlight. Antioxidant nature of lignin imparts stability to chemically unstable pesticides. General method for loading lignin with active ingredients is simple. Dry lignin powder is mixed with saturated pesticide solutions. The mixture is later dried and granulated. Some CRS based on lignin were reported to be effective for more than 7 weeks. (Dellicolli, 1977)

In one study, granules of lignin, PEG, and pesticide chloridazon were coated with varying amounts of ethyl cellulose to obtain different shell thicknesses. At optimum conditions, these granules released the entire pesticide in 800 hours. (Fernández-Pérez et al., 2011) In another promising study, lignin-Diuron pesticide coprecipitates were produced via vigorous stirring in their non-solvent, hence a nano-suspension was obtained. This

formulation achieved an impressively slow release – 80% after 120 days. (Yearla & Padmasree, 2016)

2.2.1.3. Cellulose

Cellulose has high affinity towards water, which enhances the release of pesticides impregnated in cellulose-based CRS. However, this water uptake can also impoverish the mechanical strength of cellulose structures. To alleviate this impact on structural integrity, cellulosic nanostructures, such as nanocrystals and nanofibrils can be utilized. (Mattos, Tardy, et al., 2017)

One group added thymol in the cellulose matrix through supercritical impregnation at 10 MPa and 35 C. The resultant CRS achieved pesticide release for over 4000 minutes. (Milovanovic et al., 2016) In another study, microcrystalline cellulose was used to prepare cross-linked structures for UV protection, in addition to controlling their release. (Pang et al., 2016) Moreover, cellulose nanofibrils were combined with biogenic silica to synthesize nanocomposites for tebuconazole sustained release. A slower release was achieved with the nanocomposite compared to silica alone – 30-45% release after 15 days, compared to 95%. (Mattos & Magalhães, 2016)

2.2.1.4. Inorganic carriers

Nanoparticles of biogenic silica can be obtained from Equisetum arvense and utilized as carrier material for an eco-friendly pesticide comprising neem bark extract cross-linked with polycarboxylic acids. Such formulations released 60-75% of active molecules in 30 days. (Mattos, Rojas, et al., 2017)

Halloysite nanotubes (HNT) are naturally occurring aluminosilicate nanotubes which can successfully be used as pesticide carriers in CRS. One such application is the loading of deltamethrin insecticide into HNT through vacuum suction; and subsequent impregnation of these loaded HNT into LLDPE to be used as greenhouse films. These films exhibited

active agent release for 60 days. (S. A. Seven et al., 2019) In another study, polysaccharides, starch and alginate, and clays, kaolin and bentonite, were incorporated to form beads. The above-mentioned ingredients and pesticide thiram were dispersed in hot water to obtain a homogenous mixture. Then, the mixture was added slowly into a 0.1 M CaCl2 solution; hence forming beads. Pesticide entrapment efficiency was 97%, and higher clay content tended to delay release. (B. Singh et al., 2009)

2.2.2. Structure and Properties of Halloysite Nanotubes

In this study, halloysite nanotubes (HNT) were employed as carrier materials. HNT is an aluminosilicate clay characterized by its submicron hollow tubular structure, composed of alternating bilayers of aluminum and silicon oxides. The external surfaces of HNT predominantly have siloxane groups (-Si-O-Si-), along with aluminol (-Al-OH) and silanol (-Si-OH) groups, while its inner lumen exclusively consists of aluminol groups. (Gianni et al., 2023; Heidari Pebdani, 2023)

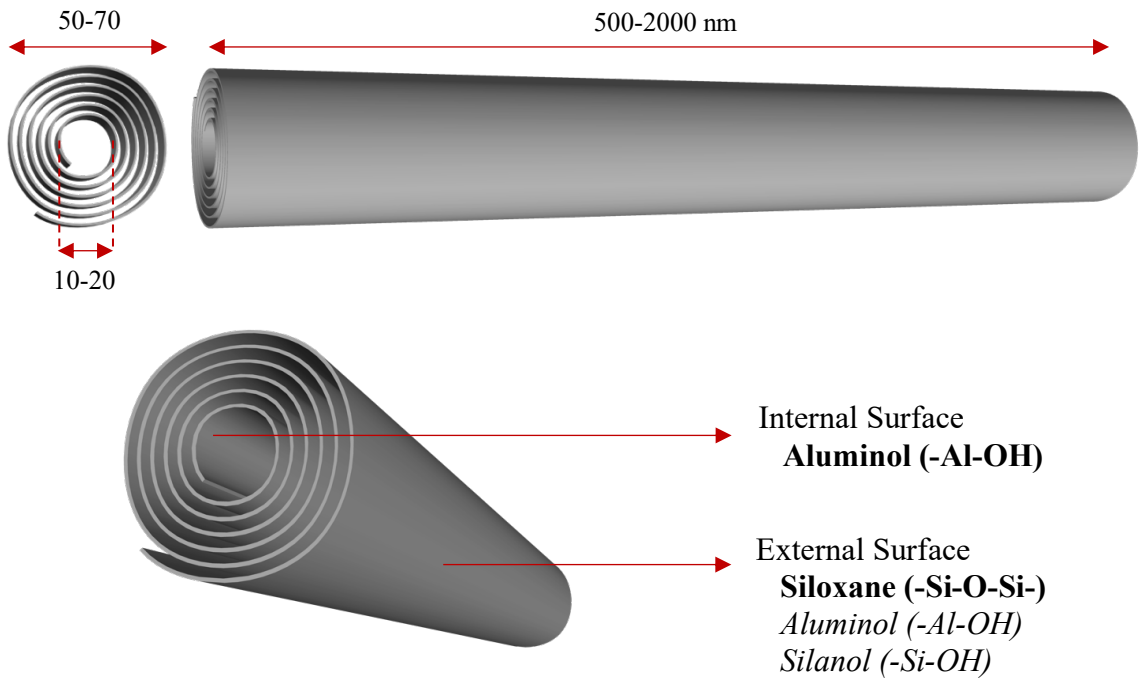

Figure 2: Structure of Halloysite Nanotubes

The unique spiraling structure of HNT comprises alternating layers of SiO_4 tetrahedra and AlO_6 octahedra, typically intercalated with a weakly held monolayer of water. Although the chemical composition of HNT shares similarities with nanoclays, its

structural characteristics closely resemble those of carbon nanotubes (CNT), particularly multi-walled carbon nanotubes (MWCNT). Due to its tubular form and micron-scale length, HNT imparts novel capabilities to nanocomposite systems. As a nanofiller, HNT is utilized to enhance mechanical and thermal properties while improving non-flammability characteristics. Key attributes such as nano-scale size, high surface area, and high length-to-diameter ratio make HNT a suitable choice for modifying polymer properties with low nanofiller content. (Dantas de Oliveira & Augusto Gonçalves Beatrice, 2019)

The distinctive structural composition of HNT leads to different electrical zeta-potentials on its various surfaces. The outermost surface bears a negative charge, while the inner lumen carries a positive charge. This feature allows for easy functionalization of HNT with different chemicals on both the inner and outer surfaces. Active agents can be loaded on both the surface of the HNT and on its inner lumen, with or without surface functionalization.

HNT is sourced from nature and has significant reserves in Turkey. It is a cost-effective and abundant material. Its biocompatibility enables its use as a drug carrier even within the human body, a concept first explored in 2000. (R. Price, 2001) Consequently, research in this area remains relatively new.

Given its natural origin, the mechanical properties of HNT are challenging to precisely define and vary depending on the geometry. In the literature, Young's modulus of HNT is commonly reported to be up to 300 GPa. (Heidari Pebdani, 2023) In a study by Song et. al., halloysite’s tensile modulus is reported as 600 GPa. (K. Song, 2017) Such a high modulus enables HNT to be used extensively as a strengthening nanofiller in polymer nanocomposite systems. (Tu et al., 2013)

2.2.3. Active Agent Incorporation on HNT

2.2.3.1. Pesticide Loading on HNT

A vacuum suction method was employed as a simple yet efficient approach for loading active agents onto Halloysite Nanotubes (HNTs). Initial trials involved the use of different fungicides, namely propiconazole, imidazole, guazatine, and imazalil.

2.2.3.2. Uridine loading on HNT

Uridine is crucial type of pyrimidine nucleoside, which plays a significant role in brain function. It is linked to nucleotides through a phosphate group, contributing to the synthesis of DNA, RNA, membrane components, and glycosylation processes. (Dobolyi et al., 2011) Besides its importance in the brain, uridine can also find applications in agriculture to enhance plant tolerance against various biotic and abiotic stress factors. Biotic stress encompasses challenges posed by pathogens, microorganisms, weeds, insects, and similar entities, while abiotic stress includes environmental factors such as temperature, drought, radiation, salinity, nutrient availability, light exposure, mechanical impacts (e.g., floods, wind, snow, ice), air pollution, and toxins. (Cansev et al., 2014)

A joint project was initiated with professors Asuman Cansev and Mehmet Cansev from Uludağ University in Bursa, who are two of the investors of the EU patent EP 2 967 061 B1, which relates to the "Use of Uridine for Enhancement of Plant Stress Tolerance". (Europe Patent No. EP 2 967 061 B1, 2014)

Uridine is applied in very small doses. According to the method outlined in the above-mentioned patent, 0.244 to 24.4 mg of uridine is dissolved in 1 litre of water, and this solution is used for irrigating the plants.

2.3. Integration of Water Management with Efficient PPP and Nutrient Use

Mineral fertilizers are imperative to maximize crop yields, and pesticides are crucial to combat pests, which can cause crop yield losses of up to 70%. Integrating nutrients or pesticides with superabsorbent polymers (SAPs) not only introduces new functionality to SAP applications but also enhances the efficiency of these agricultural products. When fertilizers or pesticides are incorporated into SAPs, their release to plants is significantly delayed compared to conventional methods, resulting in increased utilization efficiency. Furthermore, SAPs have the ability to swell with water that contains dissolved minerals and pesticides, thereby prolonging their presence near plant roots and reducing their leaching. As a result, SAPs can improve the use efficiency of applied fertilizers and pesticides.

Both macro- and micro- nutrients are essential for plant growth, even though they are applied at varying doses.

Potassium is one of the three main macronutrients, along with nitrogen and phosphorus, as plants take up considerable quantities throughout their life process. Hence the name NPK is used for the most common commercial fertilizer, denoting their mixture. Potassium is the activator of various enzymes used in protein synthesis, N and C metabolism, photosynthesis, and sugar transport. Having strong mobility, K also regulates osmotic pressure in cells and balances the anion and cations in the cytoplasm. Hence, K is vital for regulating stomatal opening and closing, cell elongation, and other processes. (Fernandez et al., 2020)

Calcium is also a vital plant nutrient. Its divalent cation Ca^{2+} is needed for cell walls and membranes. The cytosolic Ca^{2+} concentration is also very important for intracellular messenger, which is responsible for responding to various developmental and environmental cues. (WHITE, 2003)

Albeit toxic in excess, zinc, as a micronutrient, is a vital constituent of many plant proteins. Biofortification through the incorporation of zinc is used to increase the Zn

content of certain plant species and ultimately alleviate human dietary Zn deficiencies. (Broadley et al., 2007)

Plants need magnesium to synthesize chlorophyll. Additionally, in the chloroplast, Mg takes part in CO_2 assimilation reactions. A large portion of magnesium in plants is required for the structure and function of ribosomes, which enable protein biosynthesis. In fact, 75% of Mg in leaves is associated with protein biosynthesis. (Chaudhry et al., 2021)

Water is essential for food production, which consumes 70% of global water resources. For optimum plant health, water delivery should be regulated. During heavy rainfalls, fertilizers and pesticides leach into the environment. During drought, fertilizers and pesticides cannot dissolve in the soil. Superabsorbent polymers (SAP) offer a solution as an underground water reservoir, by absorbing water during rainfall and releasing it during dry periods. Thereby, SAPs allow plants to have access to water during drought, leading to increased biomass and yield. Fertilizer- and Pesticide-SAP composites can also slow down the release of nutrients and pesticides, prevent their run-offs due to heavy rainfalls, and keep them closer to the root area, for optimum plant uptake.

There have been numerous studies in the literature investigating the effectiveness of fertilizer- and pesticide-incorporated SAPs on plant growth. (Y.-C. Chen & Chen, 2019; Guo et al., 2006; S. Jin et al., 2011; León et al., 2019; Skrzypczak et al., 2019; Tubert et al., 2018; Wei et al., 2019)

In a study conducted in Argentina in 2017, Tubert et al. synthesized a superabsorbent-fertilizer composite and tested its performance on Eucalyptus plants. The composite was prepared through bulk polymerization of acrylic acid (AA), followed by neutralization using potassium hydroxide (KOH) and hydroxyethyl cellulose (HEC). To incorporate nutrients into the structure, a fertilizer solution mix tailored for Eucalyptus (BAL) was added to the reaction media after neutralization. Two SAP composites were prepared with fertilizer contents of 14 wt.% and 28 wt.%, respectively. A similar composite was synthesized using an NPK nutrient mix instead of BAL. (Tubert et al., 2018)

To evaluate the effectiveness of the fertilizer-loaded SAP composites, unloaded SAP, BAL, and NPK-loaded SAP samples were tested in both field and greenhouse conditions. Additionally, a control group and a treatment with unloaded SAP combined with solid granulated NPK pellets were included. Plant growth was assessed by monitoring plant height, dry weight, and stomatal conductance. The plants treated with fertilizers showed greater growth compared to those treated with SAPs alone and the control group. However, plants treated with fertilizer-loaded SAP composites exhibited significantly higher growth compared to all other treatment groups. Optimal fertilizer content is crucial for maximizing plant growth, as the SAP composite with 14 wt.% fertilizer outperformed the one with 28 wt.% in terms of dry plant weight.

In a 2019 study by Joshi et al., the bioinsecticide Bacillus thuringiensis (Bt) and a fertilizer mix were encapsulated within sodium alginate-based SAP microbeads using a wet-extrusion process. The efficacy of Bt-loaded microbeads was tested against Heliothis cirescens larvae and compared to the direct application of Bt powder. In trials without Bt, larval survival rates exceeded 72%. Although the microbeads released Bt and increased larval mortality compared to the control groups, the survival rate did not reach zero within 72-144 hours of exposure as observed with Bt powder. Encapsulated Bt in SAPs exhibited a slower reduction in larval survival compared to Bt incorporated into their diet. Despite the slower rate of reduction, encapsulation in superabsorbent polymers can enhance the long-term effectiveness of Bt or other pesticides under environmental conditions such as sunlight and rain. (Joshi et al., 2020)

2.4. Bio-Based Superabsorbent Polymers

In literature, novel bio-based SAP formulations are being reported. (Kuang et al., 2011; X. Liu et al., 2019; Llanes et al., 2020; Saruchi et al., 2019; X. Wang et al., 2014; F. Wu et al., 2012) These novel bio-based SAPs incorporate various naturally derived compounds, such as cellulose (Arredondo et al., 2023), starch (Dispat et al., 2020), chitin (J. Chen et al., 2022), chitosan (Fang et al., 2019), alginate (Mignon et al., 2019), guar gum (Sami et al., 2018), citric acid (H. J. Kim et al., 2017), poly(lactic acid) (Sartore et al., 2017), poly(itaconic acid) (Choi et al., 2022; H. C. Kim et al., 2022; Sand et al., 2021),

poly(amino acid), various proteins such as collagens, gelatin, and canola proteins. (J. Chen et al., 2022)

In an Italian study, Calcagnile et al. developed a biodegradable SAP composite that also serves as a fertilizer reservoir for agricultural applications. The composite was fabricated using carboxymethylcellulose sodium salt (CMCNa) and hydroxyethylcellulose (HEC) as precursors, with the addition of poly(lactic acid) (PLA) in some samples. To load nutrients, the SAP samples were immersed in various concentrations of a water-based KNO3 solution. After swelling in the solutions for 24 hours, the samples were dried in an oven at 45°C for 24 hours. The researchers argue that the inclusion of PLA in the CMCNa-HEC hydrogel contributed to the delayed absorption and release mechanisms of the hydrogel. Consequently, KNO3 release was prolonged in the PLA-containing samples, as depicted in the accompanying figures. (Calcagnile et al., 2019)

The hydrogel composite developed in this study was tested in two different Mediterranean cultivations of Pomodoro di Marciano di Leuca. The results indicated that increasing the hydrogel content in the PLA/SAP composites resulted in higher fruit yields. The weight difference was particularly significant for the PLA/H10/K100 samples tested in red soil.

In another study from India, Supare et al. reported an SAP based on starch-modified poly(acrylic acid). Starch and acrylic acid were used as monomers in a free-radical solution polymerization process, employing MBA as a cross-linker and APS as an initiator. The researchers achieved an absorption capacity of 700 g/g. Additionally, urea was encapsulated within the hydrogel structure by grafting starch with acrylic acid in the presence of urea and MBA. (Supare & Mahanwar, 2021)

The hydrogel composite produced in this study was tested in the cultivation of chickpea plants. Three soils were prepared in paper cups: (i) control soil without any hydrogel, (ii) 20 g of soil mixed with 0.05 g of urea-coated hydrogel, and (iii) 20 g of soil mixed with 0.05 g of hydrogel without urea. 30 mL of water was added in each cup, and chickpea seeds were subsequently buried for germination.

The addition of SAP had a significant impact on plant growth. After 2 days, the urea-encapsulated hydrogel resulted in a shoot length of 2.8 cm, whereas the control soil produced a shoot length of only 0.5 cm. After 15 days, plant heights of 1 cm and 5 cm were observed for the hydrogel-treated and urea-encapsulated hydrogel-treated soils, respectively. In contrast, the untreated soil exhibited no effective plant growth due to rapid vaporization.

Ding et al. mixed spent mushroom substrates (SMS) with acrylic acid at a mass ration between 0 to 100 wt% to synthesize superabsorbent polymers. SMS-AA composite achieved a maximum water absorption of 458 g/g with 25 wt% SMS; and authors argue that this composite hydrogel has two times more gel strength compared to non-composited polyacrylates. In another study, bio-based SAPs were synthesized using biomass lignin as raw material and poly(vinyl alcohol) as matrix template. Various sources of lignin were tested at different weight ratios, and both parameters affected swelling behaviour. Approximately 500 g/g swelling capacity was reported from optimum SAP synthesis conditions.(Ding & Gong, 2013)

In yet other studies, biodegradable SAPs were produced from various bio-based raw materials: (i) cellulose from sugarcane begasse and acrylic acid (Neamjan et al., 2019), (ii) chitosan and poly(vinyl alcohol) with lignin nanoparticles (W. Yang et al., 2018), (iii) biomass-based itaconic acid and vinyl sulfonic acid (Y. J. Kim, Hong, Shin, Kwon, Lim, Kim, Kim, et al., 2020), (iv) red liquor (byproduct of paper industry) and acrylic acid (Meng et al., 2019), (v) cellulose from flax shive and acrylic acid (Feng et al., 2010), (vi) citric acid and sodium bicarbonate (H. J. Kim et al., 2017), (vii) chitin and succinic anhydride. (Yoshimura et al., 2005)

In the literature, the studies on bio-based SAPs do not cover a wide range of biomaterial concentrations. In the papers by Kim et. al. and Fu et. al., SAPs with 2 wt% nanocellulose, and 5 wt% alpha-cellulose additions are presented. These SAPs can swell with water up to 300 and 440 times their own weight, respectively. (Fu et al., 2022; Y. J. Kim, Hong, Shin, Kwon, Lim, Kim, Choi, et al., 2020) These represent the lower end of cellulose incorporations in bio-based SAP formulations found in the literature. Increasing the cellulose content in the SAPs towards approximately 20 wt% generally results in an improvement in the water absorption performance. For example, in a study by Khoo et.

al., an SAP with 12 wt% cellulose is synthesized, which reached an absorption rate of 554 g/g in water. (Khoo et al., 2014) In another article by Arredondo et. al., an SAP with 20 wt% cellulose is presented, which achieved a swelling rate of 475 g/g. (Arredondo et al., 2023) Both absorption values are significantly better than that of the former SAPs that incorporate 2 and 5 wt% cellulose. There are also accounts of other studies that further increased the cellulose percentage of the bio-based SAPs to 23 and 24.5 wt%, by Wang at. al. and Barajas-Ledesma et. al., respectively. However, the SAPs in these works could only achieve water absorption values of 263 and 200 g/g, respectively. (Barajas-Ledesma et al., 2020, 2022; W. Wang et al., 2020b)

Amongst SAPs incorporating a greater percentage of bio-based materials, there exist studies presenting SAPs with 70 wt% or higher cellulose contents. The water absorption capacities of such bio-SAPs are highly limited, and they are unsuitable for both agricultural and personal hygiene applications. For example, in a study by Ibrahim et. al., CMC-Acrylamide copolymer SAPs with 70, 80, 90, and 100 wt% CMC are developed. The water absorption capacities of these bio-based SAPs are approximately 70, 70, 60, and 45 g/g, respectively. (Ibrahim et al., 2007) These values are almost 10 times lower compared to many commercial SAPs. Other examples of completely bio-based SAPs can be found in the works of Lee et. al, and Chaiyasat et. al., which have water absorption capacities of 87 and 125 g/g, respectively. (Chaiyasat et al., 2019; Lee et al., 2018) It can be said that, completely bio-based SAPs are not yet suitable for agricultural applications.

In conclusion, numerous studies have focused on developing SAPs from bio-based and biodegradable materials. These advancements pave the way for environmentally friendly SAPs with potential applications in agriculture and beyond.

Chapter 3

MATERIALS AND METHODOLOGY

3.1. Materials

Halloysite nanotube (HNT), in purified form, was generously provided by Eczacıbaşı ESAN, in Türkiye. Polyethylene glycol 400, 1000, and 4000, for synthesis (CAS 25322-68-3) were obtained from Merck. Toluene, anhydrous (CAS 108-88-3) was purchased from Merck. Triethoxy(3-isocyanatopropyl)silane (IPTS, CAS 24801-88-5) was purchased from Momentive Performance Materials.

Acrylic acid (CAS 79-10-7) and acrylamide, for synthesis, (CAS 79-06-1) was purchased from Sigma-Aldrich. 2-acrylamido-2-methylpropanesulfonic acid (AMPS) was purchased from Toagosei Co., Ltd., Japan. Potassium hydroxide, reagent grade, (CAS 1310-58-3) was purchased from Sigma-Aldrich. Crosslinking agent vinyltrimethoxysilane, (VTMS, CAS 2768-02-7) was obtained from Momentive Performance Chemicals. Initiator ammonium persulfate (APS), ACS reagent, (CAS 7727-54-0) was purchased from Sigma-Aldrich.

Carboxymethyl cellulose (CMC, CAS 9004-32-4) was kindly provided by USK Kimya A.Ş., Türkiye. Halloysite nanotube (HNT), in purified form, was generously provided by Eczacıbaşı ESAN, in Turkey.

Calcium nitrate tetrahydrate (CAS 13477-34-4) and zinc sulfate heptahydrate (CAS 7446-20-0) were purchased from Merck. Commercial calcium nitrate and zinc sulfate fertilizers were purchased from Gübretaş in Türkiye.

For nutrient-SAP composites, calcium and sulfate fertilizers were used. For the HNT loading experiment, calcium nitrate and zinc sulfate fertilizers from Gübretaş were used. These commercial fertilizers were used again for the first micronutrient integration tests in SAP structure, by directly mixing fertilizer and SAP solutions, after polymerization. In the final nutrient-SAP composite syntheses, obtained by direct mixing of SAP and nutrient solutions, calcium nitrate and zinc sulfate from Merck were used.

Cellulase enzymes from Novozyme were used in this study. Enzymes were kindly provided by Prof. Günseli Bayram Akçapınar from Acıbadem University.

DI water was obtained from Merck Milli-Q® Elix Essential 5 and Milli-Q® Reference water purification systems. All chemicals were used without further purification.

3.2. Superabsorbent Polymers

The SAPs developed in this study are derived from the synthetic SAP formulation described in the patent PCT/TR2021/050162, “A polymer matrix based superabsorbent material”. (M. S. Seven et al., 2020) The SAP described in this patent incorporates one or more water-soluble monomers suitable for radical polymerization, and an alkoxysilane derivative crosslinking agent. The monomers used in this study were acrylic acid, acrylamide, and AMPS; and the silane cross-linking agent was vinyltrimethoxysilane (VTMS). Ammonium persulfate (APS) was used as the initiator. Potassium hydroxide was used as the neutralizing agent. This patent also claims a nanoparticle addition, in the size range of 0.1-500 nm. This nanoparticle is selected as halloysite nanotubes (HNTs), which can also act as a carrier material for various active agents. For the bio-based superabsorbent polymer formulations, the nanoparticle is replaced with carboxymethyl cellulose. Deionized water was used as the solvent.

According to the literature, the copolymerization of acrylic acid and acrylamide improves the performance of superabsorbent polymer, in terms of water absorption capacity. Furthermore, the inclusion of AMPS in the copolymer favors its stability under high salinity and temperature.

The use of nanofillers in the synthesis of superabsorbent polymer results in mechanical strengthening. The nanofillers in the superabsorbent polymer become additional crosslinking points, which improve the structural integrity of the structure. This strengthening would result in a higher water absorption ratio under load, which is an important performance indicator for agricultural applications, under the soil. Furthermore, a higher mechanical strength increases the water retention duration of the superabsorbent polymer. This property would allow the SAP to supply its surrounding soil with water for a longer duration.

To serve as a water reservoir for plants and as a host for carrier materials such as nutrient-loaded HNTs, we synthesized a superabsorbent polymer based on acrylamide and acrylic acid. Initially, the monomers acrylamide, acrylic acid, and AMPS were mixed in deionized water. Subsequently, the pH was adjusted to a range of 7-8 using sodium hydroxide or potassium hydroxide. In the initial syntheses, sodium hydroxide was used, as it is the most common neutralizing agent used for commercial superabsorbent polymers. Sodium ions can displace other mineral nutrients in the soil, which leads to nutrient deficiencies. So, sodium is not desired in farming. On the other hand, potassium is one of the essential macronutrients. Therefore, to make the SAP formulation more suited for agricultural applications, potassium hydroxide was used as the neutralizing agent, instead of sodium hydroxide. Therefore, in the later syntheses, neutralizing agent was re-selected as potassium hydroxide. Potassium is an essential macronutrient necessary for plant growth.

Once pH stabilization was achieved, HNTs were added to the mixture, and the resulting solution was transferred into a reactor. The reactor was connected to a reflux system to collect the evaporated solvent and purged with nitrogen gas to establish an inert atmosphere before introducing the crosslinker (VTMS) and initiator (APS). Following the addition of the initiator, the polymerization solution was heated to 75 °C and maintained under constant stirring for 2 hours. The resulting SAP solution was then

precipitated in ethanol. The resulting SAP was subsequently cut into small pieces and dried at 70 °C for 18 hours, facilitating further crosslinking.

However, the current method employed in the polymerization reaction, which consists of 5% solids content, necessitates precipitation in ethanol after removal from the reaction. This approach presents certain drawbacks in terms of production efficiency and economic feasibility. Precipitation represents an additional step that requires extra resources and prolongs the total production time. If this method were to be implemented on a large scale, the ethanol used for precipitation would need to be filtered and reintroduced into the production line. Implementing a filtration system would burden the facility with additional requirements. Consequently, completely eliminating the precipitation stage could yield significant economic advantages.

As a potential solution, we plan to initially explore bulk or near-bulk polymerization methods. However, a major drawback of these systems may be the high viscosity of the resulting polymer, requiring manual extraction from the reactor instead of pouring it out in a liquid state. If this approach proves unsuccessful, we will increase the solid content of the current polymerization reaction to a more moderate ratio. Subsequently, the resulting solution will be cast after polymerization and dried in an oven, thereby eliminating the need for ethanol precipitation.

By evaluating these alternative approaches, we aim to enhance production efficiency and improve the economic feasibility of our SAP synthesis process while maintaining the desired properties and performance of the final product.

3.2.3. Scale-Up of SAP Production

The main purpose of this study was to develop novel superabsorbent polymers (SAPs) for use in large-scale commercial agriculture. To persuade farmers to embrace new technologies on the field, it is very important that the product or service offers significant economic advantages. Moreover, farmers place great importance on solid results, not only from small-scale greenhouse trials but also from large open fields. Therefore, for a technology to achieve commercial success in large-scale agricultural settings, it must first

demonstrate adaptability to large-scale production. The daily production capacity plays a critical role in ensuring the economically viable production of SAPs.

Initially, the applied method was to precipitate the polymer solution in ethanol, after synthesis. However, in this approach, the polymerization reaction only has 5% solids. If the solids ratio is increased beyond this point, the precipitation stage becomes cumbersome. The viscosity of the polymer solution is increased, and precipitation becomes less effective. Thus, more ethanol needs to be used. However, to make the SAP production more efficient, the output needs to be increased.

3.2.3.1. Near bulk polymerization of SAP

Since our primary objective was to maximize the production of superabsorbent polymers (SAPs) within a given reactor, we initially conducted trials aiming to increase the monomer content through bulk polymerization. However, due to the insufficient quantity of acrylic acid monomer to dissolve the other monomers, a true bulk polymerization could not be achieved. Instead, an adequate amount of water was added to facilitate the dissolution of all monomers, resulting in a solids ratio of 60%.

The polymerization reaction proceeded as before, without any adjustments to the crosslinker or initiator amounts. The viscosity of the solution significantly increased compared to the initial formulation with 5% solid content, which posed a challenge in terms of magnetic stirring. Although our laboratory is equipped with a mechanical stirrer suitable for larger reactors, for the initial trials, we had to employ an oil bath setup as per standard practice for small-scale experiments.

During the initial trials, polyethylene (PE) water cups were utilized to test near-bulk polymerization. This approach aimed to prevent any damage to the reactors and facilitate the subsequent removal of the resulting polymer. Since the polymerization was carried out at a temperature of 75 °C, which would not cause deterioration of PE, a PE cup was placed inside a beaker, and the space between the two was filled with water to enhance heat transfer from the oil bath. As a reflux system was not feasible for this setup, the beaker was covered with two paraffin films punctured with syringe needles, allowing for

gas purging. Nitrogen gas was employed to purge the oxygen at the beginning of the reaction.

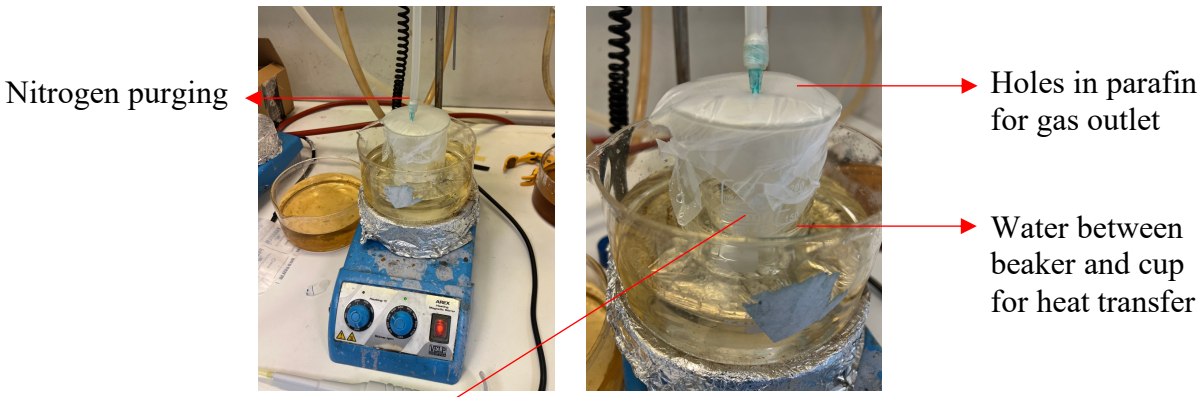

Figure 3: Synthesis Setup for Near Bulk Polymerization of SAP.

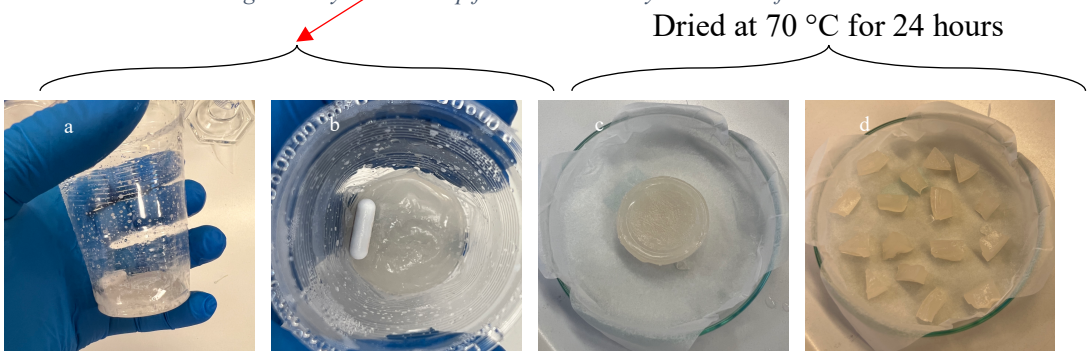

Figure 4: SAP after Near Bulk Polymerization - (a,b) in PE cup; (c,d) prepared for drying.

3.2.3.2. Polymer solution casting of SAP

To eliminate the ethanol precipitation stage and thus simplify the post-synthesis processing, reacted SAP solution was dried in a laboratory drying oven. The solid content of this polymerization reaction was increased, compared to that of the initial syntheses (5 wt.%), which was done to significantly reduce the drying time, and to increase SAP output per reaction. Solids content of 8 to 15 wt% was tested.

SAP synthesis formulation (i.e., monomer ratios, crosslinker and initiator quantities), and reaction parameters (i.e., nitrogen purging duration, reaction temperature and time) were all kept the same as 5% polymerization that was followed by precipitation. The photographs below depict the SAP solution before and after drying in Teflon mold.

Figure 5: (left) SAP solution after polymerization, (right) solid SAP after drying.

3.2.4. Drying and Storage of SAP

Once polymerization is completed after 2 hours, the resultant solution is poured into Teflon molds, at approximately 5-7 mm thickness. The molds are later transferred to a ventilated drying oven operating at 70 °C and let dry for 20 hours. When fully dried, the thickness of the sheets reduces to approximately one-tenth of their initial value, to 0.5-0.7 mm.

The final product is broken down by hand into rough pieces, and kept in close-capped falcon tubes, to prevent exposure to humidity. Since SAP is hydrophilic, it absorbs humidity in the air, the effect of which is noticeable even in 30 minutes. For example, when the SAP sheet is taken out of the oven after drying, it is highly brittle, such that even a small bend to the sheet results in shattering. However, after even 30 minutes, the brittle nature of the SAP is lost; after 1-2 hours it becomes bendable to a certain extent;

and after 1 or 2 days, depending on the thickness, the SAP sheet becomes structurally like rubber.

3.2.5. Improving Mechanical Properties of SAPs with HNTs

In this study, halloysite nanotubes (HNTs) were utilized as nanofillers in a nanocomposite superabsorbent polymer (SAP). The primary role of HNTs, along with incorporating active agents, is to enhance the structural durability of the SAPs.

In this study, HNTs were incorporated at a concentration of 5% w/w in the SAP. The density of HNT was reported as 2.5 g/cm^3 in literature. By employing Archimedes' principle, the density of the resulting SAP from our formulation was calculated as 1.6 g/cm^3. Consequently, the corresponding volume fraction of HNT was calculated as 3.2% v/v. According to the paper published by Zare and Rhee, such level of halloysite incorporation is sufficient to impart strengthening.

The HNTs used in our experiments were kindly provided by Eczacıbaşı ESAN, who supplied both standard (containing impurities) and purified (with minimal impurities) HNTs. Purified HNT was used for all active agent loadings and SAP syntheses.

3.2.5.1. Rheological properties of SAP and SAP-HNT

The effect of halloysite nanotube addition on the mechanical properties of the SAP was evaluated by rheology. The rheological properties of two SAPs were evaluated and compared. The first one is the control SAP used in this study, which incorporates 5 wt% halloysite nanotubes in its structure, without any fertilizer additions. The other SAP that was tested is the same superabsorbent polymer, without the addition of halloysite nanotubes as nanofillers.

Ramazani-Harandi et. al. published a comprehensive study on the rheological determination of the swollen gel strength of SAPs. (Ramazani-Harandi et al., 2006b) The test performed in this study is a modified version of the strain sweep test described in

their article. 0.5-gram test samples were allowed to swell in 50 mL distilled water in a falcon tube, for one day, such that their final water absorption rates reached approximately 100 g/g. The rheological measurements were performed by Anton-Paar oscillatory rheometer. Parallel plate geometry was utilized, with a gap of 1.5 mm between the plates. The tests were conducted at a room temperature of 25 °C. A strain sweep test was conducted, at a constant frequency. The storage and loss moduli were determined from the linear viscoelastic (LVE) zone.

The storage and loss moduli represent the elastic and viscous portions of the viscoelastic behaviour, respectively. Elastic and viscous portions depict the solid-state and liquid-state behaviours of the samples, respectively. Storage modulus is an indication of the superabsorbent polymer's ability to store deformation energy elastically. This stored energy is released after the mechanical stress is released. On the other hand, loss modulus represents the energy dissipated as heat through friction. (Anton Paar, n.d.)

3.2.6. Water Retention Performance of Superabsorbent Polymers

The water retention capabilities of the SAPs were also evaluated. All samples were placed in beakers filled with 250 mL of deionized water and allowed to swell for 2 days. Once filtered, the weights of the swollen gels were recorded. The swollen gels were left in their beakers under standard room temperature and pressure. Every day, during the first week of the test, the gels were filtered again to get rid of any excess water, and their weights were recorded. Consequent measurements were taken on day 10, day 14, and every other week.

The water retention ratio, given as a percentage, was calculated by comparing the current weight of the gels to their initial weights, according to the following formula:

$$Water\ Retention\ (\%) = \frac{W_g}{W_i} \times 100$$

$$W_g: weight\ of\ swollen\ gel, W_i: initial\ weight\ of\ SAP$$

3.2.7. Reusability – Reswelling Capacity of Superabsorbent Polymers

The reusability of superabsorbent polymers is determined by how their absorption capacities and dry weights are affected after swell-dry cycles. To determine their reswelling capacity, completely dried 0.05 g SAP samples were placed in 50 mL falcon tubes and immersed in 50 mL of deionized water. All samples were tested in triplicates. The SAP samples were allowed to swell in the water for 24 hours. Subsequently, the swollen gels were filtered to remove the excess water and placed back in their respective falcon tubes. The weights of falcon tubes were recorded. The caps of all the falcon tubes were removed and placed on racks. The racks were placed in a drying oven at 70 °C. The samples were taken out once all the samples were completely dried. Next, the tubes were closed with their respective caps and weighed. This swell-dry procedure was repeated three times.

3.3. Efficient Use of Plant Protection Products (PPP) and Nutrients

One objective of this study was to enhance the efficiency of various agrochemicals, including pesticides, uridine, and fertilizers, by developing a system that enables the sustained delivery of these active agents. To accomplish this, these active agents are initially loaded onto carrier materials, which can later be impregnated into a matrix material for application in the field.

It is desirable to utilize carrier materials that are highly abundant, cost-effective, and safe, while also offering sufficient loading capacities. Therefore, halloysite nanotubes (HNTs) were chosen as an ideal option for this investigation. HNTs possess ample reserves in Turkey, feature surface groups suitable for functionalization, and exhibit an optimal hollow tubular structure for loading active agents. Given that pesticides in sustained release systems are applied in low dosages, the loading capacity of HNTs proves to be adequate.

Halloysite nanotubes are aluminosilicate clays characterized by a submicron hollow tubular configuration, composed of alternating layers of alumina and silica. These layered structures accommodate water molecules. The external surfaces of HNTs primarily consist of siloxane groups, along with aluminol and silanol groups, while their inner lumen exclusively contains aluminol groups. HNTs are natural, cost-effective, and abundant, with significant reserves found in Turkey. Moreover, they exhibit biocompatibility, enabling their utilization as drug carriers within the human body. With a Young's modulus of approximately 300 GPA, they can also serve as strengthening nanofillers in nanocomposites. The initial application of HNTs as a drug carrier dates to 2001, making this research area relatively novel. Active agents can be loaded onto both the surface and inner lumen of HNTs.

Surface modification of HNTs was employed to introduce functional groups onto their surface, rendering them receptive to desired molecules and enhancing their loading capacities.

In summary, this study aims to improve the efficiency of agrochemicals through the development of a sustained delivery systems. Halloysite nanotubes were selected as carrier materials due to their abundance, affordability, and loading capacities. Their unique hollow tubular structure, along with surface modification techniques, allows for the successful loading of active agents.

3.3.1. BET and SEM Characterization of HNT

Two HNT samples were generously provided to us by Eczacıbaşı ESAN: the unpurified, or standard, HNT sample, and the purified HNT sample. To evaluate their tube dimensions and pore volume distributions, both samples underwent SEM and BET characterization.

For the BET analyses, three replicates were tested from each HNT sample. A comprehensive isotherm analysis was conducted to obtain detailed information on pore volume and surface area across all pore sizes. The results from the BET analyses revealed some significant differences between the purified and standard HNT samples.

3.3.2. Active Agent Incorporation on HNT

3.3.2.1. Pesticide loading on HNTs

To begin, HNTs were dispersed in distilled water, and the fungicide solution was added. The resulting mixture underwent shear mixing for 15 minutes at 8000 rpm to ensure effective mixing and size homogenization of the HNTs. Subsequently, the mixture was transferred to a vacuum filter flask equipped with a magnetic stirrer, and the flask was sealed with a rubber septum. While continuously stirring, a vacuum pump was connected to the flask, gradually reducing the pressure inside. This process led to the observation of bubbles, indicating the removal of air from the interior of the HNTs. Vacuuming continued until no bubbles were detected, at which point the vacuum was released. The sudden return to atmospheric pressure facilitated the ingress of fungicide molecules into the HNTs. The solution was then vacuum filtered using a filter paper, and ethanol was added during the filtration process to remove any unloaded fungicide molecules. This solvent washing step aimed to reduce the adsorption of molecules on the outer surface of the HNTs, enabling a higher concentration of loaded molecules within the inner lumen. Molecules within the inner lumen are known to be released at a slower rate compared to those on the outer surface, thus extending the release duration. Finally, the resulting slurry was dried at room temperature.

3.3.2.2. Uridine Loading on HNT

To explore the potential benefits of uridine in enhancing plant stress tolerance, a collaborative project was initiated with Professors Asuman Cansev and Mehmet Cansev from Uludağ University in Bursa, who are inventors in the EU patent EP2967061B1 titled “Use of Uridine for Enhancement of Plant Stress Tolerance”. The objective of our joint project was to devise a suitable delivery matrix for uridine, enabling its incorporation and sustained release in the soil. To achieve this, we employed the following approach: (i) incorporating uridine onto Halloysite Nanotubes (HNTs), both on their outer surfaces and within the inner lumen, and (ii) utilizing the uridine-loaded HNTs in the synthesis of

Superabsorbent Polymers (SAPs). The vacuum suction method was employed to load uridine onto the HNTs.

3.3.2.3. Bio-pesticide loading on HNT

We met with Prof. Selçuk Hazır from Adnan Menderes University and learned about their research on biological pest management methods. A total of 4 biological materials of two types have been received from Selçuk Aydın's research group labeled AF (1,2) and VOC (1,2). AF denotes anti-fungal, and VOC denotes volatile organic compounds. In this study, the VOCs are used for repelling insects. These bio-pesticides were loaded HNTs through the vacuum suction method. Bio-pesticide-loaded HNTs were incorporated in the SAP matrix during synthesis. AF- and VOC-loaded SAPs were sent back to his research group, which tested their efficacy against target pests in tomatoes.

3.3.3. Nutrient Loading on HNT

To load HNTs with nutrients, a three-step procedure was used. First, the surface of HNTs were functionalization with silane coupling agent 3-(Isocyanatopropyl)triethoxysilane (IPTS). This reaction was carried out in toluene solvent, at 120 °C, for 20 hours. Next, PEG chains were added to the mixture, and the reaction was continued for another 20 hours. This allowed PEG chains to be bonded to the functionalization surface of HNTs. This reaction was continued just after functionalization, in the same solvent. In this study PEG 400, PEG 1000, and PEG 4000 was used. The product was filtered and ground once dry. Finally, synthesized HNT complexes were mixed with different nutrients in the water, and the solution was stirred for 12 hours.

3.3.3.1. Surface functionalization of HNT with IPTS

Silane coupling agents are used to chemically bond different materials. Generally, they act as interfaces that bond organic and inorganic materials. A common example of their utilization is the matrix-filler bonding in polymeric composites reinforced with inorganic reinforcements, such as wood fibers. (Coleman, 2011; Dillingham, 2002)

There are two methods to apply silane coupling agents: (i) in the first method the silane can be used to treat the surface of inorganic material prior to mixing with the organic phase, or alternatively (ii) it can be mixed directly with the organic phase. The latter method is preferred in the industry, due to superior process efficiency. However, it is not appropriate for our work, as the inorganic material we utilize (HNT) is not used as a conventional filler as in traditional composite applications. As opposed to polymeric composites that generally contain 1-10 wt.% filler, the main component of our system is the inorganic material (HNT), to the surface of which we aim to bond PEG chains.

Surface treatment of inorganic materials can be done by either the wet or the dry method. The wet method was preferred in our study to obtain a more uniform treatment. The dry method is more suitable for large-scale production, as it is much faster and generates very little waste, at the expense of uniform treatment.

In the wet method, a dilute solution of silane is added to a slurry of the inorganic material, and the mixture is stirred. Constant stirring allows for a homogeneous distribution of the inorganic material and the silane, which results in more uniform and precise surface treatment of the inorganic material. (HENGDA, n.d.)

In this work 3-(Isocyanatopropyl)triethoxysilane (IPTS) is used as the silane coupling agent. IPTS is mainly used for crosslinking various copolymers, such as ethylene-vinyl acetate and ethylene-acrylic acid-acetic acid. Moreover, it is suitable for different resins - such as polycrystalline, epoxy, and phenolic resins, and fiber-reinforced plastic (FRP) materials.

IPTS contains two active groups, namely isocyanate, and ethoxy. These end groups couple inorganic fillers (e.g., HNT) with organic molecules (e.g., PEG chains). Suitable

polymers for use with IPTS include polyacrylic acid. (Jayasuriya, 2017; Verma & Gope, 2015) The SAP synthesized in this project is a copolymer of acrylic acid, acrylamide, and AMPS.

To attain silane coupling to the HNT surface, first, 1.6 g of HNT was dispersed in 80 mL of toluene. Next, 5.64 mL of IPTS was added to the mixture. Under constant stirring, the solution was kept at 120 °C for 20 hours, by placing the reactor in a hot oil bath.

3.3.3.2. Forming HNT-PEG complexes

To encapsulate and form a chelate with metal-bearing nutrients, PEG chains were attached to the HNT surface. PEG 400, 1000, 2000, and 4000 were used to test the efficiency of chains of different molecular weights.

PEG chains were attached to the HNT surface through silane coupling agent IPTS. After HNT and IPTS were allowed to react in toluene for 20 hours at 120 °C, PEG was dissolved in toluene (0.5g/20mL) and added to the reaction mixture with the help of a syringe, through one of the necks of the reactor. The reaction was then allowed to continue for another 20 hours, at 120 °C.

Once the reaction was completed, the resultant solution was filtered using vacuum filtering; and washed with toluene to get rid of free IPTS molecules and PEG chains. The product (HNT-IPTS-PEG complex) was ground once completely dry.

3.3.3.3. Loading nutrients on HNT-PEG complexes

Finally, synthesized HNT-IPTS-PEG complexes were mixed with calcium nitrate and zinc sulfate micronutrients in the water. 0.4g of HNT-IPTS-PEG complex were dissolved in 4 mL of deionized water, and different amounts of nutrients were added. The mixtures were stirred for 12 hours. During mechanical mixing, the micronutrients were expected to be trapped within the PEG chains.

3.3.3.4. Quantifying IPTS, PEG, and micronutrient loading with TGA

Nutrient loading ratios on HNTs were determined from thermal gravimetric analysis, by comparing the weight loss. Weight loss up to 160 °C is attributed to moisture. So, non-water mass losses of all samples were compared, to calculate loading ratios. During the analyses, temperature was raised from 30 to 1000 °C at a temperature increase rate of 10 °C/min. Nitrogen atmosphere was attained in the chamber through purging at a flow rate of 85 mL/min.

To demonstrate and quantify IPTS, PEG, and micronutrient loading, loaded and unloaded HNT samples were analyzed with thermal gravimetric analysis (TGA). Non-humidity mass losses of all samples were compared, to calculate loading ratios.

3.4. Integration of Water Management and Efficient PPP and Nutrient Use

To maximize their uptake by the plants, and to limit their loss to the environment, we studied different ways of integrating fertilizers in superabsorbent polymers. By applying fertilizer-containing SAP composites near the root area of the plants, nutrients can be made readily available for plant uptake. Also, the dissolution and leaching of fertilizers into the soil will be delayed owed to SAPs, which will act as a host matrix for these nutrients.

In the first approach, micronutrients were first attached to halloysite nanotubes (HNT) by means of PEG chelating. Then, these nutrient loaded HNTs were used in the synthesis of SAP. With this method a very limited nutrient loading on HNT could be achieved. Therefore, in the second approach, fertilizers were directly incorporated in the SAP. To do so, the nutrients were mixed with the polymer solution, and dried together.

The water absorption capacities of nutrient-SAP composites are evaluated, along with their release kinetics. A synergistic effect was achieved, and nutrient incorporation improved water absorption capacity of SAPs, contrary to initial expectations.

In most sustained or controlled delivery systems, carrier and host materials serve only one purpose: to load the materials in, and to host the carriers, respectively. In this study, our carrier material HNT, and host matrix SAP serve a dual-purpose. Our matrix SAP both hosts active agent loaded HNTs and acts as a water reservoir for plants itself. On the other hand, in addition to their main function as active agent carriers, HNTs act as strengthening fillers in the SAP matrix, which improves mechanical properties, increases water absorption under load, and prolongs water release duration. Indeed, the water release duration of our SAP is superior compared to commercially available SAPs.

We used HNT-nutrient complexes, and pesticide loaded HNTs in SAP synthesis to produce SAP-HNT nanocomposites with loaded nutrients, Ca, Fe, and Zn, along with fungicide loaded SAP nanocomposites. All synthesis were successful. SAP synthesis described in detail in the previous section was repeated with active agent loaded HNTs.

Other successful approaches to impregnate nutrients in SAP are to introduce nutrient solutions directly during or after polymer synthesis. After synthesis, polymer solution can either be precipitated in ethanol, or directly dried in the oven at 70 °C for 18 hours.

Another way of introducing nutrients in SAP structure is rather a direct approach of allowing already synthesized SAPs to swell with a nutrient solution, and later drying swollen gels in oven. Since here the interaction between nutrient molecules and SAP is only physical, the retention time of nutrients in the SAP is thought to be short and hence their dissolution in soil is expected to be rapid. However, this is an extremely simple method of loading nutrients in SAPs, without any required changes in the synthesis procedure.

The final approach is to mechanically compact fertilizer and SAP powders in a pressing machine. This approach seems counterintuitive regarding slow-release mechanisms. Attaining a slow release of fertilizers is especially important when there is adequate or excessive water delivery to plants. However, if there is a water shortage, solid fertilizers

may not be able to dissolve in soil. SAPs are hydrophilic and will swell with water, which will cause the fertilizer-SAP hybrid structure to increase in volume and burst. Upon bursting, fertilizer particles will be broken into smaller pieces, and their total surface area will greatly increase, thus allowing a faster dissolution in soil.

3.4.1. SAP Synthesis with Uridine-loaded HNT

Following the successful loading of HNTs with uridine, two SAP-HNT-uridine samples were synthesized, containing 1 and 5 wt.% HNT-uridine relative to the total solid weight of the SAPs. Consequently, the 1 and 5 wt% SAPs were expected to contain a maximum of 0.18 and 0.92 wt% uridine, respectively. However, it was important to determine the actual concentration of uridine in the synthesized SAPs, considering potential losses during the synthesis process. Additionally, investigating the release kinetics of uridine from the SAP-HNT-uridine composites in water was of interest.

To accomplish this, the synthesized SAP composites were sent to Uludağ University for temporal High-Performance Liquid Chromatography (HPLC) analysis, aiming to measure both the uridine concentration and the release profile of uridine over time. Unfortunately, the project faced technical complications during the analysis of the samples at Uludağ University, leading to the suspension of further experiments in this project.

3.4.2. Nutrient Incorporation in SAP

The initial micronutrient loading studies on HNT-PEG complexes, following HNT surface functionalization with IPTS and PEG, were very low in weight percentages. For example, maximum calcium and zinc loadings were recorded as **2.05** and **1.84 % w/w**, respectively. If we combine this with the fact that HNT is added to the SAP synthesis at only up to 10 % w/w, the effective loading of said nutrients in the SAP can only reach up to 0.2 % w/w in ideal circumstances. If we further consider the application dose of SAP in the field, which is approximately 1-2 kg / 1 da, the resultant application dose of nutrients to the field with this method would be highly inadequate. For example, 2 kg

SAP containing 0.2 % w/w of Ca in its structure, can only release up to 4 grams of calcium to the field, which is insignificant. Depending on plant type, 2-10 kg of Ca is removed annually from 1 Da of soil by cultivated crops, which needs to be replenished with chemical (mostly Calcium Ammonium Nitrate, i.e., CAN) or natural fertilizers.

Therefore, in subsequent studies, new fertilizer incorporation methods were tested, to achieve considerably higher fertilizer loadings. One method was to load nutrients on SAP through swelling and drying. However, this method is not economically feasible, due to extra processing steps. Other facile incorporation methods include mixing micronutrient solutions with the polymerization solution, both during and after synthesis. The latter approach proved to be more effective, in terms of ease of processing.

3.4.2.1. Nutrient-SAP compaction

One of the main limiting factors of applying mineral fertilizers is the need to form them into relatively large granular shapes. The reason behind this requirement is to attain compatibility with agricultural fertilizer spreader machines. These machines take in various kinds of fertilizers in solid form and spread them evenly on the field, through the action of either drop or broadcast spreaders.

If fertilizer granules are too large, they can get stuck in the machinery, especially in drop spreaders, by plugging its ports. Plugging can also be a problem for broadcast spreaders, which have larger ports compared to drop spreaders. On the other hand, if fertilizer particles are too small, i.e., in powder form, they will readily become airborne upon spreading action of said machinery, which would be a more pronounced problem with broadcast spreaders, as they will cause fertilizer powders to disperse over a wide area uncontrollably.

As with any active agent, the rate of interaction of fertilizer particles with their surroundings, and therefore their uptake by the soil and trees, depends on their surface area that is in direct contact with their surroundings. As we increase their total surface area, we will speed up their dissolution in soil and allow them to reach plants faster. To

do so, we need to lower their particle size, but we are limited by the agricultural fertilizer spreader machines' minimum granule size criteria.

So, we need to take on another approach to accelerate large fertilizer granules' dissolution in soil. Along with a large surface area, high humidity is key in terms of dissolving mineral fertilizers rapidly. We propose that integrating super absorbent polymer in the structure of a mineral fertilizer granule will speed up its dissolution in the soil through two modes of action. We envision this material having a core-shell structure, with SAP comprising the core and fertilizer the shell. Firstly, hydrophilic SAP will absorb water in its structure and retain it for a prolonged time, allowing fertilizer to be in contact with water for a longer time, compared to the typical case in bare soil. Secondly, since SAP will swell upon absorbing water, it will want to expand, and this increase in the internal pressure will cause the SAP-fertilizer granule to burst. This will break down the granule into smaller particles, which will further accelerate the dissolution process, as the total surface area is increased.

Two micronutrient and two macronutrient fertilizers were used in the nutrient – SAP compaction process. These fertilizers were mixed with fine-granulated SAP at a weight ratio of 90:10 (fertilizer to SAP). These fertilizer-SAP mixtures were loaded into a mechanical pressing machine with a small cylindrical mold and pressed at a pressure of 50 MPa for 120 seconds. Also, to assess and confirm the effect of SAP addition on dissolution kinetics, fertilizers were pressed without SAP, as control groups, with the same compaction parameters.

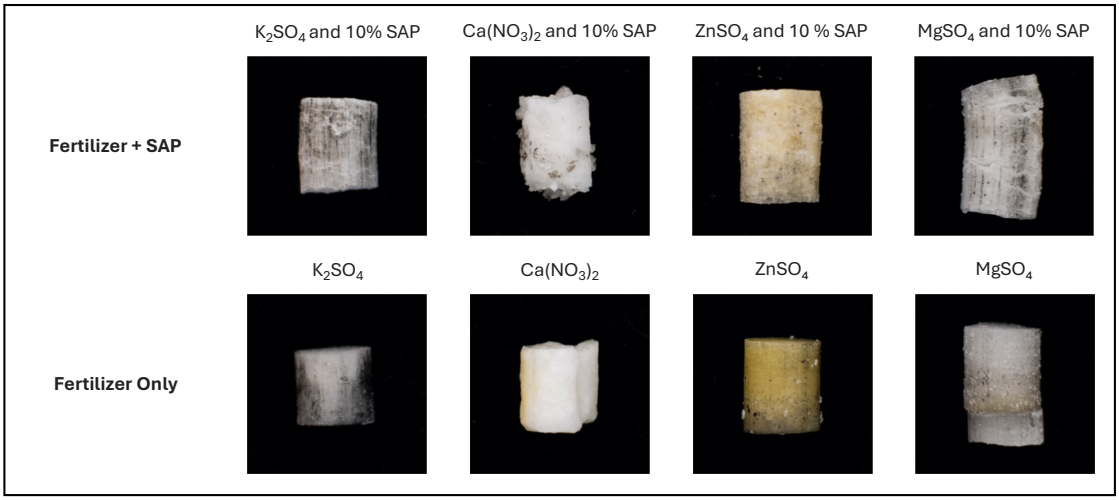

Figure 6: Compacted (Fertilizer + SAP) and (Fertilizer Only).

As macronutrients, K_2SO_4 and $MgSO_4$ were used; and $Ca(NO_3)_2$ and $ZnSO_4$ were used as micronutrients. All fertilizers were purchased from Gübretaş. In the tables below, the compositions of the above-mentioned fertilizers are listed:

Table 2: Chemical Composition of Potassium Sulfate Fertilizer.

Potassium Sulfate - K2SO4					
Atomic Weights			**Atomic Weight Ratios**	**Weight Ratios**	
K (u)	O (u)	K2O (u)	K2O/K	**K (w/w)%**	**K2O (w/w)%**
39.098	15.999	94.195	2.409	**20.8**	**50**
S (u)	O (u)	SO4 (u)	SO4/S	**S (w/w)%**	**SO4 (w/w)%**
32.065	15.999	96.061	2.996	**16.7**	**50**

Table 3: Chemical Composition of Calcium Nitrate Fertilizer.

BESTCALNI - CaNO3					
Atomic Weights			**Atomic Weight Ratios**	**Weight Ratios**	
Ca (u)	O (u)	CaO (u)	CaO (u) /Ca (u)	**Ca (w/w)%**	**CaO (w/w)%**
40.078	15.999	56.077	1.399	**26**	**36.4**
N (u)	H (u)	NH4 (u)	NH4 (u) /N (u)	**N (w/w)%**	**NH4 (w/w)%**
16.007	1.008	20.039	1.252	**1.1**	**1.4**
N (u)	O (u)	NO3 (u)	NO3 (u) /N (u)	**N (w/w)%**	**NO3 (w/w)%**
16.007	15.999	64.004	3.999	**14.4**	**57.6**

Table 4: Chemical Composition of Zinc Sulfate Fertilizer.

Zinc Sulfate (Hydrated) - Zinc Sulfate (Hydrated)					
Atomic Weights				Atomic Weight Ratio	Weight Ratio
Zn (u)	S (u)	O (u)	ZnSO4 (u)		
65.38	32.065	15.999	161.441	ZnSO4.7H2O (u) / Zn (u)	**Zn (w/w)%**
H (u)	O (u)		7H2O (u)		
1.008	15.999		126.105	4.398	**22**

Table 5: Chemical Composition of Magnesium Sulfate Fertilizer.

MAGSUL - MgSO4					
Atomic Weights			Atomic Weight Ratios	Weight Ratios	
Mg (u)	O (u)	MgO (u)	MgO (u) / Mg (u)	**Mg (w/w)%**	**MgO (w/w)%**
24.305	15.999	40.304	1.658	**16**	**26.5**
S (u)	O (u)	SO3 (u)	SO3 (u) / S (u)	**S (w/w)%**	**SO3 (w/w)%**
32.065	15.999	80.062	2.497	**32**	**79.9**

3.4.2.2. Nutrient loading on SAP through swelling

One way of introducing nutrients in SAP structure is a direct approach of allowing already synthesized SAPs to swell with a nutrient solution, and later drying swollen gels in the oven. Since here the interaction between nutrient molecules and SAP is only physical, the retention time of nutrients in the SAP is expected to be short and hence their dissolution in the soil is expected to be rapid. However, this is an extremely simple method of loading nutrients in SAPs, without any required changes in the synthesis procedure.

SAPs were put in zinc sulfate solutions of different concentrations. For each nutrient, 1 gram of SAP was mixed with 0.1, 0.2, 0.3, 0.4, and 0.5 grams of nutrient, in 100 mL of deionized water. After the SAPs were allowed to swell with the nutrient solutions for 2 days, they were dried in the oven at 70 °C for 15 hours.

The color was used as a qualitative property to indicate successful fertilizer loading on SAPs. For example, since zinc sulfate has a yellowish color, the resultant nutrient-SAPs exhibited color change. SAPs swollen with higher concentrations of nutrient solutions

displayed a more yellow color, which is an indicator of a higher nutrient concentration in the SAP-nutrient composite.

3.4.2.3. Nutrient loading during polymerization

In this approach, fertilizer solutions, i.e., commercial micronutrient granules dissolved in deionized water, were added to the polymerization mixture containing monomers, crosslinker, initiator, and solvent. Upon nutrient addition, pH was once again checked. If the pH was out of the 7-8 range, it was adjusted by adding NaOH or acrylic acid. Next, the temperature of the reactor was increased, and polymerization was then allowed to take place as usual, without any alterations to reaction temperature or duration. The resultant solution was poured into ethanol, and nutrient-SAP was precipitated.

For ethanol precipitation, the solid ratio of the polymerization reaction was 5% w/w. Alternatively, SAP could have been obtained through drying after synthesis, in which case the solid ratio would have been raised to 10% w/w.

3.4.2.4. Nutrient loading after polymerization

In the second approach, polymerization was carried out exactly like that of unloaded SAP. The resultant solution was taken out of the reactor and transferred to a beaker. Using 20 mL syringes without the needle, 30 mL of SAP solution was transferred to 6 different beakers. 30 mL of polymer solution contains approximately 2 grams of SAP.

Next, each nutrient was weighed six times according to the following weight ratios.

$$20; 40; 60; 80; 150\ \% \ \frac{Nutrient\ (g)}{SAP\ (g)} = 0.4; 0.8; 1.2; 1.6; 3\ g\ nutrient$$

Aqueous nutrient solutions were prepared at a 1:10 fertilizer:water weight ratio and mixed thoroughly with SAP solutions. The mixtures were cast on Teflon molds and placed in the oven at 70 °C for 18 hours.

Four commercial fertilizers were used: (i) Magnesium sulfate, (ii) zinc sulfate, (iii) calcium nitrate, and (iv) potassium sulfate. All fertilizers were purchased from Gübretaş.

In the first trials, this method was found the be the most effective and practical among the above-mentioned nutrient loading techniques tested. Therefore, in this study, the following syntheses of fertilizer-SAP composites were carried out according to this method. The following sections will describe the subsequent syntheses of nutrient loaded SAPs, and the methods used to evaluate their water absorption and desorption kinetics.

3.4.3. Synthesis of Superabsorbent Polymer - Fertilizer Composites

A copolymer consisting of three monomers was synthesized using by free-radical polymerization. The process involved preparing a polymerization solution by mixing the monomers in deionized water. In a beaker, Acrylamide and AMPS were dissolved in water by magnetic stirring. Acrylic acid was then carefully measured and added to the solution using a micropipette. To adjust the pH of the monomer solution to a range of 7-8, potassium hydroxide was introduced. HNT was gradually added to the mixture while stirring continuously to prevent coagulation. Following the addition of HNT, the pH was readjusted to a range of 7-8, if needed.

The solution was subsequently transferred into a 250 mL three-neck borosilicate 3.3 round bottom flask, using a funnel. Rubber septa were used to seal the two side necks to prevent solvent loss during polymerization. To conserve solvent during polymerization, the reactor was connected to a reflux system with a condensing tube cooled by tap water. Prior to initiating the reaction, nitrogen gas was purged through one of the side necks to minimize oxygen in the reactor. Air was allowed to escape through another needle placed at the end of the reflux system, confirmed by feeling the airflow on the skin and hissing sound.

After a 10-minute purge of nitrogen gas, the crosslinker, vinyltrimethoxysilane (VTMS), was introduced. Purging was continued for an additional 5 minutes, followed by the addition of the initiator, ammonium persulfate (APS). To reduce material loss, VTMS

and APS were mixed with 2 mL of deionized water, then transferred to a syringe and injected into the reaction mixture using a needle inserted through the septa of either side neck. Once APS was added, the temperature of the oil bath was set to 75 °C using a temperature controller with a thermocouple immersed in the oil bath. The controller's timer was set for a duration of 2 hours. Purging was sustained for another 5 minutes, and the reaction proceeded for 2 hours under constant magnetic stirring. Upon completion, the heating was turned off, and the reactor was removed from the oil bath.

In the first approach, nutrient loaded HNTs were used in SAP syntheses. The resultant polymer solutions were precipitated in ethanol. The SAP obtained was cut into small pieces with scissors and dried at 70 °C for 18 hours, where further crosslinking took place. The dried SAP pieces were conserved in falcon tubes. However, as previously noted, nutrient loading on HNT was roughly 2 wt%. Even with a 10 wt% incorporation of HNT in the SAP synthesis, only 0.2 wt% of nutrients could be loaded in the SAP composite.

In the "nutrient loading after polymerization" method, pristine HNT was used in the polymerization reactions. Upon completion of synthesis, the resultant polymer solutions were mixed with appropriate fertilizer-water solutions. In the first trial $20; 40; 60; 80; 150\ \% \frac{Nutrient\ (g)}{SAP\ (g)}$ concentrations were tested. However, the water absorption performance of 150% nutrient/SAP was poor. Therefore, this concentration was eliminated in the following syntheses. 80% and 100% nutrient:SAP composites were replaced with only 100% nutrient:SAP composite. Also, the effect of lower nutrient concentration on the water absorption behaviour of SAP was sought for. Therefore, a new 10% nutrient:SAP composite was added to the list.

The mixtures were poured into rectangular Teflon molds and subjected to further crosslinking during drying in an oven at 70 °C for 18 hours. The dried product in film form was brittle and was manually broken into pieces, which were then stored in closed falcon tubes to prevent moisture absorption.

The following table provides the composition of the synthesized SAPs, including the monomer, KOH, cross-linker, initiator, and solvent contents:

Table 6: Synthesis Parameters for Superabsorbent Polymer

Superabsorbent Polymer Reaction Parameters		
Monomers	**Acrylamide (g)**	9.6
	Acrylic Acid (mL)	10.85
	AMPS (g)	1.92
Nano-filler	**HNT (g)**	1.2
Solvent	**H2O (mL)**	350
Neutralizing agent	**KOH (g)**	0.135
Crosslinker	**VTMS (mL)**	0.48
Initiator	**APS (mg)**	10.7
	Solids Ratio (%)	10
	Temperature (°C)	75
	Duration (h)	2

Table 7: SAP - Fertilizer Composites with Zinc and Calcium Fertilizers

SAP - Fertilizer (Zinc Sulfate and Calcium Nitrate) Composites						
Fertilizer Ratio (%)	**0%**	**9.1%**	**16.7%**	**28.6%**	**37.5%**	**50.0%**
SAP Solution (mL)	50					
SAP Solid Content (g)	5					
Fertilizer (g)	0	0.5	1	2	3	5
Water (mL)	0	2.5	5	10	15	25
Fertilizer:SAP (w:w)	0:1	10:100	20:100	40:100	60:100	1:1

3.4.4. Water and Saline Absorption Performance of Nutrient-SAP Composites

Nutrient-loaded SAP composites were evaluated for their water and saline absorption capacities. All samples were prepared in triplicates. Each replicate consisted of 0.15-0.2 grams of SAP placed in a beaker filled with 250 mL of deionized water. Prior to starting the test, the empty weights of the beakers and the precise weights of the SAPs were recorded on a label. To determine the weight of the swollen gel, the contents of the beaker

were emptied into a plastic sieve. Any excess water was eliminated by scraping the sieve's bottom using a spoon spatula. The gel was then placed back into the beaker and weighed. By subtracting the initial weight of the empty beaker from this measurement, the weight of the swollen gel was obtained.

The water absorption ratio was determined by dividing the weight of the water absorbed by the gel by the initial dry weight of the SAP. The formula used for this calculation is as follows:

$$Water\ Absorption\ (g/g) = \frac{W_g - W_i}{W_i}$$

$$W_g: weight\ of\ swollen\ gel, W_i: initial\ weight\ of\ SAP$$

In the first approach, the SAPs were obtained in a relatively large granular shape, with a low surface area. To achieve better water absorption performance, the SAPs were ground using ceramic mortar and sieved to 1 mm.

In the second approach, the SAPs were obtained in thin film form. For water absorption tests, these samples were cut into one or more pieces by hand, to match approximately 0.2 grams.

3.4.5. Nutrient Release Kinetics

Conductivity can be used as a representative measure of the nutrients released into a solution. Therefore, to deduce nutrient release kinetics, we monitored the conductivity of the water solution in which nutrient-SAP composites were allowed to swell freely. Both calcium nitrate and zinc sulfate-loaded SAP composites were evaluated.

Approximately 0.1 grams of SAP sample was placed in a beaker containing 250 mL of distilled water. Three replicates were prepared for each sample. On the first day, measurements were taken after 30 minutes, 1 hour, 2 hours, and 4 hours. The subsequent conductivity data were recorded after 1, 2, 3, 4, and 7 days.

The nutrient release kinetics of composite SAPs with varying levels of calcium and zinc nutrient concentrations were evaluated. The nutrient release kinetics were deduced from the conductivity of the solutions in which the SAPs are allowed to swell.

3.5. Bio-Based Superabsorbent Polymers

In many of the literature studies, biomaterial addition to the SAP composition is limited, e.g., 5-10 wt.%. On the other hand, there are reports on fully bio-based or mostly bio-based SAPs. (H. J. Kim et al., 2017; Lacoste et al., 2019; Neamjan et al., 2019; Patiño-Masó et al., 2019) However, the swelling capacities of those polymers are in the range of 10 to 100, and hence they are not suitable for agricultural applications. In our study, we successfully integrated carboxymethyl cellulose (CMC) into SAP matrix, at a weight ratio of up to 50%, in acrylate-based SAP, while maintaining similar water absorption capacity compared to synthetic SAPs.

The synthesis procedure was almost identical to the one used in non-CMC SAP. Cellulose was added to the reaction mixture upon pH adjustment. In some trials, HNT was added along with cellulose. Maximum swelling rates of cellulose-SAPs were comparable to that of regular SAPs throughout different cellulose percentages. However, especially SAPs that contained 40 and 50 wt.% cellulose were not able to retain water in their structure for an extended period, due to mechanical failure after approximately one week. Altering the initiator and crosslinker ratios of these hybrid SAPs and including HNT along with cellulose in the SAP in the synthesis reaction are different approaches that we are testing to improve the mechanical properties of these SAPs and to prolong the water retention duration.

In the literature, there are studies on SAPs containing biomaterials, including cellulose. However, the studied formulations either contain very small amounts of cellulose, around 5 wt%, and have good water absorption, or they are almost entirely bio-based, but their water absorption capacities are very low, around 10 times their own weight, which is not

suitable at all to be used in diapers or for agriculture. Almost all such studies up to date report only one or two SAP formulations. In this study, we wanted to understand how varying the CMC content in the SAP affects the material properties, water absorption performance, and biodegradability. To achieve this, we successfully synthesized and tested 7 CMC-SAP formulations.

Our aim in this study is to develop an SAP using more sustainable raw materials and prevent polymer contamination in agricultural lands due to their use. To do so, we incorporated a bio-based material, carboxymethyl cellulose, in an otherwise synthetic SAP formulation described in the patent application PCT/TR2021/050162, "A polymer matrix based superabsorbent material", to improve its biodegradability, while maintaining, and even improving its water absorption characteristics. We synthesized 7 different bio-based SAPs, containing 5 to 60 wt% CMC. Their water absorption capacities, and biodegradability are discussed in this paper, along with their surface morphologies.

3.5.1. Synthesis of CMC-Based Superabsorbent Polymers

A copolymer of three monomers was synthesized through free-radical polymerization. To prepare the polymerization solution, first, the monomers were mixed in deionized (DI) water. Acrylamide and AMPS were weighed and transferred to a beaker. The appropriate amount of DI water was added, and monomers were dissolved by magnetic stirring. Next, the appropriate amount of acrylic acid was measured by a micropipette and transferred into the reaction media. Next, the pH of the monomer solution was brought to between 6-7 by adding potassium hydroxide. Subsequently, carboxymethyl cellulose (CMC) was added very slowly to the mixture, under constant stirring, to prevent coagulation. After the addition of CMC, the pH of the solution was adjusted again to between 7-8. Next, the solution was transferred into the reactor.

The reactors used in this study were 250 mL three-neck round bottom flasks made from borosilicate 3.3. The polymerization mixture was poured from the wider top neck, with the help of a funnel. Next, the two side necks were closed with rubber septa. In order not to lose the solvent during polymerization, the reactor was connected to a reflux system,

which incorporated a reflux condensing tube cooled with running tap water. Upon setting up the reaction system, nitrogen gas was purged with the help of a needle, from one of the side necks, to minimize the oxygen present in the system. The air inside was allowed to discharge by placing another needle at the end of the reflux system. Gas flow at the discharge needle was checked by feeling the airflow on the skin and hearing the hissing sound.

After 10 minutes of nitrogen gas purging, the crosslinker, vinyltrimethoxysilane (VTMS) was added. Next, purging was continued for 5 minutes, after which the initiator, ammonium persulfate (APS), was added. To minimize material loss, both VTMS and APS were mixed with 2 mL of DI water, transferred to a syringe, and added with the help of a needle, from either of the side necks, by injecting the needle through the septa. Upon APS addition, the temperature of the oil bath was set to 75 °C, through a temperature controller with its thermocouple immersed in the oil bath. The timer on the controller was set to 2 hours. Purging was continued for another 5 minutes, and the reaction was allowed to take place for 2 hours, under constant magnetic stirring. Once complete, the heating was shut down and the reactor was brought out of the oil bath. The polymer solution was poured into a rectangular Teflon mold and dried in a drying oven, at 70 °C, for 18 hours, where further crosslinking took place. Once dry, the product becomes brittle and breaks easily. The product was broken by hand and placed in closed falcon tubes, to prevent any moisture absorption.

Generally, to increase efficiency, three reaction systems were set up in parallel, and three polymerization reactions with different synthesis parameters were initiated consecutively.

In the table below, the monomer, CMC, KOH, cross-linker, initiator, and solvent contents of the synthesized SAPs are listed:

Table 8: Synthesis parameters of carboxymethyl cellulose - superabsorbent polymers.

Reactants	Carboxymethyl Cellulose - Superabsorbent Polymers							
	Control	5% CMC	10% CMC	20% CMC	30% CMC	40% CMC	50% CMC	60% CMC
Acrylamide (g)	2							
Acrylic Acid (mL)	2.38							
AMPS (g)	0.4							
KOH (g)	2.1							
H20 (mL)	50	53	56	63	72	84	101	150
CMC (g)	0	0.265	0.56	1.26	2.16	3.36	5.04	7.55
VTMS (mL)	0.1							
APS (g)	0.03							

Reaction Duration:	2 hrs after APS	**Nitrogen Purging:**	10 mins before VTMS
Reaction Temperature:	75 °C		5 mins before APS
			5 mins after APS

As can be seen from the table, only the CMC and solvent quantities were changed throughout different formulations. This was done to deduce the effect of increasing only the CMC content would have on the physical properties and performance of SAPs.

When planning the syntheses, the quantity of potassium hydroxide (KOH) that would be required to bring the pH of the polymerization mixture to a level between 7 and 8 was not known. Therefore, the CMC ratios to be tested were determined by taking the other reactants into account – monomers, crosslinker, and initiator. So, the actual CMC ratio is lower than what is written in the name of the samples. Since the initiator and crosslinker quantities are almost negligible, the CMC percentages in the names represent weight percentages of CMC within total monomer weight. For example:

$$20\%\ CMC = \frac{CMC\ (g)}{Acrylic\ Acid\ (g) + Acrylamide\ (g) + AMPS\ (g) + CMC\ (g)}$$

$$= \frac{1.26\ g}{2\ g + 2.5\ g + 0.4\ g + 1.26\ g} \times 100\% = 20.5\ wt\%\ CMC$$

3.5.2. Water and Saline Absorption Performance of CMC-Based Superabsorbent Polymers

The absorption capacities of CMC incorporating bio-SAPs were tested in deionized water and saline solution. The CMC-SAPs continued to absorb and retain more water over a long period of time. Therefore, the swelling test was conducted over a period of six months. Measurement frequencies were lower in the later stages of the test. In literature, most SAPs reach an equilibrium swelling in a matter of days, and they are not tested beyond that stage.

All samples were tested in triplicates. For each replicate, approximately 0.2 grams of SAP in film form was placed in a beaker, and 250 mL of DI water was poured into each beaker. Before initiating the test, the empty weights of the beakers and the exact weights of the SAPs were noted on a label. To measure the weight of the swollen gel, the contents of the beaker were poured into a simple plastic sieve. By scraping the bottom of the sieve with a spoon spatula, the excess water was removed. The remaining gel was poured back into the beaker and weighed. The weight of the gel was calculated by subtracting the empty beaker weight from this measurement.

For saline absorption tests, a 0.9% w/v of NaCl solution of water was prepared. The other parameters of this test were the same as that of water absorption tests.

The water and saline absorption ratios were calculated by dividing the weights of the liquid absorbed by the gel by the initial dry weights of the SAPs. The relevant formula is shown below:

$$Absorption\ (g/g) = \frac{W_g - W_i}{W_i}$$

$$W_g: weight\ of\ swollen\ gel, W_i: initial\ weight\ of\ SAP$$

3.5.4. Biodegradability of CMC-Based Superabsorbent Polymers

The first purpose behind using CMC in SAP synthesis is to make use of renewable natural resources and hence impart sustainability to the product. Many polymeric materials are used in agriculture, and they pose a waste problem after they finish serving their purpose. A common example is PE-based mulch films, which are used extensively for crops like tomatoes and strawberries to prevent contamination of the crops, suppress weeds and conserve soil moisture. They are useful during the growing season and no longer needed after the harvesting season. Ideally, they should be collected by the farmers and properly recycled. However, almost all mulch film is left on the field after harvest, as collecting it is an additional labor cost for the producers. Accumulated film over time results in microplastic contamination. Currently, there are a few companies that produce biodegradable mulch film, which is hoped to alleviate the current plastic accumulation problem. Similar to PE films, superabsorbent polymers also pose a waste concern. Moreover, since SAP is applied in the soil rather than on top of the soil, it is virtually impossible to collect it from the field after harvest. SAPs are generally regarded as safe and non-toxic for animals; however, the long-term potential harmful effects of SAPs in the soil have not been studied extensively. Therefore, it would be the best practice to improve the biodegradability of SAPs in soil. This is the second reason behind using CMC in SAP synthesis.

3.5.4.1. Testing biodegradability in soil

Soil consists of three major components. Inorganic mineral matter makes up roughly 45% of total soil volume. Water and air constitute 50%, and organic matter accounts for only the remaining 5% of total soil volume. (McClellan, n.d.) Soils are classified according to their horizons. In this regard, soil layers are named (i) O horizon, (ii) A horizon, (iii) B horizon or subsoil, and (iv) C horizon or soil base. The O horizon is approximately 5 cm deep, and it constitutes freshly decomposing organic matter. At its base, there is decomposed vegetation. Horizons O and A are rich in humus, which is responsible for enriching the soil with nutrients, and aiding moisture retention. A horizon, also called the topsoil, is rich in organic material, such as dried leaves, grasses, and surface organisms such as earthworms, fungi, and bacteria. Seed germination and microbial processes takes

place in this layer, and thus it is called the “workhorse” of plant production. These top 2 layers have a dark color, due to high organic content. (VORONEY, 2007)

For soil biodegradation test, top 10 cm of the soil, collected from Kemerburgaz / Istanbul, was used, which consists of the O and the A horizons. Due to high organic content and microbial activity, SAPs can biodegrade in these layers. At the end of the biodegradation test, a logical method of separating the soil from the SAP is washing the soil with water, on a sieve. For this method to work, the soil size should be smaller than the sieve diameter. To facilitate size reduction, the soil was placed on a table in a greenhouse and let dry for two days. Later, the soil was crushed into smaller pieces with a rolling pin.

Figure 7: Drying (left) and Grinding (right) of Soil from Organic Layer.

Subsequently, the dried and crushed soil was passed through a sieve with an opening of approximately 3 mm.

Figure 8: Sieving of Dried and Ground Soil by a Coarse Sieve (3 mm).

Figure 9: Dried and Ground Soil Sieved to < 3 mm.

After this rough size reduction, the soil was sieved once again with a lab-scale sieve shaker. The soil was passed through sieves with 2 mm, 1 mm, and 60 um, and 10 um openings. The soil that did not pass from the 2 mm or 1 mm sieves were discarded. Only the soil that has passed from the 1 mm sieve was used.

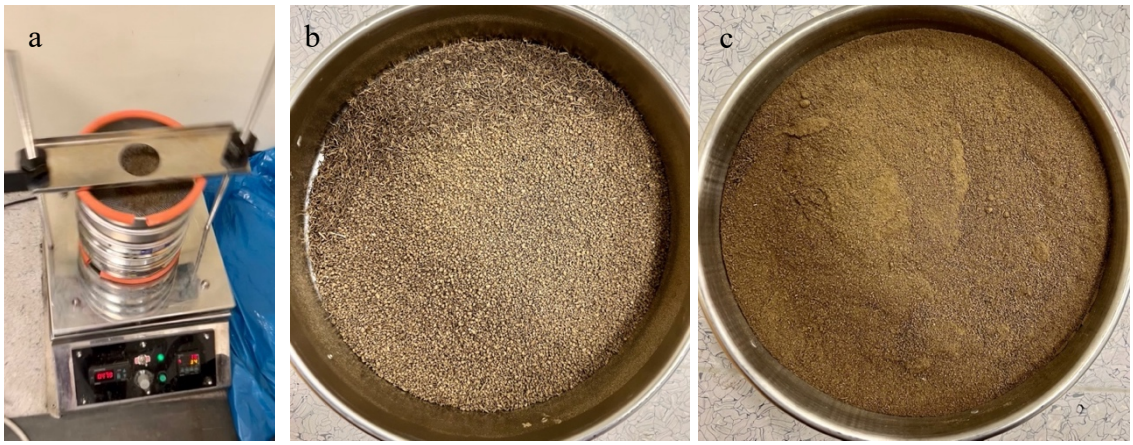

Figure 10: (a) Lab-Scale Sieve Shaker, (b) Soil Sieved to < 2 mm, (c) Soil Sieved to < 1 mm.

To assess the level of biodegradation, approximately 0.2 grams of 8 CMC-SAPs and 1 control SAP were placed in pots filled with 300 grams of soil. First, pots were filled with 100 grams of soil, then the SAPs were placed, and the remaining soil was added over the SAP.

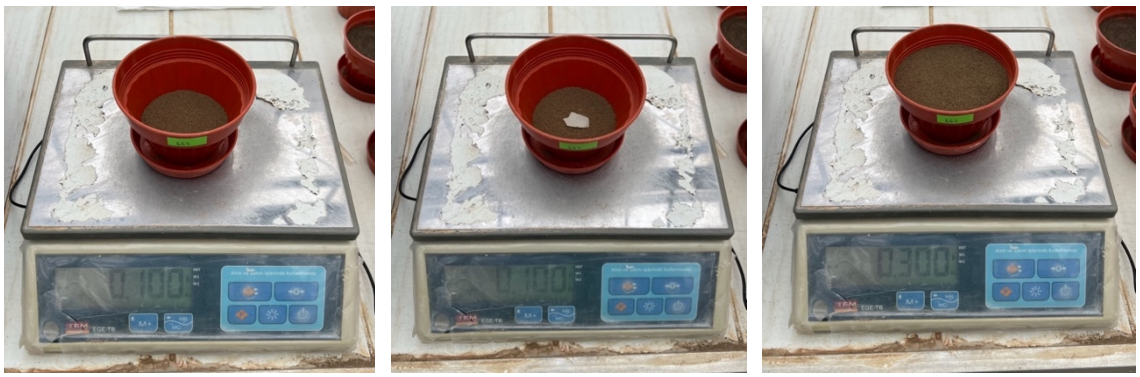

Figure 11: Preparation for Soil Biodegradation Test - 300 grams of Soil and 0.2 grams of CMC-SAP.

Swollen SAPs were extracted from the pots at the end of 3, 6, 10, and 15 weeks, to assess biodegradation kinetics. For each time test, triplicates were prepared per SAP formulation, and the weights of all SAPs were recorded before the test. Therefore, 12 replicates for each CMC-SAP formulation, totaling 108 pots, were used in this study. At the beginning of the test, all pots were irrigated to 80% of field capacity.

Field capacity denotes the amount of water that a soil can hold, without leaking. To measure field capacity, a pot with holes on the bottom, was filled with a known amount of soil, which was 300 grams in this case. The initial weight of the filled pot recorded. Later, the pot is irrigated until water starts leaking from the bottom holes. Then, it is waited for leaking to stop, and the pot is weighed again. The difference between the final and initial weighs represents the amount of water that 300 grams of soil can hold, which is the field capacity. In this experiment, field capacity was roughly 140-145 mL per 300 grams of soil. Therefore, 80% of field capacity corresponds to 114 mL of water per pot.

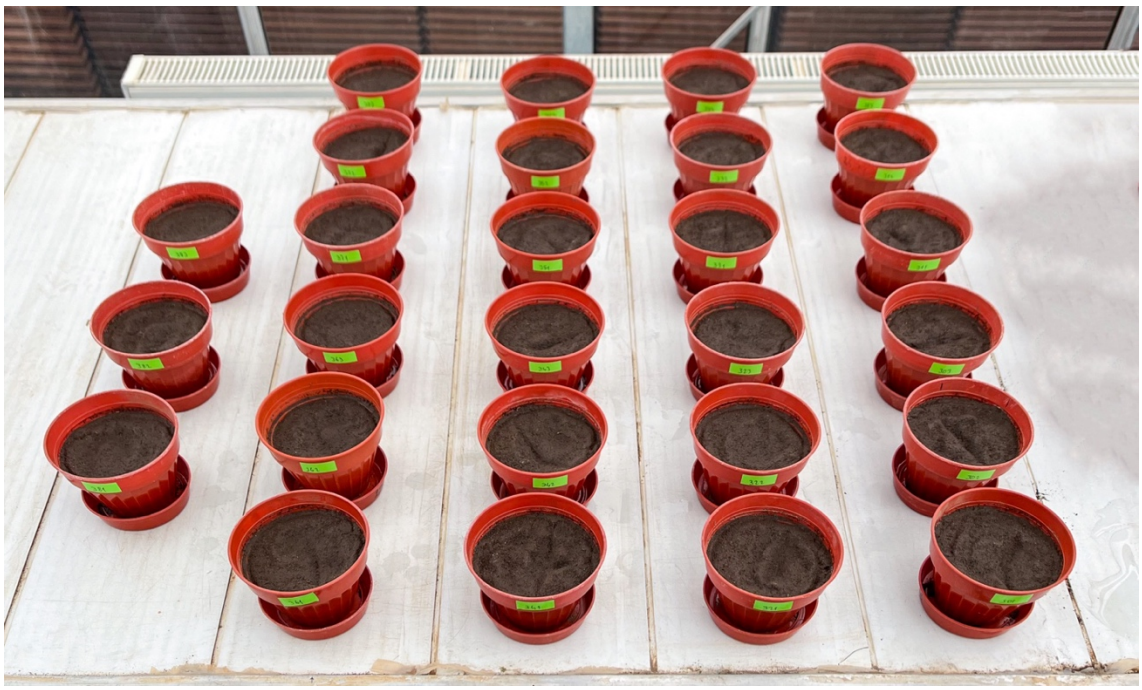

Figure 12: Pots Containing Soil and SAP for Soil Degradation Tests.

3.5.4.2. Enzymatic degradation of CMC-Based Superabsorbent Polymers

Various microorganisms, such as fungi and bacteria, are known to have plastic degrading capabilities, owed to certain enzymes found in these organisms. Such microorganisms use plastics as their only carbon source, and can live on plastic waste, under ideal conditions. Microorganisms first cause a reduction in polymer size, degrading them into monomers. Monomer units are absorbed into the microbial cells, where they undergo enzymatic degradation. This degradation process can be accelerated by first treating the plastics through heating, cooling, freezing, thawing, and chemical degradation, to break down the polymer into monomer units. The end products of enzymatic degradation of polymers include CO2, H2O, CH4, N2, and other metabolic products. CH4 is a biogas, which can be used as a fuel to produce light and heat; and it is also used in the production of certain organic acids. (Mohanan et al., 2020; Nyyssölä & Ahlgren, 2019)

Enzymes are biocatalysts that act on a specific substrate by accelerating the conversion of that substrate to end products. Polymers are absorbed by microbial cells. The extracellular and intracellular enzymes found in certain microbial cells can degrade

polymers. Various enzymes have been extracted from algae, bacteria's, actinomycetes, and fungi that are already known to degrade different kinds of plastics. All enzymes that degrade plastic polymers are members of the class "Hydrolases". Common examples include cutinase, lipase, esterase, and glycoside. Enzymes in this class function in the presence of water. They cause hydrolytic cleavage of the long carbon chains. Smaller polymeric units are then absorbed into microbial cells where further enzymatic degradation takes place, and metabolic products are released. (Kaushal et al., 2021) Certain types of fungi secrete cellulase, which belong to the glycoside hydrolases family and work by cleaving the β-1,4-glucan bonds in cellulose. (J. Chen et al., 2022)

To mimic the microbial activity in soil, and to fortify SAP degradation, cellulase enzymes from Novozyme were used to degrade CMC incorporating SAPs. To assess the cellulase degradation of CMC-based SAPs, a modified version of the method described in the article of Fujita et. al. was used. (Fujita et al., 2022) Enzymes were kindly provided by Prof. Günseli Bayram Akçapınar from Acıbadem University. To dissolve the cellulase enzyme and contain the SAPs, a buffer solution was prepared. For this experiment, a 50 mM sodium acetate buffer was prepared, and its pH was brought to between 5.25 by the addition of acetic acid. Later, this solution was transferred to a glass container, which was sterilized in an autoclave at 121 °C for 20 minutes. Biodegradation tests were carried out in 15 mL, sterilized falcon tubes. In each tube 9.8 mL of buffer solution and 0.2 mL of cellulase enzyme were added, which translates to 2% v/v enzyme. For each test, approximately 0.2 grams of SAP was used.

SAP samples to be used in the biodegradation tests were prepared in a standardized way. Previously, for water absorption tests, all samples were cut out from sheets of SAP, dried in rectangular Teflon molds. Thus, each test beaker contained varying numbers of sample pieces, with inevitably different shapes. A standard sample preparation was desired to overcome any discrepancies between the biodegradation tests across samples. To achieve this, a Teflon mold was used, which was originally designed to cast dog-bone-shaped samples for mechanical tests. It contains 24 1 cm x 3 cm dog-bone shaped cavities. Each cavity holds approximately 2 mL of solution. After the polymerization reaction was complete for each CMC-SAP formulation, 2 mL of the polymer solution was poured in each cavity of the mold. The mold was then transferred to a drying oven at 70 °C for 18 hours. Once dried, they were placed in 50 mL falcon tubes.

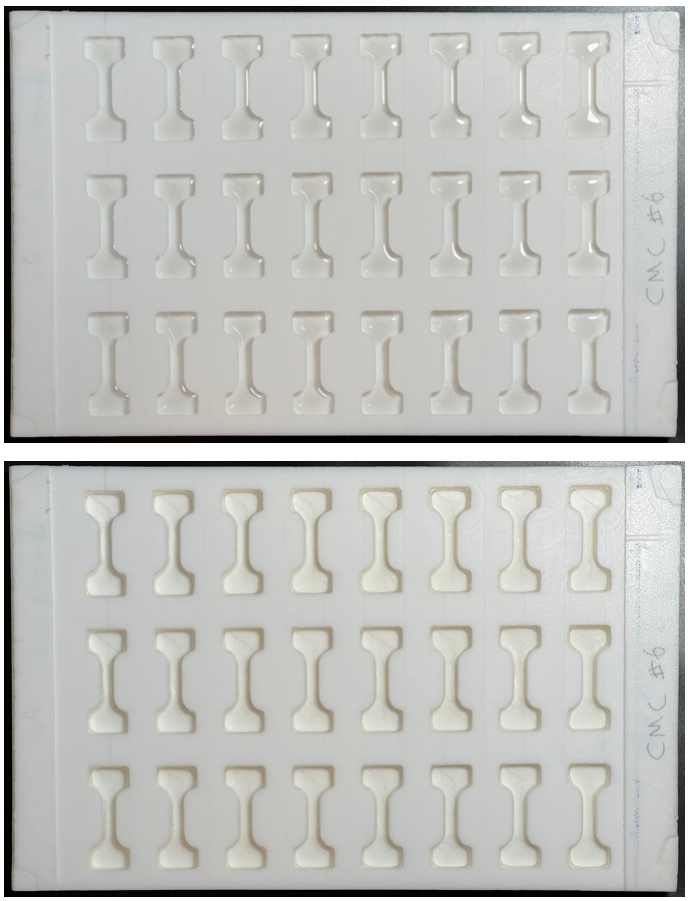

Figure 13: Biodegradation samples (top) after polymerization, and (bottom) after drying.

Measurements were taken after 1 day, 2 days, 3 days, and 5 days. All temporal biodegradation tests were performed in triplicates. Falcon tubes containing the SAP and enzyme were shaken constantly at 150 rpm in a heated incubator. The temperature was set at 50 °C for the complete duration of the test, to activate the cellulase enzyme.

It is not straightforward to convert the degradation time in enzyme containing buffer solution to the expected degradation time in soil. However, determining the correlation between the cellulose content of the SAPs and their degradation kinetics is sought-after outcome from this test.

Figure 14: SAP sample in falcon tube (left), and biodegradation test setup in incubator (right).

3.5.5. Morphology of CMC-based Superabsorbent Polymers

The morphological properties of CMC-SAPs were evaluated through Scanning Electron Microscopy (SEM). An accelerating voltage of 5 kV was used, and the working distance was kept close to 8 mm. Since our aim was to inspect the topography of the samples' surface, the CMC-SAPs were viewed by using secondary electron detection.

Chapter 4

RESULTS AND DISCUSSION

4.1. Superabsorbent Polymers

4.1.1. Scale-Up of Superabsorbent Polymer Synthesis

The main purpose of this study was to develop novel superabsorbent polymers (SAPs) for use in large-scale commercial agriculture. To persuade farmers to embrace new technologies on the field, it is very important that the product or service offers significant economic advantages. Moreover, farmers place great importance on solid results, not only from small-scale greenhouse trials but also from large open fields. Therefore, for a technology to achieve commercial success in large-scale agricultural settings, it must first demonstrate adaptability to large-scale production. The daily production capacity plays a critical role in ensuring the economically viable production of SAPs.

In the initial experiments, the SAP polymerization reaction consisted of 5 wt% solids, and the polymer solution was precipitated in ethanol after the reaction was complete. This method had some drawbacks in terms of production efficiency and economic feasibility.

Firstly, precipitation in ethanol is an extra step, which utilizes extra resources and prolongs total production time. If this method were to be used at a large-scale SAP production, ethanol used for precipitation should be filtered and brought back to the

production line. A filtration system would also be an extra burden for such a facility. Thus, the elimination of the precipitation stage altogether can have significant economic benefits.

Secondly, if the solids ratio of the polymerization reaction is increased beyond 5 wt%, for the sake of increasing the efficiency of SAP production, the precipitation stage becomes cumbersome. The viscosity of the polymer solution is increased, and precipitation becomes less effective. Thus, more ethanol needs to be used. However, to make the SAP production more efficient, the output needs to be increased.

In polymerization systems, increasing the concentration of solids in the reaction is an effective and cost-efficient approach to boost production. This method allows for greater output without the need to expand reactor capacity, resulting in reduced energy and labor costs per unit of polymer produced. However, augmenting the monomer-to-solvent ratio presents certain challenges. Specifically, since the reaction is a free radical polymerization, a higher monomer concentration intensifies the gel effect, and causes it to manifest itself earlier in the reaction. Premature gelation leads to a higher proportion of unreacted monomers, limiting further polymer chain growth and yielding a lower average molecular weight. In the context of superabsorbent polymers, shorter chains are less favorable for optimal water absorption capabilities.

4.1.1.1. Near bulk polymerization of SAP

First, near-bulk polymerization was tested. The major drawback of this method was that the resultant polymer was highly viscous and had to be manually taken out of the reactor, instead of being poured out in a liquid state.

The SAP samples from the initial trials exhibited satisfactory water absorption performance, capable of absorbing water up to 600 times their own weight. Encouraged by these results, subsequent reactions were conducted in larger reactors. Initially, a 250 mL beaker served as the reactor, also lacking a reflux system. The setup closely resembled the one involving the PE cup. The most labor-intensive aspect of this reaction was the removal of SAP from the glass beaker. Following initial cleaning, the beaker was filled

with water, enabling the remaining SAP on the glass surface to swell and facilitating easier removal the next day. In contrast, the PE cup could be easily cut off after synthesis and did not adhere to the SAP, unlike the glass beaker.

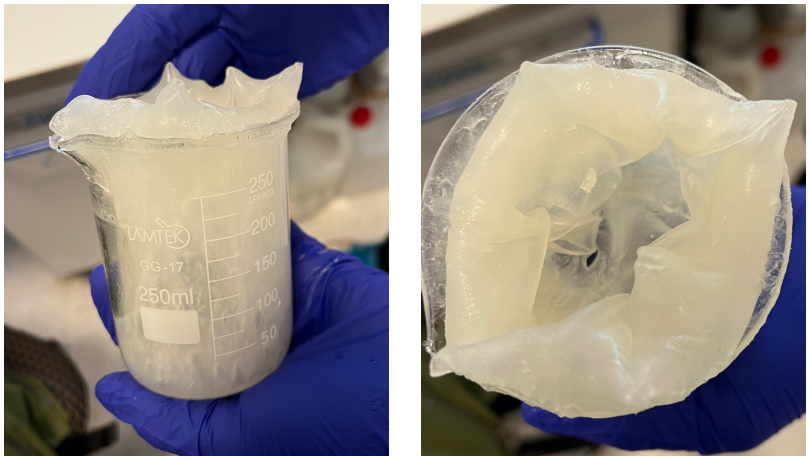

Figure 15: SAP Stuck to the Glass Beaker after Near Bulk Polymerization.

One of the challenges encountered in near-bulk polymerization was the pronounced gel effect. This phenomenon was first observed from the shape of the SAP at the end of the reaction in the 250-mL beakers. Due to the exothermal nature of radical chain polymerization, the solvent (water) readily evaporated, resulting in a mushroom-like explosion of the polymerization solution. This effect was even more pronounced and observable in the larger 3-liter reactor. Once the explosion occurred, the polymerization was effectively completed, often within one hour or even sooner. In contrast, with previous dilute formulations, the reaction was maintained at 75 °C for 2 hours.

4.1.1.2. Polymer solution casting of SAP

Near-bulk polymerization of SAP proved risky due to gel effect and subsequent explosion of the reaction solution. Therefore, the solid content of the polymerization reaction was lowered to a more modest ratio and the resultant solution was cast after polymerization and dried in an oven, thereby eliminating the ethanol precipitation stage.

Considering ease of handling polymer solution after reaction and drying time, 10-12 wt.% was found to be the optimum solid content of the polymerization reaction. This solids

content both shortened the drying time and allowed the solution to flow smoothly after the reaction was completed.

Further increasing the solid content resulted in an even shorter drying time, however, the increased viscosity hindered the flow of the polymer solution out of the reactor.

4.1.2. Effect of SAP Size on Water Absorption Characteristics

The effect of SAP size on water absorption behavior was analyzed by grinding SAPs to 4 different sizes and recording their swollen gel weights with time. S, M, L, and XL grind size denotes 0-2 mm, 2-3 mm, 3-4 mm, and 4-5 mm, respectively.

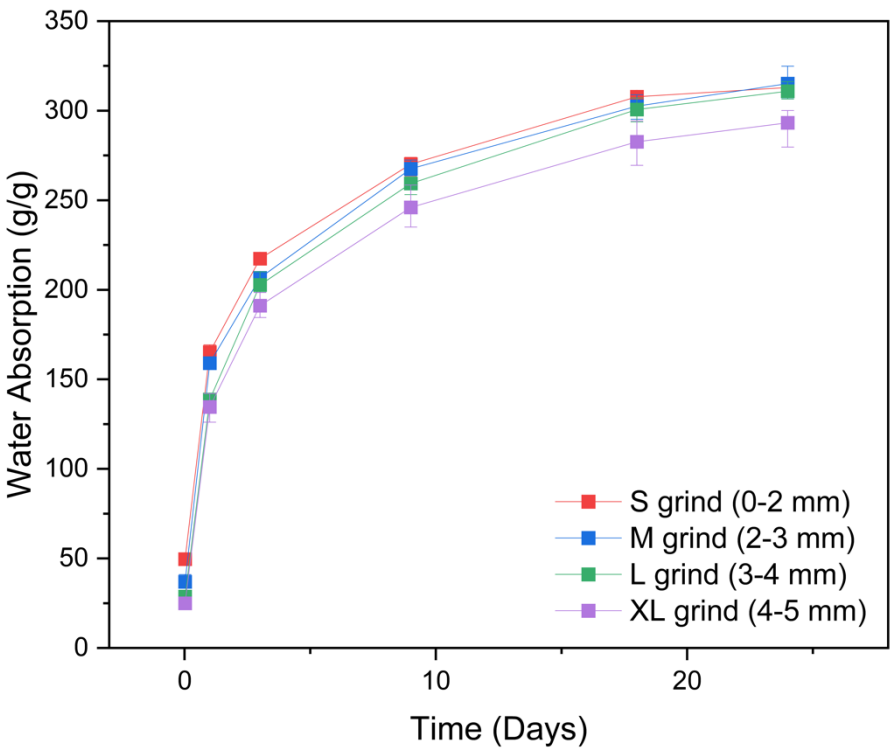

As expected, as SAPs are reduced in size, they absorb water more quickly compared to larger-sized ones. In fact, for the first week, it was observed that swelling ratios are exactly inversely related to size. After three weeks, S, M, and L grind samples reached similar swelling ratios; however, XL grind retained lower water absorption ratios throughout the end of the test, at 24 days.

Since the data points belonging to the first day overlap on this plot, a zoomed-in version is also included, which shows data for only up to 3.5 hours. Here, the difference in water absorption capacities can be seen more clearly.

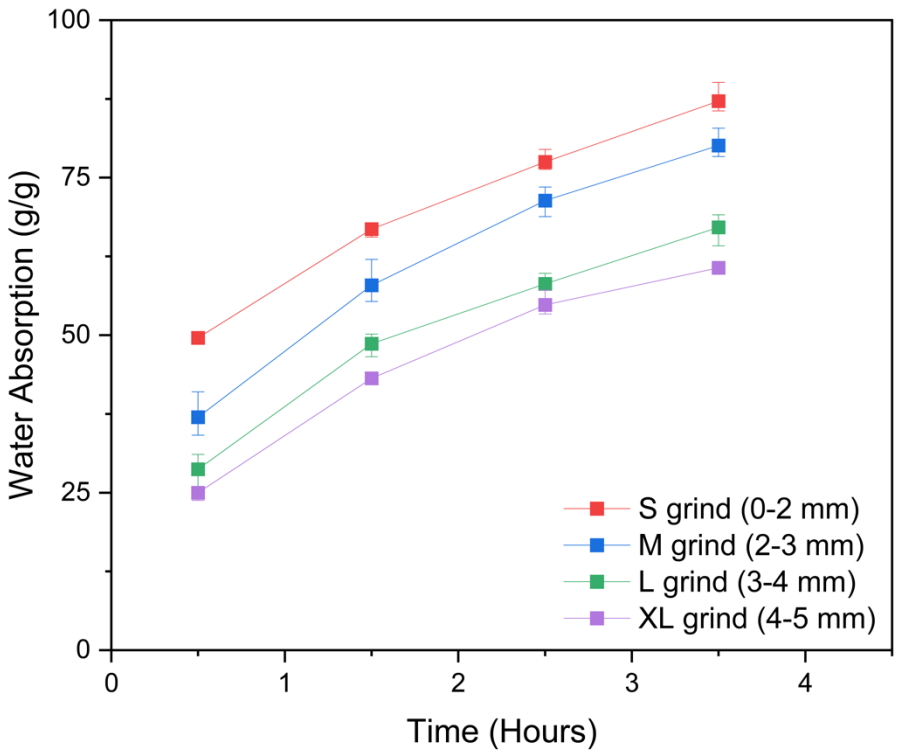

In agricultural applications, the use of powder-like, i.e., smaller-sized, granules can become airborne. Due to this, they pose a risk of being transmitted to unwanted parts of the field and result in potential environmental pollution. Moreover, since the usual plant growth durations are several months, a higher water absorption performance on day one is not a significant advantage. Furthermore, it requires more energy to break down the SAP into smaller granules. Therefore, an SAP granule size of 3-4 mm is ideal for agricultural applications. The main limitation here is the size requirements of the specific seeder equipment machine to be used, such as regular or no-till drills, pneumatic drills, or others.

4.1.2. Rheological Properties of SAP and SAP-HNT

To understand the effect of halloysite nanotube addition on the mechanical properties of the SAP, strain sweep rheology tests of pristine SAP and halloysite-SAP were performed and are presented below:

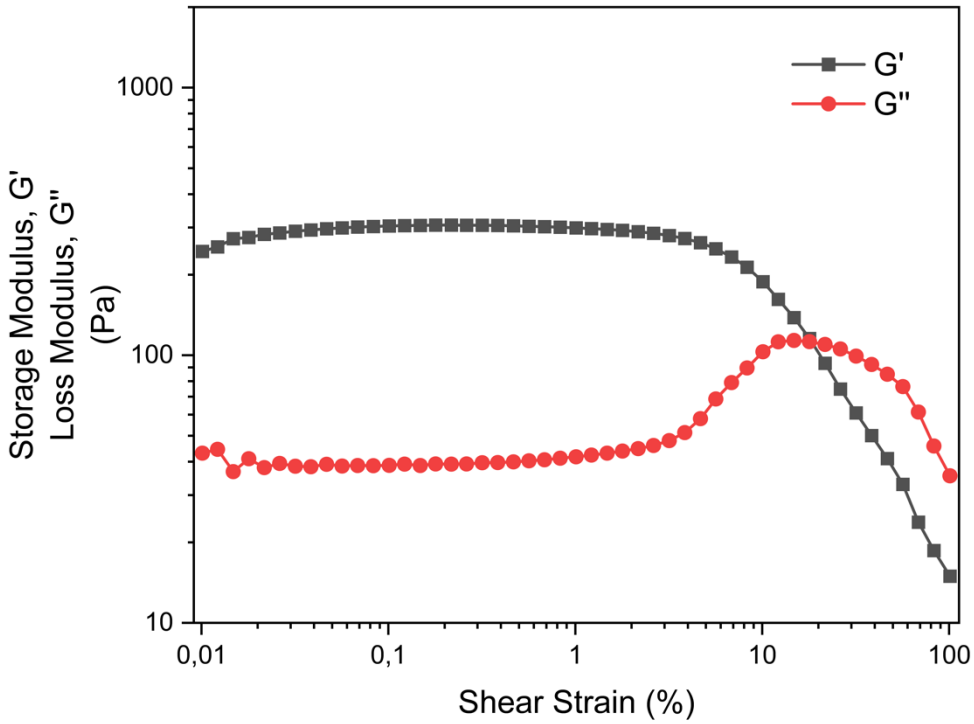

Figure 16: Strain dependence of the G' and G" at a constant angular frequency (1 rad/s) for the swollen pristine SAP sample.

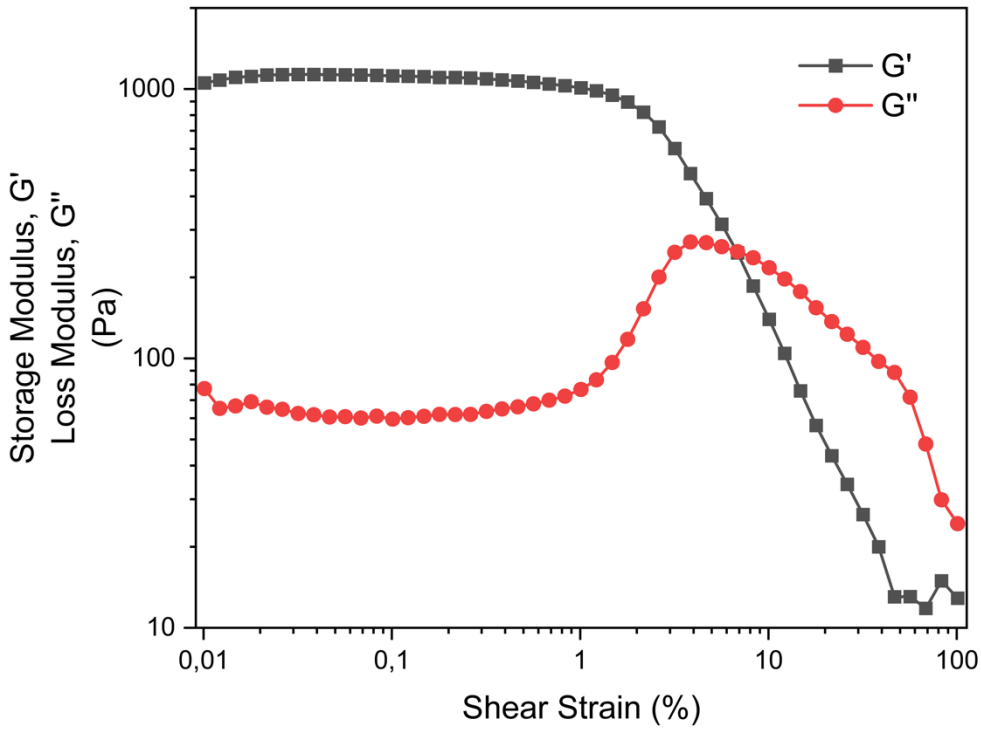

Figure 17: Strain dependence of the G' and G" at a constant angular frequency (1 rad/s) for the swollen halloysite-SAP sample.

From the strain sweep tests, conducted both at the same frequency of 1 rad/s, it was observed that the addition of halloysite nanotubes significantly increased the storage and loss moduli of superabsorbent polymer. In the LVE region, the maximum storage modulus of pristine SAP reached 306 Pa, whereas that of the halloysite-integrating SAP nanocomposite used in this study reached 1134 Pa. A mere 5 wt% incorporation of halloysite nanotubes in the polymer network allowed for approximately a 3.7-fold improvement in storage modulus. HNT also increased the loss modulus, albeit to a smaller extent. The loss modulus of pristine SAP was in the vicinity of 40 Pa throughout the LVE region, whereas that of the halloysite-SAP was approximately 62 Pa. This represents a more than 1.5-fold increase.

If the storage modulus of a material is higher than its loss modulus, it is regarded as an elastic material. The storage moduli of both superabsorbent polymer samples tested in this study are significantly higher than their loss moduli. Therefore, both SAP samples can be classified as highly elastic. The loss factor, or damping factor, is the ratio of the loss modulus to the storage modulus. A small loss factor indicates elastic behaviour, and most of the energy is stored in the superabsorbent polymer network as elastic potential energy.(H. Chen et al., 2016) The SAP with halloysite nanofillers, has a loss factor of

0.055, whereas pristine SAP has a loss factor of 0.131. HNT-SAP can store approximately 95% of applied energy as elastic potential energy, whereas this ratio is 87% for pristine SAP. Therefore, it can be said that HNT-SAP is more elastic compared to pristine SAP.

4.2. Efficient Use of Plant Protection Products (PPP) and Nutrients

4.2.1. Surface and Topography Characterization of HNT

Two HNT samples were generously provided to us by Eczacıbaşı ESAN: the unpurified, or standard, HNT sample, and the purified HNT sample. To evaluate their surface topographies, tube dimensions and pore volume distributions, both samples underwent SEM and BET characterizations.

4.2.2. SEM Analysis of HNT

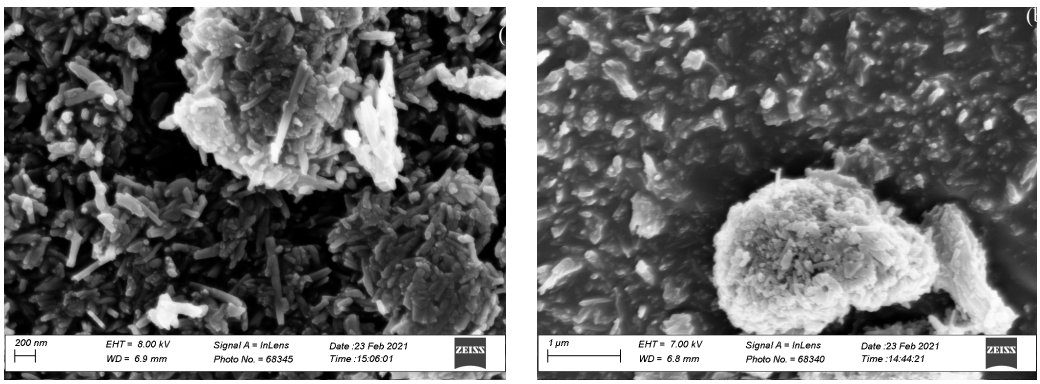

Figure 18: SEM Images of ESAN (a) unpurified HNT, and (b) purified HNT.

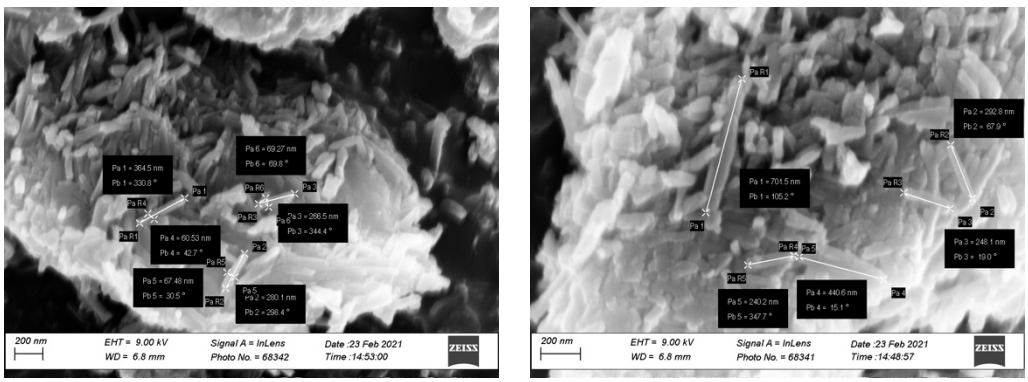

Figure 19: SEM images showing length and diameter of unpurified HNT.

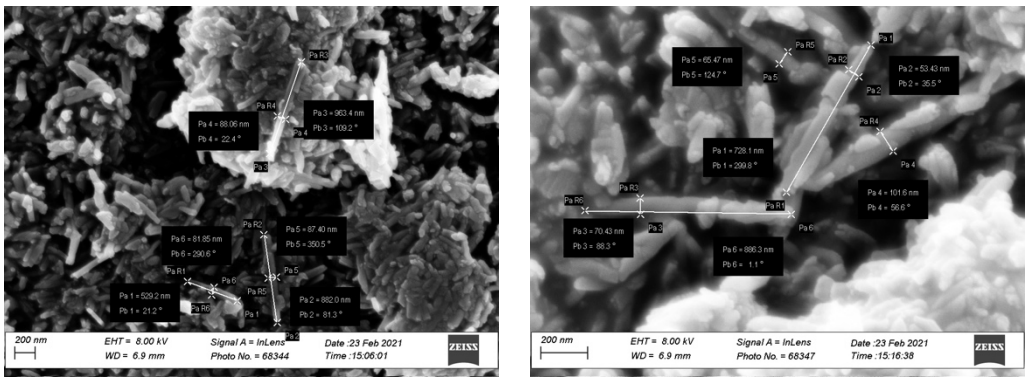

Figure 20: SEM images showing length and diameter purified HNT.

Upon examining the SEM images, a notable disparity in non-tubular impurities became evident between the unpurified standard HNT sample and the purified HNT sample. More non-tubular impurities were present in the standard HNT sample, whereas the purified HNT sample predominantly exhibited tubular structures. Furthermore, the purified HNTs displayed significantly greater length. Specifically, the average length of purified HNTs obtained from ESAN was measured at 813 nm, while the unpurified HNTs had an average length of 354 nm. Conversely, the difference in average diameters between the two samples was less prominent and may not hold statistical significance. Our SEM analysis yielded an average diameter of 84 nm for the purified HNT sample, whereas the unpurified sample exhibited an average diameter of 66 nm. One of the reasons for using purified HNT in SAP syntheses is the hypothesis that longer HNTs are more favorable as reinforcing fillers in composite systems. (Zare & Rhee, 2022b)

4.2.4. BET Analysis of HNT

Table 9: BET results of HNT supplied by ESAN.

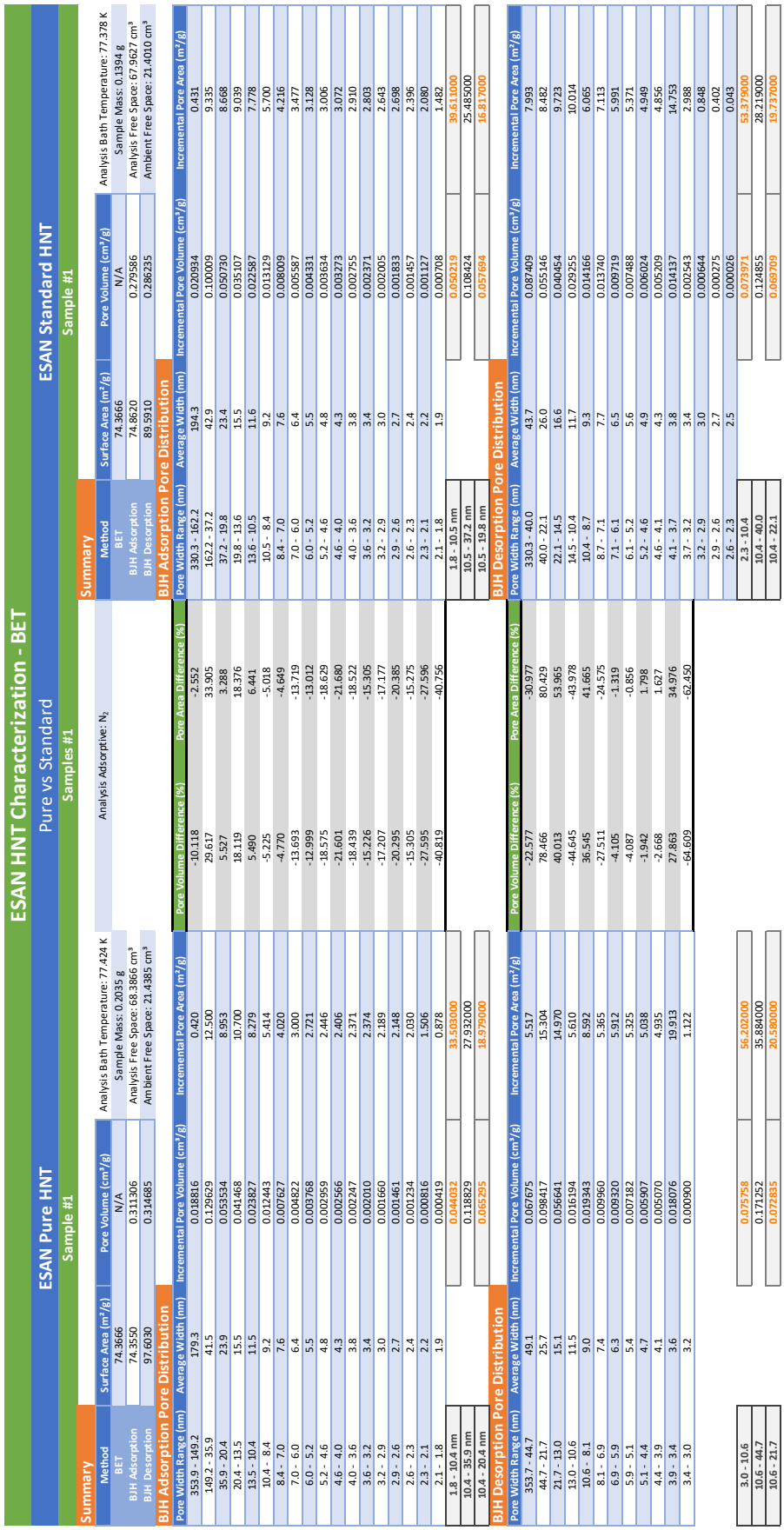

ESAN HNT Characterization - BET

ESAN Pure HNT — Sample #1

Summary

Method	Surface Area (m²/g)	Pore Volume (cm³/g)
BET	74.3666	N/A
BJH Adsorption	74.3550	0.311306
BJH Desorption	97.6030	0.314685

Analysis Bath Temperature: 77.424 K
Sample Mass: 0.2035 g
Analysis Free Space: 68.3866 cm³
Ambient Free Space: 21.4385 cm³

BJH Adsorption Pore Distribution

Pore Width Range (nm)	Average Width (nm)	Incremental Pore Volume (cm³/g)	Incremental Pore Area (m²/g)	Pore Volume Difference (%)	Pore Area Difference (%)
353.9 - 149.2	179.3	0.018816	0.420	-10.118	-2.552
149.2 - 35.9	41.5	0.129629	12.500	29.617	33.905
35.9 - 20.4	23.9	0.053534	8.953	5.527	3.288
20.4 - 13.5	15.5	0.041468	10.700	18.119	18.376
13.5 - 10.4	11.5	0.023827	8.279	5.490	6.441
10.4 - 8.4	9.2	0.012443	5.414	-5.225	-5.018
8.4 - 7.0	7.6	0.007627	4.020	-4.770	-4.649
7.0 - 6.0	6.4	0.004822	3.000	-13.693	-13.719
6.0 - 5.2	5.5	0.003768	2.721	-12.999	-13.012
5.2 - 4.6	4.8	0.002959	2.446	-18.575	-18.629
4.6 - 4.0	4.3	0.002566	2.406	-21.601	-21.680
4.0 - 3.6	3.8	0.002247	2.371	-18.439	-18.522
3.6 - 3.2	3.4	0.002010	2.374	-15.226	-15.305
3.2 - 2.9	3.0	0.001660	2.189	-17.207	-17.177
2.9 - 2.6	2.7	0.001461	2.148	-20.295	-20.385
2.6 - 2.3	2.4	0.001234	2.030	-15.305	-15.275
2.3 - 2.1	2.2	0.000816	1.506	-27.595	-27.596
2.1 - 1.8	1.9	0.000419	0.878	-40.819	-40.796
1.8 - 10.4 nm		0.044032	33.503000		
10.4 - 35.9 nm		0.118829	27.932000		
10.4 - 20.4 nm		0.065295	18.979000		

BJH Desorption Pore Distribution

Pore Width Range (nm)	Average Width (nm)	Incremental Pore Volume (cm³/g)	Incremental Pore Area (m²/g)	Pore Volume Difference (%)	Pore Area Difference (%)
353.7 - 44.7	49.1	0.067675	5.517	-22.577	-30.977
44.7 - 21.7	25.7	0.098417	15.304	78.466	80.429
21.7 - 13.0	15.1	0.056641	14.970	40.013	53.965
13.0 - 10.6	11.5	0.016194	5.610	-44.645	-43.978
10.6 - 8.1	9.0	0.019343	8.592	36.545	41.665
8.1 - 6.9	7.4	0.009960	5.365	-27.511	-24.575
6.9 - 5.9	6.3	0.009320	5.912	-4.105	-1.319
5.9 - 5.1	5.4	0.007182	5.325	-4.087	-0.856
5.1 - 4.4	4.7	0.005907	5.038	-1.942	1.798
4.4 - 3.9	4.1	0.005070	4.935	-2.668	1.627
3.9 - 3.4	3.6	0.018076	19.913	27.863	34.976
3.4 - 3.0	3.2	0.000900	1.122	-64.609	-62.450

ESAN Standard HNT — Sample #1

Summary

Method	Surface Area (m²/g)	Pore Volume (cm³/g)
BET	74.3666	N/A
BJH Adsorption	74.8620	0.279586
BJH Desorption	89.5910	0.286235

Analysis Bath Temperature: 77.378 K
Sample Mass: 0.1394 g
Analysis Free Space: 67.9627 cm³
Ambient Free Space: 21.4010 cm³

BJH Adsorption Pore Distribution

Pore Width Range (nm)	Average Width (nm)	Incremental Pore Volume (cm³/g)	Incremental Pore Area (m²/g)
330.3 - 162.2	194.3	0.020934	0.431
162.2 - 37.2	42.9	0.100009	9.335
37.2 - 19.8	23.4	0.050730	8.668
19.8 - 13.6	15.5	0.035107	9.039
13.6 - 10.5	11.6	0.022587	7.778
10.5 - 8.4	9.2	0.013129	5.700
8.4 - 7.0	7.6	0.008009	4.216
7.0 - 6.0	6.4	0.005587	3.477
6.0 - 5.2	5.5	0.004331	3.128
5.2 - 4.6	4.8	0.003634	3.006
4.6 - 4.0	4.3	0.003373	3.072
4.0 - 3.6	3.8	0.002755	2.910
3.6 - 3.2	3.4	0.002371	2.803
3.2 - 2.9	3.0	0.002005	2.643
2.9 - 2.6	2.7	0.001833	2.698
2.6 - 2.3	2.4	0.001457	2.396
2.3 - 2.1	2.2	0.001127	2.080
2.1 - 1.8	1.9	0.000708	1.482
1.8 - 10.5 nm		0.050219	39.611000
10.5 - 37.2 nm		0.108424	25.485000
10.5 - 19.8 nm		0.057694	16.817000

BJH Desorption Pore Distribution

Pore Width Range (nm)	Average Width (nm)	Incremental Pore Volume (cm³/g)	Incremental Pore Area (m²/g)
330.3 - 40.0	43.7	0.087409	7.993
40.0 - 22.1	26.0	0.055146	8.482
22.1 - 14.5	16.6	0.040454	9.723
14.5 - 10.4	11.7	0.029255	10.014
10.4 - 8.7	9.3	0.014166	6.065
8.7 - 7.1	7.7	0.013740	7.113
7.1 - 6.1	6.5	0.009719	5.991
6.1 - 5.2	5.6	0.007488	5.371
5.2 - 4.6	4.9	0.006024	4.949
4.6 - 4.1	4.3	0.005209	4.856
4.1 - 3.7	3.8	0.014137	14.753
3.7 - 3.2	3.4	0.002543	2.988
3.2 - 2.9	3.0	0.000644	0.848
2.9 - 2.6	2.7	0.000275	0.402
2.6 - 2.3	2.5	0.000026	0.043
2.3 - 10.4		0.073971	53.379000
10.4 - 40.0		0.124855	28.219000
10.4 - 22.1		0.069709	19.737000

3.0 - 10.6	0.075758	56.202000
10.6 - 44.7	0.171252	35.884000
10.6 - 21.7	0.072835	20.580000

Sample #2

Summary

Method	Surface Area (m^2/g)	Pore Volume (cm^3/g)	Analysis Bath Temperature: 77.424 K
BET	80.2504	N/A	Sample Mass: 0.1615 g
BJH Adsorption	77.9997	0.334031	Analysis Free Space: 67.5631 cm^3
BJH Desorption	103.1664	0.338564	Ambient Free Space: 21.1871 cm^3

BJH Adsorption Pore Distribution

Pore Width Range (nm)	Average Width (nm)	Incremental Pore Volume (cm^3/g)	Incremental Pore Area (m^2/g)	Pore Volume Difference (%)	Pore Area Difference (%)
371.9 - 154.2	185.4	0.027439	0.592	-19.895	-36.344
154.2 - 35.9	41.4	0.136692	13.216	43.589	52.241
35.9 - 19.7	23.2	0.059124	10.194	6.764	10.229
19.7 - 13.6	15.5	0.039547	10.224	-7.620	-6.562
13.6 - 10.5	11.6	0.024710	8.522	-8.083	-8.198
10.5 - 8.4	9.2	0.013697	5.945	-9.435	-9.678
8.4 - 7.0	7.6	0.007837	4.123	-15.267	-15.426
7.0 - 6.0	6.4	0.005181	3.225	-22.429	-22.439
6.0 - 5.2	5.5	0.003860	2.792	-26.811	-26.758
5.2 - 4.6	4.8	0.002988	2.474	-31.921	-31.977
4.6 - 4.0	4.3	0.002656	2.492	-30.234	-30.274
4.0 - 3.6	3.8	0.002255	2.382	-33.442	-33.408
3.6 - 3.2	3.4	0.002055	2.430	-29.236	-29.299
3.2 - 2.9	3.0	0.001791	2.365	-25.094	-25.087
2.9 - 2.6	2.7	0.001517	2.233	-29.703	-29.669
2.6 - 2.3	2.4	0.001306	2.146	-29.060	-29.152
2.3 - 2.1	2.2	0.000932	1.718	-33.333	-33.385
2.1 - 1.8	1.9	0.000443	0.925	-54.141	-54.208
1.8 - 10.5 nm		0.046518	35.250000		
10.4 - 35.9 nm		0.123381	28.940000		
10.4 - 20.4 nm		0.064257	18.746000		

BJH Desorption Pore Distribution

Pore Width Range (nm)	Average Width (nm)	Incremental Pore Volume (cm^3/g)	Incremental Pore Area (m^2/g)	Pore Volume Difference (%)	Pore Area Difference (%)
371.7 - 40.4	43.8	0.090650	8.282	-6.412	-12.931
40.4 - 21.2	25.1	0.093256	14.877	52.339	52.101
21.2 - 12.9	15.0	0.059492	15.888	34.206	46.433
12.9 - 10.6	11.5	0.016344	5.701	-50.363	-49.562
10.6 - 8.6	9.3	0.016110	6.908	-1.462	-1.201
8.6 - 6.9	7.6	0.014540	7.698	-10.169	-8.051
6.9 - 5.9	6.3	0.009378	5.941	-16.840	-14.419
5.9 - 5.1	5.4	0.007631	5.635	-13.106	-10.356
5.1 - 4.4	4.7	0.005940	5.051	-18.283	-15.394
4.4 - 3.9	4.1	0.005087	4.931	-15.540	-12.197
3.9 - 3.4	3.6	0.019469	21.423	17.987	24.400
3.4 - 3.1	3.2	0.000668	0.830	-77.333	-75.970
3.0 - 10.6		0.078823	58.417000		
10.6 - 44.7		0.169092	36.466000		
10.6 - 21.7		0.075836	21.589000		

Samples #2

Analysis Adsorptive: N_2

Sample #2

Summary

Method	Surface Area (m^2/g)	Pore Volume (cm^3/g)	Analysis Bath Temperature: 77.377 K
BET	94.0654	N/A	Sample Mass: 0.1370 g
BJH Adsorption	86.6960	0.000000	Analysis Free Space: 67.3772 cm^3
BJH Desorption	104.0560	0.321946	Ambient Free Space: 21.1982 cm^3

BJH Adsorption Pore Distribution

Pore Width Range (nm)	Average Width (nm)	Incremental Pore Volume (cm^3/g)	Incremental Pore Area (m^2/g)
362.4 - 123.3	147.3	0.034254	0.930
123.3 - 37.3	43.9	0.095197	8.681
37.3 - 20.3	24.0	0.055378	9.248
20.3 - 13.7	15.6	0.042809	10.942
13.7 - 10.4	11.6	0.026883	9.283
10.4 - 8.4	9.2	0.015124	6.582
8.4 - 7.0	7.6	0.009249	4.875
7.0 - 6.0	6.4	0.006679	4.158
6.0 - 5.2	5.5	0.005274	3.812
5.2 - 4.6	4.8	0.004389	3.637
4.6 - 4.0	4.3	0.003807	3.574
4.0 - 3.6	3.8	0.003388	3.577
3.6 - 3.2	3.4	0.002904	3.437
3.2 - 2.9	3.0	0.002391	3.157
2.9 - 2.6	2.7	0.002158	3.175
2.6 - 2.3	2.4	0.001841	3.029
2.3 - 2.1	2.2	0.001398	2.579
2.1 - 1.8	1.9	0.000966	2.020
1.8 - 10.4 nm		0.059568	47.612000
10.4 - 35.9 nm		0.125070	29.473000
10.4 - 20.4 nm		0.069692	20.225000

BJH Desorption Pore Distribution

Pore Width Range (nm)	Average Width (nm)	Incremental Pore Volume (cm^3/g)	Incremental Pore Area (m^2/g)
362.5 - 37.7	40.7	0.096861	9.512
37.7 - 21.3	25.0	0.061216	9.781
21.3 - 14.3	16.3	0.044329	10.850
14.3 - 10.4	11.7	0.032927	11.303
10.4 - 8.7	9.4	0.016349	6.992
8.7 - 7.1	7.7	0.016186	8.372
7.1 - 6.1	6.5	0.011277	6.942
6.1 - 5.2	5.6	0.008782	6.286
5.2 - 4.6	4.9	0.007269	5.970
4.6 - 4.1	4.3	0.006023	5.616
4.1 - 3.7	3.8	0.016501	17.221
3.7 - 3.2	3.4	0.002947	3.454
3.2 - 2.9	3.0	0.000858	1.129
2.9 - 2.6	2.7	0.000352	0.515
2.6 - 2.3	2.4	0.000069	0.113
3.0 - 10.6		0.085334	60.853000
10.6 - 44.7		0.138472	31.934000
10.6 - 21.7		0.077256	22.153000

Sample #3

Summary

Method	Surface Area (m^2/g)	Pore Volume (cm^3/g)	Analysis Bath Temperature: 77.424 K
BET	77.5296	N/A	Sample Mass: 0.1858 g
BJH Adsorption	73.7267	0.296516	Analysis Free Space: 68.0334 cm^3
BJH Desorption	96.6661	0.301569	Ambient Free Space: 21.3615 cm^3

BJH Adsorption Pore Distribution

Pore Width Range (nm)	Average Width (nm)	Incremental Pore Volume (cm^3/g)	Incremental Pore Area (m^2/g)
347.7 - 36.2	39.1	0.137229	14.045
36.2 - 20.5	24.1	0.052086	8.645
20.5 - 14.0	16.0	0.038027	9.531
14.0 - 10.4	11.7	0.026344	9.037
10.4 - 8.5	9.2	0.012374	5.368
8.5 - 7.0	7.6	0.007329	3.856
7.0 - 6.0	6.4	0.004834	3.008
6.0 - 5.2	5.5	0.003531	2.552
5.2 - 4.6	4.8	0.002822	2.335
4.6 - 4.0	4.3	0.002476	2.326
4.0 - 3.6	3.8	0.002088	2.207
3.6 - 3.2	3.4	0.001900	2.248
3.2 - 2.9	3.0	0.001638	2.162
2.9 - 2.6	2.7	0.001408	2.075
2.6 - 2.3	2.4	0.001202	1.976
2.3 - 2.1	2.2	0.000864	1.594
2.1 - 1.8	1.9	0.000364	0.761

1.8 - 10.4 nm		0.030456	27.100000
10.4 - 35.9 nm		0.076745	23.936000
10.4 - 20.4 nm		0.038718	14.405000

BJH Desorption Pore Distribution

Pore Width Range (nm)	Average Width (nm)	Incremental Pore Volume (cm^3/g)	Incremental Pore Area (m^2/g)
347.6 - 41.1	44.9	0.067454	6.015
41.1 - 20.5	24.2	0.089790	14.811
20.5 - 12.9	14.9	0.051702	13.850
12.9 - 10.6	11.5	0.015748	5.462
10.6 - 8.6	9.4	0.016040	6.848
8.6 - 7.0	7.6	0.013708	7.218
7.0 - 5.9	6.4	0.009224	5.799
5.9 - 5.1	5.5	0.007389	5.418
5.1 - 4.5	4.7	0.006039	5.101
4.5 - 3.9	4.2	0.004930	4.744
3.9 - 3.5	3.7	0.018661	20.314
3.5 - 3.1	3.3	0.000884	1.087

3.0 - 10.6		0.076875	56.529000
10.6 - 44.7		0.157240	34.123000
10.6 - 21.7		0.067450	19.312000

Samples #3

Pore Volume Difference (%)	Pore Area Difference (%)
489.117	2018.401
-16.138	48.923
5.499	54.925
0.244	34.120
-29.833	-11.652
-26.791	-11.438
-18.688	-3.898
-19.968	-6.997
-17.989	-6.150
-10.967	1.043
-17.666	-7.347
-12.964	-2.642
-10.590	-0.185
-12.329	-2.030
-14.509	-4.587
-27.027	-18.046
-62.123	-57.030

Pore Volume Difference (%)	Pore Area Difference (%)
31.423	35.017
90.973	102.668
55.098	67.899
-24.310	-23.821
42.603	41.957
29.321	31.141
24.229	26.588
26.719	29.741
26.870	30.327
27.489	31.559
71.927	79.136
-55.354	-53.308

Analysis Adsorptive: N_2

Sample #3

Summary

Method	Surface Area (m^2/g)	Pore Volume (cm^3/g)	Analysis Bath Temperature: 77.378 K
BET	61.9971	N/A	Sample Mass: 0.1440 g
BJH Adsorption	56.5560	0.204303	Analysis Free Space: 68.1689 cm^3
BJH Desorption	68.3270	0.209689	Ambient Free Space: 21.4545 cm^3

BJH Adsorption Pore Distribution

Pore Width Range (nm)	Average Width (nm)	Incremental Pore Volume (cm^3/g)	Incremental Pore Area (m^2/g)
352.9 - 117.9	140.6	0.023294	0.663
117.9 - 36.4	42.8	0.062109	5.805
36.4 - 19.9	23.4	0.036045	6.152
19.9 - 13.7	15.6	0.026280	6.738
13.7 - 10.5	11.6	0.017635	6.076
10.5 - 8.4	9.2	0.010011	4.354
8.4 - 7.0	7.6	0.005945	3.130
7.0 - 6.0	6.4	0.004412	2.744
6.0 - 5.2	5.5	0.003441	2.488
5.2 - 4.6	4.8	0.002781	2.302
4.6 - 4.0	4.3	0.002536	2.382
4.0 - 3.6	3.8	0.002183	2.309
3.6 - 3.2	3.4	0.001832	2.166
3.2 - 2.9	3.0	0.001606	2.118
2.9 - 2.6	2.7	0.001406	2.071
2.6 - 2.3	2.4	0.001184	1.945
2.3 - 2.1	2.2	0.000961	1.771
2.1 - 1.8	1.9	0.000642	1.342

1.8 - 10.4 nm		0.038940	31.122000
10.4 - 35.9 nm		0.079960	18.966000
10.4 - 20.4 nm		0.043915	12.814000

BJH Desorption Pore Distribution

Pore Width Range (nm)	Average Width (nm)	Incremental Pore Volume (cm^3/g)	Incremental Pore Area (m^2/g)
352.9 - 42.2	46.1	0.051326	4.455
42.2 - 21.8	25.7	0.047017	7.308
21.8 - 14.0	16.2	0.033335	8.249
14.0 - 10.4	11.6	0.020806	7.170
10.4 - 8.6	9.3	0.011248	4.824
8.6 - 7.1	7.7	0.010600	5.504
7.1 - 6.1	6.5	0.007425	4.581
6.1 - 5.2	5.6	0.005831	4.176
5.2 - 4.6	4.9	0.004760	3.914
4.6 - 4.1	4.3	0.003867	3.606
4.1 - 3.6	3.8	0.010854	11.340
3.6 - 3.2	3.4	0.001980	2.328
3.2 - 2.9	3.0	0.000450	0.592
2.9 - 2.6	2.7	0.000183	0.268
2.6 - 2.3	2.4	0.000007	0.012

3.0 - 10.6		0.056565	40.273000
10.6 - 44.7		0.101158	22.727000
10.6 - 21.7		0.054141	15.419000

Averages - Pure HNT

Summary

Method	Surface Area (m^2/g)	Pore Volume (cm^3/g)
BET	77.3822	N/A
BJH Adsorption	75.3605	0.313951
BJH Desorption	99.1452	0.318273

BJH Adsorption Pore Distribution

	Incremental Pore Volume (cm^3/g)	Incremental Pore Area (m^2/g)
1.8 - 10.4 nm	0.040335	31.951000
10.4 - 36 nm	0.106318	26.936000
10.4 - 20.4 nm	0.056090	17.376667
20.4 - 36 nm	0.054915	9.264000

BJH Desorption Pore Distribution

	Incremental Pore Volume (cm^3/g)	Incremental Pore Area (m^2/g)
3.1 - 10.6 nm	0.077152	57.049333
10.6 - 44.7 nm	0.165861	35.491000
10.6 - 21.1 nm	0.072040	20.493667
21.1 - 42.1 nm	0.093821	14.997

Averages

BET
BJH Adsorption
BJH Desorption

Total Pore Volume Difference (%)	Total Surface Area Difference (%)
N/A	0.745
94.642	3.653
16.744	13.536

Pore Volume Difference (%)	Pore Area Difference (%)
-18.63884836	-19.00545017
1.754962451	9.312266652
-1.769400062	4.561136072
15.89203182	**15.47282699**

Pore Volume Difference (%)	Pore Area Difference (%)
7.220086163	10.77181968
36.51700344	28.46645753
7.466211848	7.279833883
72.27611872	**75.94931759**

Averages - Standard HNT

Summary

Method	Surface Area (m^2/g)	Pore Volume (cm^3/g)
BET	76.8097	N/A
BJH Adsorption	72.7047	0.161296
BJH Desorption	87.3247	0.272623

BJH Adsorption Pore Distribution

	Incremental Pore Volume (cm^3/g)	Incremental Pore Area (m^2/g)
1.8 - 10.5 nm	0.049576	39.448333
10.4 - 37 nm	0.104485	24.641333
10.4 - 20 nm	0.057100	16.618667
20 - 37 nm	0.047384	8.023

BJH Desorption Pore Distribution

	Incremental Pore Volume (cm^3/g)	Incremental Pore Area (m^2/g)
2.3 - 10.4 nm	0.071957	51.501667
10.4 - 40 nm	0.121495	27.626667
10.4 - 21.7 nm	0.067035	19.103000
21.7 - 40 nm	0.054460	8.524

According to the BET results, the total surface area of the purified HNT was only slightly higher, by approximately 1-3%, compared to the standard HNT. However, the total pore volume of the purified HNT was approximately 18% greater than that of the standard HNT. This higher pore volume can be attributed to the increased proportion of HNT in the purified sample. Notably, most of the impurities present in the standard HNT sample lacked a tubular structure, contributing more to the surface area rather than the pore volume. Additionally, cumulative pore volume information was obtained from the BET analysis. Given that the inner lumen of the HNT has an average size of 20 nm, a comparison of the loading capability between the two samples necessitates an assessment of the total volume of pores larger than 20 nm. On average, the purified HNT samples exhibited a 44% higher total volume of larger pores. This finding further substantiates our expectation that purified HNT is more advantageous for incorporating active agents, thereby reinforcing the rationale behind using purified HNT in the synthesis of superabsorbent polymers (SAPs).

4.2.3. Active Agent Incorporation on HNT

4.2.3.1. Pesticide loading on HNTs

In this study, various combinations of four different HNT/water ratios and three different fungicide/HNT concentrations were investigated, resulting in a total of 12 experiments conducted under different conditions as listed below.

Table 10: Vacuum Suction Loading of Fungicide Highlife 250 EC (250 g/L Propiconazole) on Halloysite Nanotubes - Loading Mixture.

Fungicide Loading Mixture

Sample	HNT	Water	Propiconazole	HNT	Propiconazole
	(g)	*(mL)*	*(mL)*	*(wt% in water)*	*(wt% in HNT)*
5H10F	5	95	2	5	10
5H20F	5	95	4	5	20
5H30F	5	95	6	5	30
10H10F	10	90	4	10	10
10H20F	10	90	8	10	20
10H30F	10	90	12	10	30
15H10F	15	85	6	15	10
15H20F	15	85	12	15	20
15H30F	15	85	18	15	30
20H10F	20	80	8	20	10
20H20F	20	80	16	20	20
20H30F	20	80	24	20	30

Fungicide Loading Parameters

Shear mixing	Vacuum	Drying
10 min at 8,000 rpm	3 x 15 min	Vacuum filter

The fill ratios of the resultant HNTs are their most important property, as they show the efficacy of the active agent loading procedure. By determining the amount of HNT powder used and evaluating the fill ratios, it becomes possible to estimate the quantity of fungicide to be released from the HNTs. Thermal gravimetric analyses (TGA) were performed on all samples to calculate the fill ratios of the HNTs. The TGA results depicting weight loss across the temperature range of 30-1000 °C, for all samples, are presented in the table below.

Table 11: Vacuum Suction Loading of Fungicide Highlife 250 EC (250 g/L Propiconazole) on Halloysite Nanotubes - TGA Results.

	Fungicide Loading - TGA Results			
Sample	**Total Weight Loss**	**Moisture content**	**Weight Loss**	**Fungicide Loading (wt%)**
	(%)	*[until 200 C] (%)*	*[from 200 to 1000 C] (%)*	*Weight Loss Compared to HNT*
5H10F	18.85	4.61	14.24	0.94
5H20F	20.12	4.71	15.41	2.11
5H30F	23.51	3.99	19.52	6.22
10H10F	19.37	4.83	14.54	1.24
10H20F	29.03	3.24	25.79	12.49
10H30F	27.32	3.38	23.94	10.64
15H10F	23.17	3.72	19.45	6.15
15H20F	21.6	3.56	18.04	4.74
15H30F	33.89	3.58	30.31	17.01
20H10F	21.44	3.61	17.83	4.53
20H20F	26.51	3.43	23.08	9.78
20H30F	21.59	3.72	17.87	4.57
Pristine HNT	18.98	5.68	13.3	0

TGA Parameters			
N2 Flow rate	**Heating Rate**	**Atmosphere**	**Temperature Range**
50 ml/min	10 °C/min	Nitrogen	30 - 1000 °C

Based on the TGA analyses, it can be inferred that fungicide/HNT ratios exceeding 20% do not yield a significant increase in fill ratios (i.e., the fungicide content within the HNTs). Furthermore, in certain cases, a 30% fungicide concentration resulted in lower fill ratios compared to a 20% concentration. Although this discrepancy may be attributed to experimental errors, no significant correlation between fungicide/HNT ratios and fill ratios within the range of 20% to 30% fungicide concentrations was observed.

Additionally, different HNT/water concentrations were compared by analyzing TGA plots for samples with identical fungicide concentrations (e.g., samples 5H10F, 10H10F, 15H10F, and 20H10F). Overall, it was concluded that HNT concentrations of 10% and 15% in water yielded the highest fill ratios. Consequently, the optimal parameters for the fungicide loading experiment were determined to be 10 wt% HNT/water and 20 wt% fungicide/HNT.

To assess the potential accumulation of molecules on the outer surface of the HNTs, the samples were analyzed using scanning electron microscopy (SEM). The provided images include five HNT+fungicide samples along with an empty HNT control sample.

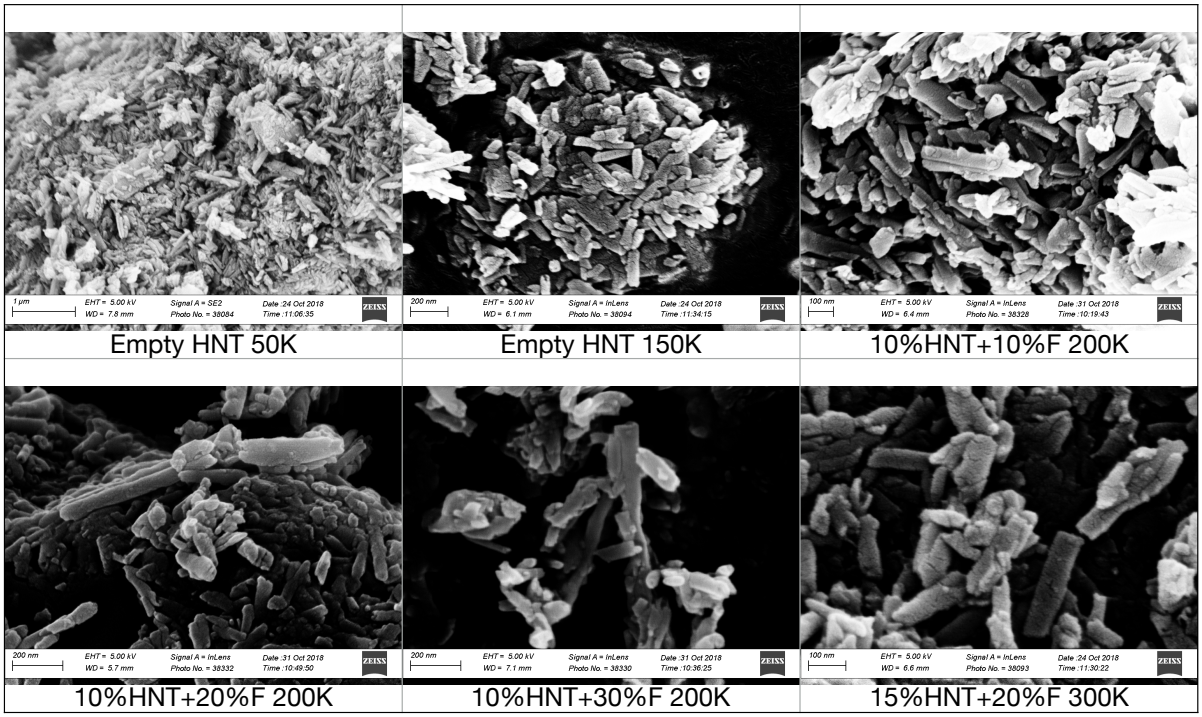

Figure 21: SEM Images of Pristine and Fungicide-Loaded HNTs.

The first two images of the empty HNT sample depict pristine outer surfaces of the nanotubes without any adsorption of molecules. However, the remaining images reveal nanotubes that are covered with a substance. It is presumed that this substance adsorbed onto the outer surface of the HNTs is either the fungicide active agent or solvent molecules from the fungicide solution.

Furthermore, it was anticipated that this coverage or adsorption would correlate with the fungicide-to-HNT ratio. Although a systematic calculation of adsorption was not conducted, analysis of the SEM images led to the deduction that there is no direct interdependence between the coverage of the outer surface of the HNTs and the fungicide concentration. As expected, HNTs from the 10% fungicide sample exhibited lower coverage compared to the others. However, no significant difference in coverage was observed between the 20% and 30% fungicide samples. Thus, it can be concluded that the coverage issue is likely attributed to the cleaning process employed during the filtration step, as well as an excess concentration of fungicide.

4.2.3.2. Uridine loading on HNT

Uridine-loaded and unloaded -pristine- HNT samples were evaluated using Thermal Gravimetric Analysis (TGA), to assess the actual uridine loading achieved by using the vacuum suction method. TGA results are presented below:

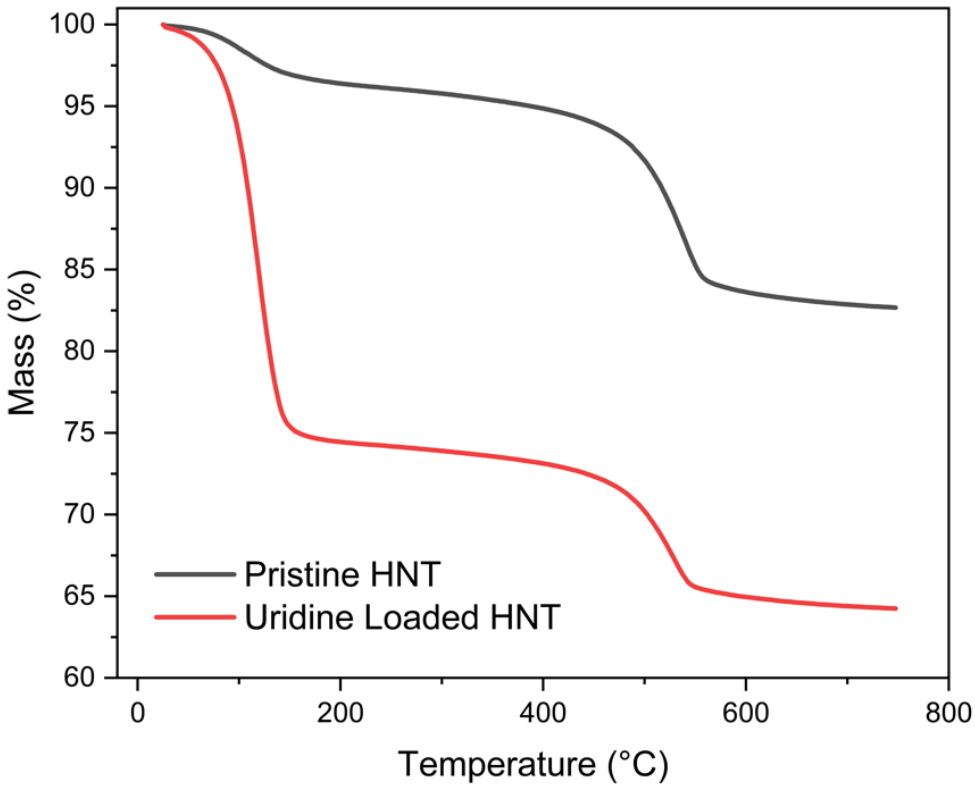

Figure 22: Thermogravimetric Analysis of Unloaded Pristine HNT and Uridine Loaded HNT.

By comparing the differences in mass loss between the pure HNTs and the uridine-loaded HNT samples, an approximate uridine loading of 18.4 wt.% was calculated. In this calculation, the temperature range corresponding to the mass loss attributed to humidity was taken into account, as uridine undergoes thermal decomposition near 110 °C. Therefore, both samples were assumed to have experienced similar levels of humidity loss during the analysis.

4.2.3.1.1. SAP synthesis with uridine-loaded HNT

Next, two SAP-HNT-uridine samples were synthesized at 1 and 5 wt.% HNT-uridine -compared to total solid weight -. Thus, the 1 and 5 wt.% SAPs consist of at most 0.18 and

0.92 wt.% of uridine respectively. However, due to potential losses during synthesis, the actual uridine concentration should also be measured after synthesis. To do so, and to measure the release kinetics of uridine from the SAP-HNT-uridine composite, in water; synthesized SAP composites were sent to Uludağ University for temporal HPLC analysis. Unfortunately, due to some technical complications in analyzing the samples on their side, this project was suspended.

4.2.4. Nutrient Loading on HNT

To bind nutrients onto HNT we utilized PEG chelation to bind PEG polymer chains, first, HNT surfaces needed to be functionalized with a coupling agent. In our study, we used 3-(Triethoxysilyl)propyl isocyanate (IPTS) as the silane coupling agent. Next, PEG 400, 1000, and 4000 were added to the reaction mixture, to attach to HNT surface, through bonding with IPTS.

According to the following thermal gravimetric analysis results, we calculated that silane coupling agent, IPTS, loading on pure HNT was 6 wt%, PEG loading was 2 to 5 wt%, and nutrient loading was approximately 1 to 2 wt% of HNT. To achieve these numbers, we subtracted non-water mass loss percentage of a certain sample, for example, HNT-IPTS, from that of pure HNT.

Below, the TGA results are displayed as a table:

Table 12: Nutrient Loading on HNT Calculated from TGA Results

TGA Results and Analysis	Temperature Range and Mass Loss		Mass Loss Difference (Loading)
	Water	Non-water	
Pure HNT	*26.6 - 143.6 °C* 1.92%	*143.6 - 995.3 °C* 14.48%	
HNT - IPTS	*26.6 - 143.6 °C* 0.77%	*144.1 - 993.58 °C* 20.50%	*Relative to Pure HNT* **6.02%**
HNT - IPTS - PEG 400	*26.5 - 143.5 °C* 0.77%	*143.6 - 993.3 °C* 24.01%	*Relative to HNT-IPTS* **3.50%**
HNT - IPTS - PEG 1000	*26.5 - 143.5 °C* 0.67%	*143.7 - 993.9 °C* 22.55%	*Relative to HNT-IPTS* **2.05%**
HNT - IPTS - PEG 4000	*26.5 - 143.5 °C* 0.65%	*143.5 - 993.8 °C* 25.83%	*Relative to HNT-IPTS* **5.33%**
HNT - IPTS - PEG 400 + Ca	*26.5 - 141.9 °C* 1.04%	*141.9 - 992.6 °C* 22.73%	*Relative to HNT-IPTS-PEG 400* **-1.28%**
HNT - IPTS - PEG 400 + Zn	*26.5 - 142.0 °C* 1.07%	*142.0 - 993.1 °C* 23.22%	*Relative to HNT-IPTS-PEG 400* **-0.78%**
HNT - IPTS - PEG 1000 + Ca	*26.6 - 140.4 °C* 0.90%	*140.9 - 993.2 °C* 21.62%	*Relative to HNT-IPTS -PEG 1000* **-0.93%**
HNT - IPTS - PEG 1000 + Zn	*26.5 - 140.3 °C* 1.02%	*140.8 - 992.5 °C* 21.51%	*Relative to HNT-IPTS -PEG 1000* **-1.04%**
HNT - IPTS - PEG 4000 + Ca	*26.6 - 141.9 °C* 1.05%	*142.5 - 985.3 °C* 23.78%	*Relative to HNT-IPTS-PEG 4000* **-2.05%**
HNT - IPTS - PEG 4000 + Zn	*26.6 - 143.1 °C* 0.94%	*143.6 - 992.9 °C* 23.99%	*Relative to HNT-IPTS-PEG 4000* **-1.84%**

These mass loss differences give the weight percentages of IPTS, PEG, and micronutrients in the entire structure. IPTS loading on HNT was calculated to be **6.02 % w/w**. PEG loading was **3.5**, **2.05**, and **5.33 % w/w** for PEG- 400, 1000, and 4000, respectively. Calcium loadings were **1.28**, **0.93**, and **2.05 % w/w** for HNT-IPTS-PEG-400, 1000, and 4000 complexes respectively. Similarly, zinc loadings were calculated as **0.78**, **1.04**, and **1.84 % w/w**.

4.3. Integration of Water Management and Efficient PPP and Nutrient Use

4.3.1. Halloysite as a Carrier Material in SAPs

The SAP synthesized in this study has a nanocomposite structure that incorporates 5 wt% halloysite nanotubes (HNT). HNT is an aluminosilicate clay with a submicron hollow tubular structure and has alternating layers of alumina and silica. Active agents can be loaded on both the outside surface of the HNT and on its inner lumen.

In literature, HNT has been shown to increase the release duration of fertilizers, when integrated in polymers used for their encapsulation, as nanofillers. Furthermore, HNT has been used in novel microbial fertilizer formulations to host microbial cells, enable their slow release even after 15 days, and improve their survival stability. Clay-based nanocomposites have been developed as slow-release fertilizers, including NPK and urea. Further still, other clay-based pesticide formulations have been developed to hinder volatilization and photodegradation of the absorbed pesticides, such as herbicides. Due to its limited loading capacity, HNT is more suited for the delivery of certain pesticides, microbial fertilizers, or other active agents such as enzymes, such as uridine, that are applied at small doses. Traditional fertilizers and most micronutrients are applied at such high doses such that the loading capacity of HNT is not sufficient.

Active agent loading is not the only purpose clay-based materials can serve in nanocomposites. In literature, HNT is known to improve the mechanical properties of polymer nanocomposites. In this regard, pristine HNT, with a Young's modulus of approximately 300 GPA, can act as a strengthening filler in superabsorbent polymer nanocomposites.

Indeed, the reason for HNT incorporation in our study was to impart mechanical strengthening to the SAP structure. SAPs are applied underground, where the pressure limits their water absorption capacities. SAP-HNT can better maintain its structural integrity, which allows higher water absorption under pressure.

4.3.2. Swelling and Dissolution Speeds of Compacted SAP-Fertilizer and Fertilizer

Fertilizers compacted with 10 wt.% SAP dissolved more readily in water, compared to only fertilizers. This photograph is a still image taken from a video showing the dissolution of fertilizers, together with the swelling of SAP. Although it is much easier to observe it in a video, one can also notice the difference between the two groups from this image. For example, if we pay attention to the bottom-right portion, we can notice that the fertilizer pellet has not disintegrated yet, whereas the fertilizer-SAP pellet has already disintegrated and dissolved considerably. This is a great example showing the internal "burst effect" enabled by the swelling of the SAP. The grease observed on the surface of the water comes from the lubricant used during the compaction process.

4.3.3. Water and Saline Absorption Performance of Nutrient Loaded Superabsorbent Polymers

In this study, SAPs loaded with nutrients after polymerization was evaluated. Water absorption performances of SAPs loaded with varying contents of zinc, calcium, and magnesium fertilizers were measured.

The water absorption ratio of the SAPs was calculated from the swollen gel weights and initial dry SAP weights, according to the following formula:

$$Water\ Absorption\ Ratio\ (\%) = \frac{Swollen\ Gel\ Weight - Initial\ SAP\ Weight}{Initial\ SA\ Weight} \cdot 100$$

In the first test, magnesium sulfate loaded SAPs (Mg:SAP) were evaluated. As expected, SAP composites with higher amounts of fertilizers integrated into their structure have deteriorated water absorption capacities. However, this decrease in swelling rates did not linearly correlate with decreasing SAP percentages in the composite.

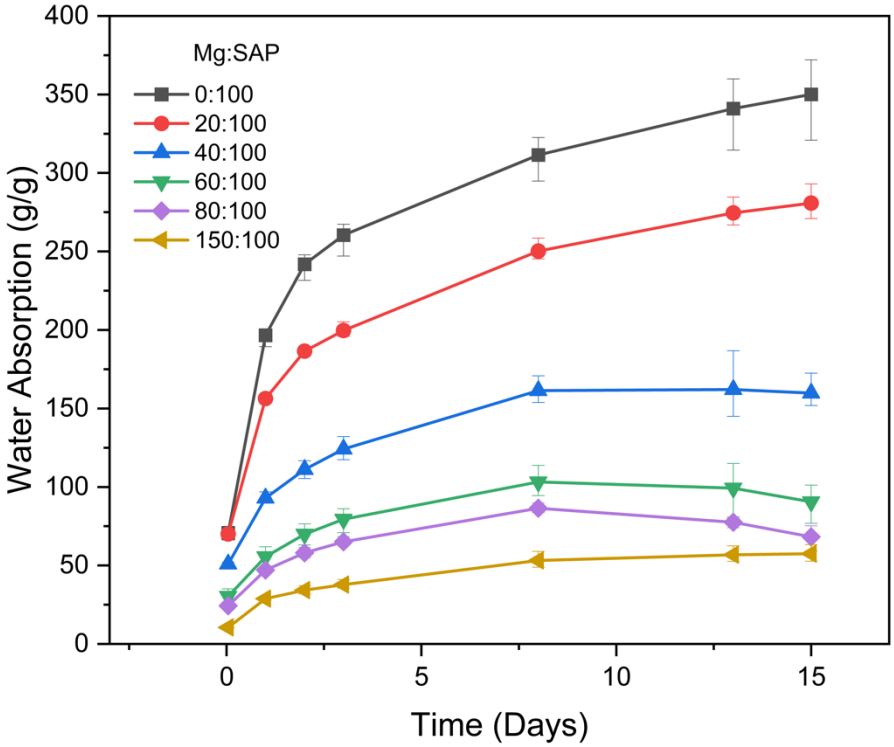

Figure 23: Water Absorption Kinetics of Mg:SAP.

One effective way to assess to assess this correlation, and the impact of nutrient addition on the water retention capability of SAPs, is by measuring the amount of water absorbed per unit of the polymer in the composite SAP. To achieve this, a new set of data, called the adjusted water absorption, was derived from the existing data. The adjusted water absorption capacity of a nutrient-SAP composite is obtained by dividing its true water absorption by the proportion of the polymer's weight in its composition. Both data sets are presented in this section. So, for example, for a nutrient-loaded SAP containing 40% SAP and 60% fertilizer, a swelling ratio of 100x will give an adjusted swelling ratio of ${}^{100x}/_{0.4} = 250x$. The adjusted swelling ratio can be thought of as the true swelling ratio of the SAP present in the composite since the fertilizer dissolves in water without providing additional mass to the swollen gel.

$$Adjusted\ Water\ Absorption = \frac{True\ Water\ Absorption}{Weight\ Fraction\ of\ Synthetic\ Polymer}$$

For example, a composite with a 40:100 nutrient:SAP composition, has an SAP weight fraction of $W_{SAP} = \frac{100}{100+40} = 0.714$. Such a composite with a true water absorption ratio of 300 g/g has an adjusted water absorption ratio of $\frac{300\ g/g}{0.714} = 420\ g/g$.

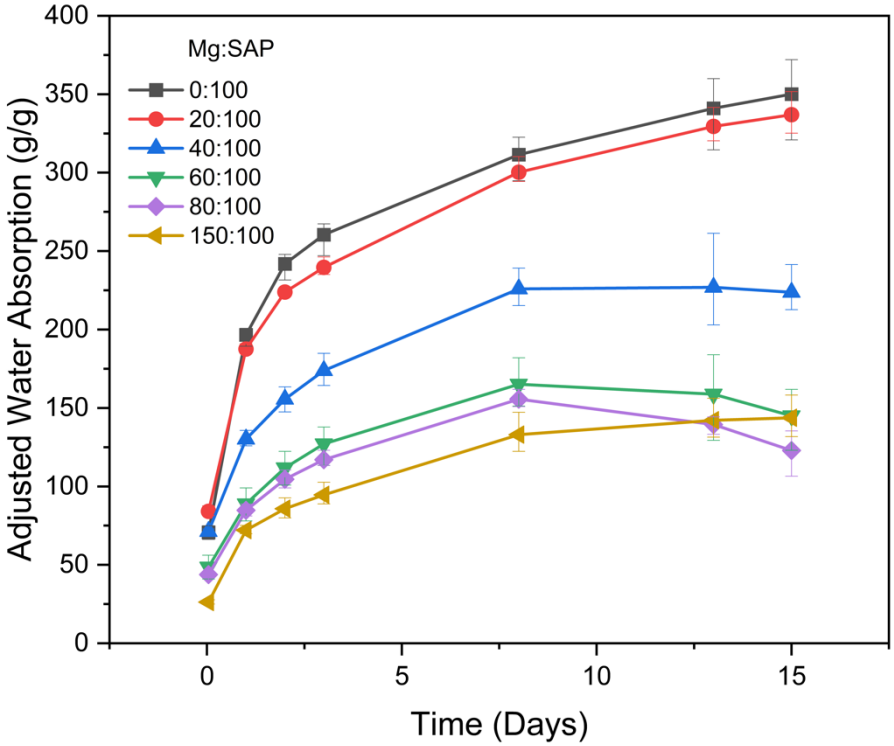

Figure 24: Adjusted Water Absorption Kinetics of Mg:SAP.

Increasing the magnesium fertilizer ratio in the composites resulted in a decrease in the water absorption performance. This outcome was expected, because, as the amount of SAP in the structure is decreased, the swelling capacity should be degraded. Moreover, these lower SAP contents were accounted for with the adjusted swelling ratios, which were obtained by dividing the actual swelling ratios by the SAP weight fraction. Even in those results, the adjusted swelling ratios of Mg:SAP composites with higher nutrient ratios, were lower than that of pure SAP. In fact, the swelling ranking of Mg:SAP composites were the same for the actual and adjusted swelling ratios. This meant that the water absorption ability of the SAP degraded when it was brought together with the fertilizer.

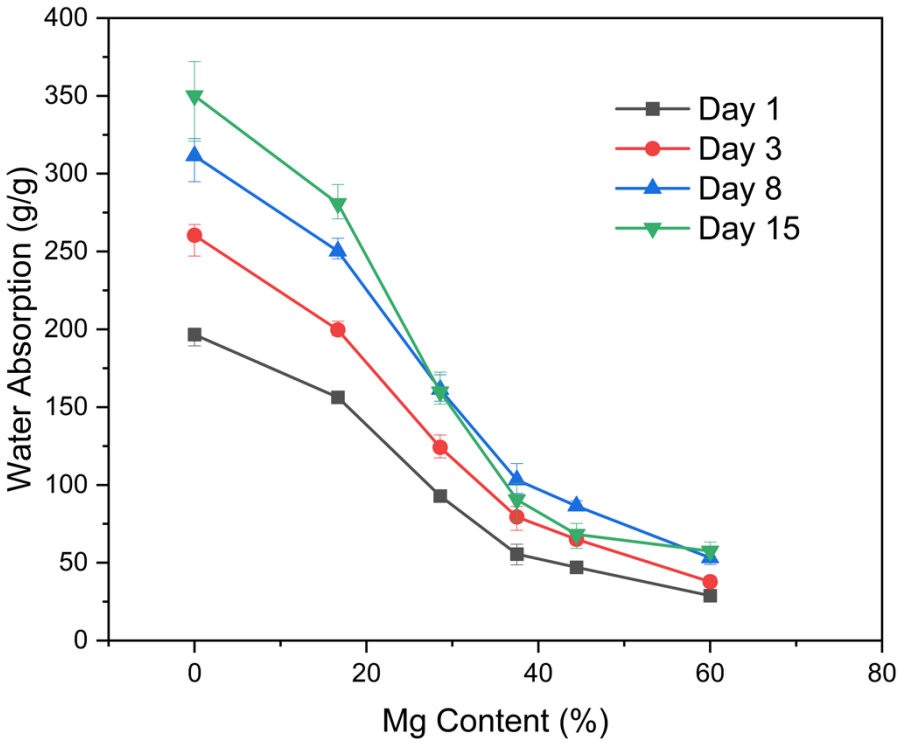

Figure 25: Water Absorption vs Mg Content.

However, in the water absorption tests of the calcium nitrate:SAP (Ca:SAP) composites, a completely different phenomenon was perceived, from the one that was understood from the initial set of Mg:SAP samples. Increasing the calcium nitrate ratio in the SAP was expected to result in a decrease in the water absorption performance. However, in the initial water absorption test of Ca:SAP samples, the 20:100 Ca:SAP composite displayed the best water absorption performance. This was unexpected, as it had less SAP than the pure SAP control sample.

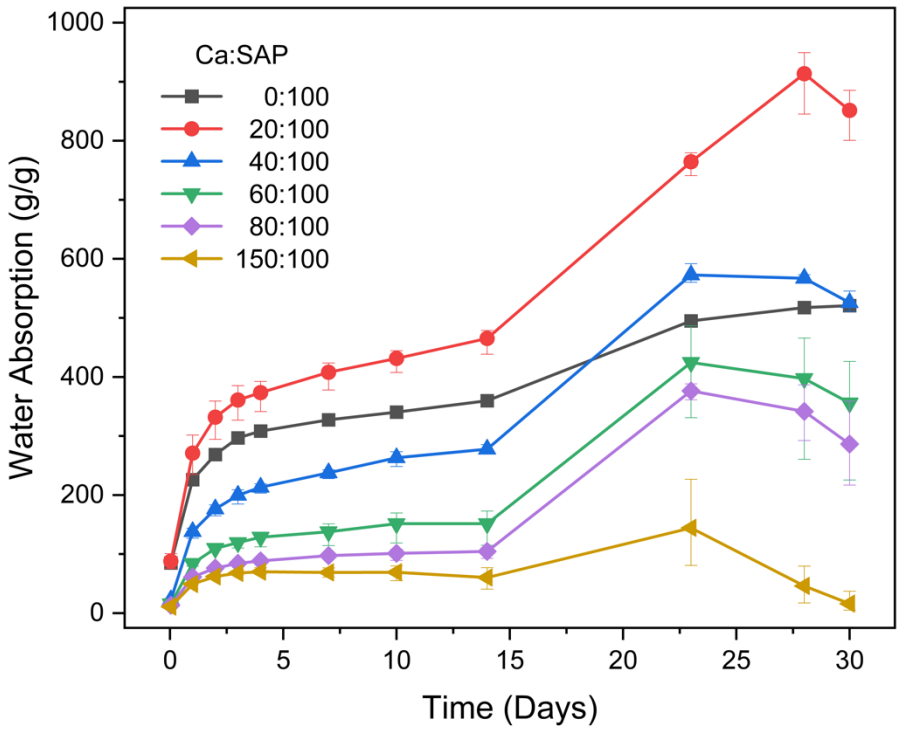

Figure 26: Water Absorption Kinetics of Ca:SAP.

As can be seen from the plots, the water absorption capacities are not exactly inversely correlated with nutrient ratios. For example, 20:100 Ca:SAP displayed the best water absorption performance, with a significantly higher swelling ratio compared to pure SAP. This was unexpected, as it had less SAP than the pure SAP control sample.

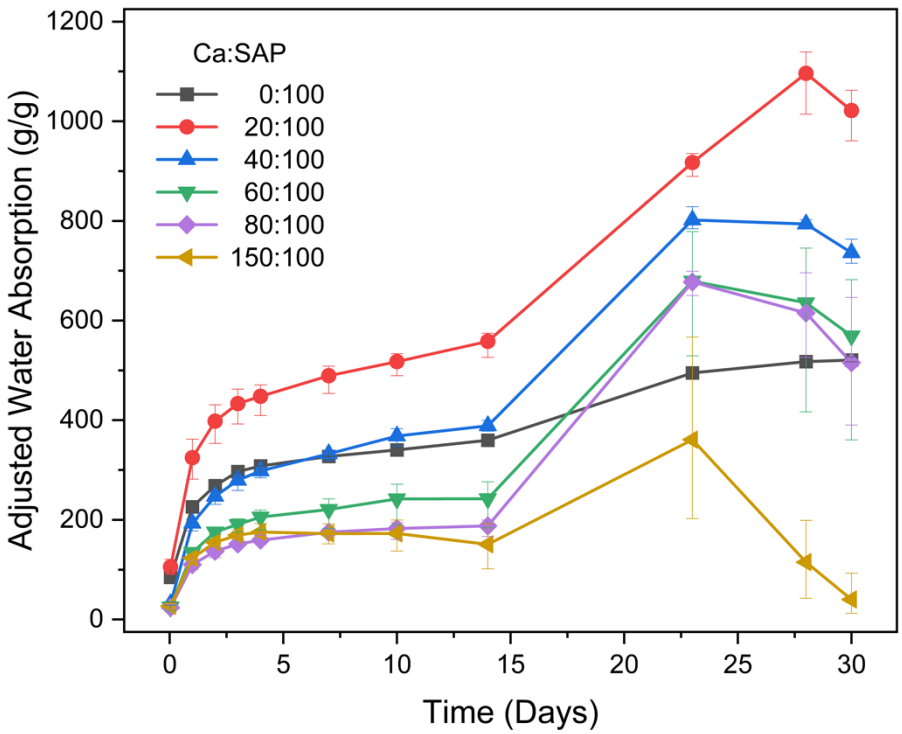

Figure 27: Adjusted Water Absorption Kinetics of Ca:SAP.

Also, if we look at the adjusted swelling ratios, 40:100 Ca:SAP surpassed the control after the first week. Moreover, the adjusted swelling ratios of all composites except for the 150:100 Ca:SAP composite were all higher than pure SAP.

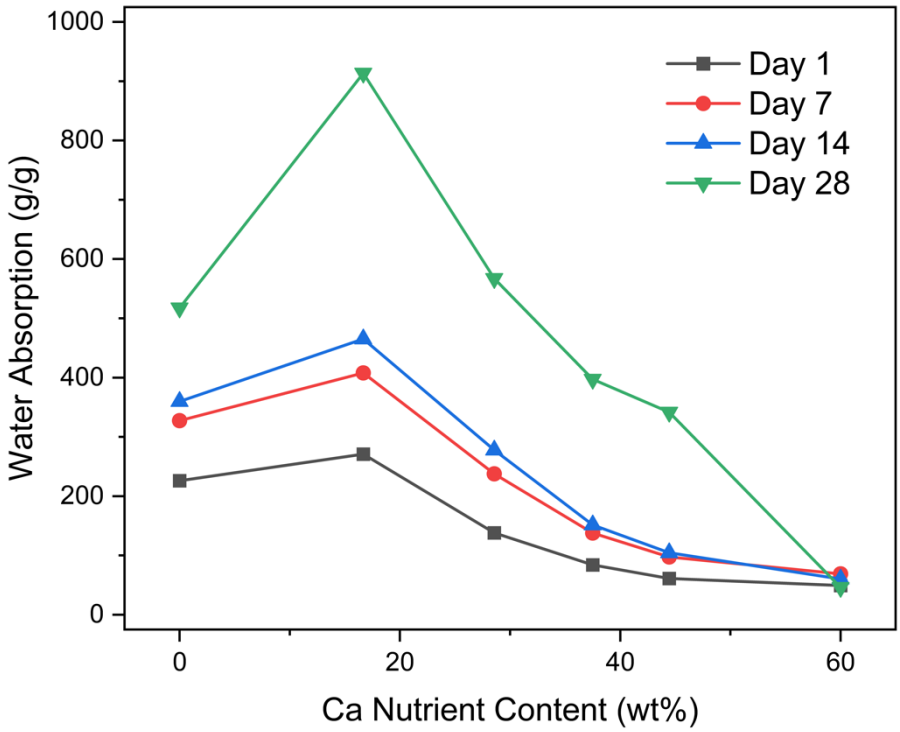

Figure 28: Swelling Ratio vs Ca Nutrient Content.

Although it sounds counterintuitive at first, this phenomenon can be explained by the ion balance between the water in the SAP and the water surrounding the SAP. As water enters the SAP structure, the nutrients readily dissolve and generate ions, which increases the ionic concentration in the water withheld by the SAP. This creates an ionic concentration gradient that drives more water to enter inside the SAP to approach the ionic balance.

The reasoning behind the increase in water absorption following an increase in nutrient content, despite a reduction is SAP amount, is attributed to the ionic concentration gradient across the gel. In the example of calcium nitrate:SAP composite, the inside of the gel has a high concentration of Ca ions, whereas the body of water surrounding the gel has a lower Ca concentration. Therefore, water must flow from the outside of the gel to the inside of the gel, to lower this concentration gradient. However, there is also a diffusion of nutrient ions from the SAP to the surrounding water, which lowers the ionic concentration gradient. Since the water is not changed during the swelling tests, the ionic

balance can be reached within a short time, which would alter the effect the initial nutrient content would have on the water absorption performance of nutrient:SAP composites.

Following the understanding of how the ionic concentration in and out of the gel affects water absorption, to prove this reasoning, and to observe how a higher ionic concentration gradient would affect the water absorption potential of the Ca:SAP composites, the water in test beakers was changed after two weeks. After the replenishment with fresh water, water absorption capacities of all Ca:SAP composites increased radically. Changing the water was expected to result in a greater increase for fertilizer-loaded SAPs, since it should greatly increase the ionic concentration gradient across the gel.

This substantial effect can be observed on the previous "Swelling Kinetics of Ca-SAP" plot. The swelling ratios of all calcium nitrate:SAP composites increased sharply, whereas the increase in the control group (pure SAP) was minimal. All but the 20:100 composites reached their maximum swelling ratios on day 23. The best performer 20:100 composite reached its highest absorption on day 28, by swelling with water that is more than 900 times its own weight. Whereas this ratio was slightly over 500x for pure SAP.

To allow fertilizer-loaded SAPs to exhibit their optimum water absorption performance, a new water absorption test was devised, in which the water change was planned to be performed on every measurement day. In fact, compared to the previous Ca:SAP test, the absorption rates of gels increased and reached higher values earlier.

For the upcoming water absorption tests, Calcium nitrate:SAP and Zinc sulfate:SAP composites were synthesized again. The following table provides the composition of the SAP-fertilizer composites:

Table 13: SAP - Fertilizer Composites with Zinc and Calcium Fertilizers.

SAP - Fertilizer (Zinc Sulfate and Calcium Nitrate) Composites						
Fertilizer Ratio (wt%)	**0**	**9.1**	**16.7**	**28.6**	**37.5**	**50.0**
SAP Solution (mL)	50					
SAP Solid Content (g)	5					
Fertilizer (g)	0	0.5	1	2	3	5
Water (mL)	0	2.5	5	10	15	25
Fertilizer:SAP (w:w)	0:1	10:100	20:100	40:100	60:100	1:1

In the initial test, Ca:SAP composite with the highest fertilizer concentration (60 wt%) exhibited very limited water absorption. Hence, this ratio in the subsequent test was lowered to 50 wt%. Only 100:100 fertilizer:SAP (50 wt%) composites were prepared in the upcoming syntheses, in place of 80:100 and 150:100 versions. The SAP with the lowest fertilizer concentration (20:100) performed best in the initial test. To determine whether a lower fertilizer concentration would favor higher water absorption, and eventually establish the optimum fertilizer concentration, a nutrient:SAP composites with a 10:100 ratio was prepared.

The water absorption kinetics of SAPs with varying levels of calcium and zinc nutrient additions are evaluated. Swelling tests were conducted in triplicate with the new samples. From each fertilizer-SAP synthesis, a control group, i.e., pure SAP, and 5 composites at varying nutrient ratios were evaluated. For 3 fertilizers, a total of 18 samples were tested. A total of 54 250 mL beakers were prepared. In each beaker, approximately 0.15 grams of SAP was placed, and it was filled with 250 mL of deionized water. However, due to water absorption ratios exceeding 1000 g/g, gels of some beakers were completely filled with swollen SAP. To allow for further proper water absorption, 9 of these beakers were changed with 400 mL beakers. These test beakers belonged to 20:100 and 40:100 Ca:SAP and 20:100 Zn:SAP samples. Water absorption tests were continued for 4 weeks.

In the plots below, the water absorption kinetics of Ca:SAP and Zn:SAP composites are shown across a time span of 14 days. Furthermore, another set of graphs displays water absorption capacities against nutrient weight fractions, for us to understand how nutrient

content affects water retention ratios of SAPs more clearly. There are two versions of these plots, presenting true and adjusted water absorption ratios.

In this water absorption test, the water in the beakers was changed with fresh deionized water after 1 day and on every measurement day. This procedure eliminates the nutrient ions in the water containing the SAPs, hence resulting in a greater ionic concentration gradient between the inside and outside of the SAP. Subsequently, to lower this concentration gradient, more water from the outside enters the SAP. In the meantime, however, the nutrient ions inside the SAP continue to diffuse to the outside of the gel. Over time, this ion transport results in an increased ionic concentration in the water surrounding the gel and lowers the concentration gradient. Whenever this water is replaced with fresh water, the concentration gradient is increased again. So, by repeating this procedure frequently, the ionic concentration gradient is maintained at a high level throughout the test. Therefore, the optimum water absorption capacities of fertilizer:SAP composites could be measured. For saline absorption tests, a 0.9% w/v of NaCl solution of water was prepared. The other parameters were the same as that of water absorption tests.

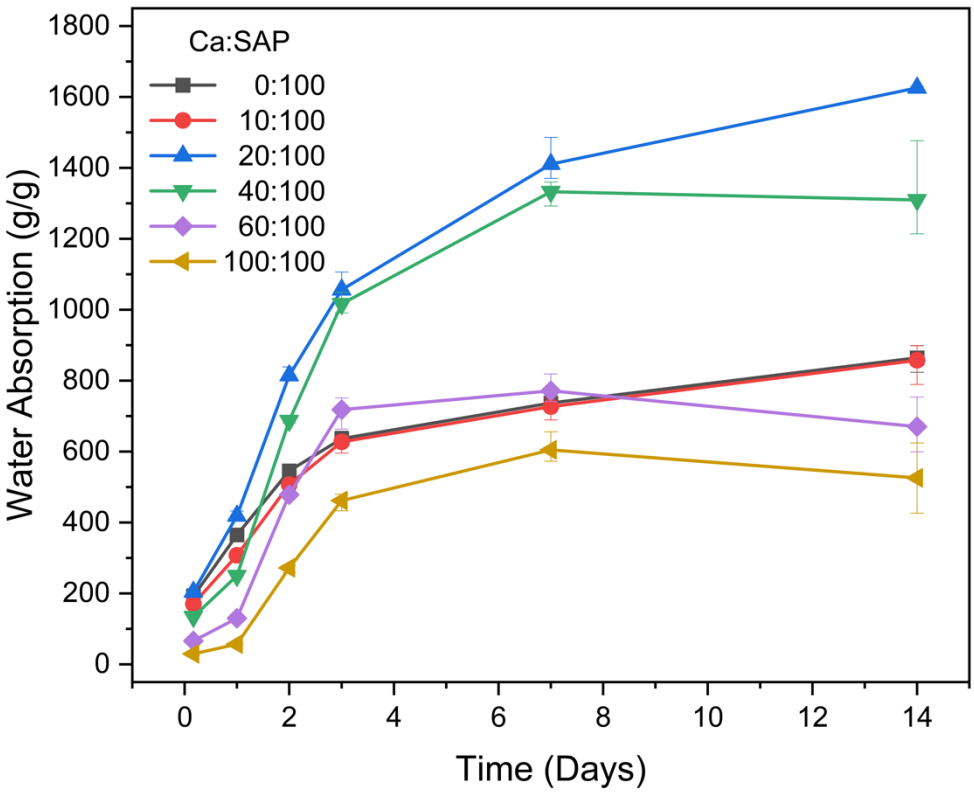

Figure 29: Ca:SAP water absorption (g/g) vs time (days).

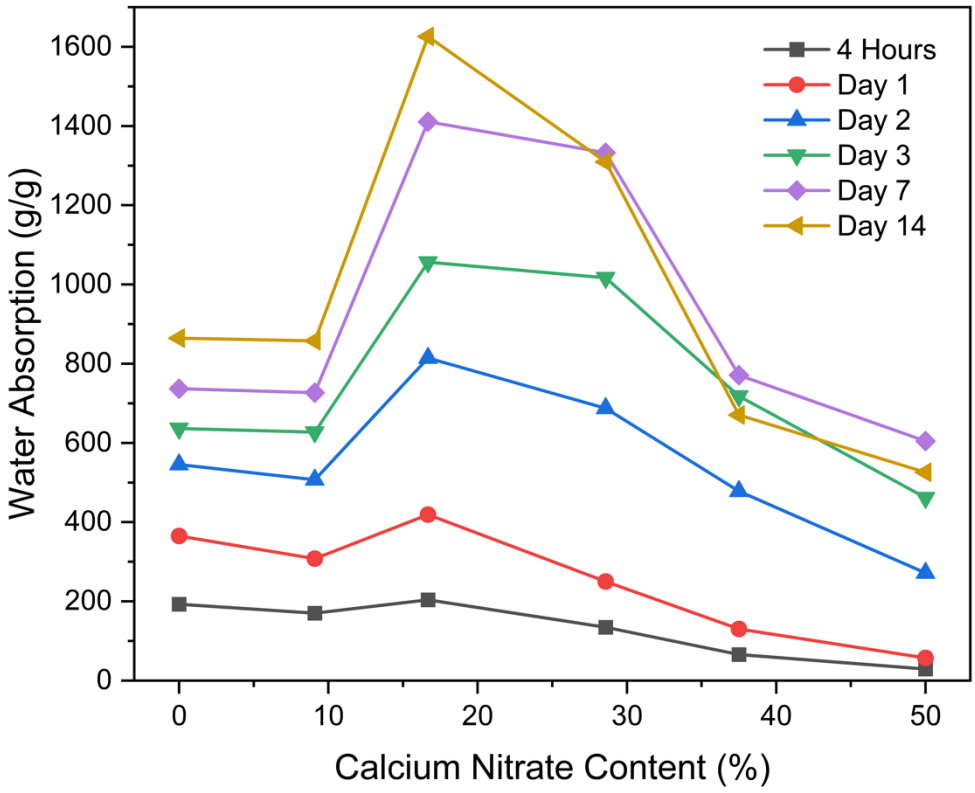

Figure 30: Ca:SAP water absorption (g/g) vs calcium nitrate content (wt%).

From the plots, the effect of replacing the water with fresh deionized water on the water absorption capacity can be easily observed. The first water change took place on day 1. On the plot, the slope of water absorption from day 1 to day 2 is significantly more than the one up to day 1. In the initial part of the graph, this effect can be observed from the changing slopes of all samples except for pure SAP and 10:100 fertilizer:SAP samples. Pure SAP is expected to show a negligible response to the water change, as the water is not expected to be rich in ions. 10:100 fertilizer:SAPs have a very low ratio of fertilizer in their structure. So, the dissolved nutrient ions were not able to create a strong ionic concentration gradient that would positively affect water absorption. In fact, throughout the test, the water absorption capacities of pure SAP and that of 10:100 fertilizer:SAP composites were almost identical.

As in the previous test, the best performer was 20:100 Ca:SAP composite, with a water absorption capacity of 1625 g/g after 2 weeks. It is followed by 40:100 Ca:SAP, which reached a water absorption of 1332 g/g after 1 week. In contrast, pure SAP could only achieve an 864 g/g water absorption after 14 days. All the other samples performed worse than pure SAP. The minimum water absorption was 526 g/g by SAP containing 50 wt%

calcium nitrate fertilizer. Even this water absorption performance is comparable to most commercial SAPs. This shows how effective loading an SAP with a fertilizer can be in terms of improving its water absorption capacity. To understand the effect of fertilizer content better, it is best to analyze the adjusted water absorption data set.

All Ca:SAP composites performed better than pure SAP in terms of the water absorption capacities of their SAP sections. The optimum fertilizer content in this regard was between 16.7 and 28.6 wt% calcium nitrate corresponding to 20:100 and 40:100 Fertilizer:SAPs, respectively.

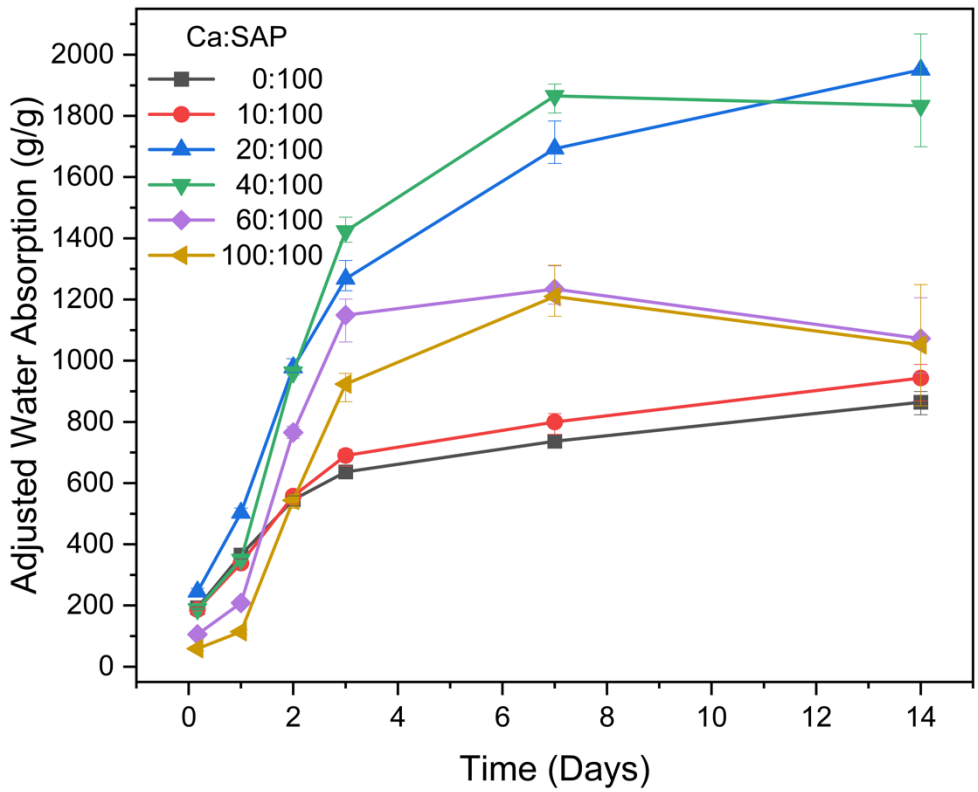

Figure 31: Ca:SAP adjusted water absorption (g/g) vs time (days).

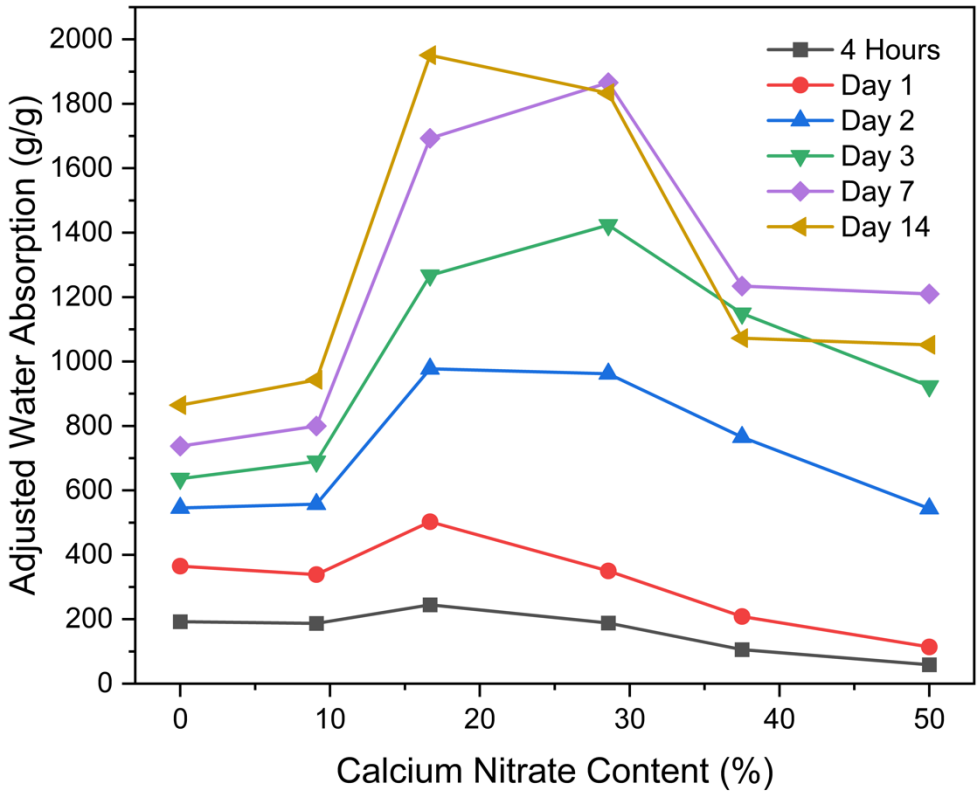

Figure 32: Ca:SAP adjusted water absorption (g/g) vs calcium nitrate content (wt%).

According to adjusted swelling data, the SAP portions of these two formulations achieved water absorption ratios of 2276 and 2136 g/g. Compared to pure SAP, these results correspond to a significant increase of 163 and 147%. In simpler terms, the calcium nitrate fertilizer incorporations in SAP improved its water absorption capacity by 2.63 and 2.47 times, upon 16.7 and 28.6 wt% fertilizer addition. In addition to significantly improved water absorption capacities, adding fertilizer in SAPs gives them the further benefit of supplying the nutrient demand of the soil. Hence, adding calcium nitrate fertilizers in an SAP formulation can be said to have a synergistic effect. Next, the water absorption performance of Zn:SAP composites was evaluated.

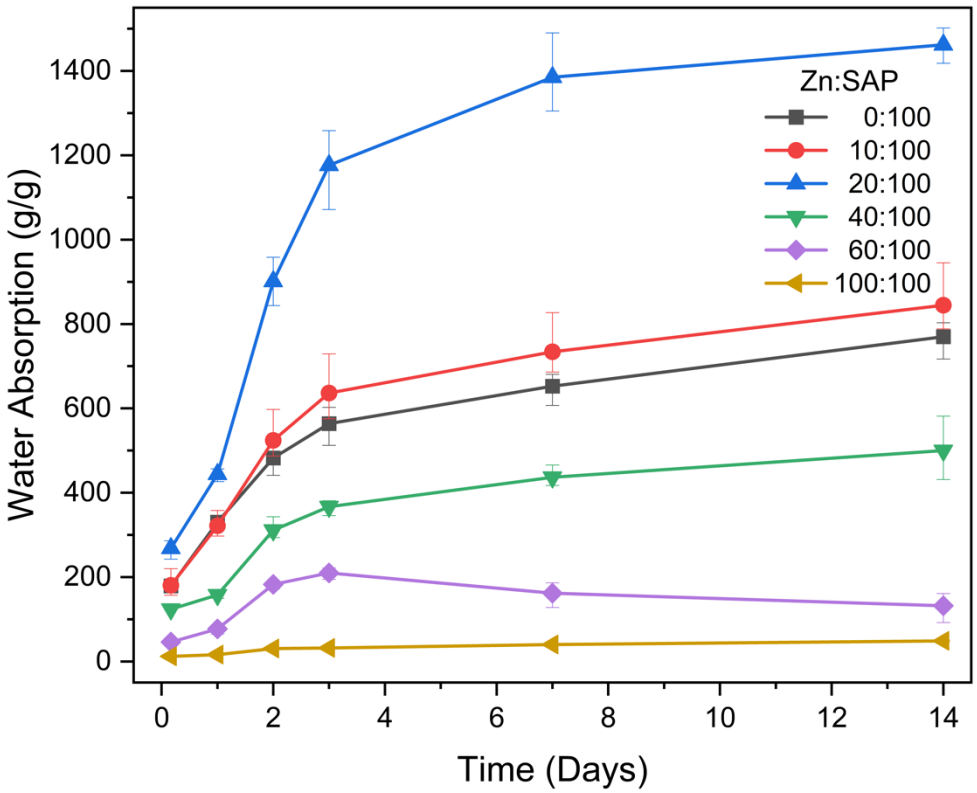

Figure 33: Zn:SAP water absorption (g/g) vs time (days).

Zn:SAP composites with low fertilizer loadings exhibited similar water absorption trends compared to their Ca:SAP counterparts. For example, the best performer was the composite SAP with 16.7 wt% zinc sulfate. Moreover, the water absorption kinetics of pure SAP and 10:100 Zn:SAP was highly similar. However, unlike Ca:SAP composites, the synergistic effect of fertilizer incorporation in SAPs in terms of better water absorption, could not be observed for composite SAPs with higher zinc sulfate ratios, which displayed highly deteriorated water absorption performances. For instance, composite SAP with 37.5 wt% Zn reached peak water absorption of 210 g/g, whereas the SAP with 50 wt% Zn only achieved 45 g/g absorption. In comparison, their Ca-SAP counterparts reached 720 and 605 g/g absorption.

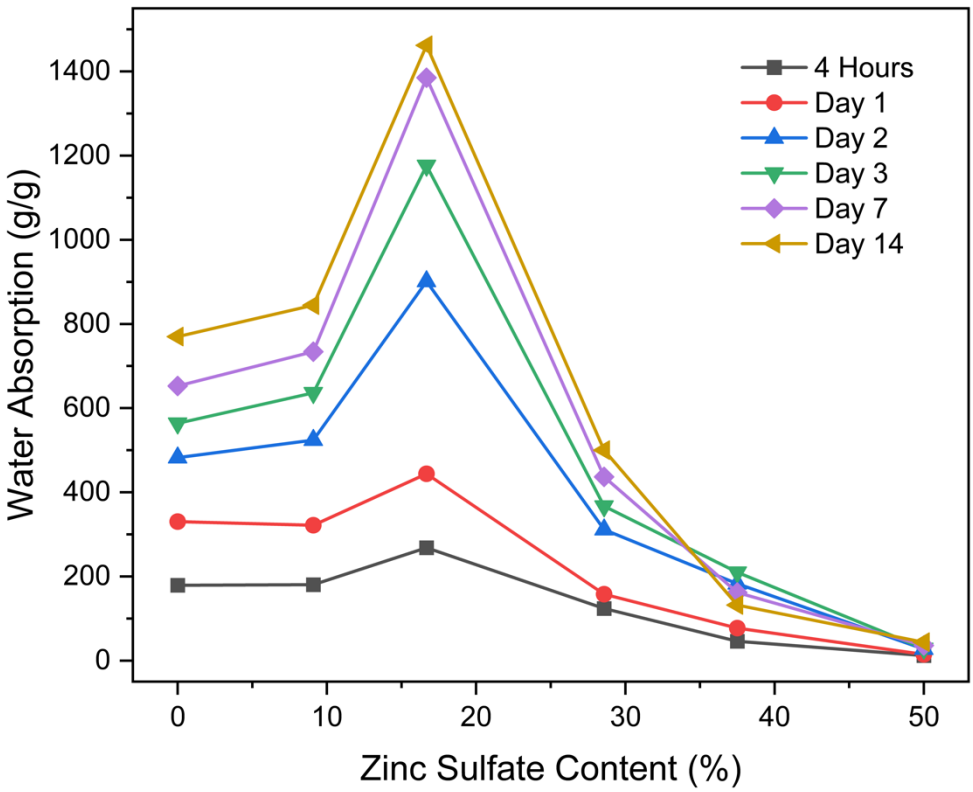

Figure 34: Zn:SAP water absorption (g/g) vs zinc sulfate content (wt%).

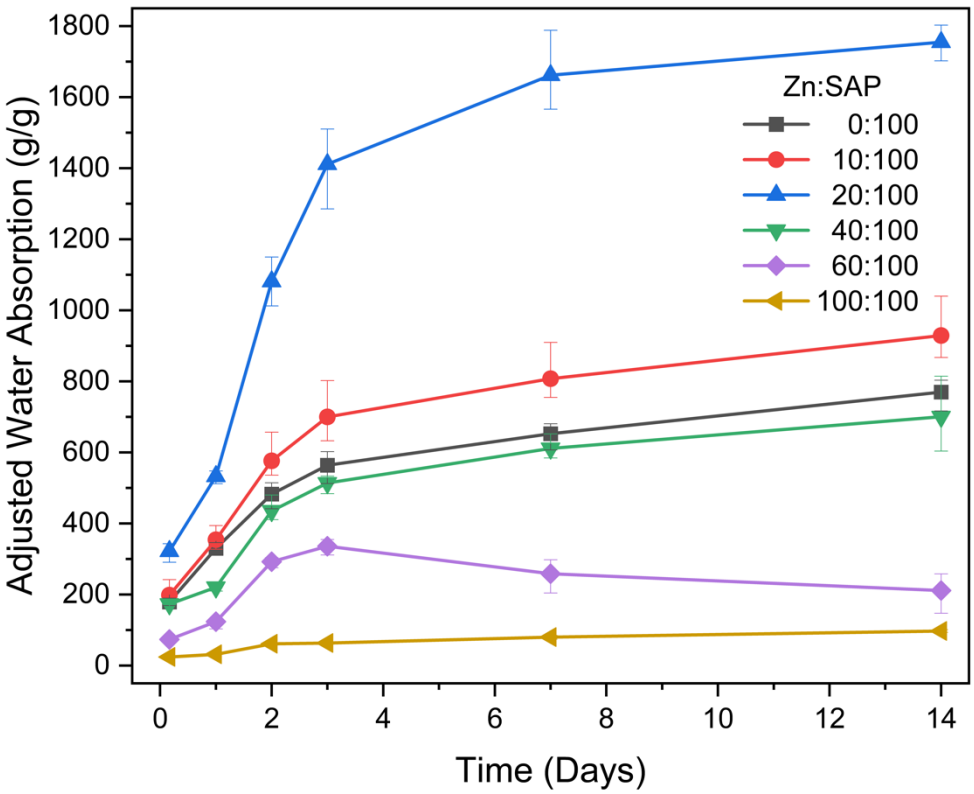

Figure 35: Zn:SAP adjusted water absorption (g/g) vs time (days).

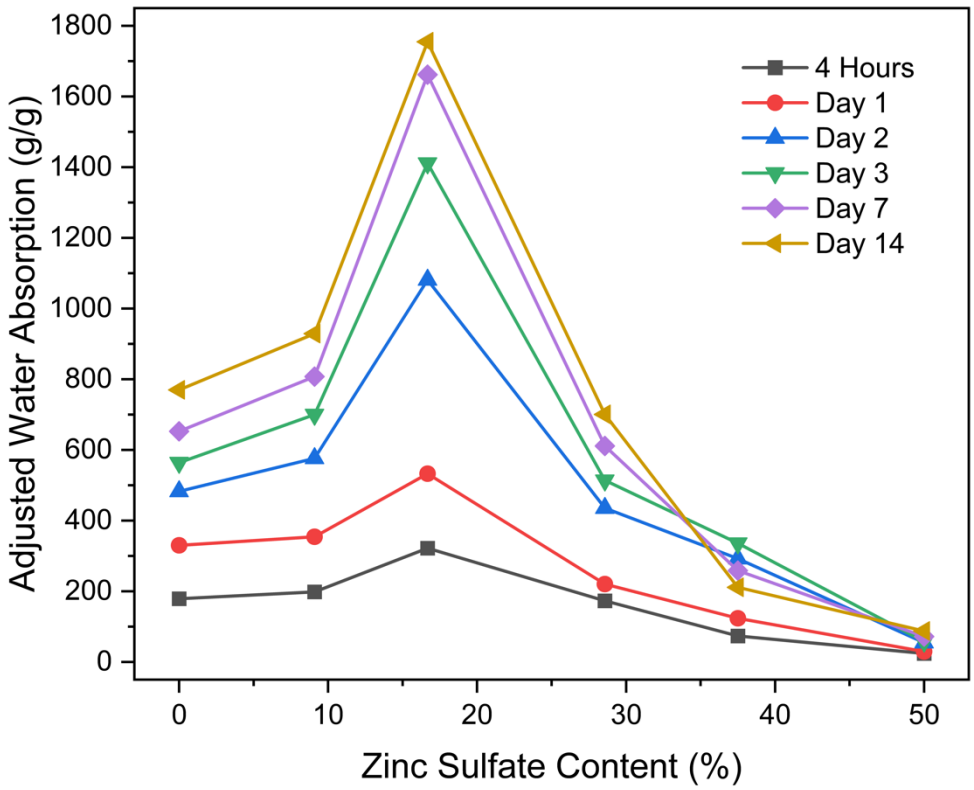

Figure 36: Zn:SAP adjusted water absorption (g/g) vs zinc sulfate content (wt%).

SAP composites with 17 wt% (20:100) calcium sulfate and zinc nitrate achieved superior water absorptions of 1626 and 1462 g/g, respectively. In comparison, most commercial SAPs have water absorption capacities of 400-800 g/g.

The effect of ionic concentration gradient can be used to explain the enhanced water absorption performance of fertilizer-SAP composites compared to pure SAP. However, the same reasoning cannot be used to explain the discrepancy between the water absorption performances of zinc sulfate – SAP and calcium nitrate – SAP composites. The addition of calcium nitrate enhances the water absorption performance of SAPs more than zinc sulfate does. To elucidate this phenomenon, we need to investigate the solubilities of zinc and calcium nutrients in water. Ionic interactions, hydration energy, and lattice energy are the main factors that contribute to the solubility of zinc and calcium ions in water.

Both calcium and zinc have a +2 charge. However, zinc has a higher charge density due to its smaller ionic radius than calcium. The sulfate ion has a double negative charge, whereas the nitrate ion has a single negative charge. Sulfate is a larger ion compared to nitrate, due to its higher charge, and consequently has an increased ionic radius. The

larger size and higher charge of sulfate ions contribute to the stronger ionic interactions and lattice energies of their compounds, compared to compounds of nitrate ions.
Lattice energy depends on the ionic charge and the distance between ions. Higher lattice energy is an indication of a stronger attraction between the ions and a lower solubility. The smaller ionic radius of zinc and the higher charge on the sulfate ions compared to nitrate contribute to stronger electrostatic interactions and higher lattice energy of zinc sulfate compared to calcium nitrate. The interaction between Ca and nitrate ions is weaker, which favors solubility in water.

The hydration energy of an ion is affected by its charge and ionic radius. Higher charge and smaller ionic radius usually favor higher hydration energy due to stronger electrostatic attraction between the ion and water molecules. Zn^{2+} has a smaller ionic radius compared to Ca^{2+}. Although both ions have the same charge, the smaller size of zinc results in a significantly higher hydration energy of zinc sulfate.
The coordination number also influences the solubility of a compound in water. Compounds with a higher coordination number can form more stable complexes, owing to more interactions with water molecules. This results in enhanced solubility, due to ions being more stabilized in the solution. In contrast, compounds with lower coordination numbers have reduced stabilization in solution, and lower solubilities.
Ca^{2+} ion in calcium nitrate tetrahydrate ($Ca(NO_3)_2 \cdot 4H_2O$) is coordinated by 8 oxygen atoms. These atoms include 4 oxygen atoms from 4 water molecules and 4 oxygen atoms from 2 nitrate ions. Therefore, the coordination number of Ca^{2+} is 8. In zinc sulfate heptahydrate ($ZnSO_4 \cdot 7H_2O$), Zn^{2+} ions are coordinated by 6 oxygen atoms. These atoms include 4 atoms from the water molecules and 2 oxygen molecules from the sulfate ion. Similarly, in magnesium sulfate ($MgSO_4 \cdot 7H_2O$), Mg^{2+} ions are coordinated by 6 oxygen atoms – 4 from water molecules and 2 from the sulfate ion. Therefore, both Zn^{2+} and Mg^{2+} ions have a coordination number of 6 in their sulfates, compared to the coordination number of 8 for Ca^{2+} in its nitrate. This is another factor that favors the solubility of Ca^{2+} ions from calcium nitrate, compared to Zn^{2+} from zinc sulfate and Mg^{2+} ions from magnesium sulfate.

Calcium nitrate has higher solubility in water compared to zinc sulfate and magnesium sulfate. The higher solubility of calcium nitrate accelerates its dissolution in water and results in a faster increase in the ionic concentration of the water surrounding the SAP-

calcium nitrate composite. Subsequently, the ionic concentration gradient effect can be observed more for SAP composites with calcium nitrate, rather than SAP composites with zinc- or magnesium- sulfate.

Following deionized water, the SAP-fertilizer composites were tested in a saline solution. For this test, an aqueous 0.9 wt% NaCl solution was prepared. In the following plots, the saline absorption performances of Ca- and Zn-SAPs are presented.

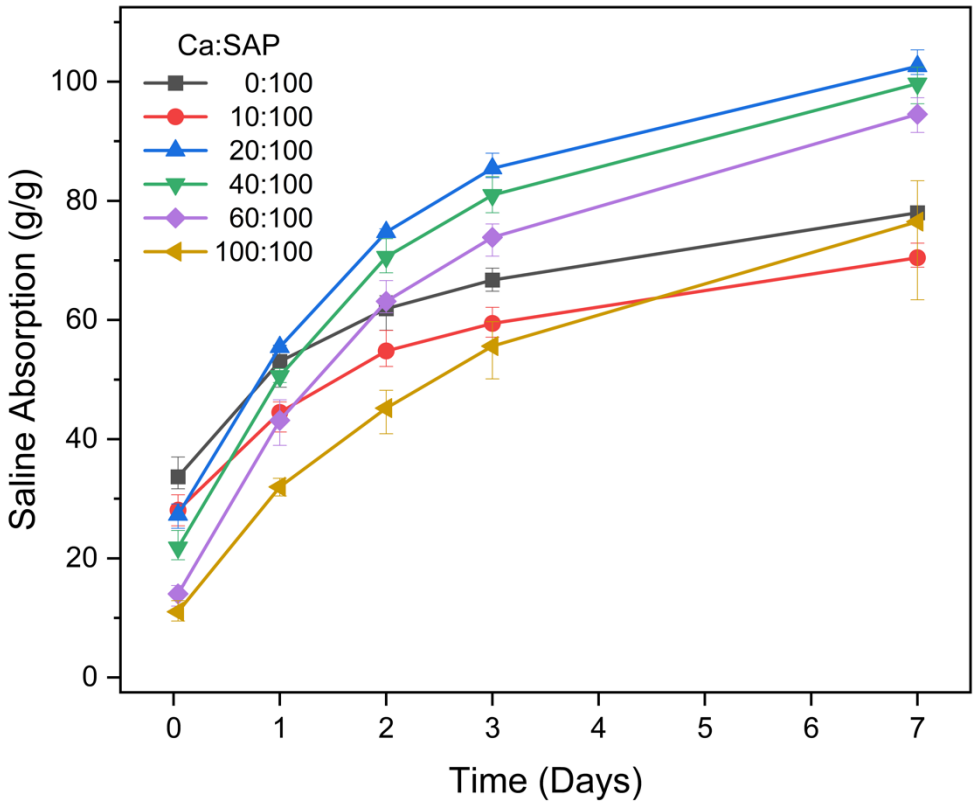

Figure 37: Ca:SAP saline absorption (g/g) vs time (days).

From the beginning of the test, until day 1, pure SAP performed better than Ca-SAP composites. However, on the following days, until day 7, Ca:SAPs incorporating 16.7% to 37.5% calcium nitrate, absorbed more saline compared to pure SAP. These findings are in line with the water absorption test.

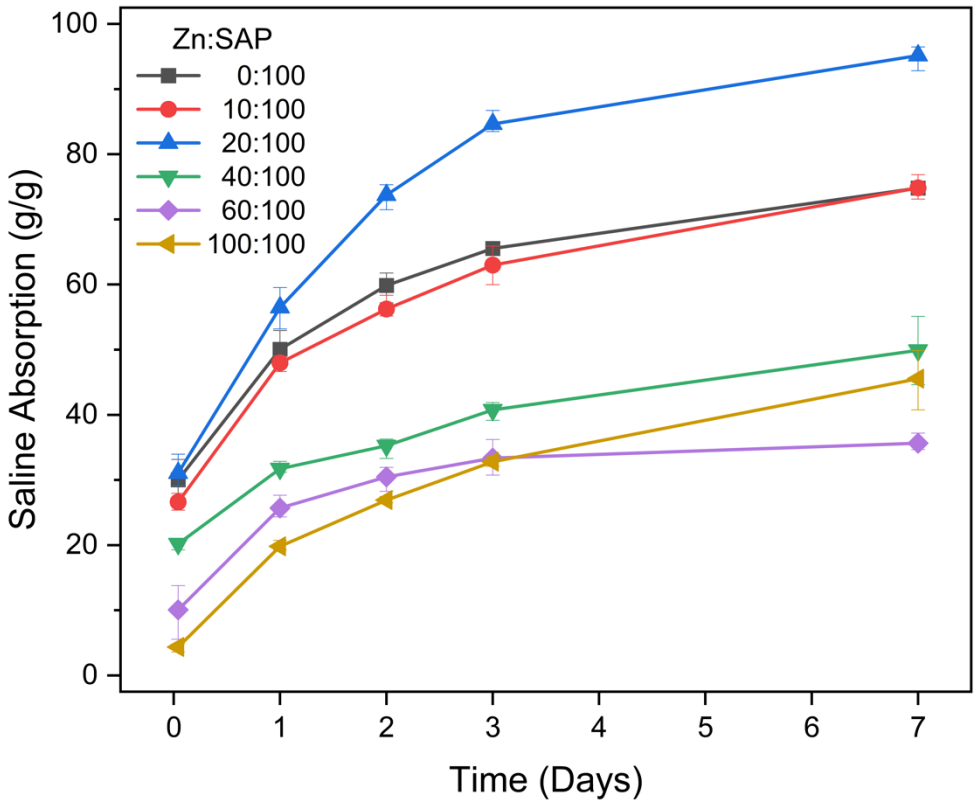

Figure 38: Zn:SAP saline absorption (g/g) vs time (days).

From the beginning of the test, Zn:SAP with 16.7% zinc sulfate performed better than all other samples. In contrast with Ca:SAP samples, pure SAP performed better than SAPs with 28.6% to 38.5% zinc fertilizer addition. These findings are also in line with the outcome of the corresponding water absorption test.

4.3.4. Water Retention Performance of Nutrient Loaded Superabsorbent Polymers

Water retention capacity holds particular significance as a performance metric for SAPs intended for agricultural applications. The longer an SAP can retain water within its structure, the more advantageous it becomes during drought conditions, because it can continuously supply water to plants. While the test conditions did not replicate farming settings, they enabled us to compare different samples under uniform conditions. Furthermore, in soil tests, extracting the swollen gel alongside soil contaminants posed challenges to accurate weight measurements. Therefore, the only viable method to assess water retention would be through soil moisture measurement. However, this method does

not provide data on the weight of water retained by the SAP. As a result, a true water retention test would not be possible in soil. Therefore, the swollen gels were allowed to release water in beakers to prevent any contamination. In the upcoming graph, the water retention ratios are plotted over time.

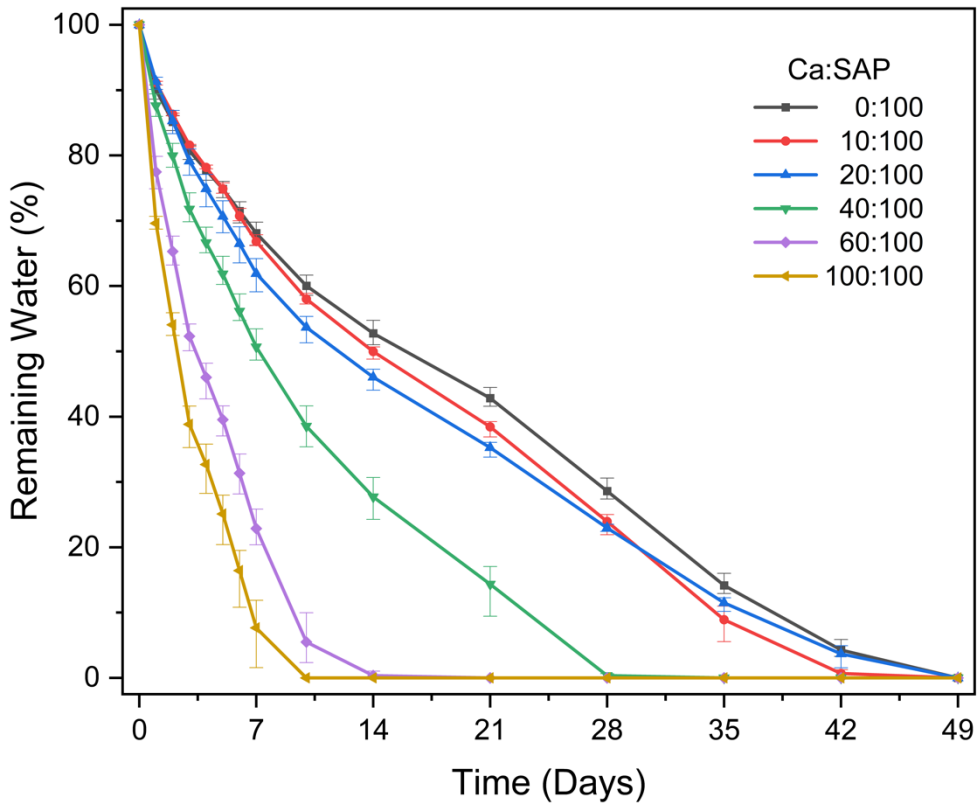

Figure 39: Ca:SAP water retention (%) vs time (days).

Pure SAP outperformed both Ca- and Zn-SAP composites in terms of water retention. Among Ca-SAPs, 10:100 and 20:100 composites performed slightly worse compared to pure SAP. After 14 days, their water retention ratios were 3 and 7% less than pure SAP, respectively, which withheld 53% of initial water. However, the 40:100 composite performed significantly worse and could only withhold 28% of the initial water in its structure, after 14 days. SAP with 38% calcium nitrate exhibited complete water release after 10-14 days. SAP containing 50% calcium nitrate dried completely after 7-10 days.

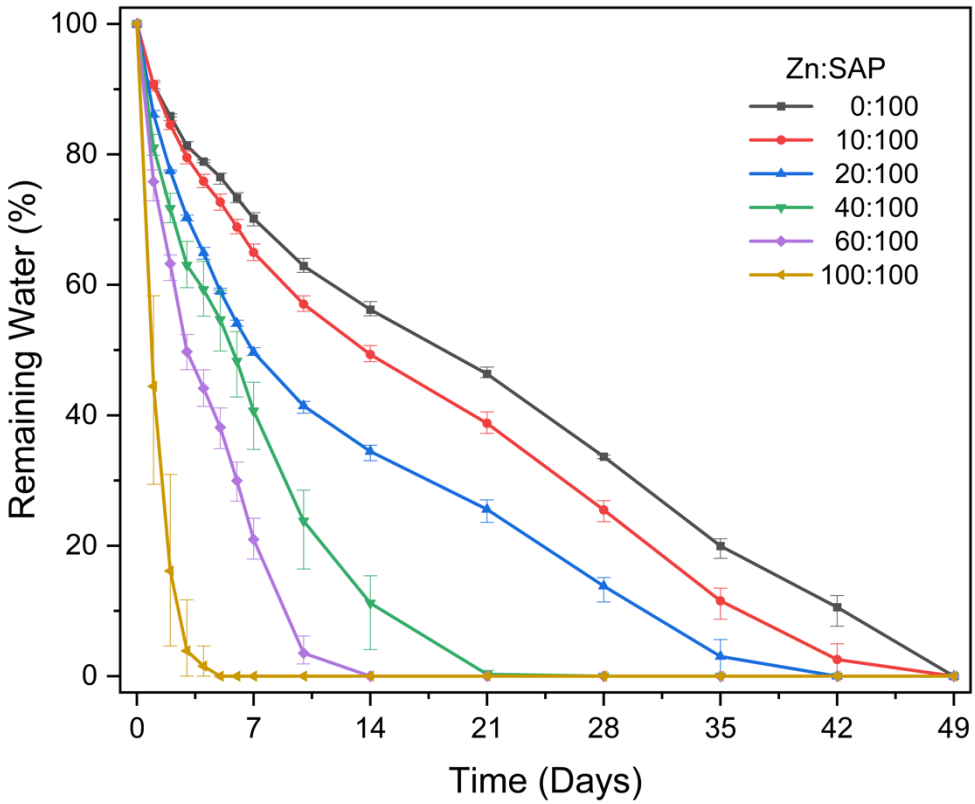

Figure 40: Zn:SAP water retention (%) vs time (days).

A similar trend was observed among Zn-SAP composites, which performed worse than Ca-SAP samples. The water retention capacity of 10:100 Zn:SAP composite was similar to that of Ca:SAP. However, the 20:100 composite released significantly more water compared to its Ca counterpart, with only 34% of initial water retained in its crosslinked structure after 14 days. The 40:100 composite dried completely on day 21, whereas its Ca equivalent still retained 14% of the initial water. Moreover, SAP containing 50% zinc sulfate released the water completely in four days.

Based on these findings, it is reasonable to conclude that SAPs with high fertilizer contents are not suitable for long-term agricultural applications. Nevertheless, they hold potential for short-term soil applications. For instance, such SAPs could be applied as coatings on seeds to enhance their chances of sprouting under drought conditions. Given that the germination phase is typically brief for crops like wheat – around 3 to 5 days – the SAP can function as a water and nutrient reservoir. Using an SAP rich in fertilizer can even be more favorable compared to pure SAP under such circumstances. The inferior swelling ratios of fertilizer-SAPs are sufficient to maintain a moist surrounding for seeds, and they can provide more nutrients for the seeds and the soil. Conversely, SAPs with

low fertilizer contents prove more suitable for extended soil applications, to provide water during prolonged drought periods.

4.3.5. Reusability - Reswelling Capacity of Nutrient Loaded Superabsorbent Polymers

The dry weights and the water absorption ratios of all calcium nitrate and zinc sulfate fertilizer-incorporated SAP samples are plotted throughout three swell-dry cycles. The dry weights are not plotted in units of mass (gram), but rather in terms of the percentage of the original weight remaining. This is done to make a better comparison among samples. The swelling ratio is represented in units of g/g (g of absorbed water / g of initial dry SAP). The x-axes of both plots represent the number of swell-dry cycles.

In the upcoming graphs, the dry weights of calcium nitrate and zinc sulfate fertilizer-incorporated SAPs, after each swell-dry cycle, are plotted.

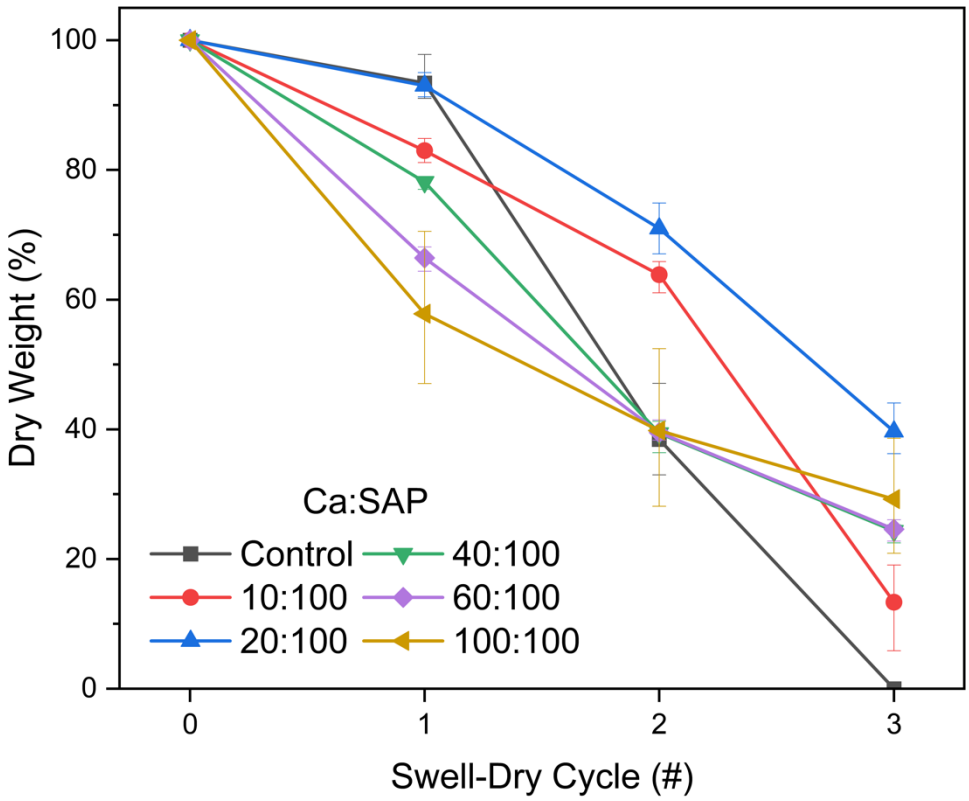

Figure 41: Ca:SAP Retained Dry Weight (%) vs Swell-Dry Cycle.

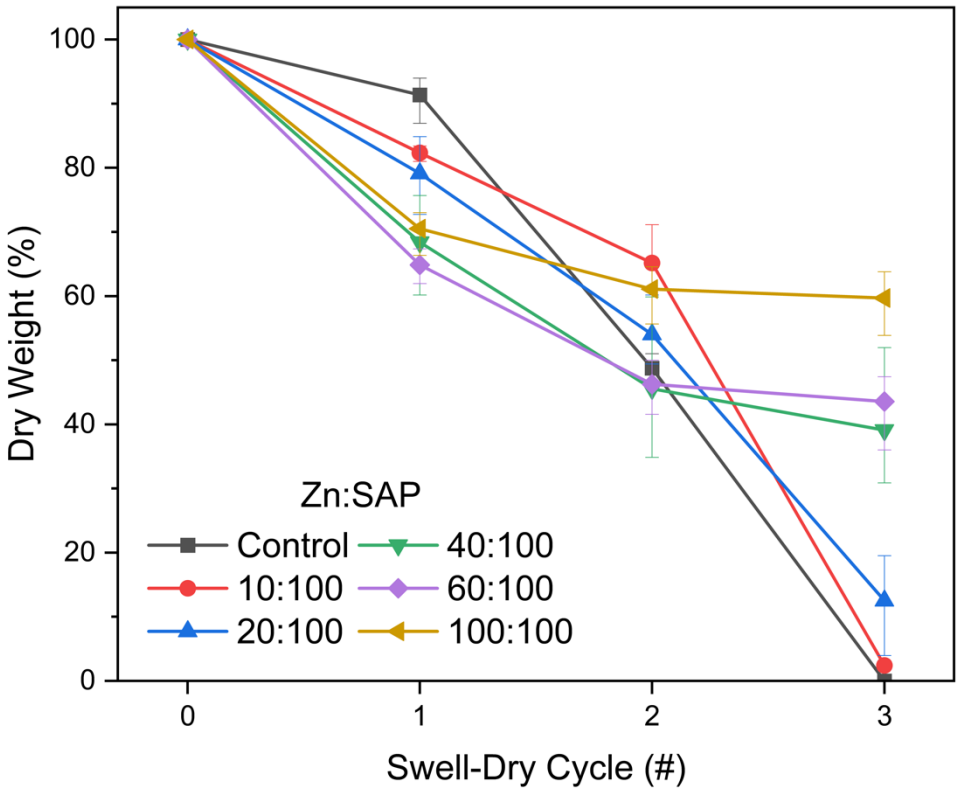

Figure 42: Zn:SAP Retained Dry Weight (%) vs Swell-Dry Cycle.

Fertilizer-SAP samples lost their dry weight after each swell-dry cycle. The amount of weight loss varied across different fertilizer incorporations. A direct correlation between fertilizer content and weight loss could not be observed during the first and second swell-dry cycles. However, at the end of three swell-dry cycles, the percent retained weight of fertilizer-SAPs was directly correlated to the fertilizer ratio in the SAP structure. In other words, at the end of swell-dry cycles, SAPs with more fertilizer content retained a higher proportion of their initial dry weights. This outcome is justifiable, because, since the SAPs are allowed to swell for only 24 hours per cycle, the fertilizer in the SAP structure do not have enough time to completely release into the surrounding water. Therefore, upon swell-dry cycles, the SAPs with initially more fertilizer content could retain more fertilizer in their structures that add to their total dry weights.

The water absorption ratios of fertilizer incorporated SAP samples, after each swelling cycle, are presented in the following plot:

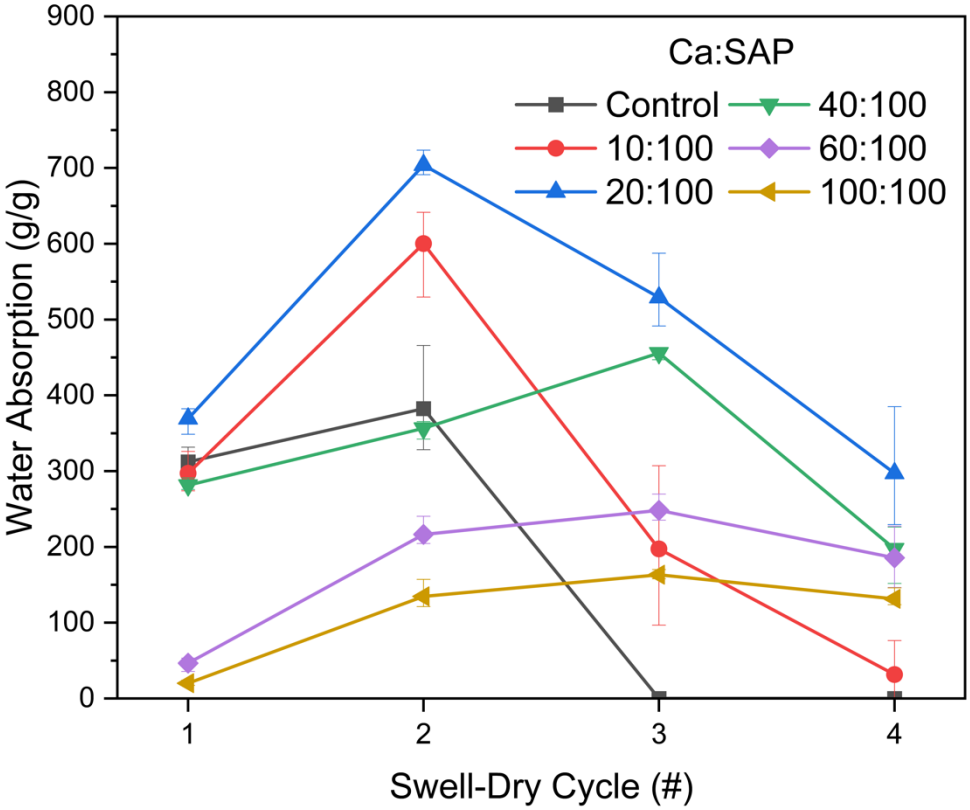

Figure 43: Ca-SAP Water Absorption (g/g) vs Swell-Dry Cycle.

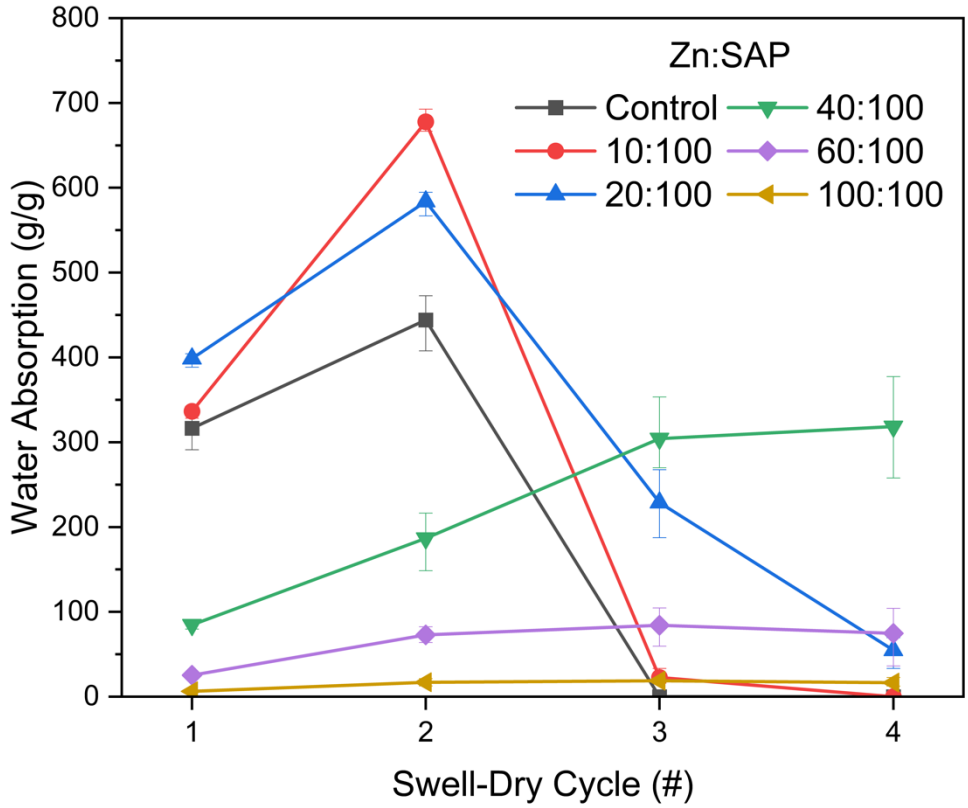

Figure 44: Zn-SAP Water Absorption (g/g) vs Swell-Dry Cycle.

The change in total water absorbed going from swell cycle #1 to #2, follows a trend similar to that of bio-SAP samples. Like CMC incorporated SAPs, the 24-hour swelling capacity of fertilizer-SAPs of every fertilizer concentration increased in the second swelling cycle. This was highly expected since the same surface area expansion phenomenon took place. As previously mentioned, following the first swell cycle, tiny pieces of SAP samples reached expansive volumes. Once dried, these samples occupied a much greater surface area compared to their initial state. As mentioned before, the swelling test in these evaluations are only for 24 hours, so they measure the kinetics of water absorption, rather than equilibrium swelling capacities. Therefore, the gel weights following the second swell cycle were all higher than those belonging to the first swell cycle.

As one can note, only cycles #1 and #2 were mentioned in terms of similarities in changing swelling kinetics. This is because the total water absorptions of lower fertilizer containing SAPs, at the end of the 3rd and 4th swell cycles, were considerably lower compared to the first two cycles. This was not the case for CMC-SAP samples. In fact, an opposite trend was observed for bio-SAPs. Most cellulose incorporated SAPs increased their water absorption up until the 3rd swell cycle, with only two samples (50 and 60 wt% CMC-SAP) having a slightly reduced gel weight compared to 2nd swelling cycle. Water absorption capacities of Bio-SAP samples started to deteriorate only at the end of the 4th swelling cycle. Even so, most samples did hold approximately 60% of their water absorption capacities compared to the previous swell cycle.

When we analyze the water absorptions of calcium nitrate incorporated SAPs, the most apparent trend going from swell cycle #2 to #3 is the deteriorated swelling capacities of pristine SAP, 10:100 Ca:SAP, and 20:100 Ca:SAP samples. On the other hand, other samples slightly increased their water absorption. However, in the final swelling cycle, all samples showed weakened absorption capabilities. A very similar trend was observed for zinc sulfate incorporated SAPs. The main difference was that Zn-SAPs had overall lower swelling capacities, especially for higher fertilizer concentrations.

An interesting and unexpected outcome from both the Ca- and Zn-SAP swelling tests was the fact that pristine SAPs, without any fertilizer addition, completely lost their swelling ability on the third swelling cycle. This situation was not observed for any of the samples

in the CMC-SAP range. The following note is important in this regard. The main difference between the “pristine” SAP versions in the fertilizer:SAP and CMC-SAP samples was the addition of halloysite nanotubes (HNT) during the polymerization of SAP that was used for fertilizer incorporation studies. The optimum SAP formulation in this study contained HNT, which enhanced mechanical properties substantially, as was shown by rheological studies. Therefore, it was not expected for HNT-SAP to perform poorly in swell-dry-reswell cycles. However, this result was observed for 2 different HNT-SAP samples, synthesized in two different polymerization reactions, each tested with 3 replicates.

On the other hand, carboxymethyl cellulose incorporated SAPs (CMC-SAP) performed significantly better than HNT-SAP (at 5 wt% HNT) throughout all CMC concentrations tested.

4.3.6. Nutrient Release Kinetics

The first set of plots presents the conductivities of the solution to which nutrients are released over time. The next set of plots displays the representative nutrient release kinetics of both Ca and Zn-SAP samples.

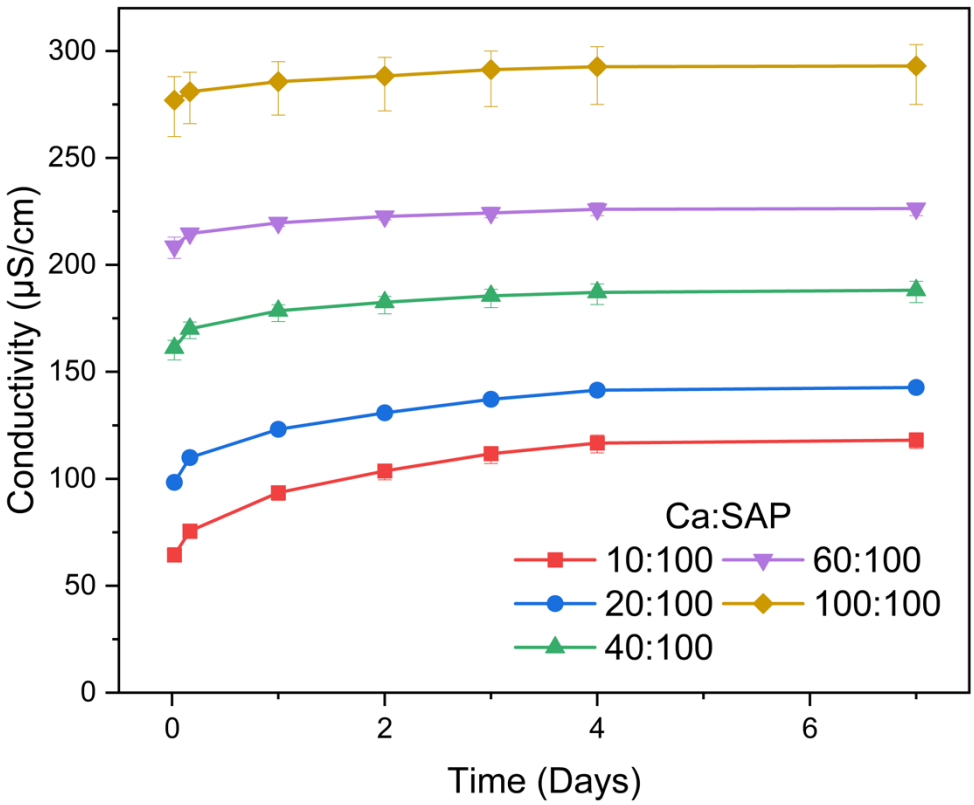

Figure 45: Conductivity of solutions in which calcium nitrate - SAP composites are allowed to swell.

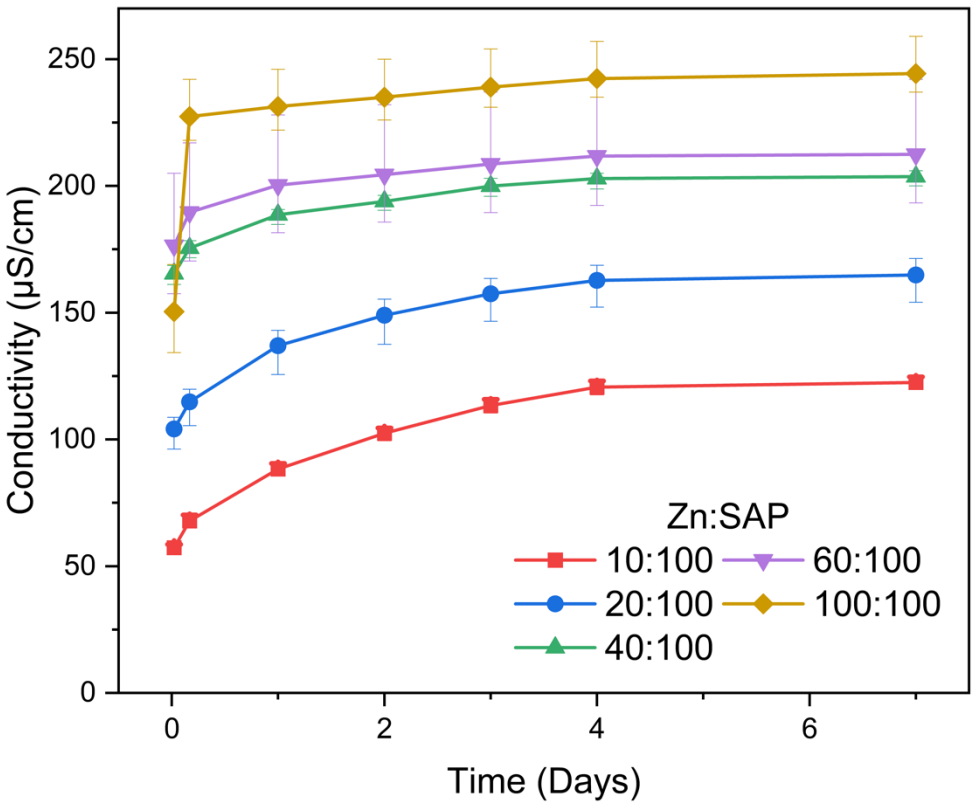

Figure 46: Conductivity of solutions in which zinc sulfate - SAP composites are allowed to swell.

As expected, the conductivity of solutions in which the highest nutrient-containing SAP composites reached the highest values. The only anomaly observed is in the conductivity plot of 100:100 Zn:SAP sample. On the first measurement at 30 minutes, the conductivity of its solution is lower compared to that of 40:100 and 60:100 samples, which is not expected as it contains more nutrients. However, there is a reasonable explanation. The water absorption capacity of 100:100 Zn:SAP sample is highly limited compared to the latter. A low water absorption significantly limits the dissolution and release of nutrients inside the SAP structure into the swelling medium. Nonetheless, after day 1, sufficient nutrients were released to bring the conductivity higher than that of the other samples.

A limiting condition was necessary for the conductivity-to-release conversion. The nutrient release from all samples was assumed to have been completed by day 7. Also, the conductivity ratios were assumed to be equivalent to release ratios. So, for example, the conductivity on day 1 divided by the final conductivity on day 7 represents the ratio of nutrients released into the solution. The second set of percent nutrient release plots is derived according to this calculation method.

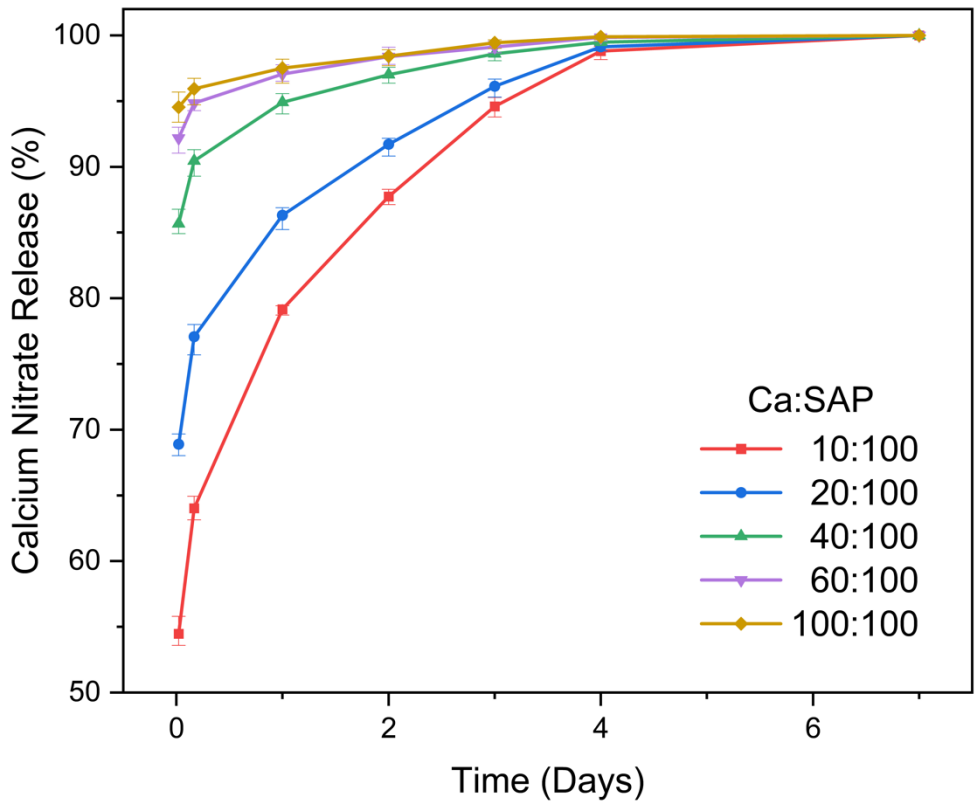

Figure 47: Calcium nitrate release from Ca:SAP samples, deduced from conductivity data.

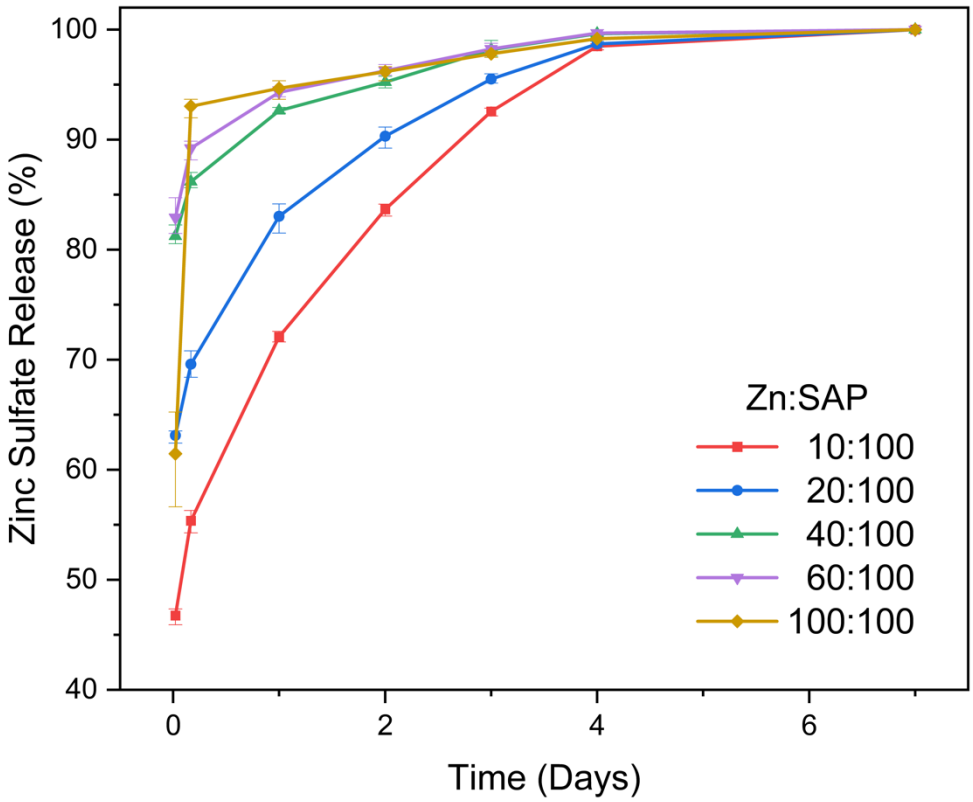

Figure 48: Zinc sulfate release from Zn:SAP samples, deduced from conductivity data.

The nutrient ratio in the SAP composites determines the nutrient release kinetics. The most important and apparent trend observed here is that a lower nutrient concentration in the SAP composite favors a slower release of nutrients into the swelling medium. For example, among Ca:SAP composites, the slowest nutrient release after day 1 is observed for the 10:100 sample, at 79%. Whereas, the 1-day nutrient release rates for the remaining samples are 86, 95, 97, and 98% for the 20:100, 40:100, 60:100, and 100:100 samples, respectively.

4.3.7. Finding the Optimum Fertilizer-SAP Ratio

SAPs are generally applied to large, open agricultural fields. The main type of plant grown on such fields is grains. The amount of fertilizer to be applied is determined according to the demand of the specific crop and nutrients already available in the soil. The latter depends on the cultivation techniques used by the farmer. For example,

conventional farming relies mostly on chemical fertilizers; does not incorporate regenerative agriculture practices such as cover cropping, crop rotation, or no-till; and does not make use of compost or manure as nutrient sources. Therefore, for conventional agriculture, most of the nutrient demand of the plant needs to be replenished by chemical fertilizers during each cultivation cycle.

Sadeghi et. al. analyzed the combined effect of the application of varying rates of zinc and magnesium fertilizers on wheat yield. They concluded that 60 kg ha^{-1} of zinc sulfate and 140 kg ha^{-1} of magnesium sulfate increased wheat yield. (Sadeghi & Soleimani, 2012) The recommended dose of calcium nitrate depends on the produce, but the minimum dose ranges from 100 to 300 kg ha^{-1}. (Georges Chidiac, n.d.)

The suggested application dose of SAPs is approximately 45 kg per hectare. (Y. Yang et al., 2022) This dose changes according to the swelling capacity of the SAP, which is measured in distilled water. For example, an SAP with a swelling ratio of 1000x can be applied roughly half as much as an SAP that can swell up to 500x its own weight. However, the important criterion here is the swelling performance of SAPs under the soil, which is not listed by the manufacturers.

It is interesting to note that most studies in the literature focus on incorporating urea and NPK fertilizers in soil, rather than micronutrients. (Che Ani et al., 2022; Rashidzadeh & Olad, 2014; Sarkar et al., 2014; Sarkar & Datta, 2014; Xu et al., 2019) Considering the recommended dose of SAPs, the amount of fertilizer that can be delivered to the soil is negligible. Even with very high fertilizer incorporation of 50 wt%, only 22.5 kg/ha of urea or NPK can be applied, which is 15-22% of the recommended dose. Therefore, SAPs are inadequate as macronutrient reservoirs.

On the other hand, calcium and zinc fertilizers are applied in much lower quantities. For instance, zinc sulfate and calcium nitrate have recommended doses of 3-8 kg/ha (Zinc Nutrient Initiative) and 5-30 kg/ha (Incitec Pivot Fertilisers, 2021) for most crops, respectively. Zinc-incorporated SAPs can provide the bulk of the recommended dose of the nutrient. A 20:100 Zn-SAP composite comprises 7.4 kg/ha of zinc sulfate for 45 kg/ha SAP application and has superior water absorption capacity, compared to pure SAP. Therefore, the composite SAP can act both as a water reservoir during drought and as an

ample supply of zinc micronutrients. Calcium has a higher application rate compared to zinc. Therefore, 40:100 Ca:SAP can be preferred, which contains 12.8 kg/ha of calcium nitrate for the same SAP application rate. Accordingly, Ca:SAP composites can supply a significant portion of the nutrient while acting as an adequate water reservoir.

SAP-fertilizer composites would be even more effective for micronutrients that require lower application doses, such as boron (0.6-2.0 kg ha^{-1}) (Mousavi & Raiesi, 2022), copper (5-10 kg ha^{-1}) (Incitec Pivot Fertilisers, 2022a), iron (0.5-8 kg ha^{-1}) (Incitec Pivot Fertilisers, 2022b), manganese (3.4-16.8 kg ha^{-1}) (International Plant Nutrition Institute, n.d.), molybdenum (0.6-2.2 kg ha^{-1}) (International Plant Nutrition Institute, n.d.; KAISER et al., 2005), and zinc (3-8 kg ha^{-1}) (Zinc Nutrient Initiative, 2015).

For micronutrients applied at very low doses, the recommended fertilizer-SAP composition would be 10:100, 20:100 or 40:100. The water absorption capacities of these fertilizer-SAPs are similar, if not superior compared to pure SAP. Hence, it is not necessary to increase the amount of polymer to attain the same level of water-holding capacity of the soil. For a 20:100 fertilizer:SAP composite, a dose of 45 kg ha^{-1} of SAP-fertilizer translates to $\frac{20}{120}$ (45 kg ha^{-1}) = 9 kg ha^{-1} of fertilizer. This range covers the recommended doses of boron, copper, iron, manganese, molybdenum, and zinc. Alternatively, an SAP-fertilizer with a ratio of 40:100 can be used. In this case, the relative nutrient application dose would be $\frac{40}{140}$ (45 kg ha^{-1}) = 12.86 kg ha^{-1}.

4.4. Bio-based Superabsorbent Polymers

The aim of this study was to develop carboxymethyl cellulose (CMC) based SAPs and to understand how varying the CMC content affects material properties, water absorption performance, and biodegradability. Maximum water absorption of 600 g/g was achieved by SAP with 10 wt% CMC. SAPs with 20 and 30 wt% CMC exhibited water absorption performance comparable to synthetic SAP. SAPs with more than 40 wt% CMC biodegraded completely by cellulase enzyme after 3 days.

4.4.1. Synthesis of CMC-Based Superabsorbent Polymers

Almost all commercially available SAPs are derived from acrylic acid and/or acrylamide monomers, use sodium hydroxide as the neutralizing agent, and incorporate a cross-linker, which forms the bridge between polymer chains. In our study, a similar SAP formulation was developed, with a few modifications to make them more suitable for use in agriculture.

The SAP in this study is a copolymer of three monomers, acrylic acid, acrylamide, and AMPS. In a previous study, the copolymerization of acrylamide and AMPS improved the stability of the main chain under high salinity and temperature. In another study, an ionic comonomer, acrylic acid, is included in the reaction mixture, along with acrylamide. The resultant copolymer had a higher swelling capacity and improved pH sensitivity. Therefore, to optimize swelling capacity, and to improve stability under high salinity conditions, a copolymer with these three monomers was developed.

Sodium ions can displace other mineral nutrients in the soil, which leads to nutrient deficiencies. So, sodium is not desired in farming. On the other hand, potassium is one of the essential macronutrients. Therefore, to make the SAP formulation more suited for agricultural applications, potassium hydroxide was used as the neutralizing agent, instead of sodium hydroxide.

In this study, carboxymethyl cellulose (CMC) was incorporated in an otherwise synthetic SAP formulation, at varying weight fractions. A total of 7 CMC-SAPs, with a wide range of CMC concentrations, were synthesized. The tested CMC weight fractions were 5, 10, 20, 30, 40, 50, and 60% out of the total CMC-SAP weight. A fully synthetic SAP, with no CMC, was also synthesized to act as the reference control group.

4.4.2. Morphology of CMC-Based Superabsorbent Polymers

The surface morphologies of CMC and CMC incorporating SAPs were evaluated by SEM. The SEM micrographs presented below show the shape of CMC particles, and the cross-sectional surfaces of the CMC-SAP samples.

4.4.2.1. Carboxymethyl Cellulose

Figure 49: SEM images of carboxymethyl cellulose

CMC mostly has a fibrous structure. The diameter of most fibers approximately ranges from 10 to 30 micrometers.

4.4.2.2. Control – Pure SAP

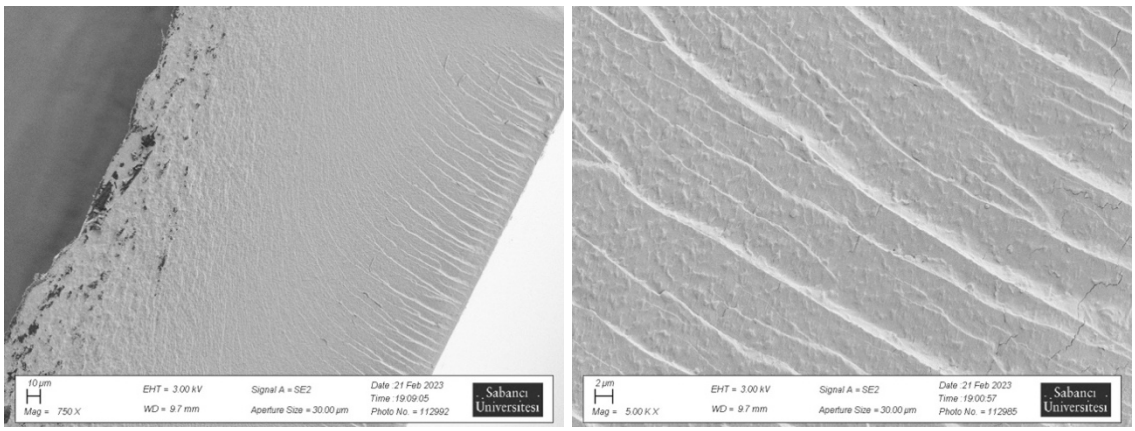

Figure 50: SEM images of control SAP

Pure SAP, without any CMC addition, has a very smooth cross-sectional surface, as expected, without any fillers. Only small surface cracks can be observed, due to fracture.

4.4.2.4. SAP with 5 wt% CMC

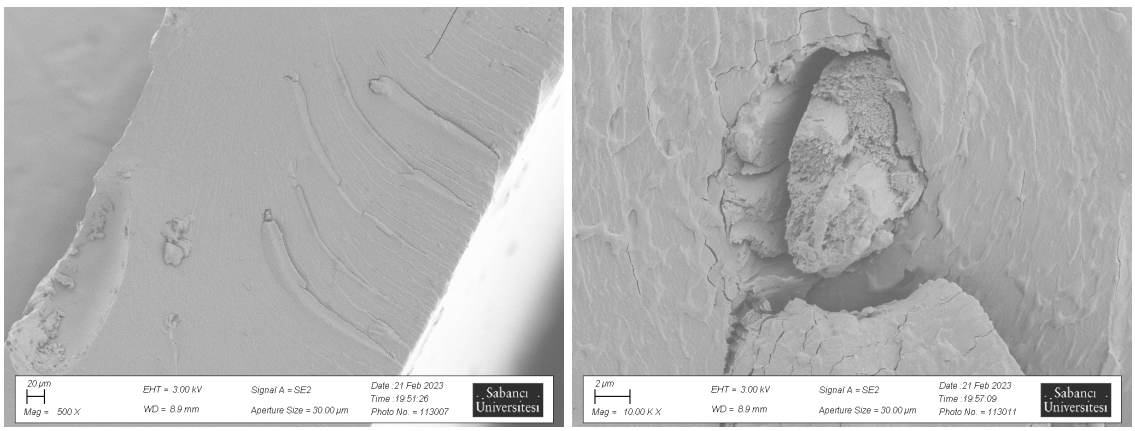

Figure 51: SEM images of SAP with 5 wt% CMC

As we start to incorporate CMC in the SAP structure, we start to see some fiber-like fillers in the matrix. At 5 wt%, CMC particles can be observed along the edges of the SAP sample. More instances of clusters of CMC fibers can be observed in the middle section of the cross section, penetrating through the surface. Similarly, most CMC fillers can be observed along the edge, on the left-hand-side of this particular image. However, other than these regions, the surface is very smooth, similar to pure SAP.

4.4.2.5. SAP with 10 wt% CMC

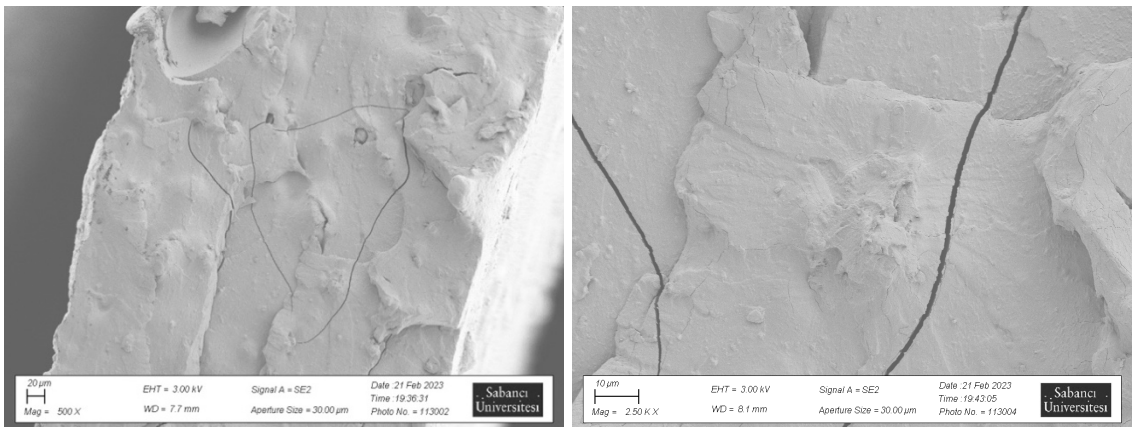

Figure 52: SEM images of SAP with 10 wt% CMC

As the CMC content is increased to 10 wt%, a significant increase in the roughness of the surface is observed. However, the CMC fibers are still neither widespread nor clearly visible.

4.4.2.6. SAP with 20 wt% CMC

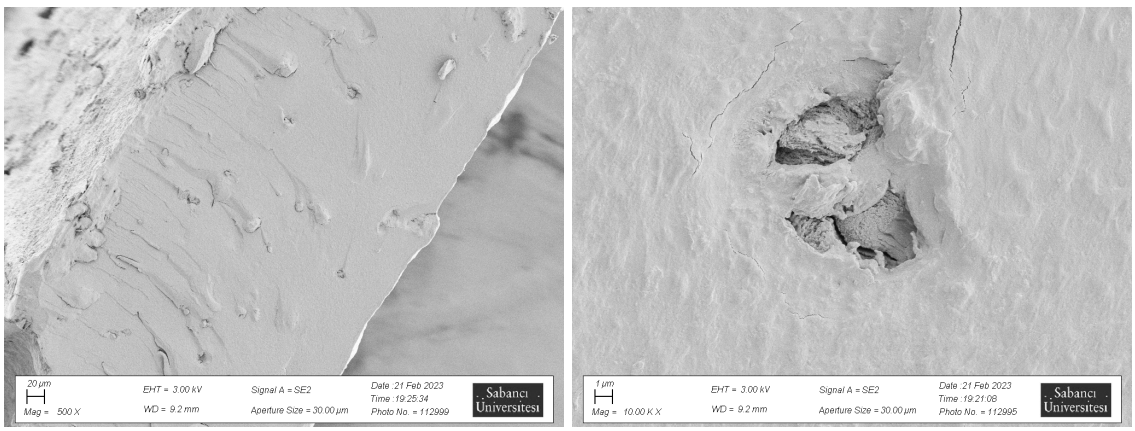

Figure 53: SEM images of SAP with 20 wt% CMC

When the CMC ratio is increased to 20 wt%, more CMC fibres throughout the entire cross-sectional surface can be observed.

4.4.2.7. SAP with 30 wt% CMC

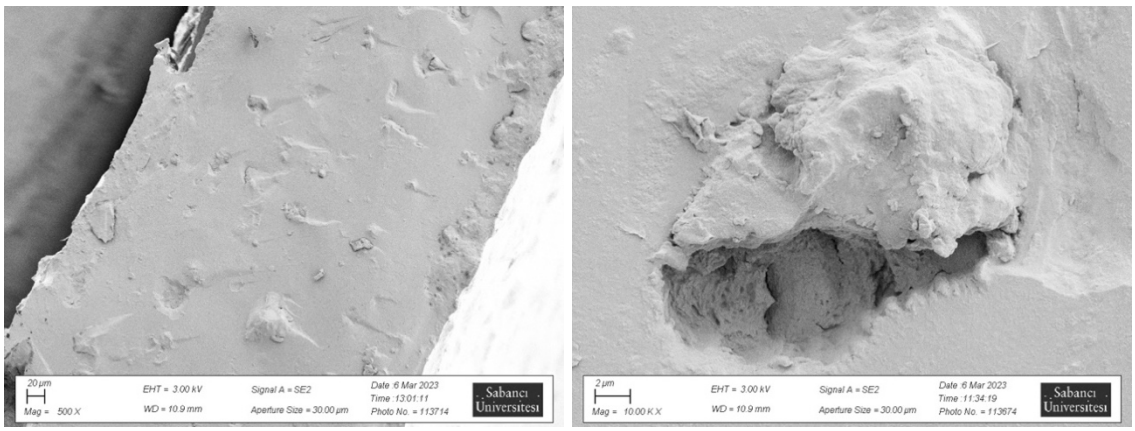

Figure 54: SEM images of SAP with 30 wt% CMC

As we further increase the CMC ratio in the SAP to 30 wt%, we observe more fillers penetrating through the cross-sectional surface, compared to 20 wt% CMC-SAP. However, the instances of CMC fillers present on the surface is significantly less than one would expect from a material containing 30 wt% CMC. Also, the overall roughness of the surface does not seem to increase noticeably.

4.4.2.8. SAP with 40 wt% CMC

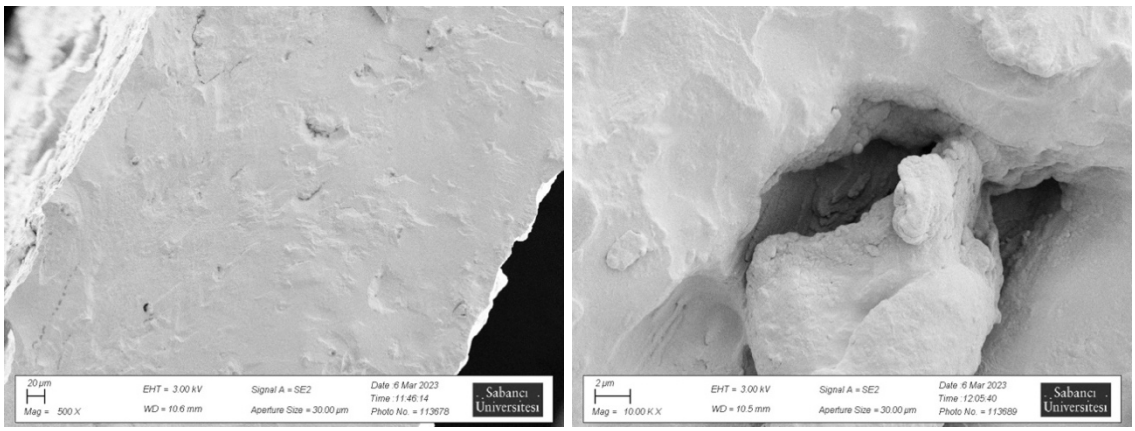

Figure 55: SEM images of SAP with 40 wt% CMC

As the CMC ratio in the SAP reaches 40 wt%, total instances of CMC fillers on the surface do not significantly increase. However, the cross-sectional surface appears to be rougher, overall. Yet, the appearance of the SAP is highly uniform, despite a high ratio of CMC fillers.

4.4.2.9. SAP with 50 wt% CMC

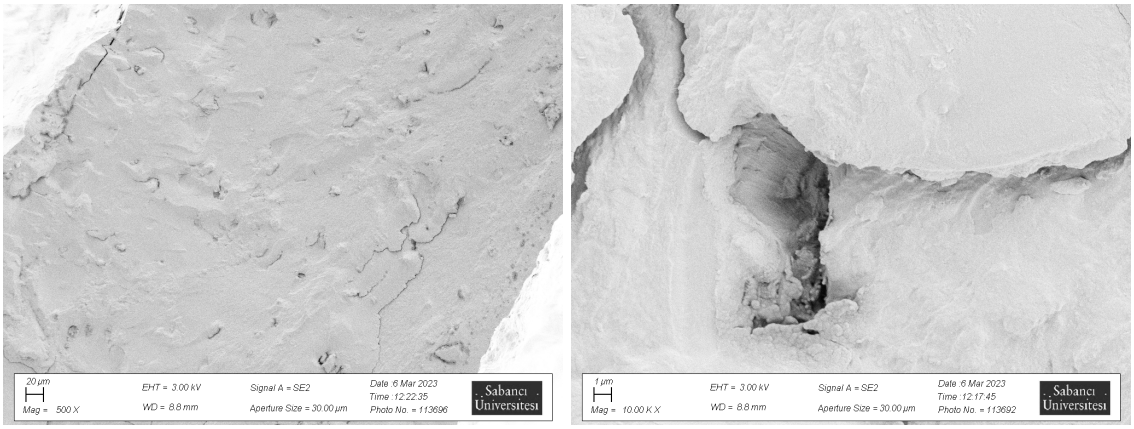

Figure 56: SEM images of SAP with 50 wt% CMC

The cross-sectional surface of SAP with 50 wt% CMC displays noticeably more occurrences of fillers than SAPs with lower CMC contents. Also, the overall appearance of the surface is rougher. Yet, the appearance of the SAP is highly homogeneous, despite a very high concentration of CMC fillers.

4.4.2.10. SAP with 60 wt% CMC

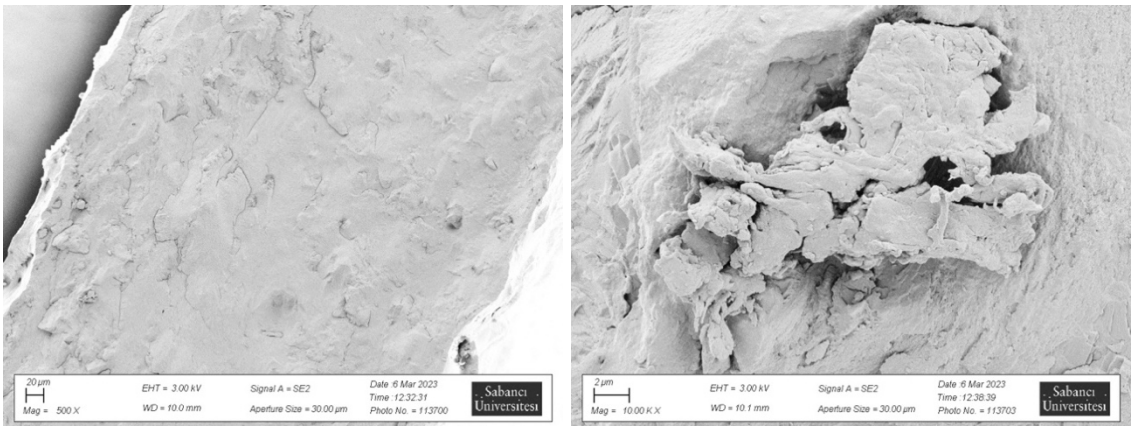

Figure 57: SEM images of SAP with 60 wt% CMC

At 60 wt% CMC, we see the most instances of CMC fillers on the surface, and the cross-sectional surface appears to be rougher than all the other samples. However, the surface still appears to be notably coherent, given 60 wt% of this material is made up of CMC. The fact that we observe a highly coherent/homogeneous cross-sectional surface throughout all CMC-SAP samples suggests that the incorporation of CMC in the polymer structure was successful during the syntheses.

4.4.3. Water and Saline Absorption Performance of CMC-Based Superabsorbent Polymers

In the plots below, the water absorption kinetics of CMC-SAPs with varying levels of carboxymethyl cellulose are shown.

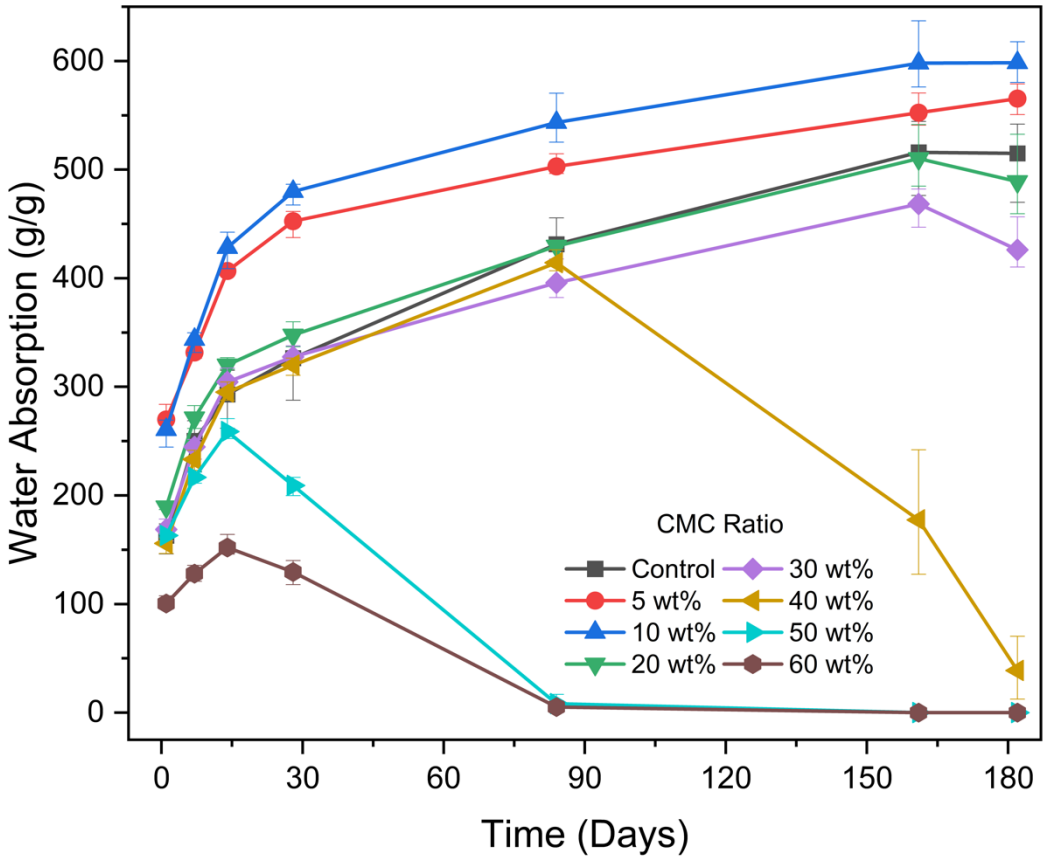

Figure 58: CMC-SAP water absorption (g/g) vs time (days).

As the CMC content of the SAP increases until a certain point, water absorption increases, but drops afterward. Initial explanations for this are the hydrophilic nature of CMC and the rough surface area of the CMC-SAPs, which improve water absorption. Another reason can be the lower initiator and crosslinker ratios of these polymers.

In this study, throughout the SAP formulations, only the CMC content of the SAP was changed, whereas the monomer, crosslinker, and initiator quantities were kept the same. The consequences of this situation should be kept in mind when comparing the water absorption capacities of CMC-SAPs.

As the CMC ratio of the SAP is increased, the crosslinker and initiator ratios decrease. Since CMC is incorporated in the polymer backbone, the average length of the polymer chains is expected to increase, as the initiator content remains the same. Similarly, the degree of crosslinking is expected to be lowered, due to the decreasing ratio of VTMS in CMC-containing polymerization solutions.

For water absorption, there is an optimum degree of crosslinking. Until that point, reducing the degree of crosslinking results in an increase in water absorption capacity. As polymer chains are less restricted with fewer crosslinking points, they can expand more to swell with more water. However, further reducing the degree of crosslinking would cause the number of crosslinking points to be insufficient to hold the polymer chains together upon a critical level of water absorption.

Initiator content is critical for governing the polymer chain length, as it determines the number of active sites available for polymerization. If the initiator content is too high, there are many growing polymer chains with active sites. In such a scenario, monomer units readily bond to many growing polymer chains, and this results in a lower average molecular weight, which negatively impacts the water-holding capability of the SAP structure. Longer chains that are sufficiently crosslinked can expand to a greater extent and hold more water inside, whereas short chains do not have the same expanding capabilities. In contrast, when the initiator concentration is very low, there are not enough active sites, hence not enough growing polymer chains that monomers can readily attach to. This results in a lower rate of polymerization and a lower conversion, compared to a synthesis having sufficient active sites.

This explanation agrees with the finding that, as CMC ratios increase beyond 20 wt%, the water absorption capacities of SAP degrade significantly. SAPs with high CMC ratios have much more lightly crosslinked polymer networks compared to SAPs with less than 10 wt% CMC. For example, pure SAP incorporates 2 wt% VTMS (crosslinker) in its polymerization mixture, whereas 60% CMC-SAP only has 0.8 wt% VTMS in its synthesis composition.

SAPs with 50 and 60 wt% CMC achieved their highest water absorption rates of 152 and 259 g/g, respectively, after 2 weeks. Then, due to the mechanical failure of their

crosslinked structures upon hydrolytic degradation, they were not able to retain as much water. In fact, after 2 to 3 months, their water-holding capacities were completely degraded.

Another meaningful way to assess the effect of CMC addition on the water-holding capacity of an otherwise synthetic polymer is to calculate the amount of water bio-SAP absorbs per its synthetic portion. Therefore, a derivative data set was reproduced from the existing data, called the adjusted water absorption. The adjusted water absorption capacity of a bio-SAP is calculated by dividing its true water absorption by the weight fraction of the synthetic polymer in its structure.

$$Adjusted\ Water\ Absorption = \frac{True\ Water\ Absorption}{Weight\ Fraction\ of\ Synthetic\ Polymer}$$

For example, let's say a bio-SAP with 50 wt% CMC in its structure has a water absorption capacity of 200 g/g. Its adjusted water absorption would be $\frac{200 g/g}{0.5} = 400\ g/g$.

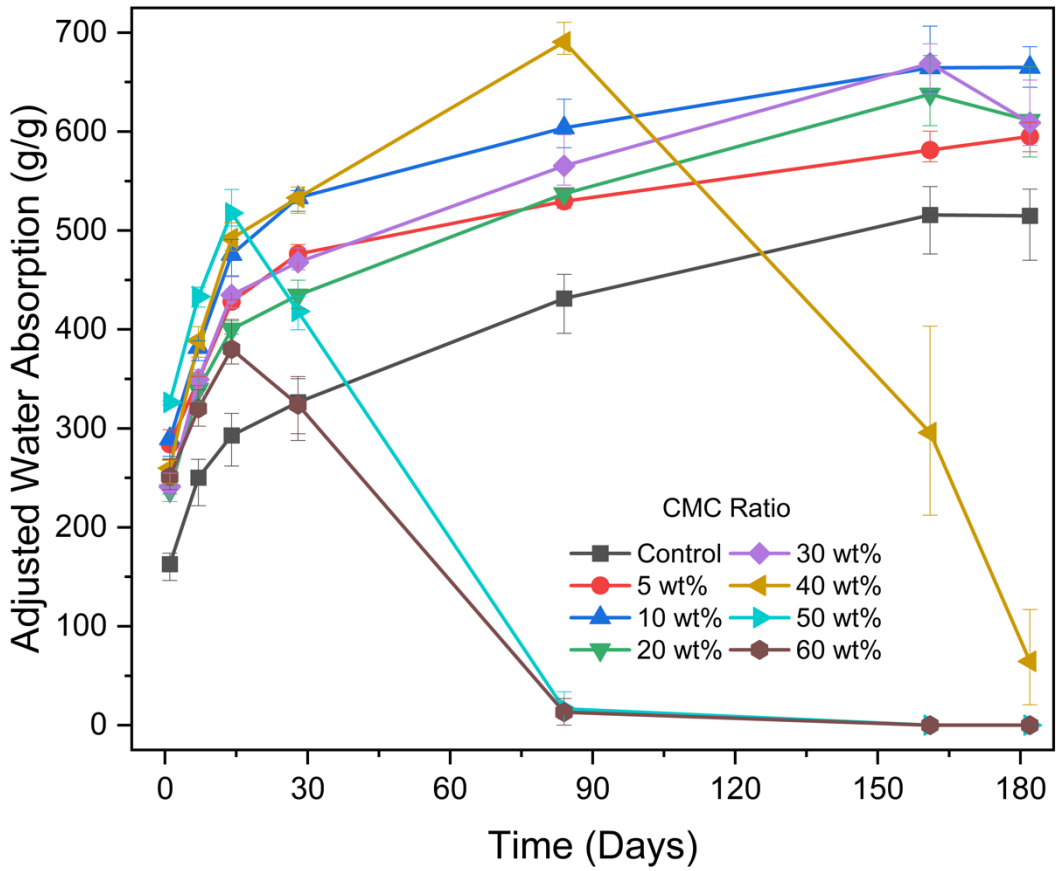

Figure 59: CMC-SAP adjusted water absorption (g/g) vs time (days).

The true water absorption capacity of pure SAP is comparable to that of the SAP with 20 wt% CMC, and better than that of SAPs with higher ratios of CMC. However, if we compare their adjusted water absorption capacities, we notice that SAPs with 20 and 30 wt% CMC are superior to pure SAP. Moreover, during the first 3 months, SAP with 40 wt% CMC has a higher adjusted water absorption. In fact, for the first 2 weeks, pure SAP has the lowest adjusted water absorption amongst all samples. This means that the synthetic portions of all bio-SAPs were more efficient in absorbing water than the fully synthetic SAP.

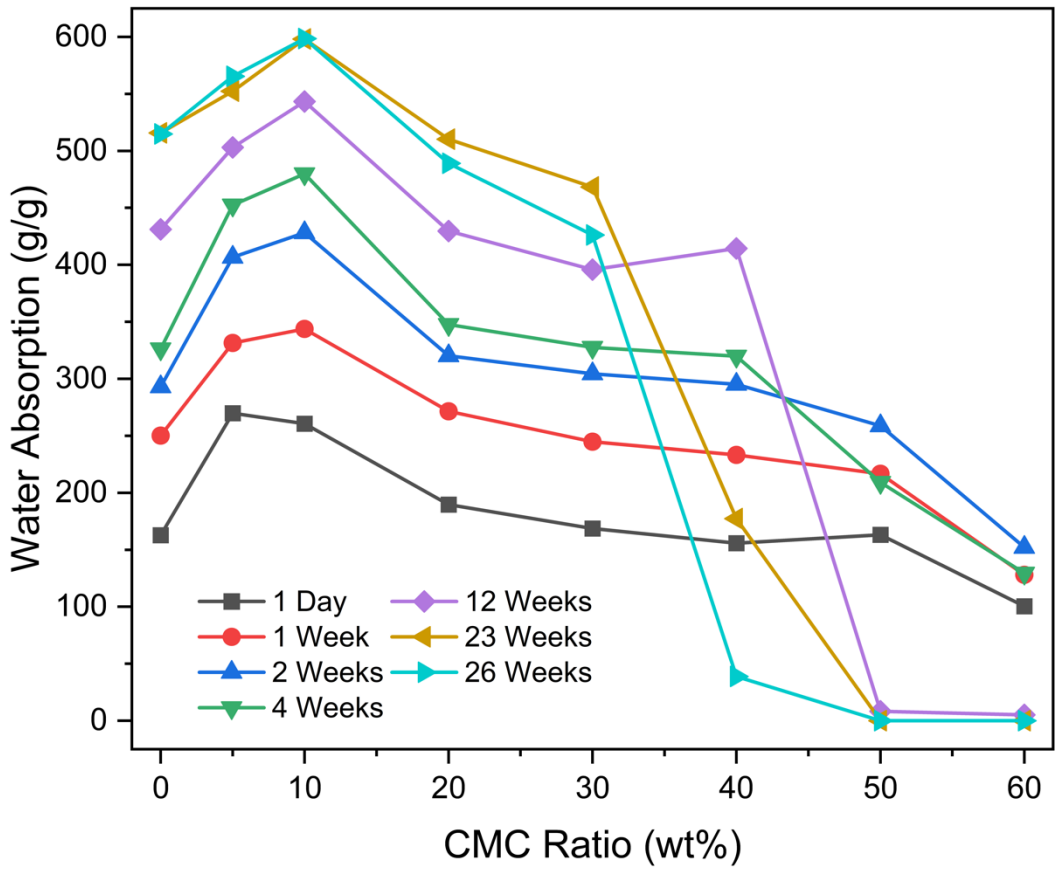

Figure 60: CMC-SAP water absorption (g/g) vs CMC ratio (wt%).

To observe the effect of the CMC ratio more clearly, water absorption capacity was plotted as a function of the CMC ratio (wt%). Individual lines represent measurement times. By looking at the left side of the plot, it can be easily seen that, until 10 wt% CMC, the water absorption capacities of CMC-SAPs increase. For example, after 4 weeks, represented here by the green line, pure SAP absorbed 326 g/g of water. Whereas the water absorptions of 5% and 10% CMC-SAPs reached 452, and 480 g/g, respectively. In other words, 10% CMC-SAP absorbed almost 50% more water compared to pure SAP, which is a significant improvement.

Another version of this plot is given below, representing adjusted water absorption capacities versus the CMC ratio (wt%):

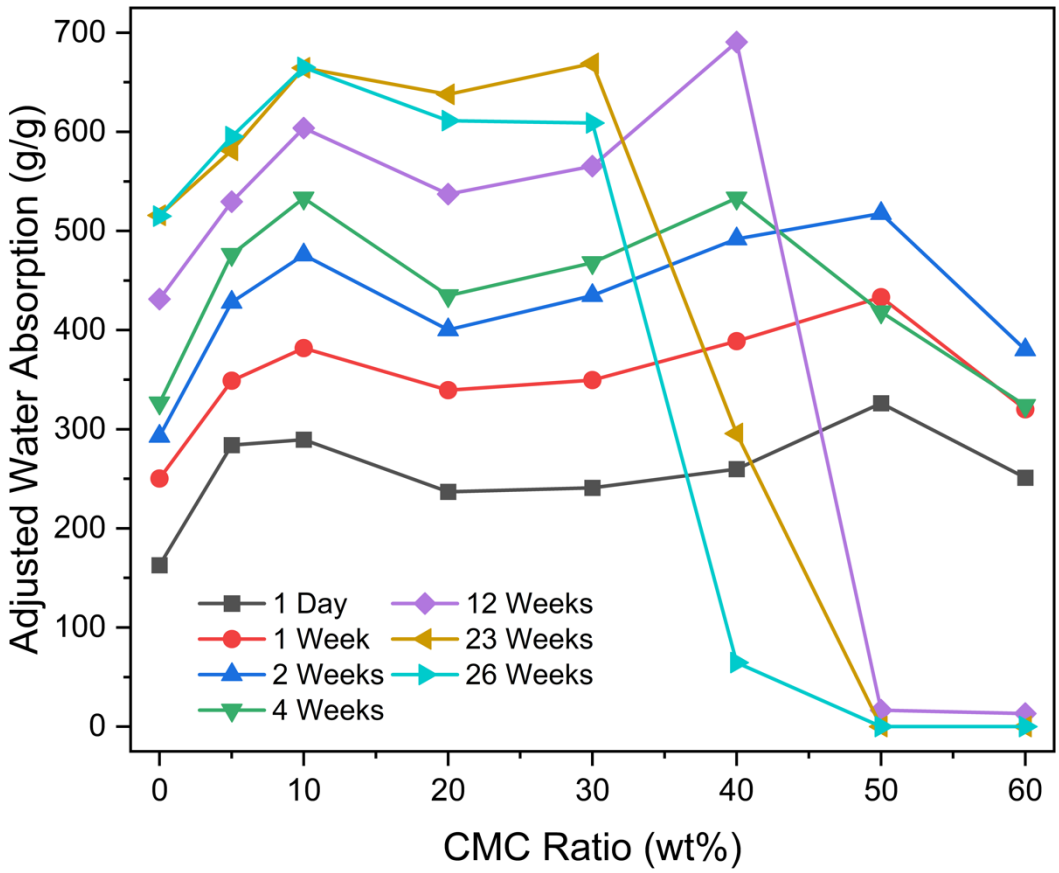

Figure 61: CMC-SAP adjusted water absorption (g/g) vs CMC ratio (wt%).

The water absorption capacities of CMC-SAPs in this study were adequate for agriculture applications. For example, SAPs with 30 and 40 wt% CMC reached water holding capacities of approximately 500 and 400 g/g respectively, which are comparable to most commercial synthetic SAPs. However, there is still room for improvement. SAPs with even higher CMC contents can reach similar water absorption capacities. To optimize water absorption, the amount of crosslinker and initiator ratios in the synthesis for CMC-SAPs can be adjusted according to the respective CMC ratios of the polymer.

In the following plots, the saline absorption performance of CMC-SAPs is presented.

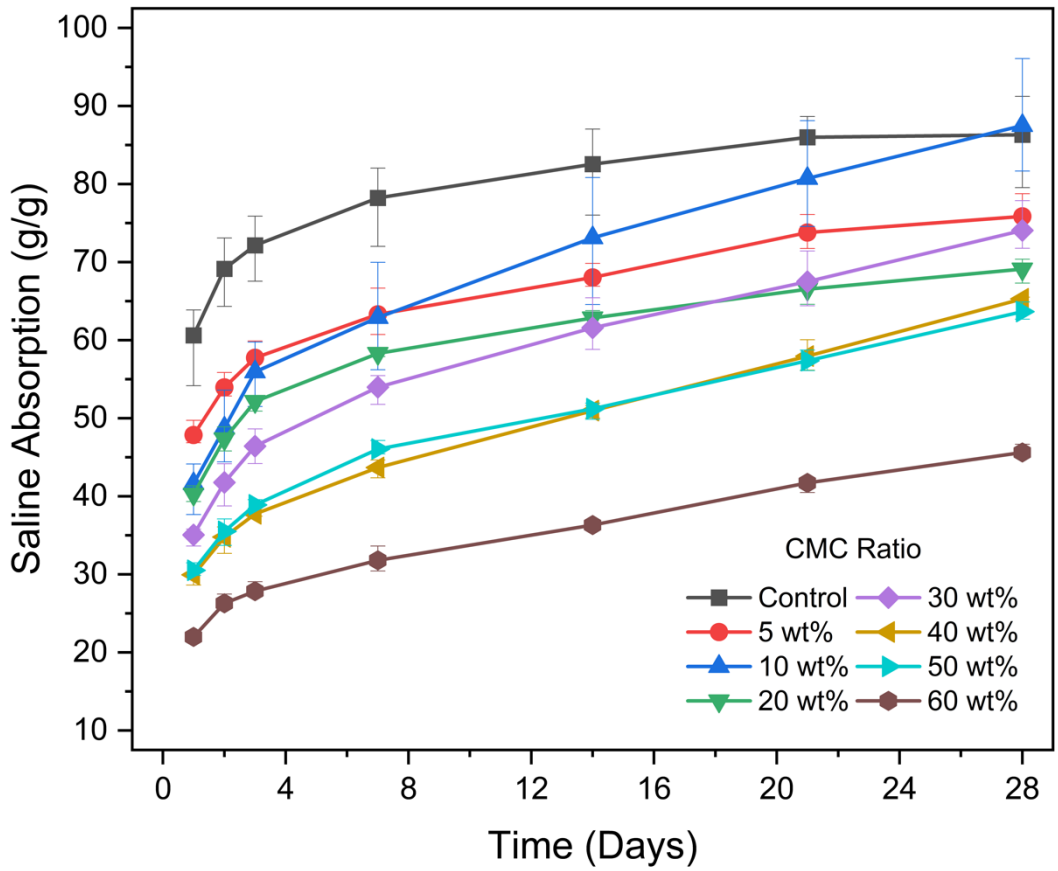

Figure 62: CMC-SAP saline absorption (g/g) vs time (days).

From the beginning of the test, pure SAP performed better than its bio-based counterparts. SAP with 10 wt% CMC slightly surpassed the water absorption capacity of pure SAP only after 4 weeks. Despite their superior water absorption performance compared to pure SAP, SAPs with 5 and 10 wt% CMC could not outperform fully synthetic SAP in terms of absorption in saline solution.

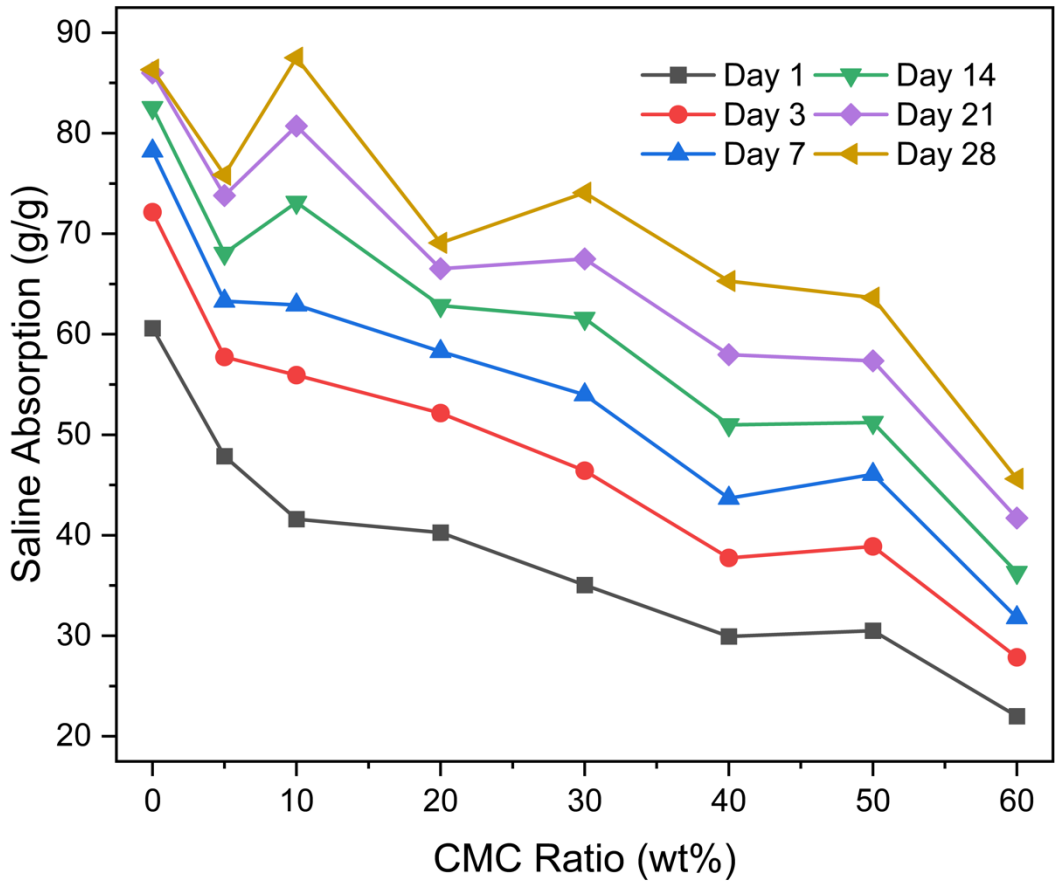

Figure 63: CMC-SAP saline absorption (g/g) vs CMC ratio (wt%).

To better visualize the effect of CMC concentration on the saline absorption capacity of bio-SAPs, the absorption values are plotted against CMC ratio (wt%) on the graph above.

4.4.4. Water Retention Performance of CMC-Based Superabsorbent Polymers

Water retention capacity is an especially important performance parameter for SAPs intended for agricultural use. The longer the SAP can withhold water in its structure, the more favorable it is during drought, because it can supply water to plants for a longer time. Although the test conditions did not recreate farming conditions, it allowed us to compare the samples under the same conditions. Moreover, in soil tests, the swollen gels could not be taken out without soil contaminants, which affect weight measurements, therefore, the only way to assess water retention could be through soil moisture measurement. However, this method does not provide the weight of the water retained by the swollen gel. Hence, a true water retention test would not be possible. Therefore, the

swollen gels were allowed to release water in beakers. This prevented any contamination, which would affect weight measurements. In the next plot, the ratios of retained water are plotted as a function of time.

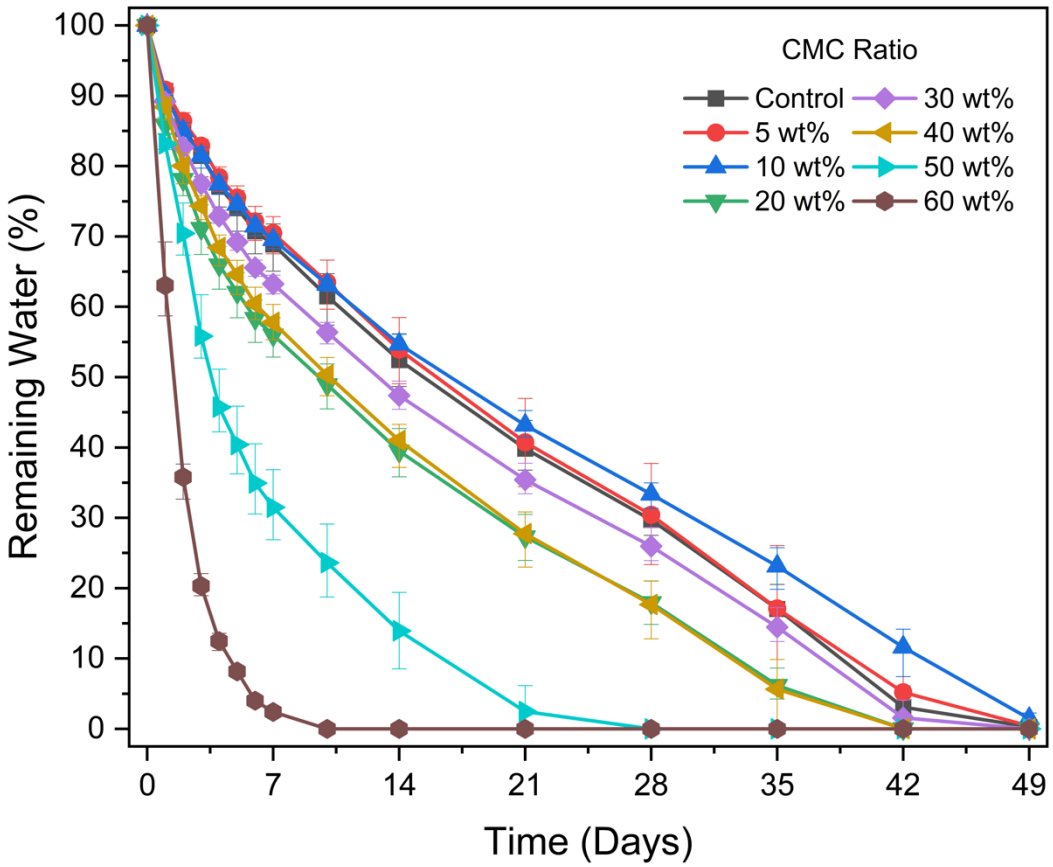

Figure 64: CMC-SAP remaining water (%) vs time (days).

Throughout the test, SAPs with 5 and 10 wt% CMC were able to retain somewhat more water compared to pure SAP, in their crosslinked structure. However, these three samples performed better than the remaining bio-SAPs, which contained more CMC. Moreover, SAPs with 60 and 50 wt% CMC exhibited complete water release after 1 week and 3 weeks, respectively. Considering these results, it is safe to say that SAPs with such high CMC contents are not suitable for long-term agricultural applications. However, they can still be suitable for short-term application in soil. For example, such SAPs can be coated on seeds to increase their chances of germination under drought conditions. Since the germination period is usually short for grains, for example, 3 to 5 days for wheat, these SAPs can serve as a water reservoir and maintain a moist surrounding for the seeds. Using a higher bio-content in SAPs can even be more favorable compared to pure SAP under such circumstances, as they can readily degrade after serving their purpose. On the other

hand, SAPs with less cellulose content are more suitable for longer-term soil applications, to provide water during extended drought conditions.

4.4.5. Reusability - Reswelling Capacity of CMC-SAPs

The dry weights and the water absorption ratios of all CMC-SAP samples are plotted throughout three swell-dry cycles. The dry weights are not plotted in units of mass (gram), but rather in terms of the percentage of the original weight remaining. This is done to make a better comparison among samples. The swelling ratio is represented in units of g/g (g of absorbed water / g of initial dry SAP). The x-axes of both plots represent the number of swell-dry cycles.

The dry SAP weights of CMC-SAP samples after each swell-dry cycle are presented in the plot below:

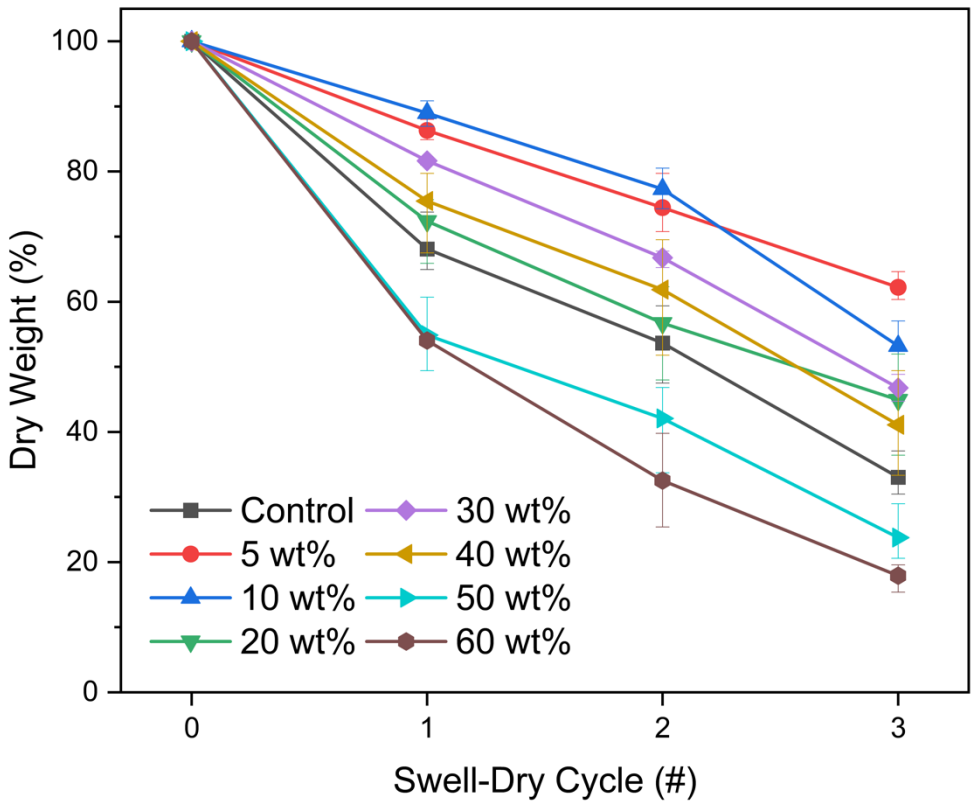

Figure 65: CMC-SAP Retained Dry Weight (%) vs Swell-Dry Cycle.

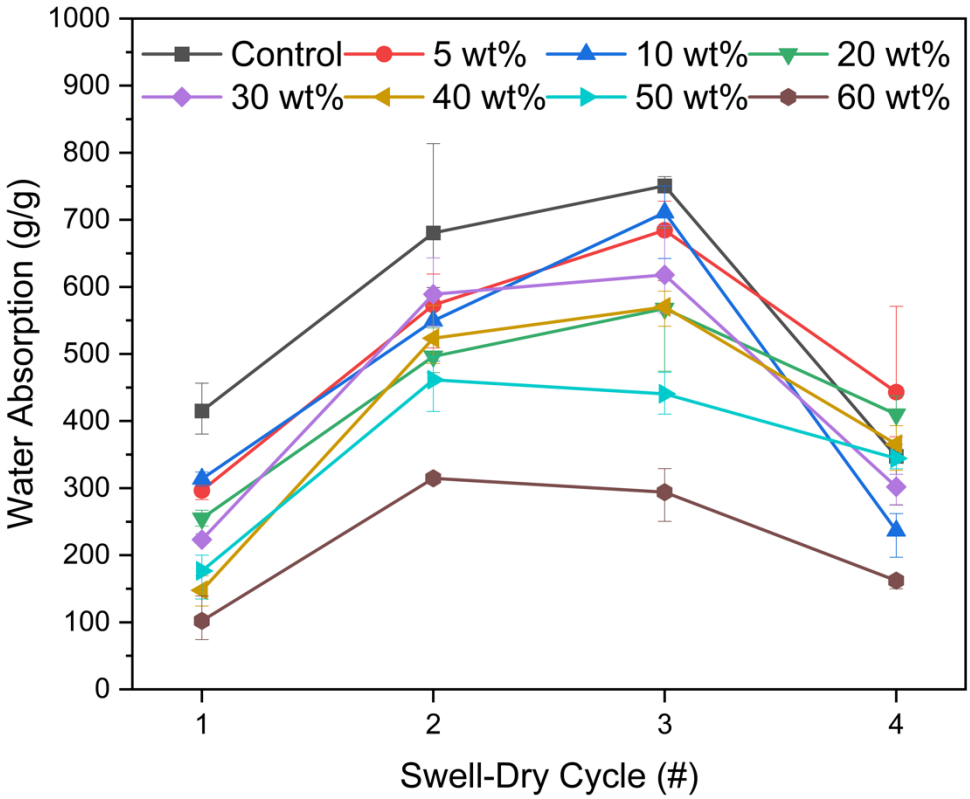

Figure 66: CMC-SAP Water Absorption (g/g) vs Swell-Dry Cycle.

Weight loss occurred for all the dry bio-SAP samples following each swell-dry cycle. The amount of weight loss differed across SAPs with varying ratios of CMC. It was observed that, as a general trend, a low to moderate CMC incorporation in the SAP structure, significantly improved its resistance to dry weight loss. However, when CMC constitutes the majority of the SAP structure, the ability to withstand weight loss is greatly reduced.

A rather unusual trend was observed regarding reswelling capacities. The water absorption ratios in the second, and for most samples, both the second and the third swelling cycles were greater than the absorption in the first swelling cycle. At first, this seemed like an unexpected and improbable outcome. However, there was a rational explanation. The most important parameters that affect the 24-hour swelling ratio are the surface area to mass ratio and dry SAP weight. A higher surface area translates to faster-swelling kinetics. Since this is a time-limited test, kinetics is crucial. Dry SAP weight determines the inherent water uptake capacity of the SAP gel, at equilibrium.

Initially, all samples were cut out from dried sheets of SAP. Hence, there was only one or a few pieces of SAP samples, which totaled approximately 0.05 grams, inside each falcon tube. Accordingly, the surface area of the samples was very low, compared to what it would have been if the SAP samples consisted of small granules. Since the surface area to mass ratio directly affects the kinetics of water absorption, the water absorption was relatively slow in the first swelling cycle. During the first cycle, the SAPs swelled to an expansive volume. When these gels were dried in an oven, they did not return to their original shape; rather they dried along the walls of the falcon tube and hence occupied a greater surface area. Hence their surface area-to-mass ratios increased remarkably. Therefore, during the second swelling cycle, their water absorption kinetics were much faster than in the first cycle. Accordingly, the samples were able to absorb more water during the 24 hours and occupied a greater volume than in the first cycle. When the gels were put in the oven, they dried along the walls of the falcon tubes again, however, this time they occupied even more surface area. Therefore, the water absorption kinetics during the third swelling cycle was greater, owing to an even higher surface area-to-mass ratio.

The only two samples, for which the water absorption ratio after the third cycle swelling cycle is lower than that after the second swelling cycle, are 50% and 60% CMC-SAP. This outcome was expected as these two samples were also the ones that suffered the greatest weight loss. After the first cycle, these samples were able to retain only 55% of their initial dry weight. After the second cycle, this ratio decreased to 42 and 33%, respectively. Therefore, the high CMC incorporating SAPs were not able to increase their swelling rates albeit with higher surface area to mass ratios. In comparison, the dry weight retention of low to moderate CMC-incorporating samples ranged from 57 to 77%, after the second swell-dry cycle. Therefore, the samples were still able to increase their 24-hour water absorption ratios, owing to increased surface areas. However, upon final 24-hour swelling, the water absorption ratios of all samples were reduced, due to extensive dry weight loss following third swell-dry cycle.

4.4.6. Biodegradability of CMC-SAPs

4.4.6.1. Degradation In Soil

Unfortunately, I was not able to generate a meaningful outcome from the soil degradation tests of CMC-SAP. When preparing the soil for the tests, my plan of action was to be able to easily separate the soil from the SAP by only using a 1 mm sieve. To do so, I sieved the dried soil to be used in the tests below 1 mm. This way I thought the small soil particles would easily pass through the 1 mm sieve while the swollen SAPs would not pass through. However, I didn't take into account the powder-like soil particles that could easily stick to the SAP surface. At the end of the tests, SAPs could easily be retrieved, however they were surrounded by soil. This mixture of SAP and soil had a structure similar to thick mud, and a relatively dark color. This mixture of soil and SAP was further washed under running water.

Although most soil particles were thereby eliminated, there were still very small, powder-like soil particles that were attached to the SAP surface, which could also be perceived from the slightly dark color. Examples of soil-covered SAPs retrieved from the soil degradation tests are shown on the image on the left-hand side. When the filtered SAP particles were dried, they shrunk in size, and the soil particles around them became more concentrated. The amount of soil attached to the SAPs were inevitably different from sample to sample. Also, for some samples, the final SAP weight was higher than its initial weight, due to these attached soil particles. Therefore, a rational and consistent biodegradation data could not be generated from this test.

4.4.6.2. Enzymatic Degradation

Although it is not straightforward to convert the degradation time in enzyme containing buffer solution to the expected degradation time in soil, determining the correlation between the cellulose content of the SAPs and their degradation kinetics is the most important outcome.

At the end of the enzymatic biodegradation tests, buffer solutions containing the SAP and the enzyme were filtered using a vacuum filter with a 200-mesh nylon filter, corresponding to a pore size of 75 microns. Therefore, SAPs with a size of more than 75 microns were considered in the final weight, whereas smaller SAP particles were considered degraded. Next, the SAP that stayed on the nylon filter was put back into their respective falcon tubes.

In the photographs below, the biodegradation test samples from the 5th day can be seen. Tubes on the left-hand side are unfiltered, and tubes on the right-hand side contain the SAPs after filtration. In the middle, the amount of filtered SAP can be observed.

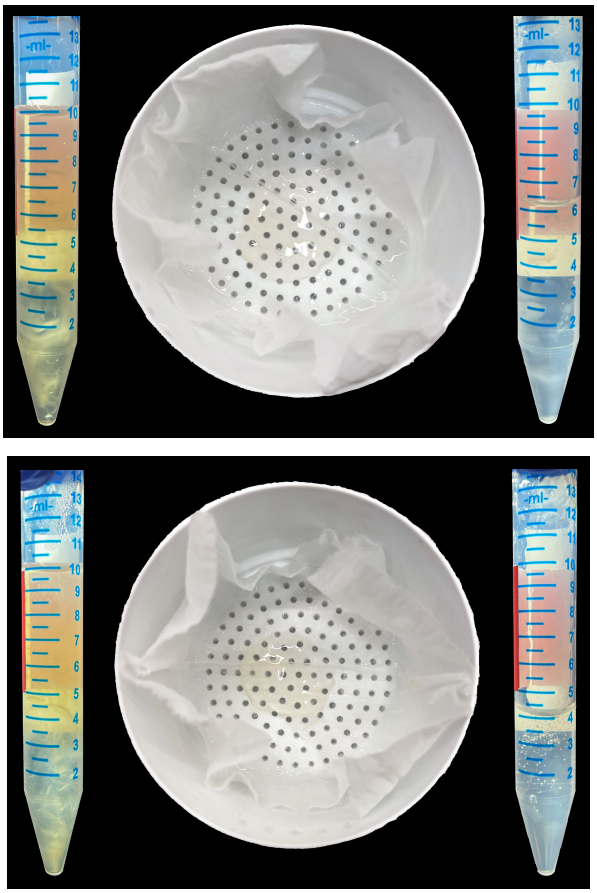

Figure 67: 5-Day Biodegradation Test Before and After Filtration: (a) Control SAP, (b) SAP with 20 wt% CMC.

The image on the left belongs to pure SAP, and the one on the right belongs to SAP incorporating 20 wt% of CMC. Notice the slight yellow color of the unfiltered test tubes containing the buffer solution with degraded SAP and the enzyme. In contrast, the filtered solutions inside the tubes on the right-hand side are colorless. This yellow color comes

from the cellulase enzyme. The enzyme used in this study had a rich dark brown color. Although it was only used at a concentration of 2 v/v%, it changed the color of the buffer solution to yellow. The fact that this color was eliminated in the filtered SAP solution shows that the enzyme was successfully filtered and would not be included in the final weight of the SAP.

The white material with a cloud-like shape in the solution is the SAP. It is easily visible in the degraded samples above, of pure SAP (a) and 20 wt% CMC-SAP (b).

In the photographs below, the 5-day biodegradation test samples of SAPs with 30 wt% and 60 wt% CMC are shown below, on the left and right-hand side respectively.

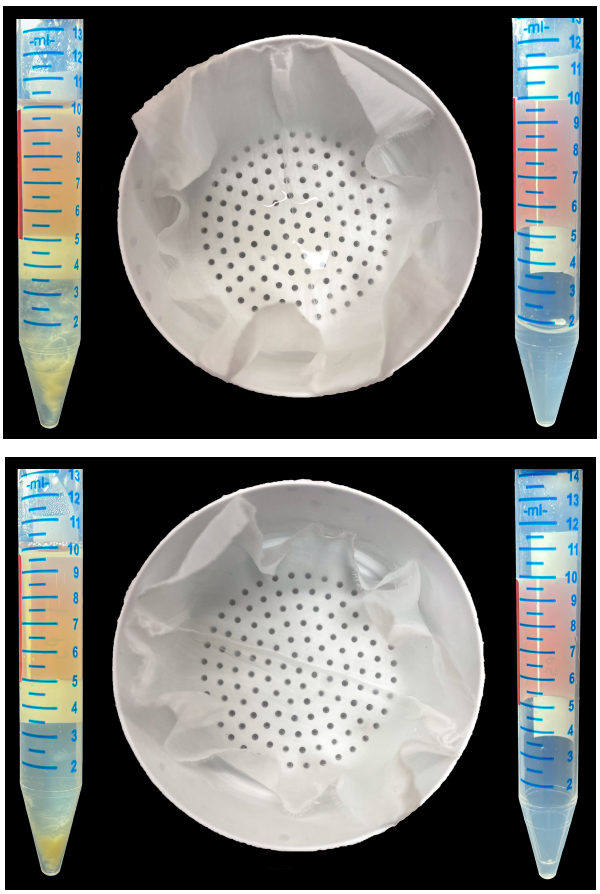

Figure 68: 5-Day Biodegradation Test Before and After Filtration: (a) SAP with 30 wt% CMC, (b) SAP with 60 wt% CMC.

Compared to previous examples of pure SAP, and CMC-SAP with a lower CMC concentration, the unfiltered solutions on the left-hand side contain a very small amount of white, cloud-like substance that represents the SAP. For example, the white substance

belonging to 30 wt% CMC-SAP appears to be in a lower amount, and highly disintegrated compared to that of pure SAP. Furthermore, the unfiltered solution on the right-hand side, belonging to 60 wt% CMC-SAP, contains no white, cloud-like substance belonging to SAP. The SAP has degraded to such an extent, that the solution containing it became completely transparent. In fact, all the solution readily passed through the 75-micron nylon filter during vacuum filtration, and no SAP was left on the filter. So, this SAP achieved 100% biodegradation. In the 5-day biodegradation test, SAPs that contained 40, 50, and 60 wt% CMC achieved complete biodegradation.

After the filtration step was complete, all the test tubes containing the filtered SAPs were frozen at -80 °C for 4 hours and freeze-dried for 3 days. Since 15 mL falcon tubes have very small openings, and the depth of the SAP inside the tubes is very high, it could have taken a very long time to dry these samples in a drying oven. Therefore, freeze-drying was preferred.

Figure 69: SAP Samples from Biodegradation Tests in Freeze Dryer.

The test tubes were covered with Parafilm to prevent sample discharge due to high vacuum. However, 4-5 holes were opened at the top of the tubes, with a needle, to allow water vapor to be released easily. A wide enough container could not be found, to place all the test tubes inside. So, all the tubes were assembled to stand together by wrapping parafilm around them.

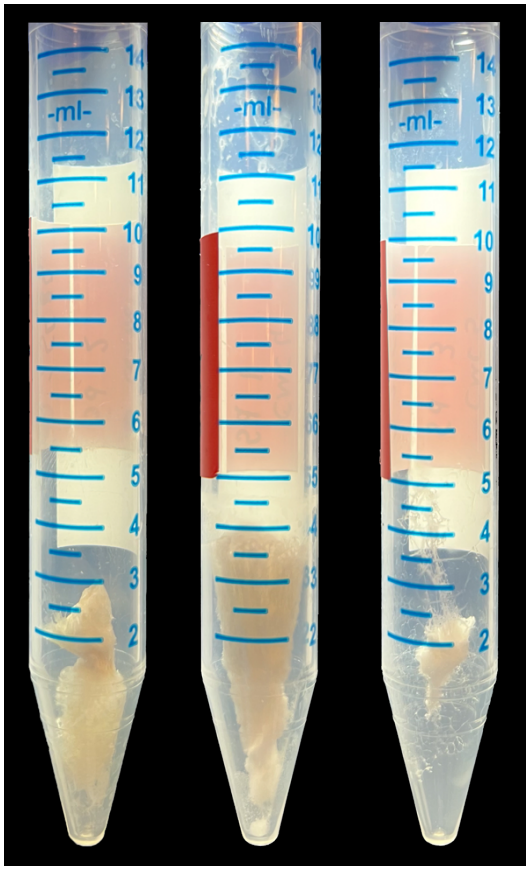

Figure 70: Free-dried SAP samples after biodegradation test.

On the left-hand side, the freeze-dried pure SAP, that has been exposed to enzymatic degradation for 5 days, is shown. In the middle, 20 wt% CMC-SAP is shown, subject to the same degradation conditions. Finally, on the right-hand side, freeze-dried 30 wt% CMC-SAP can be seen, belonging to the same degradation test group. The latter sample, with the highest CMC content, is visually smaller than the other samples, which is consistent with the weight measurements. This is expected since a higher cellulose content would result in higher degradation. The dried SAP in the middle appear to be more than the SAP on the left-hand side. However, this is due to the many air pockets present in the sample; and the weight of this sample belonging to 20 wt% CMC-SAP is lower than that of pure SAP.

Biodegradation was determined by comparing the initial and final weights of SAP samples, according to the formula below:

$$Biodegradation\ (\%)\ = \frac{W_{initial} - W_{final}}{W_{initial}}\ x\ 100$$

$$W_{initial}: weight\ of\ SAP\ before\ the\ test$$
$$W_{final}: weight\ of\ SAP\ after\ the\ test$$

This study was successful in drawing a correlation between the cellulose content of the SAPs and their degradation kinetics. As a general trend, increasing the CMC content in the SAP results in higher rates of degradation in cellulase containing buffer solutions.

In the plot below, the biodegradation ratio (%) of CMC-SAPs are plotted as a function of time. Compared to pure SAP, SAPs with notable CMC in their structures displayed significantly higher biodegradation upon exposure to cellulase enzyme.

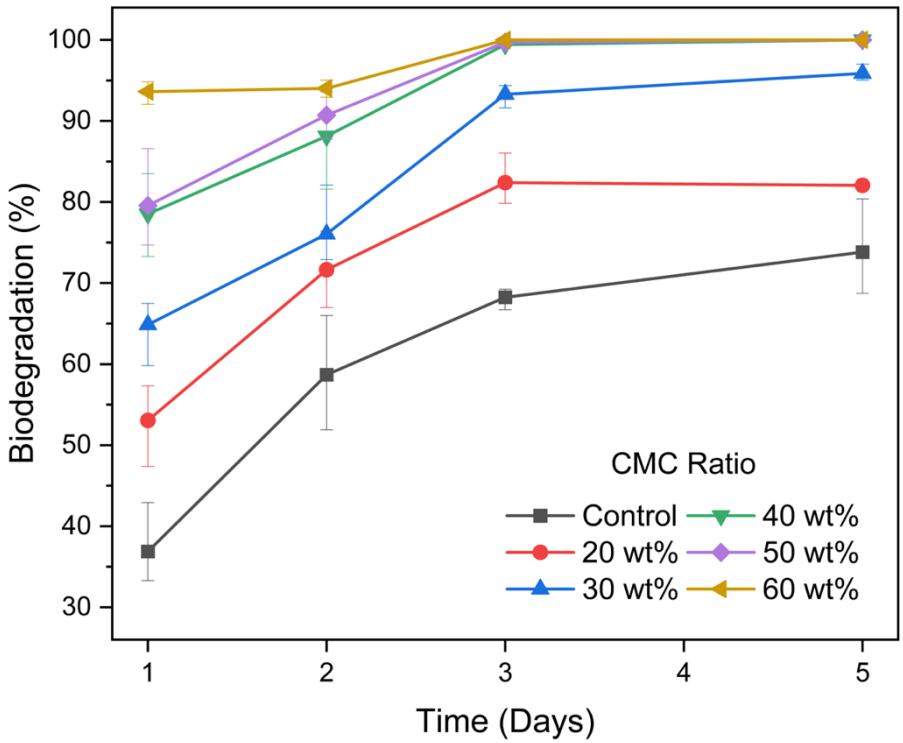

Figure 71: CMC-SAP biodegradation (%) vs time (days).

After 3 days, CMCs with 50 and 60 wt% CMC degraded completely. After 5 days, CMC-SAP samples with 40% or more CMC by weight, degraded entirely.

In the next plot below, biodegradation percent is plotted against CMC weight percent, so it can be more clearly observed how the CMC ratio affects the biodegradation rate of SAPs.

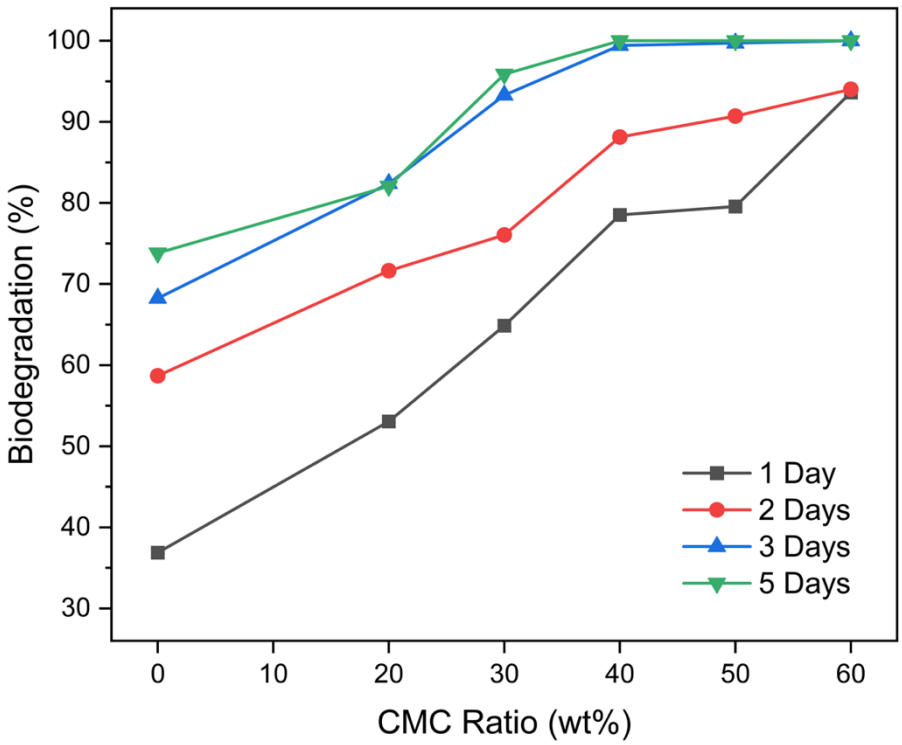

Figure 72: CMC-SAP biodegradation (%) vs CMC ratio (wt%).

After 1 day of exposure to cellulase enzyme, degradation of SAP with 60 wt% CMC reached 94%, whereas that of pure SAP stayed at approximately 37%.

The optimum CMC-SAP formulations that combine significant cellulose contents and sufficient water absorption capacities are 20,30, and 40 wt% CMC-SAP. Since their CMC content is substantial, their biodegradation rates are expected to be considerably higher than that of pure SAP. Therefore, in the following part, the biodegradation rates of those SAPs are compared with pure SAP, along with the SAPs containing 50 and 60 wt% CMC.

4.4.7. Recommendations for Future Work

4.4.7.1. Effects of Crosslinker and Initiator

In this study, only the CMC content of the SAP was changed, whereas the monomer, crosslinker, and initiator quantities were kept the same. The consequences of this situation should be kept in mind when comparing the properties of CMC-SAPs.

As the CMC ratio of the SAP is increased, the crosslinker and initiator ratios decrease. Since CMC is incorporated in the polymer backbone, the average length of the polymer chains is expected to increase, as the initiator content remains the same. Similarly, the degree of crosslinking is expected to be lowered, due to the decreasing ratio of VTMS in CMC-containing polymerization solutions.

For water absorption, there is an optimum degree of crosslinking. Until that point, reducing the degree of crosslinking results in an increase in water absorption capacity. As polymer chains are less restricted with fewer crosslinking points, they can expand more to swell with more water. However, further reducing the degree of crosslinking would cause the number of crosslinking points to be insufficient to hold the polymer chains together upon a critical level of water absorption.

Initiator content is critical for governing the polymer chain length, as it determines the number of active sites available for polymerization. If the initiator content is too high, there are many growing polymer chains with active sites. In such a scenario, monomer units readily bond to many growing polymer chains, and this results in a lower average molecular weight, which negatively impacts the water-holding capability of the SAP structure. Longer chains that are sufficiently crosslinked can expand to a greater extent and hold more water inside, whereas short chains do not have the same expanding capabilities. In contrast, when the initiator concentration is very low, there are not enough active sites, hence not enough growing polymer chains that monomers can readily attach to. This results in a lower rate of polymerization and a lower conversion, compared to a synthesis having sufficient active sites.

As a recommendation for a future work, the amount of crosslinker and initiator in the synthesis for CMC-SAPs can be increased according to the respective CMC ratios of the polymer. As an optimum crosslinker and initiator amount is approached, the water absorption capabilities of CMC-SAPs are expected to improve.

4.4.7.2. Soil Biodegradation Test

For this study, a cumbersome soil biodegradation test was devised and performed. Unfortunately, a meaningful outcome from these tests could not be generated. When preparing the soil for the tests, the plan of action was to be able to easily separate the soil from the SAP by only using a 1 mm sieve. To do so, dried soil was sieved to below 1 mm. This way the small soil particles would easily pass through the 1 mm sieve while the swollen SAPs would not pass through. However, the powder-like soil particles readily stuck to the SAP surface. At the end of the tests, SAPs could easily be retrieved, however they were surrounded by soil. This mixture of SAP and soil had a structure similar to thick mud, and a relatively dark color. This mixture of soil and SAP was further washed under running water.

Although most soil particles were thereby eliminated, there were still very small, powder-like soil particles that were attached to the SAP surface, which could also be perceived from the slightly dark color. The amount of soil attached to the SAPs were inevitably different from sample to sample. Also, for some samples, the final SAP weight was higher than its initial weight, due to these attached soil particles. Therefore, a rational and consistent biodegradation data could not be generated from this test.

In a future work, a new soil biodegradation test can be devised, in which the SAPs can be easily separated from the soil, without any residue on polymer surface. One suggestion would be to eliminate powder-like soil, under a certain size.

Chapter 5

CONCLUSION

5.1. Superabsorbent Polymers

Despite their current predominant utilization in the hygiene sector, superabsorbent polymers were first developed in 1960s with the intention to improve water conservation in soil. However, their first commercial use in 1970s was in disposable hygienic products, such as feminine sanitary napkins and incontinence products. Subsequently, SAP's first use in baby diapers was only in 1982. (Gelok International Corporation, n.d.)

The most important property of an SAP in the hygiene sector is fast liquid absorption, so that it can take up body fluids as quickly as possible. However, this property in not particularly important for an SAP intended as soil water reservoir. The two most important properties of agricultural SAPs are high water holding capacities and long water retention durations, so that it can supply plant roots with water for an extended period. Therefore, it is critical to develop new formulations for SAPs intended to be used as soil amendments, rather than reusing conventional formulations.

Recently, owed to improved formulations and enhanced water holding capacities, SAPs started to gain commercial success as soil amendment for increasing crop yields and reducing water losses in agriculture. However, compared to SAP in hygiene products,

SAP as water reservoir in soil is still relatively at its infancy, regarding optimum formulation and application methods. Moreover, there is a tremendous amount of possible synergistic incorporations of different products with SAP, which can further alleviate yield losses or boost plant growth.

Until today, SAPs intended for large-scale commercial use, have been manufactured with 100% petroleum-based monomers. Acrylate-based SAPs can have very high water-absorption capacities owed to high molecular weight and optimally cross-linked structures; however, these characteristics also render them difficult to biodegrade. Current studies in this field, including the last chapter of this thesis, focuses on developing novel bio-degradable SAPs.

5.2. Efficient Use of Plant Protection Products (PPP) and Nutrients

One of the most plausible approaches to fight world hunger is to increase crop productivity. Enhanced crop productivity usually derives from more effective crop protection, that is better fighting with harmful pests. Pesticides have long been used in farming to fight pests and prevent crop loses. However, current formulations have not only been very effective in terms of saving crops, but they also have been polluting the environment more than any sector. Controlled release systems are put forward as an alternative crop protection strategy, which enable the sustained release of pesticides in smaller but effective quantities. This way, pesticides are not only used much less compared to conventional methods, but also pose significantly less environmental threat. Due to less pesticide use, CRS improve the safety of occupational workers and due to much less, if any pesticide residue on harvest, enhances the health of consumers. The need for less applications with CRS compared to traditional techniques allows for reduced energy costs for farmers.

In conclusion, controlled release systems offer promising solutions for sustainable agriculture by addressing the challenges associated with pesticide use. By selecting appropriate carrier materials, designing optimal architectures, and understanding the complex interactions involved, it is possible to achieve the desired sustained release of

pesticides, leading to improved efficiency, reduced environmental contamination, and minimized pesticide usage in crop protection.

Current findings in the area of controlled release suggest these systems can be promising solutions for achieving sustainable agriculture required to feed ten billion people in 2050. People tend to have confirmation bias as we tend to use any information supporting our claims to further prove our point. However, in order to truly analyze the situation thoroughly, we need to consider the shortcomings of our hypothesis. The study of controlled release systems for agriculture is at nascent stages, and there is insufficient data regarding their efficacy in the fields and their potential environmental and health hazards. There is a strong demand to confirm the real advantages of new CRS over conventional methods in the field, in terms of both efficacy in crop protection and environmental and health impact, as such informational is mostly lacking. This represents a significant research gap in literature, and a fertile area of study for many enthusiastic scientists.

5.3. Integration of Water Management and Efficient PPP and Nutrient Use

The suggested application dose of SAPs is approximately 45 kg per hectare. (Y. Yang et al., 2022) It is interesting to note that most studies in the literature focus on incorporating urea and NPK fertilizers in soil, rather than micronutrients. (Che Ani et al., 2022; Rashidzadeh & Olad, 2014; Sarkar et al., 2014; Sarkar & Datta, 2014; Xu et al., 2019) Considering the recommended dose of SAPs, the amount of fertilizer that can be delivered to the soil is negligible. Even with very high fertilizer incorporation of 50 wt%, only 22.5 kg/ha of urea or NPK can be applied, which is 15-22% of the recommended dose. Therefore, SAPs are inadequate as macronutrient reservoirs.

On the other hand, calcium and zinc fertilizers are applied in much lower quantities. For instance, zinc sulfate and calcium nitrate have recommended doses of 3-8 kg/ha (Zinc Nutrient Initiative) and 5-30 kg/ha (Incitec Pivot Fertilisers, 2021) for most crops, respectively. Zinc-incorporated SAPs can provide the bulk of the recommended dose of the nutrient. A 20:100 Zn-SAP composite comprises 7.4 kg/ha of zinc sulfate for 45 kg/ha

SAP application and has superior water absorption capacity, compared to pure SAP. Therefore, the composite SAP can act both as a water reservoir during drought and as an ample supply of zinc micronutrients. Calcium has a higher application rate compared to zinc. Therefore, 40:100 Ca:SAP can be preferred, which contains 12.8 kg/ha of calcium nitrate for the same SAP application rate. Accordingly, Ca:SAP composites can supply a significant portion of the nutrient while acting as an adequate water reservoir.

Superabsorbent polymers (SAP) are applied together with the seeds. They help farmers combat drought conditions by acting as a water reservoir and providing water to plant roots. On the other hand, fertilizers are indispensable to replenish soil nutrients for plant growth. Traditionally, fertilizers and SAPs are applied in granular form, by spreading machines. Incorporating fertilizers in SAPs can reduce the number of fertilizer applications by serving a dual purpose: water reservoir and nutrient supply. Fertilizers are applied at a dose of approximately 150 kg/ha, of which urea and NPK constitute the most. Whereas nutrients such as calcium, zinc, iron, copper, and magnesium are applied at considerably lower doses. SAPs, on the other hand, are applied at a dose of 15-45 kg/ha. Considering their low application rates, our focus in this study has been on developing Ca and Zn-SAP composites. At low nutrient incorporations, these composite SAPs have superior water absorption performance compared to pure SAP, and their saline absorption performances are comparable. For example, a Zn:SAP composite with a 20:100 composition can supply the recommended zinc sulfate. Similarly, Ca:SAP composites can provide the majority of the recommended calcium nitrate dose while acting as a water reservoir under drought conditions.

5.4. Bio-based Superabsorbent Polymers

In the literature, there are examples of bio-based SAPs. However, the studied formulations either contain very small amounts of cellulose, e.g., around 5 wt%, and have good water absorption; or they are almost entirely bio-based, but their water absorption capacities are very limited, approximately 45-70 times their own weight, which is not suitable to be used in practical applications. Furthermore, most works study only one or two formulations. In this study, a wide range of CMC ratios from 5 to 60 wt%, were

studied. A relatively high cellulose ratio was successfully integrated into the SAP structure, and sufficiently high-water absorption capacities were achieved.

In this study, complete biodegradation of polymeric absorbent materials was achieved by incorporating more than 30% CMC in the synthesis of an otherwise synthetic SAP. SAP with 40 wt% CMC achieved a water absorption capacity of more than 400 g/g, which is sufficient to be used in the agriculture or personal hygiene sector.

Owed to their superior water absorption capacities, SAPs can be used in agriculture to allow better water use efficiency, enable water savings, and improve crop yields, especially in climates where the rainfall regime is highly unpredictable. The bio-SAP formulations developed in this study have high water absorption capacities, up to 600 g/g. This is comparable to, or even better than most commercially available SAPs. Hence, bio-SAPs offer the same water absorption benefits as commercial SAPs while preventing agriplastic accumulation in agricultural lands.

BIBLIOGRAPHY

1. Abalos, D., Jeffery, S., Sanz-Cobena, A., Guardia, G., & Vallejo, A. (2014). Meta-analysis of the effect of urease and nitrification inhibitors on crop productivity and nitrogen use efficiency. *Agriculture, Ecosystems & Environment*, *189*, 136–144. https://doi.org/10.1016/j.agee.2014.03.036
2. Ahmed, E. M. (2015). Hydrogel: Preparation, characterization, and applications: A review. *Journal of Advanced Research*, *6*(2), 105–121. https://doi.org/10.1016/j.jare.2013.07.006
3. Ahmed Khan, T., Zakaria, M. E. T., Kim, H., Ghazali, S., & Jamari, S. S. (2020). Carbonaceous microsphere-based superabsorbent polymer as filler for coating of NPK fertilizer: Fabrication, properties, swelling, and nitrogen release characteristics. *Journal of Applied Polymer Science*, *137*(8). https://doi.org/10.1002/app.48396
4. Alexandratos, N., & Bruinsma, J. (2012). World Agriculture towards 2030/2050: the 2012 revision. In *WORLD AGRICULTURE*. www.fao.org/economic/esa
5. Al-Jabari, M., Ghyadah, R. A., & Alokely, R. (2019). Recovery of hydrogel from baby diaper wastes and its application for enhancing soil irrigation management. *Journal of Environmental Management*, *239*, 255–261. https://doi.org/10.1016/j.jenvman.2019.03.087
6. Aljohani, W. jumah, wenchao, li, Ullah, M. W., Zhang, X., & Yang, G. (2017). Application of Sodium Alginate Hydrogel. *IOSR Journal of Biotechnology and Biochemistry*, *03*(3), 19–31. https://doi.org/10.9790/264X-03031931
7. Anil, I., Gunday, S. T., Alagha, O., & Bozkurt, A. (2019). Synthesis, Characterization, and Swelling Behaviors of Poly(acrylic acid-co-acrylamide)/Pozzolan Superabsorbent Polymers. *Journal of Polymers and the Environment*, *27*(5), 1086–1095. https://doi.org/10.1007/s10924-019-01415-0
8. Anton Paar. (n.d.). *Basics of rhelogy*. Anton Paar. Retrieved December 16, 2023, from .anton-paar.com/en/basics-of-rheology/
9. Arredondo, R., Yuan, Z., Sosa, D., Johnson, A., Beims, R. F., Li, H., Wei, Q., & Xu, C. C. (2023). Performance of a novel, eco-friendly, cellulose-based superabsorbent polymer (<scp>Cellulo-SAP</scp>): Absorbency, stability, reusability, and biodegradability. *The Canadian Journal of Chemical Engineering*, *101*(4), 1762–1771. https://doi.org/10.1002/cjce.24601
10. Arredondo Ramirez, R. M. (2022). *Production of cellulose-based superabsorbent polymers for soil water retention* [The University of Western Ontario]. https://ir.lib.uwo.ca/etd/9093
11. Bajpai, S. K., Bajpai, M., & Sharma, L. (2007). Inverse suspension polymerization of poly(methacrylic acid-co-partially neutralized acrylic acid) superabsorbent hydrogels: synthesis and water uptake behavior. *Designed Monomers and Polymers*, *10*(2), 181–192. https://doi.org/10.1163/156855507780378285
12. Bao, Y., Ma, J., & Li, N. (2011). Synthesis and swelling behaviors of sodium carboxymethyl cellulose-g-poly(AA-co-AM-co-AMPS)/MMT superabsorbent hydrogel. *Carbohydrate Polymers*, *84*(1), 76–82. https://doi.org/10.1016/j.carbpol.2010.10.061
13. Barajas-Ledesma, R. M., Patti, A. F., Wong, V. N. L., Raghuwanshi, V. S., & Garnier, G. (2020). Engineering nanocellulose superabsorbent structure by

controlling the drying rate. *Colloids and Surfaces A: Physicochemical and Engineering Aspects*, *600*, 124943. https://doi.org/10.1016/j.colsurfa.2020.124943

14. Barajas-Ledesma, R. M., Stocker, C. W., Wong, V. N. L., Little, K., Patti, A. F., & Garnier, G. (2022). Biodegradation of a Nanocellulose Superabsorbent and Its Effect on the Growth of Spinach (*Spinacea oleracea*). *ACS Agricultural Science & Technology*, *2*(1), 90–99. https://doi.org/10.1021/acsagscitech.1c00178
15. Barajas-Ledesma, R. M., Wong, V. N. L., Little, K., Patti, A. F., & Garnier, G. (2022). Carboxylated nanocellulose superabsorbent: Biodegradation and soil water retention properties. *Journal of Applied Polymer Science*, *139*(3), 51495. https://doi.org/10.1002/app.51495
16. Batista, R. A., Espitia, P. J. P., Quintans, J. de S. S., Freitas, M. M., Cerqueira, M. Â., Teixeira, J. A., & Cardoso, J. C. (2019). Hydrogel as an alternative structure for food packaging systems. *Carbohydrate Polymers*, *205*, 106–116. https://doi.org/10.1016/j.carbpol.2018.10.006
17. Behera, S., & Mahanwar, P. A. (2020). Superabsorbent polymers in agriculture and other applications: a review. *Polymer-Plastics Technology and Materials*, *59*(4), 341–356. https://doi.org/10.1080/25740881.2019.1647239
18. Braun, O., Coquery, C., Kieffer, J., Blondel, F., Favero, C., Besset, C., Mesnager, J., Voelker, F., Delorme, C., & Matioszek, D. (2021). Spotlight on the Life Cycle of Acrylamide-Based Polymers Supporting Reductions in Environmental Footprint: Review and Recent Advances. *Molecules*, *27*(1), 42. https://doi.org/10.3390/molecules27010042
19. Broadley, M. R., White, P. J., Hammond, J. P., Zelko, I., & Lux, A. (2007). Zinc in plants. *New Phytologist*, *173*(4), 677–702. https://doi.org/10.1111/j.1469-8137.2007.01996.x
20. Brookes, G., & Barfoot, P. (2018). Environmental impacts of genetically modified (GM) crop use 1996-2016: Impacts on pesticide use and carbon emissions. *GM Crops & Food*, *9*(3), 109–139. https://doi.org/10.1080/21645698.2018.1476792
21. Brouwer, C., Prins, K., & Heibloem, M. (1989). *Irrigation Water Management: Irrigation Scheduling - Annex I: Irrigation efficiencies*. FAO. https://www.fao.org/3/t7202e/t7202e08.htm
22. Bylemans, D., De Coninck, B., & Keulemans, W. (2019). *Farming without plant protection products : Can we grow without using herbicides, fungicides and insecticides?* https://doi.org/Doi: 10.2861/05433
23. Calcagnile, P., Sibillano, T., Giannini, C., Sannino, A., & Demitri, C. (2019). Biodegradable poly(lactic acid)/cellulose-based superabsorbent hydrogel composite material as water and fertilizer reservoir in agricultural applications. *Journal of Applied Polymer Science*, *136*(21), 47546. https://doi.org/10.1002/app.47546
24. Campos, E. V. R., de Oliveira, J. L., & Fraceto, L. F. (2014). Applications of Controlled Release Systems for Fungicides, Herbicides, Acaricides, Nutrients, and Plant Growth Hormones: A Review. *Advanced Science, Engineering and Medicine*, *6*(4), 373–387. https://doi.org/10.1166/asem.2014.1538
25. Cansev, A., Gülen, H., Kesici Zengin, M., Ergin, S., Cansev, M., & Kumral, N. A. (2014). *USE OF URIDINE FOR ENHANCEMENT OF PLANT STRESS TOLERANCE* (Patent EP2967061B1). European Patent Office.
26. Cerasola, V. A., Perlotti, L., Pennisi, G., Orsini, F., & Gianquinto, G. (2022). Potential Use of Superabsorbent Polymer on Drought-Stressed Processing Tomato (Solanum lycopersicum L.) in a Mediterranean Climate. *Horticulturae*, *8*(8), 718. https://doi.org/10.3390/horticulturae8080718

27. Chaiyasat, A., Jearanai, S., Christopher, L. P., & Alam, M. N. (2019). Novel superabsorbent materials from bacterial cellulose. *Polymer International*, *68*(1), 102–109. https://doi.org/10.1002/pi.5701
28. Chaudhry, A. H., Nayab, S., Hussain, S. B., Ali, M., & Pan, Z. (2021). Current Understandings on Magnesium Deficiency and Future Outlooks for Sustainable Agriculture. *International Journal of Molecular Sciences*, *22*(4), 1819. https://doi.org/10.3390/ijms22041819
29. Chauhan, G. S., Chauhan, S., Sen, U., & Garg, D. (2009). Synthesis and characterization of acrylamide and 2-hydroxyethyl methacrylate hydrogels for use in metal ion uptake studies. *Desalination*, *243*(1–3), 95–108. https://doi.org/10.1016/j.desal.2008.04.017
30. Che Ani, N., Ghazali, S., Ahmed Khan, T., Kim, H.-J., & Jamari, S. S. (2022). Nutrients Release Evaluation on NPK Fertilizer Coated by a Carbon Microspheres Superabsorbent Polymer. *Chemical Engineering & Technology*, *45*(11), 2008–2014. https://doi.org/10.1002/ceat.202200270
31. Chen, H., Hou, S., Ma, H., Li, X., & Tan, Y. (2016). Controlled gelation kinetics of cucurbit[7]uril-adamantane cross-linked supramolecular hydrogels with competing guest molecules. *Scientific Reports*, *6*(1), 20722. https://doi.org/10.1038/srep20722
32. Chen, J., Wu, J., Raffa, P., Picchioni, F., & Koning, C. E. (2022). Superabsorbent Polymers: From long-established, microplastics generating systems, to sustainable, biodegradable and future proof alternatives. *Progress in Polymer Science*, *125*, 101475. https://doi.org/10.1016/j.progpolymsci.2021.101475
33. Chen, Q., Yan, X., Zhu, L., Chen, H., Jiang, B., Wei, D., Huang, L., Yang, J., Liu, B., & Zheng, J. (2016). Improvement of Mechanical Strength and Fatigue Resistance of Double Network Hydrogels by Ionic Coordination Interactions. *Chemistry of Materials*, *28*(16), 5710–5720. https://doi.org/10.1021/acs.chemmater.6b01920
34. Chen, Y.-C., & Chen, Y.-H. (2019). Thermo and pH-responsive methylcellulose and hydroxypropyl methylcellulose hydrogels containing K2SO4 for water retention and a controlled-release water-soluble fertilizer. *Science of The Total Environment*, *655*, 958–967. https://doi.org/10.1016/j.scitotenv.2018.11.264
35. Cheng, D., Liu, Y., Yang, G., & Zhang, A. (2018). Water- and Fertilizer-Integrated Hydrogel Derived from the Polymerization of Acrylic Acid and Urea as a Slow-Release N Fertilizer and Water Retention in Agriculture. *Journal of Agricultural and Food Chemistry*, *66*(23), 5762–5769. https://doi.org/10.1021/acs.jafc.8b00872
36. Choi, H., Park, J., & Lee, J. (2022). Sustainable Bio-Based Superabsorbent Polymer: Poly(itaconic acid) with Superior Swelling Properties. *ACS Applied Polymer Materials*, *4*(6), 4098–4108. https://doi.org/10.1021/acsapm.2c00021
37. Coleman, E. A. (2011). Plastics Additives. In *Applied Plastics Engineering Handbook* (pp. 419–428). Elsevier. https://doi.org/10.1016/B978-1-4377-3514-7.10023-6
38. Cornell University Northeast Region Certified Crop Adviser (NRCCA) Study Resources. (n.d.). *Nutrient Management: Basic Concepts of Plant Nutrition*. Cornell University. Retrieved November 27, 2023, from https://nrcca.cals.cornell.edu/nutrient/CA1/CA010102.php
39. Czarnecka, E., & Nowaczyk, J. (2020). Semi-Natural Superabsorbents Based on Starch-g-poly(acrylic acid): Modification, Synthesis and Application. *Polymers*, *12*(8), 1794. https://doi.org/10.3390/polym12081794

40. Czarnecka, E., & Nowaczyk, J. (2021). Synthesis and Characterization Superabsorbent Polymers Made of Starch, Acrylic Acid, Acrylamide, Poly(Vinyl Alcohol), 2-Hydroxyethyl Methacrylate, 2-Acrylamido-2-methylpropane Sulfonic Acid. *International Journal of Molecular Sciences*, *22*(9), 4325. https://doi.org/10.3390/ijms22094325
41. Dantas de Oliveira, A., & Augusto Gonçalves Beatrice, C. (2019). Polymer Nanocomposites with Different Types of Nanofiller. In *Nanocomposites - Recent Evolutions*. IntechOpen. https://doi.org/10.5772/intechopen.81329
42. Dellicolli, H. T. (1977). Controlled Release of Pesticides from Kraft Lignin Carriers. In H. B. Scher (Ed.), *Controlled Release Pesticides* (Vol. 53, pp. 84–93). AMERICAN CHEMICAL SOCIETY. https://doi.org/10.1021/bk-1977-0053
43. Dillingham, G. (2002). Priming to improve adhesion. In *Adhesion Science and Engineering* (pp. 433–464). Elsevier. https://doi.org/10.1016/B978-044451140-9/50010-X
44. Dinescu, S., Albu Kaya, M., Chitoiu, L., Ignat, S., Kaya, D. A., & Costache, M. (2018). *Collagen-Based Hydrogels and Their Applications for Tissue Engineering and Regenerative Medicine* (pp. 1–21). https://doi.org/10.1007/978-3-319-76573-0_54-1
45. Ding, R., & Gong, K. (2013). Super-absorbent resin preparation utilizing spent mushroom substrates. *Journal of Applied Polymer Science*, *130*(2), 1098–1103. https://doi.org/10.1002/app.39285
46. Dispat, N., Poompradub, S., & Kiatkamjornwong, S. (2020). Synthesis of ZnO/SiO2-modified starch-graft-polyacrylate superabsorbent polymer for agricultural application. *Carbohydrate Polymers*, *249*, 116862. https://doi.org/10.1016/j.carbpol.2020.116862
47. Djafari Petroudy, S. R., Ranjbar, J., & Rasooly Garmaroody, E. (2018). Eco-friendly superabsorbent polymers based on carboxymethyl cellulose strengthened by TEMPO-mediated oxidation wheat straw cellulose nanofiber. *Carbohydrate Polymers*, *197*, 565–575. https://doi.org/10.1016/j.carbpol.2018.06.008
48. Dobolyi, A., Juhasz, G., Kovacs, Z., & Kardos, J. (2011). Uridine Function in the Central Nervous System. *Current Topics in Medicinal Chemistry*, *11*(8), 1058–1067. https://doi.org/10.2174/156802611795347618
49. Dowgert, M. F. (2010). *The Impact of Irrigated Agriculture on a Stable Food Supply*. 1–11.
50. Edmeades, D. C. (2004). *Nitrification and Urease Inhibitors*. Environment Bay of Plenty.
51. Elshafie, H. S., & Camele, I. (2021). Applications of Absorbent Polymers for Sustainable Plant Protection and Crop Yield. *Sustainability*, *13*(6), 3253. https://doi.org/10.3390/su13063253
52. European Environment Agency. (2021, May 11). *Population trends 1950 – 2100: globally and within Europe*. European Environment Agency. https://www.eea.europa.eu/data-and-maps/indicators/total-population-outlook-from-unstat-3/assessment-1#:~:text=The%20world's%20population%20increased%20from,under%20most%20UN%20projection%20variants.
53. Fang, S., Wang, G., Xing, R., Chen, X., Liu, S., Qin, Y., Li, K., Wang, X., Li, R., & Li, P. (2019). Synthesis of superabsorbent polymers based on chitosan derivative graft acrylic acid-co-acrylamide and its property testing. *International Journal of Biological Macromolecules*, *132*, 575–584. https://doi.org/10.1016/j.ijbiomac.2019.03.176

54. FAO. (2021, November 6). *COP26: Agricultural expansion drives almost 90 percent of global deforestation*. FAO. https://www.fao.org/newsroom/detail/cop26-agricultural-expansion-drives-almost-90-percent-of-global-deforestation/en
55. Farzanian, K., & Ghahremaninezhad, A. (2018). On the Effect of Chemical Composition on the Desorption of Superabsorbent Hydrogels in Contact with a Porous Cementitious Material. *Gels*, *4*(3), 70. https://doi.org/10.3390/gels4030070
56. Feng, H., Li, J., & Wang, L. (2010). PREPARATION OF BIODEGRADABLE FLAX SHIVE CELLULOSE-BASED SUPERABSORBENT POLYMER UNDER MICROWAVE IRRADIATION. *BioResources*, *5*(3), 1484–1795.
57. Fernandez, V., Uçgun, K., Ge, S., Jiang, Y., Xu, X., Du, X., Wang, F., Sha, J., Chen, Q., Tian, G., & Zhu, Z. (2020). *Effects of Potassium Levels on Plant Growth, Accumulation and Distribution of Carbon, and Nitrate Metabolism in Apple Dwarf Rootstock Seedlings*. https://doi.org/10.3389/fpls.2020.00904
58. Fernández-Pérez, M., Villafranca-Sánchez, M., Flores-Céspedes, F., & Daza-Fernández, I. (2011). Ethylcellulose and lignin as bearer polymers in controlled release formulations of chloridazon. *Carbohydrate Polymers*, *83*(4), 1672–1679. https://doi.org/10.1016/j.carbpol.2010.10.024
59. Food and Agriculture Organization. (2021). *Fertilizer consumption (kilograms per hectare of arable land) | Data*. https://data.worldbank.org/indicator/AG.CON.FERT.ZS
60. Fu, E., Zhang, S., Luan, Y., Zhang, Y., Saghir, S., & Xiao, Z. (2022). Novel superabsorbent polymer composites based on α-cellulose and modified zeolite: synthesis, characterization, water absorbency and water retention capacity. *Cellulose*, *29*(3), 1727–1737. https://doi.org/10.1007/s10570-021-04380-x
61. Fujita, S., Tazawa, T., & Kono, H. (2022). Preparation and Enzyme Degradability of Spherical and Water-Absorbent Gels from Sodium Carboxymethyl Cellulose. *Gels*, *8*(5), 321. https://doi.org/10.3390/gels8050321
62. Gelok International Corporation. (n.d.). *What is Super Absorbent Polymer*. Retrieved June 26, 2024, from https://gelok.com/super-absorbent-polymer-overview/#:~:text=Superabsorbent%20polymers%20were%20first%20developed,polymer%20attached%20to%20starch%20molecules.
63. Georges Chidiac. (n.d.). *Calcium Nitrate - Agricultural Grade*. Van Iperen. Retrieved June 13, 2024, from https://www.vaniperen.com/products/calcium-nitrate-agricultural-grade-fertilizer/
64. Ghazali, S., Jamari, S., Noordin, N., & Tan, K. M. (2016). Pyrolysis of carbonaceous particles and properties of Carbonaceous- *g* -Poly (acrylic acid-co-acrylamide) superabsorbent polymer for agricultural applications. *MATEC Web of Conferences*, *69*, 06001. https://doi.org/10.1051/matecconf/20166906001
65. Ghezzi, L., Spepi, A., Agnolucci, M., Cristani, C., Giovannetti, M., Tiné, M. R., & Duce, C. (2018). Kinetics of release and antibacterial activity of salicylic acid loaded into halloysite nanotubes. *Applied Clay Science*, *160*, 88–94. https://doi.org/10.1016/j.clay.2017.11.041
66. Gianni, E., Pšenička, M., Macková, K., Scholtzová, E., Jankovič, Ľ., Mareš, M., Papoulis, D., & Pospíšil, M. (2023). New detail insight into Halloysite structure: Mechanism behind nanotubular morphology described by density functional theory and molecular dynamics supported by experiments. *Journal of Molecular Structure*, *1287*, 135639. https://doi.org/10.1016/j.molstruc.2023.135639

67. Gonçalves, J. M., Miao, Q., Duarte, I. M., & Shi, H. (2021). Water-Saving Techniques and Practices for On-Farm Surface Irrigation Systems. *Biol. Life Sci. Forum 2021*.
68. Gong, J. P., Katsuyama, Y., Kurokawa, T., & Osada, Y. (2003). Double-Network Hydrogels with Extremely High Mechanical Strength. *Advanced Materials*, *15*(14), 1155–1158. https://doi.org/10.1002/adma.200304907
69. Gordon, A. (2022, September 7). *Yield Losses Due to Pests*. AGRIVI. https://www.agrivi.com/blog/yield-losses-due-to-pests/
70. Guardia, G., Marsden, K. A., Vallejo, A., Jones, D. L., & Chadwick, D. R. (2018). Determining the influence of environmental and edaphic factors on the fate of the nitrification inhibitors DCD and DMPP in soil. *Science of The Total Environment*, *624*, 1202–1212. https://doi.org/10.1016/j.scitotenv.2017.12.250
71. Guo, Liu, Zhan, & Wu, L. (2005). Preparation and Properties of a Slow-Release Membrane-Encapsulated Urea Fertilizer with Superabsorbent and Moisture Preservation. *Industrial & Engineering Chemistry Research*, *44*(12), 4206–4211. https://doi.org/10.1021/ie0489406
72. Guo, M., Liu, M., Liang, R., & Niu, A. (2006). Granular urea-formaldehyde slow-release fertilizer with superabsorbent and moisture preservation. *Journal of Applied Polymer Science*, *99*(6), 3230–3235. https://doi.org/10.1002/app.22892
73. He, F., Zhou, Q., Wang, L., Yu, G., Li, J., & Feng, Y. (2019). Fabrication of a sustained release delivery system for pesticides using interpenetrating polyacrylamide/alginate/montmorillonite nanocomposite hydrogels. *Applied Clay Science*, *183*, 105347. https://doi.org/10.1016/j.clay.2019.105347
74. Heidari Pebdani, M. (2023). Molecular insight into structural and mechanical properties of Halloysite structure. *Computational Materials Science*, *218*, 111948. https://doi.org/10.1016/j.commatsci.2022.111948
75. HENGDA. (n.d.). *How To Use Silane Coupling Agent*. Retrieved November 25, 2023, from https://www.hengdasilane.com/how-to-use-silane-coupling-agent/
76. Huang, T., Xu, H. G., Jiao, K. X., Zhu, L. P., Brown, H. R., & Wang, H. L. (2007). A Novel Hydrogel with High Mechanical Strength: A Macromolecular Microsphere Composite Hydrogel. *Advanced Materials*, *19*(12), 1622–1626. https://doi.org/10.1002/adma.200602533
77. Ibrahim, S. M., El Salmawi, K. M., & Zahran, A. H. (2007). Synthesis of crosslinked superabsorbent carboxymethyl cellulose/acrylamide hydrogels through electron-beam irradiation. *Journal of Applied Polymer Science*, *104*(3), 2003–2008. https://doi.org/10.1002/app.25916
78. Incitec Pivot Fertilisers. (2022a). *Copper*. https://www.incitecpivotfertilisers.com.au/~/media/Files/IPF/Documents/Agritopics/22%20Copper%20Agritopic.pdf
79. Incitec Pivot Fertilisers. (2022b). *Iron*. https://www.incitecpivotfertilisers.com.au/~/media/Files/IPF/Documents/Fact%20Sheets/23%20Iron%20Fact%20Sheet.pdf
80. International Fertilizer Association. (n.d.). *Organic and Mineral Fertilizers*. International Fertilizer Association. Retrieved November 27, 2023, from https://www.fertilizer.org/about-fertilizers/organic-and-mineral-fertilizers/
81. International Plant Nutrition Institute. (n.d.-a). *Manganese*. Retrieved November 20, 2023, from https://www.tfi.org/sites/default/files/tfi-manganese.pdf
82. International Plant Nutrition Institute. (n.d.-b). *Molybdenum*. Retrieved November 20, 2023, from https://www.tfi.org/sites/default/files/tfi-molybdenum.pdf

83. Islam, H. B. M. Z., Krishna, S. B. N., & Imran, A. Bin. (2023). Enhancing the mechanical properties of hydrogels with vinyl-functionalized nanocrystalline cellulose as a green crosslinker. *Nanotechnology*, *34*(50), 505706. https://doi.org/10.1088/1361-6528/acf93b
84. Jayasuriya, C. K. (2017). Interfacial Bonding in Polymer–Ceramic Nanocomposites☆. In *Reference Module in Materials Science and Materials Engineering*. Elsevier. https://doi.org/10.1016/B978-0-12-803581-8.03252-5
85. Jin, S., Yue, G., Feng, L., Han, Y., Yu, X., & Zhang, Z. (2011). Preparation and Properties of a Coated Slow-Release and Water-Retention Biuret Phosphoramide Fertilizer with Superabsorbent. *Journal of Agricultural and Food Chemistry*, *59*(1), 322–327. https://doi.org/10.1021/jf1032137
86. Jin, X., Zhang, R., Su, M., Li, H., Yue, X., Qin, D., & Jiang, Z. (2019). Functionalization of halloysite nanotubes by enlargement and layer-by-layer assembly for controlled release of the fungicide iodopropynyl butylcarbamate. *RSC Advances*, *9*(72), 42062–42070. https://doi.org/10.1039/C9RA07593C
87. Joshi, P. P., Van Cleave, A., Held, D. W., Howe, J. A., & Auad, M. L. (2020). Preparation of slow release encapsulated insecticide and fertilizer based on superabsorbent polysaccharide microbeads. *Journal of Applied Polymer Science*, *137*(39). https://doi.org/10.1002/app.49177
88. Kabir, S. M. F., Sikdar, P. P., Haque, B., Bhuiyan, M. A. R., Ali, A., & Islam, M. N. (2018). Cellulose-based hydrogel materials: chemistry, properties and their prospective applications. *Progress in Biomaterials*, *7*(3), 153–174. https://doi.org/10.1007/s40204-018-0095-0
89. Kabiri, K., Omidian, H., Zohuriaan-Mehr, M. J., & Doroudiani, S. (2011). Superabsorbent hydrogel composites and nanocomposites: A review. *Polymer Composites*, *32*(2), 277–289. https://doi.org/10.1002/pc.21046
90. KAISER, B. N., GRIDLEY, K. L., NGAIRE BRADY, J., PHILLIPS, T., & TYERMAN, S. D. (2005). The Role of Molybdenum in Agricultural Plant Production. *Annals of Botany*, *96*(5), 745–754. https://doi.org/10.1093/aob/mci226
91. Kaushal, J., Khatri, M., & Arya, S. K. (2021). Recent insight into enzymatic degradation of plastics prevalent in the environment: A mini - review. *Cleaner Engineering and Technology*, *2*, 100083. https://doi.org/10.1016/j.clet.2021.100083
92. Khoo, J. M. Y., Chee, S. Y., Lee, C. L., & Nagalingam, S. (2014). Superabsorbent polymer prepared using carboxymethyl cellulose derived from *Ceiba pentandra* (L.) Gaertn. (kapok) cotton. *Journal of Applied Polymer Science*, *131*(18). https://doi.org/10.1002/app.40808
93. Kiatkamjornwong, S. (2007). Superabsorbent Polymers and Superabsorbent Polymer Composites. *ScienceAsia*, *33(s1)*, 039. https://doi.org/10.2306/scienceasia1513-1874.2007.33(s1).039
94. Kim, H. C., Lim, S. H., Kwon, Y. R., Kim, J. S., Kim, J. H., & Kim, D. H. (2022). Itaconic Acid-based Superabsorbent Polymer Composites Using Cellulose with Enhanced Absorption Properties and Heat Resistance. *Fibers and Polymers*, *23*(4), 891–899. https://doi.org/10.1007/s12221-022-4431-6
95. Kim, H. J., Koo, J. M., Kim, S. H., Hwang, S. Y., & Im, S. S. (2017). Synthesis of super absorbent polymer using citric acid as a bio-based monomer. *Polymer Degradation and Stability*, *144*, 128–136. https://doi.org/10.1016/j.polymdegradstab.2017.07.031
96. Kim, Y. J., Hong, S. J., Shin, W. S., Kwon, Y. R., Lim, S. H., Kim, H. C., Kim, J. S., Kim, J. W., & Kim, D. H. (2020). Preparation of a biodegradable

superabsorbent polymer and measurements of changes in absorption properties depending on the type of surface-crosslinker. *Polymers for Advanced Technologies*, *31*(2), 273–283. https://doi.org/10.1002/pat.4767

97. Kim, Y. J., Hong, S. J., Shin, W. S., Kwon, Y. R., Lim, S. H., Kim, J. S., Choi, J., Kim, J. W., & Kim, D. H. (2020). Preparation and Performance of Superabsorbent Polymer with Cellulose Additives. *Fibers and Polymers*, *21*(11), 2448–2455. https://doi.org/10.1007/s12221-020-1198-5
98. Klinpituksa, P., & Kosaiyakanon, P. (2017). Superabsorbent Polymer Based on Sodium Carboxymethyl Cellulose Grafted Polyacrylic Acid by Inverse Suspension Polymerization. *International Journal of Polymer Science*, *2017*, 1–6. https://doi.org/10.1155/2017/3476921
99. Kong, X., Duan, Y., Schramm, A., Eriksen, J., & Petersen, S. O. (2016). 3,4-Dimethylpyrazole phosphate (DMPP) reduces activity of ammonia oxidizers without adverse effects on non-target soil microorganisms and functions. *Applied Soil Ecology*, *105*, 67–75. https://doi.org/10.1016/j.apsoil.2016.03.018
100. Kuang, J., Yuk, K. Y., & Huh, K. M. (2011). Polysaccharide-based superporous hydrogels with fast swelling and superabsorbent properties. *Carbohydrate Polymers*, *83*(1), 284–290. https://doi.org/10.1016/j.carbpol.2010.07.052
101. Lacoste, C., Lopez-Cuesta, J.-M., & Bergeret, A. (2019). Development of a biobased superabsorbent polymer from recycled cellulose for diapers applications. *European Polymer Journal*, *116*, 38–44. https://doi.org/10.1016/j.eurpolymj.2019.03.013
102. Lee, J., Park, S., Roh, H., Oh, S., Kim, S., Kim, M., Kim, D., & Park, J. (2018). Preparation and Characterization of Superabsorbent Polymers Based on Starch Aldehydes and Carboxymethyl Cellulose. *Polymers*, *10*(6), 605. https://doi.org/10.3390/polym10060605
103. Lehrsch, G. A., Lentz, R. D., Bjorneberg, D. L., & Sojka, R. E. (2014). Irrigation-Induced☆. In *Reference Module in Earth Systems and Environmental Sciences*. Elsevier. https://doi.org/https://doi.org/10.1016/B978-0-12-409548-9.09019-9
104. León, O., Soto, D., Antúnez, A., Fernández, R., González, J., Piña, C., Muñoz-Bonilla, A., & Fernandez-García, M. (2019). Hydrogels based on oxidized starches from different botanical sources for release of fertilizers. *International Journal of Biological Macromolecules*, *136*, 813–822. https://doi.org/10.1016/j.ijbiomac.2019.06.131
105. Li, A., Shi, Z., Yin, Y., Fan, Y., Zhang, Z., Tian, X., Yang, Y., & Pan, L. (2023). Excessive use of chemical fertilizers in catchment areas raises the seasonal pH in natural freshwater lakes of the subtropical monsoon climate region. *Ecological Indicators*, *154*, 110477. https://doi.org/10.1016/j.ecolind.2023.110477
106. Liu, B., Wang, Y., Yang, F., Wang, X., Shen, H., Cui, H., & Wu, D. (2016). Construction of a controlled-release delivery system for pesticides using biodegradable PLA-based microcapsules. *Colloids and Surfaces B: Biointerfaces*, *144*, 38–45. https://doi.org/10.1016/j.colsurfb.2016.03.084
107. Liu, G., Yang, Z., Du, J., He, A., Yang, H., Xue, G., Yu, C., & Zhang, Y. (2020). Adding NBPT to urea increases N use efficiency of maize and decreases the abundance of N-cycling soil microbes under reduced fertilizer-N rate on the North China Plain. *PLOS ONE*, *15*(10), e0240925. https://doi.org/10.1371/journal.pone.0240925
108. Liu, X., Luan, S., & Li, W. (2019). Utilization of waste hemicelluloses lye for superabsorbent hydrogel synthesis. *International Journal of Biological Macromolecules*, *132*, 954–962. https://doi.org/10.1016/j.ijbiomac.2019.04.041

109. Llanes, L., Dubessay, P., Pierre, G., Delattre, C., & Michaud, P. (2020). Biosourced Polysaccharide-Based Superabsorbents. *Polysaccharides*, *1*(1), 51–79. https://doi.org/10.3390/polysaccharides1010005
110. Macdougall, L. J., & Anseth, K. (2020). Bioerodible Hydrogels Based on Photopolymerized Poly(ethylene glycol)- *co* -poly(α-hydroxy acid) Diacrylate Macromers. *Macromolecules*, *53*(7), 2295–2298. https://doi.org/10.1021/acs.macromol.0c00030
111. Mao, S., Islam, M. R., Xue, X., Yang, X., Zhao, X., & Hu, Y. (2011). Evaluation of a water-saving superabsorbent polymer for corn (Zea mays L.) production in arid regions of Northern China. *African Journal of Agricultural Research*, *6*(17), 4108–4115.
112. Massaro, M., Campofelice, A., Colletti, C. G., Lazzara, G., Noto, R., & Riela, S. (2018). Functionalized halloysite nanotubes: Efficient carrier systems for antifungine drugs. *Applied Clay Science*, *160*, 186–192. https://doi.org/10.1016/j.clay.2018.01.005
113. Massaro, M., Cavallaro, G., Colletti, C. G., D'Azzo, G., Guernelli, S., Lazzara, G., Pieraccini, S., & Riela, S. (2018). Halloysite nanotubes for efficient loading, stabilization and controlled release of insulin. *Journal of Colloid and Interface Science*, *524*, 156–164. https://doi.org/10.1016/j.jcis.2018.04.025
114. Mattos, B. D., & Magalhães, W. L. E. (2016). Biogenic nanosilica blended by nanofibrillated cellulose as support for slow-release of tebuconazole. *Journal of Nanoparticle Research*, *18*(9), 274. https://doi.org/10.1007/s11051-016-3586-8
115. Mattos, B. D., Rojas, O. J., & Magalhães, W. L. E. (2017). Biogenic silica nanoparticles loaded with neem bark extract as green, slow-release biocide. *Journal of Cleaner Production*, *142*, 4206–4213. https://doi.org/10.1016/j.jclepro.2016.11.183
116. Mattos, B. D., Tardy, B. L., Magalhães, W. L. E., & Rojas, O. J. (2017). Controlled release for crop and wood protection: Recent progress toward sustainable and safe nanostructured biocidal systems. *Journal of Controlled Release*, *262*, 139–150. https://doi.org/10.1016/j.jconrel.2017.07.025
117. McClellan, T. (n.d.). *Soil Composition*. University of Hawai'i at Manoa, College of Tropical Agriculture and Human Resources. Retrieved November 26, 2023, from https://www.ctahr.hawaii.edu/mauisoil/a_comp.aspx
118. Meng, Y., Liu, X., Li, C., Liu, H., Cheng, Y., Lu, J., Zhang, K., & Wang, H. (2019). Super-swelling lignin-based biopolymer hydrogels for soil water retention from paper industry waste. *International Journal of Biological Macromolecules*, *135*, 815–820. https://doi.org/10.1016/j.ijbiomac.2019.05.195
119. Mignon, A., De Belie, N., Dubruel, P., & Van Vlierberghe, S. (2019). Superabsorbent polymers: A review on the characteristics and applications of synthetic, polysaccharide-based, semi-synthetic and 'smart' derivatives. *European Polymer Journal*, *117*, 165–178. https://doi.org/10.1016/j.eurpolymj.2019.04.054
120. Milovanovic, S., Markovic, D., Aksentijevic, K., Stojanovic, D. B., Ivanovic, J., & Zizovic, I. (2016). Application of cellulose acetate for controlled release of thymol. *Carbohydrate Polymers*, *147*, 344–353. https://doi.org/10.1016/j.carbpol.2016.03.093
121. Mohanan, N., Montazer, Z., Sharma, P. K., & Levin, D. B. (2020). Microbial and Enzymatic Degradation of Synthetic Plastics. *Frontiers in Microbiology*, *11*. https://doi.org/10.3389/fmicb.2020.580709

122. Mousavi, S. M., & Raiesi, T. (2022). Essentiality of boron in higher plants. In *Boron in Plants and Agriculture* (pp. 1–28). Elsevier. https://doi.org/10.1016/B978-0-323-90857-3.00008-4
123. Mulyani, S., Mawarni, A. S., & Ramadhani, D. G. (2021). CHARACTERISATION OF CARBOXYMETHYLCELLULOSE-BASED SUPERABSORBENT POLYMER HYDROGEL FOR SLOW-RELEASE OF NITROGEN-PHOSPHORUS-POTASSIUM FERTILISER. *Journal of Chemical Technology and Metallurgy*, *56*(4), 730–737.
124. Nakayama, A., Kakugo, A., Gong, J. P., Osada, Y., Takai, M., Erata, T., & Kawano, S. (2004). High Mechanical Strength Double-Network Hydrogel with Bacterial Cellulose. *Advanced Functional Materials*, *14*(11), 1124–1128. https://doi.org/10.1002/adfm.200305197
125. Neamjan, N., Wiwattananukul, R., Hiangrat, K., Matkaran, K., Na-iam, Y., Sakulsombat, M., & Sriroth, K. (2019). Preparation of Superabsorbent Polymer from Sugarcane Bagasse via Extrusion Process. *Sugar Tech*, *21*(2), 296–300. https://doi.org/10.1007/s12355-018-0670-7
126. Neem.World. (2016, February 8). *Health Risks Associated with Pesticides*. Neem.World. https://neem.world/health-risks-associated-pesticides/
127. Noppakundilograt, S., Choopromkaw, S., & Kiatkamjornwong, S. (2018). Hydrolyzed collagen-grafted-poly[(acrylic acid)- *co* -(methacrylic acid)] hydrogel for drug delivery. *Journal of Applied Polymer Science*, *135*(1). https://doi.org/10.1002/app.45654
128. Nyyssölä, A., & Ahlgren, J. (2019). Microbial degradation of polyacrylamide and the deamination product polyacrylate. *International Biodeterioration & Biodegradation*, *139*, 24–33. https://doi.org/10.1016/j.ibiod.2019.02.005
129. OERKE, E.-C. (2006). Crop losses to pests. *The Journal of Agricultural Science*, *144*(1), 31–43. https://doi.org/10.1017/S0021859605005708
130. Oladosu, Y., Rafii, M. Y., Arolu, F., Chukwu, S. C., Salisu, M. A., Fagbohun, I. K., Muftaudeen, T. K., Swaray, S., & Haliru, B. S. (2022). Superabsorbent Polymer Hydrogels for Sustainable Agriculture: A Review. *Horticulturae*, *8*(7), 605. https://doi.org/10.3390/horticulturae8070605
131. Pang, L., Gao, Z., Zhang, S., Li, Y., Hu, S., & Ren, X. (2016). Preparation and anti-UV property of modified cellulose membranes for biopesticides controlled release. *Industrial Crops and Products*, *89*, 176–181. https://doi.org/10.1016/j.indcrop.2016.05.014
132. Patachia, S., & Croitoru, C. (2015). Increasing the adsorption capacity and selectivity of poly(vinyl alcohol) hydrogels by an alternative imprinting technique. *Journal of Applied Polymer Science*, *132*(23). https://doi.org/10.1002/app.42024
133. Patel, S., Bajpai, J., Saini, R., Bajpai, A. K., & Acharya, S. (2018). Sustained release of pesticide (Cypermethrin) from nanocarriers: An effective technique for environmental and crop protection. *Process Safety and Environmental Protection*, *117*, 315–325. https://doi.org/10.1016/j.psep.2018.05.012
134. Patiño-Masó, J., Serra-Parareda, F., Tarrés, Q., Mutjé, P., Espinach, F. X., & Delgado-Aguilar, M. (2019). TEMPO-Oxidized Cellulose Nanofibers: A Potential Bio-Based Superabsorbent for Diaper Production. *Nanomaterials*, *9*(9), 1271. https://doi.org/10.3390/nano9091271
135. Pierchala, M. K., Makaremi, M., Tan, H. L., Pushpamalar, J., Muniyandy, S., Solouk, A., Lee, S. M., & Pasbakhsh, P. (2018). Nanotubes in nanofibers: Antibacterial multilayered polylactic acid/halloysite/gentamicin membranes for

bone regeneration application. *Applied Clay Science*, *160*, 95–105. https://doi.org/10.1016/j.clay.2017.12.016
136. Pimentel, D., & Burgess, M. (2012). Small amounts of pesticides reaching target insects. *Environment, Development and Sustainability*, *14*(1), 1–2. https://doi.org/10.1007/s10668-011-9325-5
137. Pimentel, D., & Levitan, L. (1986). Pesticides: Amounts Applied and Amounts Reaching Pests. *BioScience*, *36*(2), 86–91.
138. Qiao, D., Liu, H., Yu, L., Bao, X., Simon, G. P., Petinakis, E., & Chen, L. (2016). Preparation and characterization of slow-release fertilizer encapsulated by starch-based superabsorbent polymer. *Carbohydrate Polymers*, *147*, 146–154. https://doi.org/10.1016/j.carbpol.2016.04.010
139. R. Price, B. P. G. Y. L. R. (2001). In-vitro release characteristics of tetracycline HCl, khellin and nicotinamide adenine dineculeotide from halloysite; a cylindrical mineral. *Journal of Microencapsulation*, *18*(6), 713–722. https://doi.org/10.1080/02652040010019532
140. Rahman, K., & Zhang, D. (2018). Effects of Fertilizer Broadcasting on the Excessive Use of Inorganic Fertilizers and Environmental Sustainability. *Sustainability*, *10*(3), 759. https://doi.org/10.3390/su10030759
141. Ramazani-Harandi, M. J., Zohuriaan-Mehr, M. J., Yousefi, A. A., Ershad-Langroudi, A., & Kabiri, K. (2006a). Rheological determination of the swollen gel strength of superabsorbent polymer hydrogels. *Polymer Testing*, *25*(4), 470–474. https://doi.org/10.1016/j.polymertesting.2006.01.011
142. Ramazani-Harandi, M. J., Zohuriaan-Mehr, M. J., Yousefi, A. A., Ershad-Langroudi, A., & Kabiri, K. (2006b). Rheological determination of the swollen gel strength of superabsorbent polymer hydrogels. *Polymer Testing*, *25*(4), 470–474. https://doi.org/10.1016/j.polymertesting.2006.01.011
143. Rashidzadeh, A., & Olad, A. (2014). Slow-released NPK fertilizer encapsulated by NaAlg-g-poly(AA-co-AAm)/MMT superabsorbent nanocomposite. *Carbohydrate Polymers*, *114*, 269–278. https://doi.org/10.1016/j.carbpol.2014.08.010
144. Rodrigues, F. H. A., Pereira, A. G. B., Fajardo, A. R., & Muniz, E. C. (2013). Synthesis and characterization of chitosan- *graft* -poly(acrylic acid)/nontronite hydrogel composites based on a design of experiments. *Journal of Applied Polymer Science*, *128*(5), 3480–3489. https://doi.org/10.1002/app.38386
145. Rosenbom, A. E., Olsen, P., Plauborg, F., Grant, R., Juhler, R. K., Brüsch, W., & Kjær, J. (2015). Pesticide leaching through sandy and loamy fields – Long-term lessons learnt from the Danish Pesticide Leaching Assessment Programme. *Environmental Pollution*, *201*, 75–90. https://doi.org/10.1016/j.envpol.2015.03.002
146. Rossi, F., Castiglione, F., Ferro, M., Marchini, P., Mauri, E., Moioli, M., Mele, A., & Masi, M. (2015). Drug–Polymer Interactions in Hydrogel-based Drug-Delivery Systems: An Experimental and Theoretical Study. *ChemPhysChem*, *16*(13), 2818–2825. https://doi.org/10.1002/cphc.201500526
147. Sadeghi, M., & Soleimani, F. (2012). Synthesis of pH-Sensitive Hydrogel Based on Starch-Polyacrylate Superabsorbent. *Journal of Biomaterials and Nanobiotechnology*, *03*(02), 310–314. https://doi.org/10.4236/jbnb.2012.322038
148. Sami, A. J., Khalid, M., Jamil, T., Aftab, S., Mangat, S. A., Shakoori, A. R., & Iqbal, S. (2018). Formulation of novel chitosan guargum based hydrogels for sustained drug release of paracetamol. *International Journal of Biological Macromolecules*, *108*, 324–332. https://doi.org/10.1016/j.ijbiomac.2017.12.008

149. Sánchez-Correa, F., Vidaurre-Agut, C., Serrano-Aroca, Á., & Campillo-Fernández, A. J. (2018). Poly(2-hydroxyethyl acrylate) hydrogels reinforced with graphene oxide: Remarkable improvement of water diffusion and mechanical properties. *Journal of Applied Polymer Science*, *135*(15). https://doi.org/10.1002/app.46158
150. Sand, A., Shin, N.-J., Nam, H.-G., & Kwark, Y.-J. (2021). Effects of Reaction Parameters on Water Absorption of Poly(itaconic acid) Superabsorbent Particles Synthesized by Inverse Suspension Polymerization. *Fibers and Polymers*, *22*(4), 898–903. https://doi.org/10.1007/s12221-021-0459-2
151. Santos, A. C., Ferreira, C., Veiga, F., Ribeiro, A. J., Panchal, A., Lvov, Y., & Agarwal, A. (2018). Halloysite clay nanotubes for life sciences applications: From drug encapsulation to bioscaffold. *Advances in Colloid and Interface Science*, *257*, 58–70. https://doi.org/10.1016/j.cis.2018.05.007
152. Sargeant, T. D., Desai, A. P., Banerjee, S., Agawu, A., & Stopek, J. B. (2012). An in situ forming collagen–PEG hydrogel for tissue regeneration. *Acta Biomaterialia*, *8*(1), 124–132. https://doi.org/10.1016/j.actbio.2011.07.028
153. Sarkar, S., & Datta, S. C. (2014). Influence of Fertilizer Loaded Nanoclay Superabsorbent Polymer Composite (NCPC) on Dynamics of P and N Availability and their Uptake by Pearl Millet (Pennisetum glaucum) in an Inceptisols. *International Journal of Bio-Resource and Stress Management*, *5*(2), 221. https://doi.org/10.5958/0976-4038.2014.00559.4
154. Sarkar, S., Datta, S. C., & Biswas, D. R. (2014). Synthesis and characterization of nanoclay-polymer composites from soil clay with respect to their water-holding capacities and nutrient-release behavior. *Journal of Applied Polymer Science*, *131*(6), n/a-n/a. https://doi.org/10.1002/app.39951
155. Sarkar, S., Datta, S. C., & Biswas, D. R. (2015). Effect of Fertilizer Loaded Nanoclay/Superabsorbent Polymer Composites on Nitrogen and Phosphorus Release in Soil. *Proceedings of the National Academy of Sciences, India Section B: Biological Sciences*, *85*(2), 415–421. https://doi.org/10.1007/s40011-014-0371-2
156. Sarmah, D., & Karak, N. (2020). Biodegradable superabsorbent hydrogel for water holding in soil and controlled-release fertilizer. *Journal of Applied Polymer Science*, *137*(13). https://doi.org/10.1002/app.48495
157. Sartore, L., Pandini, S., Baldi, F., Bignotti, F., & Di Landro, L. (2017). Biocomposites based on poly(lactic acid) and superabsorbent sodium polyacrylate. *Journal of Applied Polymer Science*, *134*(48), 45655. https://doi.org/10.1002/app.45655
158. Saruchi, Kumar, V., Mittal, H., & Alhassan, S. M. (2019). Biodegradable hydrogels of tragacanth gum polysaccharide to improve water retention capacity of soil and environment-friendly controlled release of agrochemicals. *International Journal of Biological Macromolecules*, *132*, 1252–1261. https://doi.org/10.1016/j.ijbiomac.2019.04.023
159. Satriani, A., Catalano, M., & Scalcione, E. (2018). The role of superabsorbent hydrogel in bean crop cultivation under deficit irrigation conditions: A case-study in Southern Italy. *Agricultural Water Management*, *195*, 114–119. https://doi.org/10.1016/j.agwat.2017.10.008
160. Savary, S., Willocquet, L., Pethybridge, S. J., Esker, P., McRoberts, N., & Nelson, A. (2019). The global burden of pathogens and pests on major food crops. *Nature Ecology & Evolution*, *3*(3), 430–439. https://doi.org/10.1038/s41559-018-0793-y

161. Seufert, V., Ramankutty, N., & Foley, J. A. (2012). Comparing the yields of organic and conventional agriculture. *Nature*, *485*(7397), 229–232. https://doi.org/10.1038/nature11069
162. Seven, M. S., Menceloglu, Y., Rodop, O., & Menceloglu, Y. Z. (2020). *A POLYMER MATRIX BASED SUPERABSORBENT MATERIAL* (Patent PCT/TR2021/050162).
163. Seven, S. A., Tastan, Ö. F., Tas, C. E., Ünal, H., Ince, İ. A., & Menceloglu, Y. Z. (2019). Insecticide-releasing LLDPE films as greenhouse cover materials. *Materials Today Communications*, *19*, 170–176. https://doi.org/10.1016/j.mtcomm.2019.01.015
164. Sharma, A., Kumar, V., Shahzad, B., Tanveer, M., Sidhu, G. P. S., Handa, N., Kohli, S. K., Yadav, P., Bali, A. S., Parihar, R. D., Dar, O. I., Singh, K., Jasrotia, S., Bakshi, P., Ramakrishnan, M., Kumar, S., Bhardwaj, R., & Thukral, A. K. (2019). Worldwide pesticide usage and its impacts on ecosystem. *SN Applied Sciences*, *1*(11), 1446. https://doi.org/10.1007/s42452-019-1485-1
165. Shen, J., Cui, C., Li, J., & Wang, L. (2018). In Situ Synthesis of a Silver-Containing Superabsorbent Polymer via a Greener Method Based on Carboxymethyl Celluloses. *Molecules*, *23*(10), 2483. https://doi.org/10.3390/molecules23102483
166. Singh, A., Dhiman, N., Kar, A. K., Singh, D., Purohit, M. P., Ghosh, D., & Patnaik, S. (2020). Advances in controlled release pesticide formulations: Prospects to safer integrated pest management and sustainable agriculture. *Journal of Hazardous Materials*, *385*, 121525. https://doi.org/10.1016/j.jhazmat.2019.121525
167. Singh, B., Sharma, D. K., Kumar, R., & Gupta, A. (2009). Controlled release of the fungicide thiram from starch–alginate–clay based formulation. *Applied Clay Science*, *45*(1–2), 76–82. https://doi.org/10.1016/j.clay.2009.03.001
168. Singh, B., Sharma, D. K., Negi, S., & Dhiman, A. (2015). Synthesis and characterization of agar-starch based hydrogels for slow herbicide delivery applications. *International Journal of Plastics Technology*, *19*(2), 263–274. https://doi.org/10.1007/s12588-015-9126-z
169. Singh, R., & Mahto, V. (2017). Synthesis, characterization and evaluation of polyacrylamide graft starch/clay nanocomposite hydrogel system for enhanced oil recovery. *Petroleum Science*, *14*(4), 765–779. https://doi.org/10.1007/s12182-017-0185-y
170. Sinha, V., & Chakma, S. (2019). Advances in the preparation of hydrogel for wastewater treatment: A concise review. *Journal of Environmental Chemical Engineering*, *7*(5), 103295. https://doi.org/10.1016/j.jece.2019.103295
171. Skrzypczak, D., Witek-Krowiak, A., Dawiec-Liśniewska, A., Podstawczyk, D., Mikula, K., & Chojnacka, K. (2019). Immobilization of biosorbent in hydrogel as a new environmentally friendly fertilizer for micronutrients delivery. *Journal of Cleaner Production*, *241*, 118387. https://doi.org/10.1016/j.jclepro.2019.118387
172. Song, K. (2017). Micro- and nano-fillers used in the rubber industry. In *Progress in Rubber Nanocomposites* (pp. 41–80). Elsevier. https://doi.org/10.1016/B978-0-08-100409-8.00002-4
173. Song, S., Wang, Y., Xie, J., Sun, B., Zhou, N., Shen, H., & Shen, J. (2019). Carboxymethyl Chitosan Modified Carbon Nanoparticle for Controlled Emamectin Benzoate Delivery: Improved Solubility, pH-Responsive Release, and Sustainable Pest Control. *ACS Applied Materials & Interfaces*, *11*(37), 34258–34267. https://doi.org/10.1021/acsami.9b12564
174. Sudheer, S., Bandyopadhyay, S., & Bhat, R. (2023). Sustainable polysaccharide and protein hydrogel-based packaging materials for food products: A review.

International Journal of Biological Macromolecules, *248*, 125845. https://doi.org/10.1016/j.ijbiomac.2023.125845
175. Sun, B., Wu, H., Song, W., Li, Z., & Yu, J. (2019). Design methodology and mechanical properties of Superabsorbent Polymer (SAP) cement-based materials. *Construction and Building Materials*, *204*, 440–449. https://doi.org/10.1016/j.conbuildmat.2019.01.206
176. Supare, K., & Mahanwar, P. A. (2021). Starch-derived superabsorbent polymers in agriculture applications: an overview. *Polymer Bulletin*. https://doi.org/10.1007/s00289-021-03842-3
177. Takahashi, M., Kosaka, I., & Ohta, S. (2023). Water Retention Characteristics of Superabsorbent Polymers (SAPs) Used as Soil Amendments. *Soil Systems*, *7*(2), 58. https://doi.org/10.3390/soilsystems7020058
178. Tan, D., Yuan, P., Annabi-Bergaya, F., Dong, F., Liu, D., & He, H. (2015). A comparative study of tubular halloysite and platy kaolinite as carriers for the loading and release of the herbicide amitrole. *Applied Clay Science*, *114*, 190–196. https://doi.org/10.1016/j.clay.2015.05.024
179. Tang, Y., Guan, C., Liu, Y., Zhang, Z., Li, B., & Zhu, L. (2019). Preparation and absorption studies of poly(acrylic acid-co-2-acrylamide-2-methyl-1-propane sulfonic acid)/graphene oxide superabsorbent composite. *Polymer Bulletin*, *76*(3), 1383–1399. https://doi.org/10.1007/s00289-018-2446-3
180. Tharmavaram, M., Pandey, G., & Rawtani, D. (2018). Surface modified halloysite nanotubes: A flexible interface for biological, environmental and catalytic applications. *Advances in Colloid and Interface Science*, *261*, 82–101. https://doi.org/10.1016/j.cis.2018.09.001
181. The World Bank. (n.d.-a). *Annual freshwater withdrawals, agriculture*. The World Bank. Retrieved October 18, 2022, from https://data.worldbank.org/indicator/er.h2o.fwag.zs?type=shaded&view=map&year=2018
182. The World Bank. (n.d.-b). *Arable land (hectares per person)*. The World Bank. Retrieved October 20, 2022, from https://data.worldbank.org/indicator/AG.LND.ARBL.HA.PC
183. The World Bank. (n.d.-c). *Water in Agriculture*. The World Bank. Retrieved October 18, 2022, from https://www.worldbank.org/en/topic/water-in-agriculture
184. Tu, J., Cao, Z., Jing, Y., Fan, C., Zhang, C., Liao, L., & Liu, L. (2013). Halloysite nanotube nanocomposite hydrogels with tunable mechanical properties and drug release behavior. *Composites Science and Technology*, *85*, 126–130. https://doi.org/10.1016/j.compscitech.2013.06.011
185. Tubert, E., Vitali, V. A., Alvarez, M. S., Tubert, F. A., Baroli, I., & Amodeo, G. (2018). Synthesis and evaluation of a superabsorbent-fertilizer composite for maximizing the nutrient and water use efficiency in forestry plantations. *Journal of Environmental Management*, *210*, 239–254. https://doi.org/10.1016/j.jenvman.2017.12.062
186. Venkatachalam, D., & Kaliappa, S. (2023). Superabsorbent polymers: a state-of-art review on their classification, synthesis, physicochemical properties, and applications. *Reviews in Chemical Engineering*, *39*(1), 127–171. https://doi.org/10.1515/revce-2020-0102
187. Verma, D., & Gope, P. C. (2015). The use of coir/coconut fibers as reinforcements in composites. In *Biofiber Reinforcements in Composite Materials* (pp. 285–319). Elsevier. https://doi.org/10.1533/9781782421276.3.285

188. VORONEY, R. P. (2007). THE SOIL HABITAT. In *Soil Microbiology, Ecology and Biochemistry* (pp. 25–49). Elsevier. https://doi.org/10.1016/B978-0-08-047514-1.50006-8
189. Wang, W., Yang, S., Zhang, A., & Yang, Z. (2020). Preparation and properties of novel corn straw cellulose–based superabsorbent with water-retaining and slow-release functions. *Journal of Applied Polymer Science*, *137*(32), 48951. https://doi.org/10.1002/app.48951
190. Wang, X., Zhang, Y., Hao, C., Dai, X., Zhu, F., & Ge, C. (2014). Ultrasonic synthesis and properties of a sodium lignosulfonate–grafted poly(acrylic acid-co-acryl amide) composite super absorbent polymer. *New J. Chem.*, *38*(12), 6057–6063. https://doi.org/10.1039/C4NJ01266F
191. Wang, Y., Li, C., Wang, T., Li, X., & Li, X. (2020). Polylactic Acid–Graphene Oxide-based Materials for Loading and Sustained Release of Poorly Soluble Pesticides. *Langmuir*, *36*(41), 12336–12345. https://doi.org/10.1021/acs.langmuir.0c02320
192. Wei, H., Wang, H., Chu, H., & Li, J. (2019). Preparation and characterization of slow-release and water-retention fertilizer based on starch and halloysite. *International Journal of Biological Macromolecules*, *133*, 1210–1218. https://doi.org/10.1016/j.ijbiomac.2019.04.183
193. WHITE, P. J. (2003). Calcium in Plants. *Annals of Botany*, *92*(4), 487–511. https://doi.org/10.1093/aob/mcg164
194. Wu, F., Zhang, Y., Liu, L., & Yao, J. (2012). Synthesis and characterization of a novel cellulose-g-poly(acrylic acid-co-acrylamide) superabsorbent composite based on flax yarn waste. *Carbohydrate Polymers*, *87*(4), 2519–2525. https://doi.org/10.1016/j.carbpol.2011.11.028
195. Wu, Y., Liu, T., Shi, Y., & Wang, H. (2022). Dramatically enhancing mechanical properties of hydrogels by drying reactive polymers at elevated temperatures to introduce strong physical and chemical crosslinks. *Polymer*, *249*, 124842. https://doi.org/10.1016/j.polymer.2022.124842
196. Xiao, X., Yu, L., Xie, F., Bao, X., Liu, H., Ji, Z., & Chen, L. (2017). One-step method to prepare starch-based superabsorbent polymer for slow release of fertilizer. *Chemical Engineering Journal*, *309*, 607–616. https://doi.org/10.1016/j.cej.2016.10.101
197. Xu, S., Li, X., Wang, Y., Hu, Z., & Wang, R. (2019). Characterization of slow-release collagen- *g* -poly(acrylic acid- *co* -2-acrylamido-2-methyl-1-propane sulfonic acid)–iron(III) superabsorbent polymer containing fertilizer. *Journal of Applied Polymer Science*, *136*(11). https://doi.org/10.1002/app.47178
198. Xue, Y., Zhang, J., Chen, X., Zhang, J., Chen, G., Zhang, K., Lin, J., Guo, C., & Liu, J. (2021). Trigger-Detachable Hydrogel Adhesives for Bioelectronic Interfaces. *Advanced Functional Materials*, *31*(47). https://doi.org/10.1002/adfm.202106446
199. Yamina, A. M., Fizir, M., Itatahine, A., He, H., & Dramou, P. (2018). Preparation of multifunctional PEG-graft-Halloysite Nanotubes for Controlled Drug Release, Tumor Cell Targeting, and Bio-imaging. *Colloids and Surfaces B: Biointerfaces*, *170*, 322–329. https://doi.org/10.1016/j.colsurfb.2018.06.042
200. Yang, W., Fortunati, E., Bertoglio, F., Owczarek, J. S., Bruni, G., Kozanecki, M., Kenny, J. M., Torre, L., Visai, L., & Puglia, D. (2018). Polyvinyl alcohol/chitosan hydrogels with enhanced antioxidant and antibacterial properties induced by lignin nanoparticles. *Carbohydrate Polymers*, *181*, 275–284. https://doi.org/10.1016/j.carbpol.2017.10.084

201. Yang, Y., Chen, Y., Leng, F., Huang, L., Wang, Z., & Tian, W. (2017). Recent Advances on Surface Modification of Halloysite Nanotubes for Multifunctional Applications. *Applied Sciences*, *7*(12), 1215. https://doi.org/10.3390/app7121215
202. Yang, Y., Zhang, S., Wu, J., Gao, C., Lu, D., & Tang, D. W. S. (2022). Effect of long term application of super absorbent polymer on soil structure, soil enzyme activity, photosynthetic characteristics, water and nitrogen use of winter wheat. *Frontiers in Plant Science*, *13*. https://doi.org/10.3389/fpls.2022.998494
203. Yearla, S. R., & Padmasree, K. (2016). Exploitation of subabul stem lignin as a matrix in controlled release agrochemical nanoformulations: a case study with herbicide diuron. *Environmental Science and Pollution Research*, *23*(18), 18085–18098. https://doi.org/10.1007/s11356-016-6983-8
204. Yin, H., Akasaki, T., Lin Sun, T., Nakajima, T., Kurokawa, T., Nonoyama, T., Taira, T., Saruwatari, Y., & Ping Gong, J. (2013). Double network hydrogels from polyzwitterions: high mechanical strength and excellent anti-biofouling properties. *Journal of Materials Chemistry B*, *1*(30), 3685. https://doi.org/10.1039/c3tb20324g
205. Yoshimura, T., Uchikoshi, I., Yoshiura, Y., & Fujioka, R. (2005). Synthesis and characterization of novel biodegradable superabsorbent hydrogels based on chitin and succinic anhydride. *Carbohydrate Polymers*, *61*(3), 322–326. https://doi.org/10.1016/j.carbpol.2005.06.014
206. Yuan, P., Southon, P. D., Liu, Z., Green, M. E. R., Hook, J. M., Antill, S. J., & Kepert, C. J. (2008). Functionalization of Halloysite Clay Nanotubes by Grafting with γ-Aminopropyltriethoxysilane. *The Journal of Physical Chemistry C*, *112*(40), 15742–15751. https://doi.org/10.1021/jp805657t
207. Zare, Y., & Rhee, K. Y. (2022a). Development of a model for modulus of polymer halloysite nanotube nanocomposites by the interphase zones around dispersed and networked nanotubes. *Scientific Reports*, *12*(1), 2443. https://doi.org/10.1038/s41598-022-06465-4
208. Zare, Y., & Rhee, K. Y. (2022b). Development of a model for modulus of polymer halloysite nanotube nanocomposites by the interphase zones around dispersed and networked nanotubes. *Scientific Reports*, *12*(1), 2443. https://doi.org/10.1038/s41598-022-06465-4
209. Zargarian, S. Sh., Haddadi-Asl, V., & Hematpour, H. (2015). Carboxylic acid functionalization of halloysite nanotubes for sustained release of diphenhydramine hydrochloride. *Journal of Nanoparticle Research*, *17*(5), 218. https://doi.org/10.1007/s11051-015-3032-3
210. Zeng, X., Zhong, B., Jia, Z., Zhang, Q., Chen, Y., & Jia, D. (2019). Halloysite nanotubes as nanocarriers for plant herbicide and its controlled release in biodegradable polymers composite film. *Applied Clay Science*, *171*, 20–28. https://doi.org/10.1016/j.clay.2019.01.021
211. Zhan, F., Liu, M., Guo, M., & Wu, L. (2004). Preparation of superabsorbent polymer with slow-release phosphate fertilizer. *Journal of Applied Polymer Science*, *92*(5), 3417–3421. https://doi.org/10.1002/app.20361
212. Zhang, Y., Zhao, L., & Chen, Y. (2017). Synthesis and characterization of starch-*g* -Poly(acrylic acid)/Organo-Zeolite 4A superabsorbent composites with respect to their water-holding capacities and nutrient-release behavior. *Polymer Composites*, *38*(9), 1838–1848. https://doi.org/10.1002/pc.23754
213. Zhao, M., Zhou, H., Chen, L., Hao, L., Chen, H., & Zhou, X. (2020). Carboxymethyl chitosan grafted trisiloxane surfactant nanoparticles with pH

sensitivity for sustained release of pesticide. *Carbohydrate Polymers*, *243*, 116433. https://doi.org/10.1016/j.carbpol.2020.116433

214. Zhu, J., Tan, W. K., Song, X., Gao, Z., Wen, Y., Ong, C. N., Loh, C. S., Swarup, S., & Li, J. (2020). Converting Okara to Superabsorbent Hydrogels as Soil Supplements for Enhancing the Growth of Choy Sum (*Brassica* sp.) under Water-Limited Conditions. *ACS Sustainable Chemistry & Engineering*, *8*(25), 9425–9433. https://doi.org/10.1021/acssuschemeng.0c02181
215. Zinc Nutrient Initiative. (2015). *Zinc Fact Sheet: Zinc Fertilizer Overview*. https://crops.zinc.org/wp-content/uploads/sites/11/2016/12/Zinc-Fertilizer-Overview-General-Pop-June-2015.pdf
216. Zohuriaan-Mehr, M. J., Omidian, H., Doroudiani, S., & Kabiri, K. (2010). Advances in non-hygienic applications of superabsorbent hydrogel materials. *Journal of Materials Science*, *45*(21), 5711–5735. https://doi.org/10.1007/s10853-010-4780-1
217. Zou, A., Yang, Y., Cheng, J., Garamus, V. M., & Li, N. (2018). Construction and Characterization of a Novel Sustained-Release Delivery System for Hydrophobic Pesticides Using Biodegradable Polydopamine-Based Microcapsules. *Journal of Agricultural and Food Chemistry*, *66*(25), 6262–6268. https://doi.org/10.1021/acs.jafc.8b00877